Protein-protein interactions for early intracellular vitamin B_{12} metabolism in mammals

by

Justin C. Deme

Department of Microbiology and Immunology McGill University, Montreal December 2013

A thesis submitted to McGill University in partial fulfillment of the requirements of the degree of Doctor of Philosophy

© Justin C. Deme, 2013

Table of contents

List of figures	viii
List of tables	X
List of abbreviations	Xi
Abstract	xiv
Résumé	XVi
Acknowledgments	XVIII
Preface & contribution of authors	XX
Contributions to original knowledge	xxiii
Chapter 1: Literature review and thesis objectives	
1.0 Introduction to vitamin B ₁₂	2
1.1 Historical perspectives	2
1.1.0 Pernicious anemia	2
1.1.1 Extrinsic and intrinsic factor	3
1.1.2 Pernicious anemia as an autoimmune disorder	4
1.1.3 Vitamin B ₁₂ : the extrinsic factor	4
1.1.4 Cobalamin-binding proteins	5
1.1.5 Physiological cobalamin	6
1.1.6 Folate metabolism	7
1.2 Properties of cobalamin	7
1.2.0 Corrinoid chemistry	7
1.2.1 Oxidation states	8
1.2.2 Cobalt-carbon bond	9
1.3 Cobalamin absorption, distribution, and cellular internalization	10
1.3.0 Haptocorrin	10
1 3 1 Intrinsic Factor	12

	1.3.2 Cubam receptor	12
	1.3.3 Megalin	13
	1.3.4 Intrinsic factor deficiency and Imerslund-Gräsbeck syndrome	14
	1.3.5 Internalization of cobalamin by enterocytes	15
	1.3.6 Transcobalamin	16
	1.3.7 Transcobalamin receptor	18
1.4	Cobalamin and the diet	19
	1.4.0 Food sources	19
	1.4.1 Recommended Dietary Allowance	20
	1.4.2 Deficiencies	21
	1.4.2.0 Markers	21
	1.4.2.1 Symptoms	22
	1.4.2.2 Causes	23
	1.4.3 Fortification	25
	1.4.4 Cobalamin status and health	25
	1.4.4.0 Neural tube defects	25
	1.4.4.1 Cardiovascular disease	25
	1.4.4.2 Cognitive status	26
	1.4.4.3 Bone health, age-related macular degeneration, and frailty	27
1.5	Cobalamin and bacteria	28
	1.5.0 Producing microorganisms	28
	1.5.1 Biosynthesis	28
	1.5.1.0 Production of precorrin-2	29
	1.5.1.1 Conversion to adenosylcobyric acid	31
	1.5.1.2 Generation of adenosylcobalamin	34
	1.5.2 Industrial production	36
	1.5.3 Riboswitches	37
	1.5.4 Uptake	38
	1.5.5 Cobalamin-dependent enzymes	42
	1.5.5.0 Reductive halogenases	42
	1.5.5.1 Methyltransferases	43
	1.5.5.2 Adenosylcobalamin-dependent enzymes	45

1.6 Mammalian cobalamin metabolism	46
1.6.0 Assessment of enzyme activity and complementation groups	46
1.6.1 Methionine synthase pathway	48
1.6.1.0 cblG	48
1.6.1.1 cblE	49
1.6.2 Methylmalonyl-CoA mutase pathway	51
1.6.2.0 cblA	51
1.6.2.1 cblB	52
1.6.2.2 mut	54
1.6.3 Combined defects of MeCbl and AdoCbl metabolism	57
1.6.3.0 cblF	57
1.6.3.1 cblJ	59
1.6.3.2 cblC	61
1.6.3.3 cblD	64
1.7 Model for intracellular metabolism	67
1.8 Protein-protein interactions	70
1.9 Introduction to techniques used in this thesis	72
1.9.0 Phage display	72
1.9.1 Surface plasmon resonance	73
1.9.2 Dynamic light scattering	75
1.9.3 Static light scattering	75
1.9.4 Analytical ultracentrifugation	76
1.9.5 Far UV circular dichroism	77
1.10 Rationale and thesis objectives	78
Preface to chapter 2	80

Chapter 2: Structural features of recombinant MMADHC isoforms and their interactions with MMACHC, proteins of mammalian vitamin $B_{\rm 12}$ metabolism

2.0 Summary	82
2.1 Introduction	83
2.2 Materials and methods	86
2.2.0 Cloning, expression and purification of MMADHC $\Delta 1$ -12 and MMADHC $\Delta 1$ -61	86
2.2.1 Protein purity and analyses	88
2.2.2 Western blotting	88
2.2.3 Dynamic light scattering (DLS)	89
2.2.4 Analytical ultracentrifugation (AUC)	90
2.2.5 Circular dichroism (CD)	91
2.2.6 Secondary structure (PSI-PRED) and disorder (DISOPRED2) predictions	91
2.2.7 Phage display	92
2.2.8 Surface plasmon resonance (SPR)	93
2.3 Results	94
2.3.0 Purification of recombinant MMADHC	94
2.3.1 Immunodetection of MMACHC and MMADHC in human cell lines	95
2.3.2 MMADHC is stable, monomeric, and elongated in solution	96
2.3.3 MMADHC does not bind cobalamin	101
2.3.4 Identification of MMADHC- and MMACHC-binding sites on MMACHC by phage display	104
2.3.5 MMADHC∆1-12 and MMADHC∆1-61 bind to MMACHC with similar affinity	110
2.4 Discussion	114
2.5 Acknowledgments	119
Preface to chapter 3	121
Chapter 3: Subcellular location of MMACHC and MMADHC, two human proteins central to intracellular vitamin B_{12} metabolism	1
3.0 Summary	123
3.1 Introduction	123

3.2 Materials and methods	126
3.2.0 Cloning	126
3.2.1 Gene transduction	126
3.2.2 Cell culture	127
3.2.3 Mitochondrial isolation	127
3.2.4 Immunoblotting	128
3.2.5 Immunofluorescence	129
3.2.6 Biochemical studies	129
3.3 Results	130
3.3.0 Subcellular location of MMACHC and of MMA immunofluorescence	
3.3.1 Subcellular location of MMACHC and of MMAI fractionation	
3.3.2 Biochemical studies	136
3.4 Discussion	138
3.5 Acknowledgments	
Preface to chapter 4	142
Chapter 4: The putative human lysosomal vitami and ABCD4 interact <i>in vitro</i>	n B ₁₂ transporters LMBD1
4.0 Summary	144
4.1 Introduction	144
4.2 Materials and methods	148
4.2.0 Protein purification	148
4.2.1 BN-PAGE analysis	150
4.2.2 Chemical crosslinking	150
4.2.3 SEC-MALS	151
4.2.4 Surface plasmon resonance	152

4.2.5 Phage display	154
4.3 Results	155
4.3.0 Purification of recombinant LMBD1 and ABCD4	155
4.3.1 Oligomerization of LMBD1 and ABCD4	158
4.3.2 LMBD1 and ABCD4 interact by surface plasmon resonance (SPR)	162
4.3.3 Identification of MMACHC-binding sites on LMBD1 and ABCD4 by phage display	165
4.3.4 Binary interactions of LMBD1 or ABCD4 with MMACHC or MMADHC by SPR	
4.4 Discussion	173
4.5 Acknowledgments	170
Chapter 5: Conclusions and future directions 5.0 Completion of thesis objectives	180
5.1 Directions for future research	182
5.1.0 Detection of protein complexes in vivo	182
5.1.1 Refinement of protein interaction interfaces	184
5.1.2 Mechanism for the dual-localization of MMADHC	185
5.1.3 Assessment of LMBD1 and ABCD4 activity	186
5.1.4 Structure determination of MMADHC, LMBD1, and ABCD4	187
References	190

List of Figures

Cha	pter	1

Figure 1.0. Structure of cobalamin and coordination by axial ligands.	9
Figure 1.1. Absorption and systemic distribution of dietary cobalamin	16
Figure 1.2. C-5 pathway of precorrin-2 biosynthesis	30
Figure 1.3. Biosynthesis of adenosylcobalamin from precorrin-2.	35
Figure 1.4. Vitamin B_{12} import by the B-twelve uptake (Btu) system of $E.\ coli$	41
Figure 1.5. Mammalian pathway for the synthesis of methionine from homocysteine by methionine synthase.	50
Figure 1.6. Mammalian pathway for the conversion of methylmalonyl-CoA to succinyl-CoA by methylmalonyl-CoA mutase	56
Figure 1.7. Intracellular metabolism of cobalamin in mammals	69
Chapter 2	
Figure 2.0. Recombinant MMADHC Δ 1-12 and MMADHC Δ 1-61 following size exclusion chromatography	
Figure 2.1. Immunodetection of endogenous MMACHC and MMADHC	96
Figure 2.2. Biophysical characterization of MMADHCΔ1-12 and MMADHCΔ1-61	99
Figure 2.3. Alignment of predicted structural features to sequence of MMADHC	100
Figure 2.4. Thermostability of recombinant MMADHCs in solution by DLS	103
Figure 2.5. Phage display identifies putative MMADHC binding sites on MMACHC	106
Figure 2.6. Phage display predicts self-binding regions on MMACHC	109
Figure 2.7. Real-time single-cycle kinetics of MMACHC binding to low-density MMADHCΔ1-12, MMADHCΔ1-61, and MMACHC	111
Figure 2.8. Real-time multi-cycle kinetics of MMACHC binding to low-density MMADHCΔ1-12, MMADHCΔ1-61, and MMACHC	112
Figure 2.9. Representative fitting of SPR data to steady-state affinity model	113

Chapter 3

Figure 3.0. Immunoblot of fibroblasts transduced with retroviral constructs expressing MMACHC-GFP or MMADHC-GFP isoforms	131
Figure 3.1. Immunofluorescence of fibroblasts transduced with retroviral constructs expressing MMACHC-GFP or MMADHC-GFP isoforms	132
Figure 3.2. Immunofluorescence and immunoblot of fibroblasts transduced with retroviral constructs expressing C-terminal HA or FLAG-tagged MMACHC	133
Figure 3.3. Analysis of the distribution of MMACHC and MMADHC by subcellular fractionation	135
Figure 3.4. Rescue of the biochemical defects in <i>cblC</i> - and <i>cblD</i> -patient fibroblasts transduced with retroviral vectors expressing MMACHC-GFP or MMADHC-GFP isoforms.	137
Chapter 4	
Figure 4.0. Purified, detergent-solubilized LMBD1 and ABCD4	157
Figure 4.1. Self-association of LMBD1 and ABCD4	161
Figure 4.2. Representative SPR analyses for LMBD1 binding to amine-coupled ABCD4	164
Figure 4.3. Phage display identifies putative MMACHC binding sites on LMBD1	167
Figure 4.4. Phage display identifies putative MMACHC binding sites on ABCD4	169
Figure 4.5. Representative SPR for LMBD1 and ABCD4 binding to amine-coupled MMACHC and MMADHC	171
Figure 4.6. Representative SPR for ABCD4, LMBD1, and MMACHC binding to amine-coupled MMACHC	172

List of Tables

Chapter 2	
Table 2.0. MATCH/MatchScan identification of MMADHC affinity-selected Ph.D12 and Ph.DC7C peptides aligned to sequence of MMACHC	105
Table 2.1. MATCH/MatchScan identification of MMACHC affinity-selected Ph.D12 and Ph.DC7C peptides aligned to sequence of MMACHC	108
Chapter 3	
Table 3.0. Primers used to produce MMACHC and MMADHC constructs	126
Table 3.1. Genotypes of transduced patient fibroblasts	127
Chapter 4	
Table 4.0. MatchScan identification of MMACHC affinity-selected Ph.D12 and Ph.DC7C peptides aligned to sequence of LMBD1	166
Table 4.1. MatchScan identification of MMACHC affinity-selected Ph.D12 and Ph.DC7C peptides aligned to sequence of ABCD4	168

List of abbreviations

ABC ATP-binding cassette

AdoCbl 5'-deoxyadenosylcobalamin

ALA 5-aminolevulinic acid

ALAD 5-aminolevulinic acid dehydratase

AMD Age-related macular degeneration

AMN Amnionless

ATPase Adenosine triphosphatase

ATR Adenosyltransferase

AUC Analytical ultracentrifugation

BN-PAGE Blue native polyacrylamide gel electrophoresis

BSA Bovine serum albumin

Btu B-twelve-uptake

Cba Cobamide

Cbi Cobinamide

Cbl Cobalamin

CD Circular dichroism

CM Cytoplasmic membrane

CNCbl Cyanocobalamin

CN-PAGE Clear native polyacrylamide gel electrophoresis

CUB Complement C1r/C1s, Uegf, Bmp1

CUBN Cubilin

DDH Diol dehydratase

DLS Dynamic light scattering

DMB Dimethylbenzimidazole

EGF Epidermal growth factor

GFP Green fluorescence protein

GLM Glutamate mutase

GluRS Glutamyl-tRNA synthetase

GluTR Glutamyl-tRNA reductase

GSA-AT Glutamate-1-semialdehyde aminotransferase

HBA Hydrogenobyrinic acid

HC Haptocorrin

HC Homocystinuria

Hcy Homocysteine

IF Intrinsic factor

LDL Low-density lipoprotein

LDLR Low-density lipoprotein receptor

LIMR Lipocalin-1 interacting membrane receptor

MALS Multi angle light scattering

MBP Maltose binding protein

MCM Methylmalonyl-CoA mutase

MeCbl Methylcobalamin

Met Methionine

methyl-THF 5-methyltetrahydrofolate

MMA Methylmalonic acid

MMA Methylmalonic aciduria/acidemia

MRP1 Multidrug resistance protein 1

MS Methionine synthase

MSR Methionine synthase reductase

MTHFR Methylenetetrahydrofolate reductase

MTR Methionine synthase

MTS Mitochondrial targeting sequence

MUT Methylmalonyl-CoA mutase

NBD Nucleotide binding domain

NESI Nuclear export signal-interacting protein

NTD Neural tube defect

OHCbl Hydroxocobalamin

OM Outer membrane

PBG Porphobilinogen

PBGD Porphobilinogen deaminase

PBP Periplasmic binding protein

PDC Protein-detergent complex

RNR Ribonucleotide reductase

RU Resonance unit

SAM S-adenosyl-L-methionine

SDS-PAGE Sodium dodecyl sulfate polyacrylamide gel electrophoresis

SEC Size exclusion chromatography

SLIRP Stem-loop RNA binding protein

SPR Surface plasmon resonance

SUMT Uroporphyrinogen III methyltransferase

TBDT TonB-dependent transporter

TC Transcobalamin

TCA Tricarboxylic acid

TCblR Transcobalamin receptor

TC-I Transcobalamin I

TC-II Transcobalamin II

TC-III Transcobalamin III

THF Tetrahydrofolate

UROS Uroporphyrinogen III synthase

Abstract

Vitamin B₁₂, or cobalamin, is a water soluble vitamin required as cofactor for two mammalian enzymatic processes: homocysteine remethylation to methionine in the cytoplasm using methionine synthase (MS), and fatty acid/amino acid metabolism in the mitochondrion using methylmalonyl-CoA mutase (MCM). Whereas the molecular nature of intracellular cobalamin metabolism in mammals remains poorly understood, the proteins MMACHC, MMADHC, LMBD1 and ABCD4 are implicated in its early uptake and processing. Due to the inherent challenges associated with the cellular utilization of cobalamin, we propose that these proteins mediate its early intracellular channeling; the objective of this thesis was to characterize the protein-protein interactions that coordinate this process.

To gain insight into the function of MMADHC, recombinant isoforms were purified and low-resolution structural features were determined. MMADHC is monomeric and, in solution, adopts an extended conformation, with regions of disorder identified at the N-terminal domain. Panning combinatorial phage libraries against recombinant MMADHC allowed the mapping of putative sites of interaction on MMACHC. Kinetic analyses using surface plasmon resonance (SPR) confirmed a sub-micromolar affinity for the MMACHC–MMADHC interaction. Based on these studies, we propose that the function of MMADHC is exerted through its structured C-terminal domain via interactions with MMACHC in the cytoplasm.

Clinical phenotypes and subcellular location of MS and MCM dictate that MMACHC functions in the cytoplasm while MMADHC functions at a branch point in the pathway in both the cytoplasm and the mitochondrion. To demonstrate that the MMACHC–MMADHC interaction is physiologically plausible, we used immunofluorescence and subcellular

fractionation to confirm that MMACHC is cytoplasmic while MMADHC is dual-localized to the cytoplasm and mitochondria.

Protein interaction analyses were extended by describing the recombinant production of the lysosomal membrane proteins LMBD1 and ABCD4. Detergent-solubilized LMBD1 and ABCD4 each formed homodimers in solution. SPR provided direct *in vitro* binding data for an LMBD1–ABCD4 interaction with low nanomolar affinity. Consistent with our phage display predictions, MMACHC interacted with LMBD1 and ABCD4 with high affinity.

Our results support a model whereby membrane-bound LMBD1 and ABCD4 regulate the vectorial delivery of lysosomal cobalamin to cytoplasmic MMACHC, preventing cofactor dilution to the cytoplasmic milieu and protecting against inactivating side reactions. Subsequent formation of a cytoplasmic MMACHC–MMADHC complex then processes and partitions this cofactor to the downstream enzymes MCM and MS. These studies identify and characterize multiprotein complexes, advancing our basic understanding of early intracellular cobalamin metabolism.

Résumé

La vitamine B₁₂, ou bien la cobalamine, est une vitamine soluble requise pour deux processus enzymatiques distincts chez les mammifères; la production de l'acide aminée méthionine par la méthionine synthase (MS), et le métabolisme d'acides gras et d'acides aminées par la méthylmalonyl-CoA mutase (MCM). Malgré le fait que les procédées métaboliques intracellulaires de la cobalamine restes peu bien caractérisés, les protéines dont MMACHC, MMADHC, LMBD1, et ABCD4 jouent un rôle dans l'acquisition et le traitement de ce cofacteur. Vu les difficultés intrinsèques de l'utilisation cellulaire de la cobalamine, nous proposons que ces protéines assurent l'efficacité de son canalisation. Cette thèse avait pour objectif de caractériser les interactions protéine-protéine impliquées dans ce processus.

Pour pouvoir caractériser la fonction de MMADHC, des isoformes protéiques ont été purifiées et leurs traits structurales ont étés déterminés à basse résolution. MMADHC se trouve à être monomérique et adopte une conformation étendue en solution, avec des régions non structurées dans la terminaison aminée de la protéine. Ensuite, des librairies combinatoires de phages ont été utilisées comme substrats pour tracer des sites d'interactions potentiels avec MMADHC. Les analyses kinésiques des interactions MMACHC–MMADHC ont été faites à l'aide de la résonance plasmonique de surface (SPR) et ont confirmées une intéraction d'affinité sub-micromolaire. Avec ces résultats, nous proposons que la fonction de MMADHC se fasse par sa terminaison acidique en interagissant avec MMACHC dans le cytoplasme.

Les phénotypes cliniques et la localisation subcellulaire de MS et de MCM envisagent que MMACHC joue un rôle dans le cytoplasme et que MMADHC se trouve à être impliquée

dans le processus au niveau de la mitochondrie et du milieu cytoplasmique. Pour démontrer que l'interaction MMACHC-MMADHC est physiologique, nous avons utilisé l'immunofluorescence et la fractionnement subcellulaire pour confirmer que MMACHC est cytoplasmique et que MMADHC se retrouvent au cytoplasme et au mitochondrie.

Des analyses protéiques ont également engendré LMBD1 et ABCD4. Solubilisés à l'aide de détergent, ces deux protéines prennent la conformation d'homodimères en solution. Une interaction d'affinité nanomolaire entre LMBD1 et ABCD4 a été confirmée en SPR. En lien avec nos analyses de phages, MMACHC interagit avec haute affinité avec LMBD1 et ABCD4.

Nos résultats supportent un modèle dans lequel LMBD1 et ABCD4, tous deux liés dans la membrane, régularisent l'octroi de la cobalamine lysosomale à MMACHC en prévenant la dilution de ce cofacteur dans le milieu cytoplasmique et en protégeant contre des réactions inactivant. La dissociation et le recrutement de la MMADHC cytoplasmique à MMACHC facilitent le transfert de la cobalamine vers les réactions enzymatiques catalysées par MCM et MS. L'identification et la caractérisation de ces complexes multiprotéiques font en sorte d'avancer nos connaissances générales sur le métabolisme de la cobalamine.

Acknowledgments

There are many people that I would like to thank for supporting me during my graduate studies. The Coulton lab has been like a home to me for the past 7 years; were it not for the supporting and stimulating environment provided by its members I would not have the fond memories that I have today. Dr. James W. Coulton was the first person to give me an opportunity to pursue science, and I have cherished his mentorship. Particularly, I appreciate James' encouragement in developing my scientific abilities, critical thinking, and promoting effective communication and teaching skills. James has given me all the tools required to succeed, whether it be in teaching, writing, or pursuing cutting-edge science, and for this I am deeply grateful. I would also like to thank my co-supervisor Dr. David S. Rosenblatt (Dept. of Human Genetics) for his encouragement and support throughout my Ph.D. studies. Despite coming from a different scientific background I was accepted in your group with open arms and I will cherish the insight and discussions held at your lab meetings for a long time.

I am also thankful to the members of my Advisory Committee: Dr. Benoit Cousineau (Dept. of Microbiology and Immunology), Dr. Greg Miller (Dept. of Pharmacology and Therapeutics), and Dr. Peter Pawelek (Concordia University; Dept. of Chemistry and Biochemistry) for providing critical insight and evaluation over the course of my studies. I also wish to acknowledge Dr. Liz Carpenter (SGC Oxford) and her group for making my 3-month experience in the UK a memorable one.

I also wish to thank all past and present members of the Coulton and Rosenblatt labs who provided technical/moral support, stimulating discussions and whom I call friends. Those who deserve exceptional mention include Wayne Mah, a tremendous friend and labmate throughout our joint project; Dr. David Carter, my first mentor and partner-in-crime; Dr. Karron James and

Dr. Jackie Chung, who gave me sharp doses of reality every day; Aleksandr Sverzhinsky and Nathalie Croteau for always lending an open ear. Thanks also to Dr. David Watkins for excellent advice and critical editing of manuscripts and thesis. Other people whom I am grateful to but would have to write another thesis to appreciate are Dr. Maria Plesa, Chris Ng, Andrew Cottreau, Damien Biot-Pelletier, Kristian Levey, Derek Bryant, Hubert Gagnon, Alison Brebner, and Mihaela Pupavac. I would explicitly like to thank Dr. Mark Hancock at the McGill SPR Facility for his efforts in producing top quality results.

Next, I owe an extreme debt of gratitude to my partner Alison for being just about the best person I have ever met. Through thick and thin, she has supported and encouraged me; words cannot express how much she means to me. I have cherished her guidance and care throughout our time together, and I am looking forward to the next chapter of our lives.

My family has always been supportive of my decisions to pursue science at the highest level and I am grateful for their patience, support, and encouragement over this period.

Lastly, I thank the Dept. of Microbiology and Immunology for fond memories, opportunities, and financial support, in addition to the Natural Sciences and Engineering Research Council of Canada (NSERC) and Fonds Québécois de Recherche sur la Nature et Technologies (FQRNT) for their financial support.

Preface & contribution of authors

This manuscript-based thesis is prepared in accordance with the guidelines of McGill University (http://www.mcgill.ca/gps/thesis/guidelines/preparation), in which "...thesis research may be presented as a collection of scholarly papers of which the student is the author or coauthor; that is, it can include the text of one or more manuscripts, submitted or to be submitted for publication, and/or published articles reformatted according to thesis requirements...". The following is a description of the authors' contribution to each of the manuscript-based chapters.

Chapter 2

Justin C. Deme, Isabelle R. Miousse, Maria Plesa, Jaeseung C. Kim, Mark A. Hancock, Wayne Mah, David S. Rosenblatt, James W. Coulton. (2012) Structural features of recombinant MMADHC isoforms and their interactions with MMACHC, proteins of mammalian vitamin B₁₂ metabolism. *Molecular Genetics and Metabolism* 107: 352-362.

Justin C. Deme: Cloned, expressed, and purified MMACHC and MMADHCs. Ran biophysical experiments and analyzed results. Performed disorder predictions for MMADHC. Carried out cobalamin-binding and thermostability assays. Aligned MMACHC and MMADHC affinity-selected peptides using RELIC/Matchscan. Wrote and edited manuscript.

Isabelle R. Miousse: Panned phage libraries against MMADHC. Amplified MMADHC-affinity selected phage. Purified and sequenced MMADHC-affinity-selected phage DNA.

Maria Plesa, Jaeseung C. Kim: Panned phage libraries against MMACHC. Amplified MMACHC-affinity selected phage. Purified and sequenced MMACHC-affinity-selected phage DNA.

Mark A. Hancock: Performed and analyzed surface plasmon resonance experiments, wrote

relevant sections of manuscript, edited manuscript.

Wayne Mah: Performed immunoblotting experiment, edited manuscript.

Chapter 3

Wayne Mah*, Justin C. Deme*, David Watkins, Stephen Fung, Alexandre Janer, Eric A.

Shoubridge, David S. Rosenblatt, James W. Coulton. (2013) Subcellular location of

MMACHC and MMADHC, two human proteins central to intracellular vitamin B₁₂ metabolism.

Molecular Genetics and Metabolism 108: 112-118.

*Wayne Mah and Justin C. Deme contributed equally to this publication and are considered co-authors.

Wayne Mah: Performed immunoblotting, subcellular fractionation, and immunofluorescence

experiments. Wrote and edited manuscript.

Justin C. Deme: Designed constructs and developed experimental procedures. Analyzed

immunoblotting, subcellular fractionation, and immunofluorescence results. Wrote and edited

manuscript.

David Watkins: Performed incorporation experiments, wrote relevant sections of manuscript,

edited manuscript.

Stephen Fung: Assisted with and performed cell line transfections.

Alexandre Janer: Assisted with immunofluorescence experiments.

xxi

Chapter 4

Justin C. Deme, Mark A. Hancock, Xiaobing Xia, Maria Plesa, Jaeseung C. Kim, Mark A. Hancock, Elizabeth P. Carpenter, David S. Rosenblatt, James W. Coulton. (2013). The putative lysosomal cobalamin transporters LMBD1 and ABCD4 interact *in vitro*. *In preparation*.

Justin C. Deme: Expressed and purified recombinant LMBD1 and ABCD4. Performed size exclusion and light scattering analyses of LMBD1 and ABCD4. Performed cross-linking and BN-PAGE analyses of LMBD1 and ABCD4. Performed Matchscan analyses on MMACHC affinity-selected peptides for mapping to LMBD1/ABCD4. Wrote and edited manuscript.

Mark A. Hancock: Performed and analyzed surface plasmon resonance experiments, wrote relevant sections of manuscript, edited manuscript.

Xiaobing Xia: Expressed and purified recombinant LMBD1. Performed preliminary expression and detergent screening for LMBD1.

Maria Plesa, Jaeseung C. Kim: Panned phage libraries against MMACHC. Amplified MMACHC-affinity selected phage. Purified and sequenced MMACHC-affinity-selected phage DNA.

Contributions to original knowledge

- 1. First to report recombinant production of tag-free, physiological MMADHC isoforms.
- 2. Demonstration of the endogenous expression of full-length MMACHC and MMADHC in cell lines.
- 3. Determination that recombinant MMADHC isoforms are monomeric and elongated in solution using biophysical analyses.
- 4. Estimation of the secondary structure content of MMADHC and involvement in protein conformation.
- 5. Demonstration that MMADHC does not bind or process cobalamin.
- 6. Use of phage display technology to predict and map MMACHC- and MMADHC-binding surfaces on MMACHC.
- 7. Demonstration that tag-free MMADHC and MMACHC interact *in vitro*, and that MMACHC also interacts with itself.
- 8. Determination of the subcellular location of MMACHC and MMADHC.
- 9. First to report production of recombinant LMBD1 and ABCD4.
- 10. Determination of the oligomeric state of recombinant LMBD1 and ABCD4.
- 11. Demonstration that LMBD1 and ABCD4 interact in vitro.
- 12. Use of phage display technology to predict and map regions on LMBD1 or ABCD4 involved in recruiting MMACHC.
- 13. Demonstration that LMBD1 or ABCD4 can interact in vitro with MMACHC.

Chapter 1

Literature review and thesis objectives

1.0 Introduction to vitamin B₁₂

Vitamin B_{12} , or cobalamin (Cbl), is a water soluble vitamin required by all mammals. Dubbed "nature's most beautiful cofactor" (1), Cbl is the largest of all vitamins and the most structurally complex. Because mammals lack the enzymes required for *de novo* synthesis, Cbl is acquired through the diet with meats and dairy products contributing to the majority of the daily Cbl requirements. Cbl is required as cofactor for two mammalian enzymes; methionine synthase (MS or MTR) and methylmalonyl-CoA mutase (MCM or MUT). MS is a cytoplasmic enzyme that catalyzes methionine formation by the methylation of homocysteine. MCM resides in the mitochondrion and is responsible for the terminal metabolism of odd carbon number fatty acids and the amino acids valine, methionine, isoleucine and threonine, for entry into the tricarboxylic acid (TCA) cycle. Cbl deficiencies may develop with age or can result from following a vegan diet, newborns breastfed by Cbl-deficient mothers, or genetic defects that result in impaired absorption, cellular uptake or intracellular distribution. Disorders caused by Cbl deficiency result in severe hematological and neurological symptoms. The following section is a review of relevant literature that describes historical breakthroughs in Cbl research, structure and chemistry of the Cbl molecule, biosynthesis and import of Cbl in bacteria, and absorption and intracellular processing of dietary Cbl in mammals.

1.1 Historical perspectives

1.1.0 Pernicious anemia

The history of Cbl begins with pernicious anemia, a form of non iron-deficient anemia first described by Addison over 150 years ago (2). Addison noticed that the appetite of these anemic patients diminished with time, and patients ultimately died from their affliction because no treatment options were available (3). In the 1880s, Ehrlich identified the presence of

megaloblasts in the serum of patients with pernicious anemia (4). Patients' stomachs were also compromised; Fenwick reported lesions (5); Cahn and Mering found no production of hydrochloric acid (achlorhydria) (6); and Faber and Block demonstrated that symptoms of achlorhydria presented earlier than anemia by many years (7). It wasn't until 1920 that Whipple successfully demonstrated a remedy for anemia, whereby feeding raw liver to dogs caused them to overcome anemia, an outcome not observed in dogs fed with cooked liver (8).

Minot and Murphy followed up Whipple's work by successfully treating patients with pernicious anemia using a diet of vegetables, fruits, and lightly cooked liver and muscle meat (9). Liver therapy was applied by numerous physicians starting in 1926, though the intake of large quantities of liver or liver juice resulted in poor patient compliance. Cohn pioneered a preparation of highly concentrated liver extract (10) that proved to be much more efficient than liver itself (11). By 1932 purified liver extracts suitable for intramuscular or parenteral injections appeared on the market, and in 1934 Minot, Murphy, and Whipple were awarded the Nobel Prize in Medicine and Physiology for their work on developing a cure for pernicious anemia.

1.1.1 Extrinsic and intrinsic factor

Around the same time Castle identified the biological factors involved in disease progression. Castle hypothesized that an inherent feature was missing in pernicious anemia patients for which he termed "intrinsic factor". In his famous experiment, he fed a protein meal of cooked ground beef to healthy young men and ~ 1 h later removed their gastric contents. These contents (gastric juice and partially digested beef) were then administered to anemic patients. A reticulocyte response similar to that demonstrated by Minot and Murphy was observed in these patients, whereas patients that had been administered only cooked beef or

gastric juice alone demonstrated no response (12, 13). Castle concluded that an unknown but essential interaction between an extrinsic factor found in beef and an intrinsic factor found in healthy patient gastric juice was required to treat pernicious anemia (14).

1.1.2 Pernicious anemia as an autoimmune disorder

When intrinsic factor (IF) was determined to be missing in anemic patients, a treatment consisting of defatted hog stomach was developed (15). The effectiveness of such a treatment reduced significantly with time (16), as patients developed resistance (17, 18). Pernicious anemia was later discovered to be an autoimmune disorder (19) caused by antibody production against gastric parietal cells (20) that results in atrophy and cessation of IF production (21). The development of achlorhydria arises because parietal cells also produce hydrochloric acid (22). The most common antigen is the α -subunit of the H⁺/K⁺ adenosine triphosphatase (ATPase), embedded in the membrane of parietal cells (23). Pernicious anemia has also been described in patients with auto-antibodies against IF alone and not parietal cells (24).

1.1.3 Vitamin B_{12} : the extrinsic factor

By 1945 a therapeutically effective concentrated liver extract containing Castle's extrinsic factor had been developed. In 1947 Smith (25) and Folkers (26) succeeded in crystallizing this anti-pernicious anemia factor (27). Termed "vitamin B₁₂" (26), this extrinsic factor contained cyanide and cobalt (28) for which the chemical name cyanocobalamin (CNCbl) was derived. The cyano group was an artifact of the purification procedure and CNCbl is not a naturally occurring form of Cbl. Folkers also discovered that the bacterium *Streptomyces griseus* produced Cbl in culture medium, enabling early mass production. When administered to pernicious anemia patients along with gastric juice, vitamin B₁₂ stimulated haematopoiesis, confirming Castle's hypothesis (29). Using X-ray crystallography Hodgkin later determined the

structure of CNCbl (30) and the coenzyme form of vitamin B₁₂, termed adenosylcobalamin (AdoCbl) (31). Both Cbl forms exhibited a heme-like structure called a corrin ring that coordinated a central cobalt atom; the name "cobalamin" is derived from the term "cobalt-containing vitamin". Hodgkin was awarded the Nobel Prize in Chemistry for her work on elucidating the structure of important biochemical substances. The complete synthesis of vitamin B₁₂ was reported ten years later from a collaboration between Woodward and Eschenmoser that involved more than one hundred chemists over a period of eleven years (32).

1.1.4 Cobalamin-binding proteins

Radioactive cobalt derivatives of vitamin B_{12} , namely [56 Co]-, [57 Co]-, [58 Co]- B_{12} , were generated shortly after the isolation of Cbl in order to understand absorption, tissue distribution, and turnover. A urinary excretion test that became the reference for Cbl absorption was developed in 1953 by Schilling (33). In this test, an oral administration of radiolabeled vitamin B_{12} is followed by an intramuscular injection of a large dose of non-radiolabeled vitamin B_{12} . In healthy patients, radiolabeled Cbl is absorbed by the gastrointestinal tract but is not internalized by tissue cells due to the saturation of serum Cbl binding proteins with non-radiolabeled Cbl. This results in the excretion of radiolabeled Cbl in the urine, with radioactive counts monitored over a period of 24 h. Approximately 10% of the initial radioactive dose is recovered in the urine of healthy patients, whereas < 1% is recovered in patients suffering from pernicious anemia due to poor absorption. As a follow up test for low radioactive Cbl absorption, a second dose of radioactive Cbl plus IF is administered orally. Cbl absorption is corrected only in the presence of exogenous IF in patients with pernicious anemia due to a lack of IF. This allows the differentiation between pernicious anemia and other forms of vitamin B_{12} malabsorption.

These radiolabeled Cbl derivatives were also used by Gräsbeck to show that gastric juice contained two Cbl-binding proteins with different electrophoretic mobilities (34, 35). The protein with slowest motility demonstrated IF activity, whereas the rapidly moving protein did not. The rapidly moving protein was termed R(apidly Moving) Binder, or R-binder. Gräsbeck demonstrated that saliva was rich in R-binder and that R-binder in gastric juice originated from saliva (35). The nomenclature changed following the discovery of serum Cbl-binding proteins, or "transcobalamins", in the 1950s (36, 37). Today, R-binder is less commonly used to refer to two classes of transcobalamins (I and III; TC-I and TC-III) which map to the gene encoding haptocorrin (*TCNI*) and differ only in glycosylation pattern at the protein level (*section 1.3.0*). The other Cbl-binding serum component is transcobalamin-II (TC-II), which is encoded by the *TCN2* gene (*section 1.3.6*).

1.1.5 Physiological cobalamin

In 1958 it was demonstrated that a light-sensitive derivative of Cbl (pseudovitamin B₁₂) acted as cofactor in the glutamate mutase pathway from an extract of *Clostridium tetramorphum* (38). This was shortly followed by the isolation from liver of AdoCbl, which could effectively substitute for pseudovitamin B₁₂ in this reaction (39). Methylcobalamin (MeCbl), synthesized in 1962 (40), was found to be the predominant form of Cbl in human serum (41). Only two enzymes require Cbl as cofactor in humans; methylmalonyl-CoA mutase (MCM) uses AdoCbl in the catabolism of branched chain amino acids and odd chain fatty acids, whereas methionine synthase (MS) uses MeCbl in a complex reaction that converts homocysteine (Hcy) to methionine (Met) using 5-methyltetrahydrofolate (methyl-THF) as methyl donor.

1.1.6 Folate metabolism

Apart from elevated Cbl levels, liver is also a source of folate. The MS reaction requires Cbl as cofactor but also regulates cellular folate levels by using methyl-THF as methyl donor in the MS reaction. Thus, patients with Cbl deficiencies often suffer from folate deficiencies. The folate trap hypothesis proposes that folate is irreversibly converted to methyl-THF, which cannot be effectively used in patients with defects in the MS reaction (42). This "trapping" results in decreased levels of the precursor folate required for purine and thymidine synthesis, leading to anemia. Folic acid supplementation can improve hematological disorders associated with folate deficiency but can also mask vitamin B₁₂ deficiencies (*section 1.4.3*).

1.2 Properties of cobalamin

1.2.0 Corrinoid chemistry

The general structure of Cbl involves a central cobalt atom coordinated equatorially to four nitrogens donated by a corrin ring that consists of four reduced pyrrole rings and seven amide side chains (Fig. 1.0A) (30). The largest side chain extending from the corrin ring (side chain "f") contains a nucleotide that serves as the " α -" or lower axial ligand. The nucleotide base is defined as 5,6-dimethylbenzimidazole (DMB) and further coordinates the central cobalt perpendicularly to the corrin ring (43). The identity of this nucleotide base varies within nature; cobamides (Cba) are corrin ring-containing compounds (corrinoids) with nucleotide base substitutions. For example, certain Cba found in foods have an adenine instead of DMB as nucleotide base and are designated pseudovitamin B_{12} . These forms have low affinity for Cbl-binding proteins and cannot be used by Cbl-dependent enzymes. Corrinoids that altogether lack a coordinating nucleotide are termed cobinamides (Cbi).

A sixth coordination site is provided by the " β -" or upper axial ligand and the nature of the upper axial ligand defines Cbl diversity. Cyano, methyl, hydroxy, and 5'-deoxyadenosyl groups are the upper axial ligands (or R-groups) for CNCbl, MeCbl, hydroxocobalamin (OHCbl) and AdoCbl, respectively. Depending on the upper axial ligand, the molecular masses of cobalamins range from 1.3 - 1.5 kDa. The term "vitamin B_{12} " has typically been used to describe CNCbl but has also been misrepresented to describe all potentially biologically active forms of Cbl. MeCbl and AdoCbl, found at 30-700 nM in human tissues (44), are the active coenzyme forms required for MS and MCM, respectively.

1.2.1 Oxidation states

Cobalamins exist in three different oxidation states: Co³⁺ or Co(III), Co²⁺ or Co(II), and Co⁺ or Co(I). Coordination of the upper and lower axial ligands to the central cobalt depends on the oxidation state of the cobalt. In cob(III)alamin two axial ligands coordinate the Co³⁺ core. In the Co(II) oxidation state, Cbl has no upper axial ligand and is generally referred to as cob(II)alamin or B_{12r}. Axial ligands are not engaged in coordinating the Co(I) state in cob(I)alamin or B_{12s}. The alkyl cob(III)alamins (MeCbl, AdoCbl) adopt a six-coordinate conformation at physiological pH with a methyl or 5'-deoxyadenosyl group as the upper axial ligand and DMB as lower axial ligand. When DMB acts as lower axial ligand, the coordination state is referred to as "base-on" (Fig. 1.0B). The "base-off" state is assumed upon protonation of DMB by lowering the pH. The "base-on" to "base-off" transition has pKa values of -2.13, 0.10, 2.9 and 3.67 for OHCbl, CNCbl, MeCbl, and AdoCbl, respectively (45). This makes the concentration of free "base-off" Cbl extremely low at physiological pH. Cbl-dependent enzymes that contain the conserved B₁₂-binding consensus sequence "DXHXXG" (46, 47), including

mammalian MS and MCM, substitute DMB with a histidine residue resulting in a "base-off/Hison" conformation.

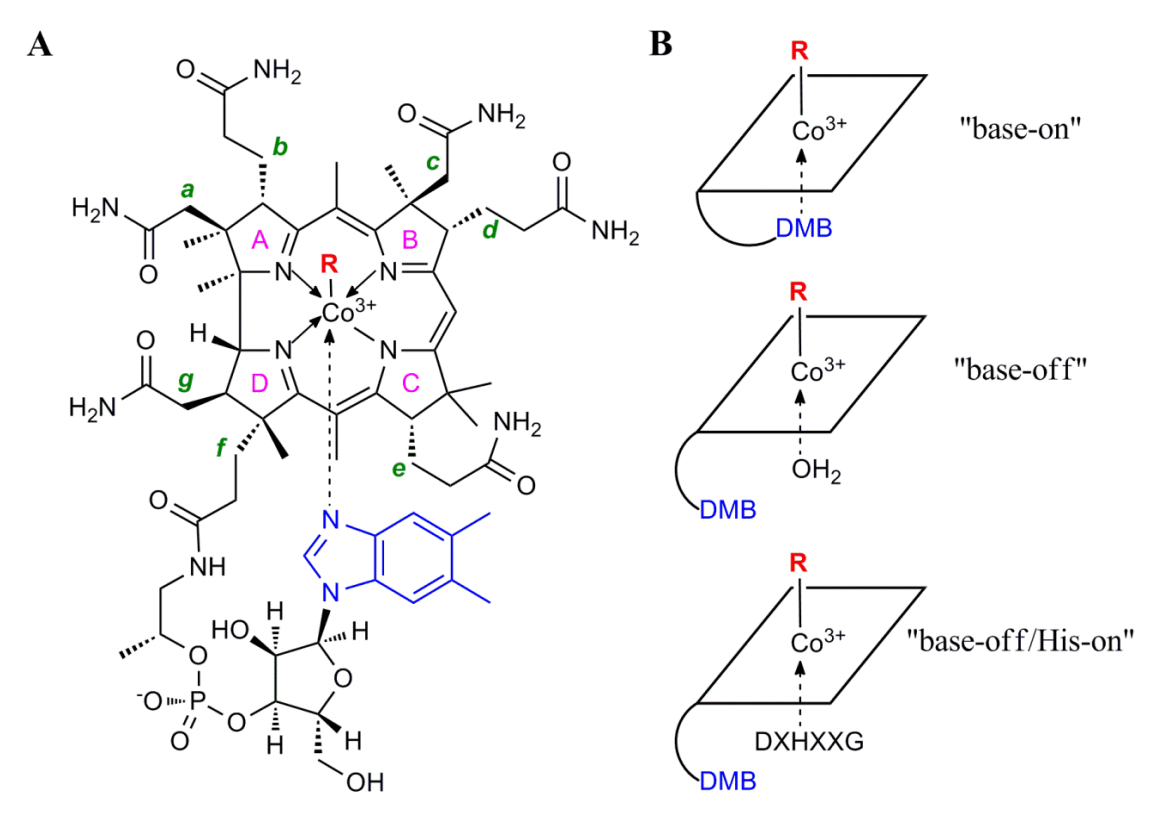


Figure 1.0. Structure of cobalamin and coordination by axial ligands. A. The central cobalt of cobalamin is coordinated equatorially by nitrogens from four pyrrole rings (pink, A-D) that form the corrin ring. Amide side chains stemming from the corrin ring are displayed in green (*a-g*). Axial ligands also contribute to cobalt coordination; the upper axial ligand (red "R") can be cyano, aquo, methyl, or 5'-deoxyadenosyl groups, and the lower axial ligand is dimethylbenzimidazole (DMB; blue) when cobalamin is in the "base-on" conformation. **B.** *Top:* the "base-on" conformation occurs when the lower axial ligand DMB coordinates the central cobalt. *Middle:* protonation of DMB results in a "base-off" state. *Bottom:* Cbl-dependent enzymes displace DMB as lower axial ligand with a histidine residue resulting in the "base-off/His-on" state.

1.2.2 Cobalt-carbon bond

Coordination of the central cobalt in AdoCbl and MeCbl is performed through a cobalt-carbon bond (Co-C). This bond is unique in nature with Cbl-dependent enzymes catalyzing the only known reactions involving such structures. The Co-C bond has a relatively weak dissociation energy of 30 and 37 kcal/mol for "base-on" forms of AdoCbl and MeCbl,

respectively (48). Fission can occur by homolytic or heterolytic cleavage. In homolytic cleavage, electrons are divided equally amongst the separated R-group and the coordinated cobalt, resulting in reduction to cob(II)alamin. In the MCM-catalyzed reaction, homolytic cleavage of the Co-C bond generates cob(II)alamin and a 5'-deoxyadenosyl radical. This radical catalyzes a carbon skeleton rearrangement on methylmalonyl-CoA to generate succinyl-CoA. In heterolytic cleavage, both electrons reduce the central cobalt to form cob(I)alamin. The MS reaction involves the heterolytic cleavage of MeCbl whereby the methyl group is transferred to homocysteine to form methionine, and the reaction intermediate cob(I)alamin. Cob(I)alamin is one of the most reactive nucleophiles known in biology (49). Cob(I)alamin undergoes rapid but sporadic oxidation in the MS reaction leading to the production of cob(II)alamin which is converted to MeCbl via reductive methylation (50). The mammalian MS and MCM reactions are described in *sections* 1.6.1 and 1.6.2.

1.3 Cobalamin absorption, distribution and cellular internalization

The absorption and transport of cobalamin is a complex process involving three transport proteins; haptocorrin (HC), intrinsic factor (IF), and transcobalamin (TC). Each transport protein binds Cbl with 1:1 stoichiometry and very high affinity ($K_d \sim 10^{-15}$ M) (51), making proteolytic degradation of the transport protein necessary for Cbl release.

1.3.0 Haptocorrin

Cbl from the diet exists predominantly in protein-bound form and only becomes released in the upper gastrointestinal tract with the help of gastric acid and the proteolytic enzyme pepsin. Haptocorrin (HC) is secreted in the saliva and binds free Cbl in the stomach. HC accounts for a family of proteins (TC-I and TC-III) that differ only in glycosylation pattern. The gene *TCNI* encodes the 410 aa mature protein with molecular weight of 45.5 kDa. HC is heavily

glycosylated which results in an apparent molecular weight increase of 30-40% (\sim 66 kDa) (52). HC has the broadest affinity for Cbl analogues out of all the transport proteins (53) and is the most abundant carrier protein found in the circulation, binding \sim 80% of total Cbl in addition to other corrinoids. The structure of deglycosylated haptocorrin complexed with CNCbl or Cbi has recently been solved (54). Despite a low overall sequence identity to IF and TC (< 25%), HC has an overall similar domain architecture consisting of two globular domains; an N-terminal α -domain (residues 1-287) and a C-terminal β -domain (residues 309-410) connected by a flexible linker (Fig. 1.1A). HC binds Cbl and Cbi through interactions between conserved residues found in IF and TC and the corrin ring. Unique residues (N120, R357 and N373) coordinate Cbi lacking DMB. A current hypothesis proposes multiple roles for HC that involve preventing the loss of free Cbl in circulation, sequestering inactive Cbl derivatives to prevent intracellular entry, and excreting inactive Cbl analogs.

HC deficiency is characterized by an overall reduction in serum Cbl, though levels of transcobalamin-bound Cbl (TC-Cbl), or holo-TC, are normal (55). Cbl uptake by peripheral cells using the transcobalamin receptor (TCblR; *section 1.3.7*) is therefore not reduced (56). Clinical symptoms for HC deficiency are not apparent. HC deficiency was identified in 15% of patients with unexplained low Cbl levels but also some patients with normal serum Cbl levels (57). Homozygous mutations in *TCN1* result in low serum Cbl levels whereas heterozygous mutations result in mildly lowered or normal levels of Cbl (58). Cbl therapy to alleviate low serum cobalamin levels is not effective for HC deficiency (56, 59). There is currently no evidence that low serum Cbl caused by HC deficiency results in clinical manisfestations of Cbl deficiency (60).

1.3.1 Intrinsic Factor

HC is digested in the intestine by pancreatic proteases resulting in the release of Cbl. Free Cbl subsequently binds to intrinsic factor (IF) secreted by gastric parietal cells. Intrinsic factor production (1-5 mg/day) far exceeds the daily required allowance of Cbl (1-5 μ g/day) (61). The gene *GIF* encodes the 417 aa protein of molecular mass 45 kDa (62). IF is glycosylated and migrates to a molecular mass of 58-60 kDa by SDS-PAGE (63). The structure of human IF in complex with CNCbl has been solved (64). Similar to HC, IF consists of an N-terminal α -domain (residues 7-273) organized as an α 6/ α 6 helical barrel and a C-terminal β -domain (residues 289-399) that contains predominantly β -strands (Fig. 1.1A). The corrin ring of Cbl forms hydrogen bonds and a salt bridge with both domains. Cbl binds IF at the α / β domain interface in a "base-on" conformation; a β -hairpin within the β -domain maintains DMB in a hydrophobic environment. IF specifically binds to Cbl and shows poor affinity towards Cbi.

1.3.2 Cubam receptor

IF-Cbl binds to the cubam receptor, formed from <u>cub</u>ilin (CUBN) and <u>am</u>nionless (AMN), on enterocytes in the distal ileum (Fig. 1.1B) (60). The human gene *CUBN* (65) encodes CUBN, a 3600 aa, 460 kDa membrane-associated protein. CUBN has three topologically distinct regions: an N-terminal domain involved in protein trimerization, an intermediary epidermal-growth factor (EGF) cluster containing eight EGF repeats and a large C-terminal cluster of 27 CUB (<u>complement C1r/C1s, Uegf, Bmp1</u>) domains. CUB domains (110 aa) are found in developmentally regulated proteins and are involved in ligand binding (66). Binding of IF-Cbl to CUBN has been mapped to CUB domains 5-8 (67), with the recent structure of IF-Cbl in complex with these domains confirming this finding (68). Consistent with the IF-Cbl structure, Cbl is bound to IF in the "base-on" conformation at the α/β-domain

interface. The α -domain interacts with CUB₆ and the β -domain interacts with CUB₈. CUB₅ and CUB₇ do not directly interact with IF but help coordinate CUB₆ and CUB₈ for interaction with IF-Cbl (68). While Cbl does not directly interact with the CUB domains, binding of Cbl to IF makes IF more compact (64) which in turn permits the IF-Cbl-CUBN interaction (68).

Because CUBN lacks transmembrane and cytoplasmic domains its internalization is dependent on other transmembrane proteins. Two proteins involved in CUBN internalization are Amnionless (AMN) (69) and Megalin (70). AMN is a 38-50 kDa single-pass transmembrane protein that colocalizes with CUBN in enterocytes (71). AMN consists of an extracellular domain containing a cysteine-rich region of unknown function and a cytoplasmic tail that drives endocytosis (72). AMN is postulated to interact with the EGF region of CUBN (71). Though the efficiency of AMN-driven CUBN endocytosis is not clearly established, AMN is necessary for plasma membrane trafficking/anchoring of CUBN in the intestine and kidney (69, 73).

1.3.3 Megalin

Megalin, or LRP2, is a heavily glycosylated protein of molecular mass 600 kDa that is structurally similar to endocytic receptors of the low-density lipoprotein (LDL) receptor family (71). Megalin has three distinct domains: a large extracellular domain, a single transmembrane domain and a short cytoplasmic tail that regulates receptor trafficking and endocytosis (Fig. 1.1B). The extracellular domain is composed of four clusters of ligand-binding, cysteine-rich complement type repeats. These clusters are separated by EGF repeats and spacer regions that are involved in the pH-dependent release of ligands in endosomal compartments and receptor recycling. Internalization by LRP2 is dependent on CUB domains 12-17 and 22-27 of CUBN which encode LRP2 binding sites; an interaction that is essential for CUBN and CUBN-ligand internalization in the kidney (74). Mutations in the gene encoding megalin (*LRP2*) cause

Donnai-Barrow syndrome, characterized by unusual facial features, hearing loss, and vision problems (75). However, patients do not suffer from Cbl deficiency suggesting that LRP2 may not be an absolute requirement for IF-Cbl-CUBN endocytosis (71). Megalin has, however, been implicated in mediating the renal reabsorption of Cbl in mice (76).

1.3.4 Intrinsic factor deficiency and Imerslund-Gräsbeck syndrome

Mutations in GIF, CUBN, and AMN all cause impaired Cbl absorption resulting in clinical deficiencies. Hereditary IF deficiency results from recessive mutations in GIF (77); a total of 18 splice site, missense, intronic, insertion-deletion and partial gene deletion mutations have been identified totaling under 100 cases (71). Imerslund-Gräsbeck syndrome is a rare (~ 400 cases) recessive inherited disorder caused by mutations in CUBN or AMN. These mutations alter the IF-Cbl binding site on CUBN or interfere with plasma membrane expression of CUBN in the ileum and renal proximal convoluted tubule epithelium (78, 79). Patients with hereditary IF deficiency or Imerslund-Gräsbeck syndrome typically present between 1-5 years of age and suffer from megaloblastic anemia and developmental delay (60). Serum Cbl levels are decreased and patients often suffer from methylmalonic acidemia/aciduria and hyperhomocysteinemia/homocystinuria. The Schilling test (section 1.1.4) is abnormal for both these disorders and uptake is corrected by exogenous IF only for patients with hereditary IF deficiency. Unlike pernicious anemia, patients with hereditary IF deficiency do not produce auto-antibodies against gastric parietal cells. Rather, mutations in GIF abrogate production of IF in gastric secretions or result in increased susceptibility to proteolysis and/or poor affinity for Cbl or CUBN (80, 81). Since the Schilling test is no longer widely used, differentiation between hereditary IF deficiency and Imerslund-Gräsbeck has become increasingly difficult, with genetic testing providing the most conclusive diagnosis (60, 71). Treatment of these disorders involves

bypassing the intestinal uptake of Cbl through intramuscular administration of OHCbl or CNCbl, with 1 mg being administered daily until sufficient stores of Cbl are replenished. Patients with Imerslund-Gräsbeck syndrome may also display a non-progressing proteinuria which reflects the role of cubam in the reabsorption of filtered proteins from the kidney; an outcome not corrected by administration of Cbl (82).

1.3.5 Internalization of cobalamin by enterocytes

Internalization of IF-Cbl-CUBN-AMN and progression into an early endosomal compartment results in dissociation of IF-Cbl from CUBN (Fig. 1.1B). Subsequent fusion with a lysosome causes the degradation of IF and release of free Cbl. It is not currently known how Cbl is transported across the lysosomal membrane but two putative transporters, LMBD1 and ABCD4, have been implicated (see sections 1.6.3.0 and 1.6.3.1). Patients with mutations in the gene encoding LMBD1 have an abnormal Schilling test, indicating its involvement in Cbl absorption in enterocytes (83). Cbl exit from enterocytes is also not well defined as egress of free Cbl into the portal circulation can occur through passive or facilitated diffusion. The ATPbinding cassette (ABC) drug transporter ABCC1, also known as the Multidrug resistance protein 1 (MRP1) was recently identified as a basolateral efflux pump of free Cbl (84). MRP1 is a 190 kDa member of the ABC transporter gene family that is expressed in various cell types. Mice lacking MRP1 have reduced levels of Cbl in plasma, liver, and kidney but increased levels in the ileum implying its role in Cbl efflux from enterocytes. Based on genetic analyses mutations in human MRP1 do not cause Cbl deficiency, proposing the existence of multiple Cbl exporters of redundant activity. It has also been proposed TC with bound Cbl (TC-Cbl) can directly exit the enterocyte (85). Additional studies are necessary to reveal how Cbl exits the cell; within the TC-Cbl complex, as free, or both.

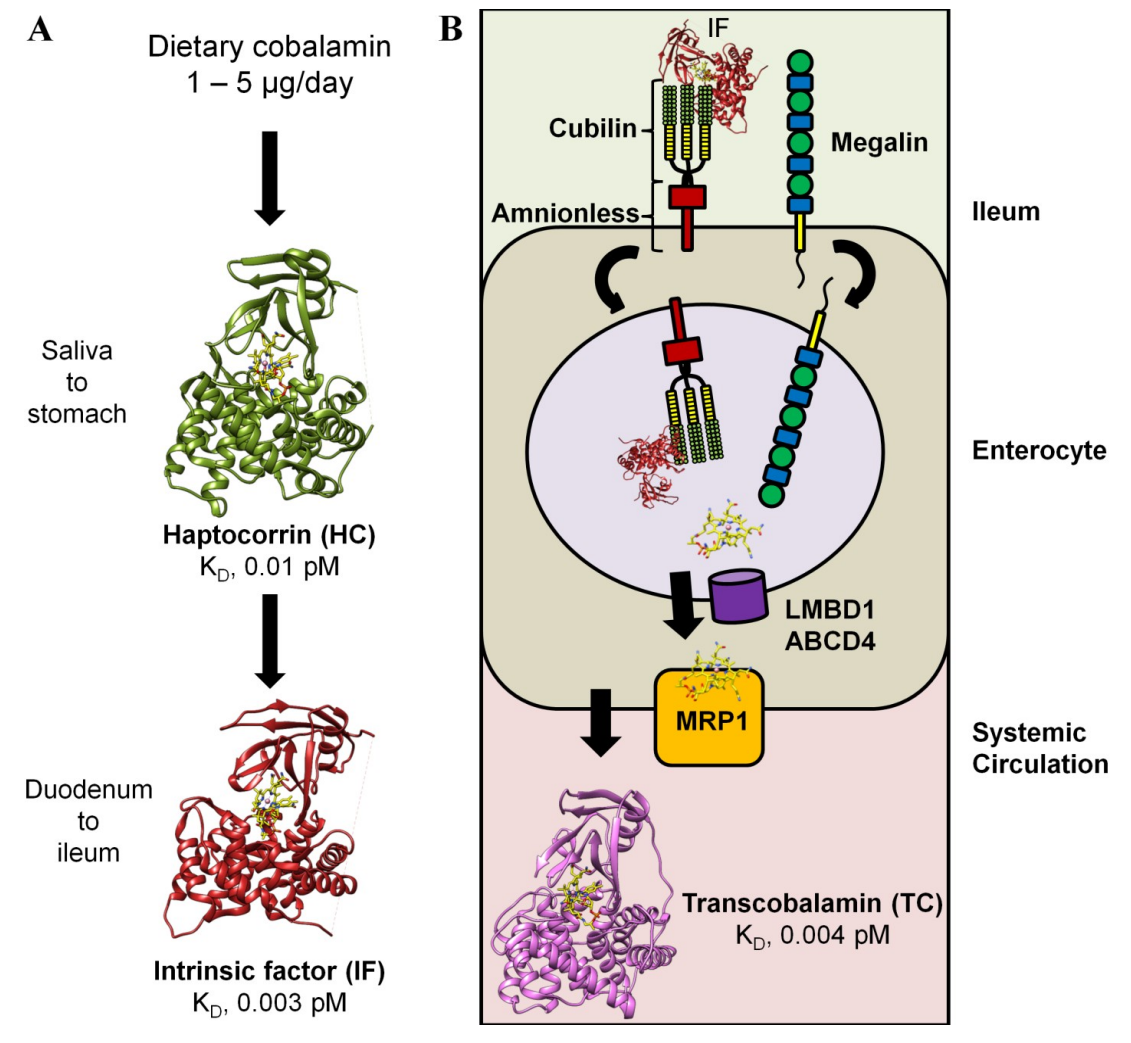


Figure 1.1. Absorption and systemic distribution of dietary cobalamin. A. Haptocorrin (HC, green) is secreted in the saliva and binds free cobalamin in the stomach. Proteolytic degradation in the duodenum results in Cbl release followed by sequestration by intrinsic factor (IF, red). IF-Cbl is internalized by enterocytes in the distal ileum. **B.** Internalization of IF-Cbl occurs through the cubam receptor composed of cubilin and amnionless; an additional membrane protein, megalin, may also be involved. Cobalamin is released from IF in the lysosome and is exported to the cytoplasm, probably through ABCD4 and/or LMBD1. Cobalamin enters systemic circulation through passive or active transport (MRP1) where it uses transcobalamin (TC, pink) as carrier protein.

1.3.6 Transcobalamin

Transcobalamin (TC-II, or TC) carries 10-30% of total serum Cbl and predominates in its apo form (apo-TC). TC binds and transports newly absorbed Cbl in the distal ileum to tissue cells throughout the body where it undergoes internalization through receptor-mediated

endocytosis (86). TC is ubiquitously expressed by all cells, with endothelial cells producing the majority of TC found in circulation (87). TC-Cbl, or holo-TC, has a short half-life of 1-2 h requiring rapid internalization by tissue cells. Encoded by TCN2, TC is a secreted and nonglycosylated protein of 409 aa (45.5 kDa). Based on gene organization and sequence homology the Cbl-binding proteins HC, IF, and TC are thought to have arisen from a common ancestral gene (88). TC demonstrates higher specificity towards Cbl than HC with amide side chains of the corrin ring mediating binding (89). Modifications to the central cobalt or ribose moiety of the nucleotide base have little effect on TC binding (89). X-ray structures of bovine and human holo-TC are currently available (90). Similar to IF and HC, the Cbl binding pocket resides between a α -domain consisting of a α 6- α 6 barrel and a β -domain formed from β -strands (Fig. 1.1B). Based on the structure of TC in addition to epitope mapping studies (91) two stretches of residues (103-159 and 207-227) within the α -domain are involved in binding the transcobalamin receptor, TCblR (92).

TC deficiency arises from mutations in the *TCN2* gene and over 40 patients have been identified. Most mutations correspond to deletions or insertions that result in protein truncation (60), though nonsense mutations (93), errors in RNA editing of the primary transcript (94), and splice site mutations (95) have also been described. Patients typically present within the first months of life with symptoms that include failure to thrive and weakness with megaloblastic anemia (96). Immunologic deficiencies and neurological problems can develop if the condition is left untreated (60). Serum Cbl levels are in the reference range or slightly reduced since TC only binds a small fraction of circulating Cbl (10-30%). TC deficiency has sometimes been misdiagnosed as leukemia due to the presence of immature white cell precursors in otherwise hypocellular bone marrow (97, 98). To date, most patients have an absence of immunologically

detectable TC (96) with others having a physiologically inactive form (99, 100). Treatment of TC deficiency is consistent with other Cbl deficiencies and consists of oral or intramuscular administration of OHCbl or CNCbl to maintain high serum Cbl concentrations (1-10 ng/ml).

1.3.7 Transcobalamin receptor

Early studies recognized that a serum component, later identified as TC, was required for cellular uptake of physiological concentrations of Cbl (66). Holo-TC in serum bound to cell surfaces and underwent internalization, a process dependent on the presence of Ca²⁺ and metabolic energy (101). Through affinity chromatography, Quadros et al. purified a receptor for TC based on its ability to retain TC throughout the purification procedure (102). This receptor had an electrophoretic mobility of 55 kDa and corresponded to the gene product of CD320 (102). The transcobalamin receptor, TCblR, is a 282 aa protein that belongs to the LDL receptor (LDLR) family and contains a large extracellular domain (198 aa), a short transmembrane helix (21 aa) and a short cytoplasmic tail (32 aa). TCblR interacts with TC solely through its extracellular domain; production of recombinant TCblR lacking the cytoplasmic and transmembrane domains maintained affinity towards TC (102). The extracellular domain of TCblR contains two LDLR type A domains linked by a 55 aa cysteine-rich CUB-like domain. The LDLR type A domains contain acidic residues that coordinate Ca²⁺ binding and are critical for binding TC (103). The cytoplasmic domain contains motifs crucial for TC-Cbl internalization (103).

TCblR expression on the cell surface is low and is regulated based on proliferative and differentiation status; maximum expression is seen in actively dividing cells whereas downregulation is observed in quiescent cells (104-106). This cell cycle regulation of TCblR expression may be physiologically relevant as increased levels of Cbl are required during DNA

synthesis (66). Early cell culture studies demonstrated TC-Cbl internalization through receptor-mediated endocytosis and recycling back to the plasma membrane, similar to the transferrin receptor (107).

TCblR deficiency has been detected in seven patients with elevated serum methylmalonic acid and in most cases hyperhomocysteinemia. Five of these patients had a homozygous deletion of three nucleotides resulting in a loss of a critical glutamic acid residue involved in coordinating Ca²⁺ within the LDLR type A domain (108). Patient fibroblasts demonstrate decreased uptake of TC-Cbl (50% of wild-type), with insertion of the missing codon restoring TCblR function. The 3-base pair deletion has a frequency of 4% in an Irish population (109). Studies performed on *CD320*-knockout mice have indicated that elimination of TCblR is nonlethal and does not result in systemic Cbl deficiency suggesting alternative mechanisms for Cbl internalization in mice (110). Despite this, severe Cbl depletion was observed in the central nervous system (CNS) suggesting that TCblR is the main receptor for Cbl uptake in the CNS (110). Patients undergoing Cbl supplementation remain asymptomatic and it is not clear if TCblR disorders have a distinct clinical phenotype.

1.4 Cobalamin and the diet

1.4.0 Food sources

Cbl is found predominantly in foods of animal origin. Meats including liver (26-58 μ g/100 g), beef (1-3 μ g/100 g), chicken (trace – 1 μ g/100 g), eggs (1-2.5 μ g/100 g) and dairy products (0.3-2.4 μ g/100 g) represent excellent sources of Cbl (111). Shellfish (0-10 μ g/100 g) and common fish (3.0-8.9 μ g/100 g) also represent significant sources (112). Due to the thermolability of Cbl, it is estimated that ~33% of Cbl is rendered inactive during the cooking process (113, 114). Plants do not produce nor require Cbl, but fertilization of crops with cow

manure can give plants Cbl content (115). These crops, in addition to Cbl-fortified cereals, represent a viable alternative for elderly patients or vegans that are at risk for Cbl deficiency. Edible seaweed and algae are also sources of Cbl; these include dried green (*Enteromorpha* sp.) and purple (*Porphyra* sp.) algae (32-78 µg/100 g). These Japanese seaweeds have been reported to prevent Cbl deficiencies in vegans (116, 117), but Cbl bioavailability from these sources remains questionable (118). Certain cyanobacteria, such as *Spirulina* sp., are sold in health food stores as Cbl supplements. However, studies have shown that cobamides, which have low affinity for IF and are not absorbed in mammalian intestines (53, 119), dominate these supplements (>80%) (120).

The bioavailability of Cbl depends on the absorption capacity of the gastrointestinal tract, for which there have been limited studies (111). Major factors affecting Cbl absorption include the quantity and nature of meal consumed. For instance, Cbl from chicken (61-66%) (121) and mutton (56-89%) (122) is readily absorbed compared to Cbl from eggs (<9%) (123). Further, the amount of absorbed Cbl increases with intake, but the rate of absorption decreases with intake. A study by Adams *et al.* (124) reported an absorption level of 50% when subjects were given 1 μ g of vitamin B₁₂, but absorption decreased to 20% and 5% when subjects were given 5 μ g and 25 μ g doses, respectively. Large doses of CNCbl (>1 mg), commonly used in supplements to treat Cbl deficiency, are poorly absorbed (~1 %) through an IF-independent mass action process. This allows patients with pernicious anemia to be effectively treated by Cbl supplementation (125).

1.4.1 Recommended Dietary Allowance

The Recommended Dietary Allowance (RDA) for vitamin B_{12} is set to prevent megaloblastic anemia and neuropathy by maintaining adequate serum concentrations (126). The

RDA for healthy adults is currently set at 2.4 μ g/day, and the median daily intake of young men and women from the United States and Canada reaches 3-7 μ g/day (126). The Dietary Reference Intakes guide assumes that 50% of dietary Cbl is absorbed by healthy adults, despite limited data on the bioavailability of vitamin B₁₂ from foods (126). It is estimated that the body excretes 2-5 μ g of Cbl a day (126). The US Institute of Medicine recommends that adults 51 years and older consume non-protein bound Cbl through intake of fortified foods such as cereals or from supplements (126). This is because elderly adults commonly suffer from atrophic gastritis which results in decreased stomach acid secretion. Atrophic gastritis causes malabsorption of protein-bound Cbl due to the inability to free up Cbl for transport by HC and IF (127). Vegans have a greater risk of developing Cbl deficiencies compared to meat eaters and should supplement their diet with Cbl-fortified foods (128).

1.4.2 Deficiencies

1.4.2.0 *Markers*

Cbl status in patients has historically been assessed by serum concentrations. The lower limit of serum Cbl is 120-180 pmol/L for adults but varies depending on testing methods. During the development of deficiency serum Cbl levels may be maintained at the expense of stored or tissue Cbl. A measured Cbl value above the cutoff point therefore may not reflect adequate Cbl status but a value below the cutoff point does define deficiency. Intermediate serum Cbl concentrations are more difficult to interpret (57).

Methylmalonic acid (MMA) and homocysteine (Hcy) are also indicators of Cbl status. Hcy and the coenzyme A (CoA) form of MMA are used by the Cbl-dependent enzymes MS and MCM, respectively. Levels of Hcy are affected in folate and vitamin B₆ deficiencies, and Hcy is therefore a less specific marker for Cbl deficiencies. Other factors, including renal impairment, medications, or mutations in the methylenetetrahydrofolate reductase (MTHFR) gene may also affect Hcy levels. MMA is a specific indicator for Cbl deficiency and serum MMA is the preferred marker of Cbl status with an expected range of 72 and 271 nmol/L for healthy individuals (126). Concentrations of propionate, the metabolic precursor to MMA, or its derivative 2-methylcitrate, can also rise in serum or cerebrospinal fluid during Cbl deficiency (129). However, the measurement of propionate or 2-methylcitrate offers no advantages over MMA for identification of Cbl deficiencies (126).

Because TC binds ~ 20% of serum Cbl, TC-Cbl (holo-TC) may provide an indication of Cbl status, though reports have demonstrated similar specificity and sensitivity as serum Cbl concentrations (130). When serum Cbl and TC-Cbl levels are determined in combination the accuracy for detecting Cbl deficiencies is significantly improved (130). Other combinations include measuring serum Cbl followed by MMA, which has been recommended as the appropriate strategy for assessment of Cbl status (131, 132). A composite criteria based on serum Cbl levels < 148 pmol/L, or 148-258 pmol/L and MMA > 0.30 μ mol/L, or Hcy > 13 nmol/L (females) and >15 nmol/L (males) has been recommended for defining inadequate Cbl status (133).

1.4.2.1 Symptoms

Anemia is the major clinical finding in severe Cbl deficiency. Hematological effects are identical to folate deficiency and include pallor of the skin with gradual onset of symptoms common in anemia, which include diminished energy, fatigue, shortness of breath, and palpitations. The underlying cause of anemia stems from interference with DNA synthesis resulting in erythrocyte enlargement (macrocytosis). Once anemia is established, a decrease in neutrophil (neutropenia) and platelet (thrombocytopenia) counts are observed due to impairment

of cell division. Hematological symptoms can be reversed through administration of folate or through injections or large oral doses of vitamin B_{12} .

Between 75 to 90% of patients with clinically observable Cbl deficiency also suffer from neurological complications and for some may be the only clinical finding. Reports have suggested that patients who are less anemic show more prominent neurological symptoms compared to patients that are more anemic (134, 135). Neurological manifestations include tingling and numbness in extremities, especially the lower limbs. Vibratory and position sense are also affected, as are motor disturbances including abnormalities of gait. Cognitive changes include loss of concentration to memory loss, disorientation, and dementia. The development of visual disturbances, insomnia, impotency, and impaired bowel and bladder control has also been reported (126). Subacute combined degeneration of the spinal cord, resulting from losses of myelin in the dorsal and lateral columns, is also associated with Cbl deficiency and results in weakness, tingling, and numbness in addition to changes in vision and mental state (136). Left untreated, many of these neurological issues are irreversible.

1.4.2.2 Causes

Cbl is continually secreted in bile and undergoes reabsorption through enterohepatic circulation. In healthy individuals the majority of Cbl is reabsorbed with some Cbl excreted in the stool; failure to produce IF increases Cbl losses. The total amount of Cbl stored in the body is estimated at 2 – 5 mg in healthy adults, with the liver accounting for over 50% of Cbl content (126). During deficiency, stores of Cbl deplete over a period of several years. The general causes for Cbl deficiency include malabsorption and dietary inadequacies, specifically in vegans and the elderly. Other causes such as atrophic gastritis, inadequate IF production, and reduced ileal uptake of Cbl due to disease, resection, bacterial interference or drug-nutrient interactions

can also contribute (126). Furthermore, rare but significant genetic defects can result in impaired absorption, cellular uptake, or intracellular processing (*section 1.6*).

Over 6% of the Western population over 60 years of age have low plasma Cbl levels, with as much as 20% having marginal status (137). Protein-bound malabsorption associated with atrophic gastritis is the most common cause of Cbl deficiency in the elderly (126). Atrophic gastritis results from inflammation of the gastric mucosa, which leads to a reduction or loss of gastric acid, plus a reduction in IF production. Administration of exogenous, nonprotein-bound Cbl is a viable treatment (126). Cbl deficiency has also been reported in patients having undergone ileal resection, a common treatment for Crohn's disease. This involves removal of part of the terminal ileum necessary for Cbl absorption by IF and the cubam receptor. Similarly, patients with bacterial overgrowth or parasitic infections can suffer from Cbl deficiency due to reduced ileal uptake caused by competition with these microorganisms (126).

Medications can also interfere with Cbl absorption. Commonly used in the elderly to treat gastroesophageal reflux disease, proton pump inhibitors cause a reduction in the secretion of gastric acid and pepsin. This effectively prevents release and absorption of food-bound Cbl, though a consensus on the effect of these medications on Cbl deficiency has yet to be reached (138-140). Patients taking metformin, used in the treatment of non-insulin dependent diabetes, have reported developing megaloblastic anemia (141, 142). A recent rat study demonstrated a reduction in Cbl serum levels with accumulation in the liver, suggesting that metformin alters overall tissue distribution but may not reflect impaired Cbl status (143). The anesthetic nitrous oxide (N₂O) inactivates MeCbl-bound methionine synthase (MS) that can result in severe irreversible neurological damage (144).

1.4.3 Fortification

Safety concerns over the effects of folate supplementation masking Cbl deficiency have been debated. Folate, obtained through supplements or fortified foods, corrects the hematological but not the neurological conditions associated with Cbl deficiency. Between 20 and 30% of Cbl-deficient patients have neurological problems without anemia (57), leading to the proposal of fortifying foods, including flour or milk, with vitamin B₁₂. Those with poor dietary intake of Cbl such as vegans as well as the elderly may benefit from such fortification.

1.4.4 Cobalamin status and health

1.4.4.0 Neural tube defects

Neural tube defects (NTD) are caused by failure of the neural tube to close during gestation. Risk factors for NTD include folate deficiency in addition to genetic and environmental factors (145, 146). Since the introduction of folate fortification of the Canadian food supply in 1998, the incidence of NTD has decreased over 50% (147). Because the Cbl-dependent enzyme MS directly influences intracellular levels of folate, low Cbl status is a risk factor for NTD. As deficiency develops, the impaired MS reaction results in the trapping of folate as methyl-THF which ultimately prevents DNA synthesis and cell division. Studies have reported a 2-4 fold increase in the risk of NTD in patients with low Cbl status (146, 148, 149).

1.4.4.1 Cardiovascular disease

Elevated levels of serum Hcy may represent a risk factor or marker of cardiovascular disease progression. Several meta-analyses have associated Hcy with an increased risk of cardiovascular disease (150, 151). In a recent study, Cbl supplementation resulted in a ~7% reduction in Hcy levels in serum whereas folate supplementation resulted in a 10-30% reduction (152). Patients taking high doses of Cbl had a 21% reduction in risk of coronary events

compared to patients on lower doses (153). For patients with adequate folate status, Cbl is the major determinant of serum Hcy concentrations (154). Recent meta-analyses have indicated that B vitamin supplementation reduces overall plasma Hcy but does not alter the risk of cardiovascular disease (155, 156).

1.4.4.2 Cognitive status

The effects of subclinical Cbl deficiency on cognitive status are not fully understood. While the assessment of Cbl status forms part of the screening process for dementia, studies investigating cognitive decline caused by Cbl status have been inconclusive (157). Elevated levels of MMA are associated with cognitive decline and Alzheimer disease (158). In elderly subjects, the rate of cognitive decline correlates with the level of holo-TC, MMA, and the ratio of holo-TC to serum Cbl (159, 160). High serum folate is associated with cognitive impairment in Cbl deficient patients, whereas high serum folate is protective in subjects with normal Cbl levels (161). Few studies have examined the direct relationship between Cbl and cognitive function in the elderly, with one review recognizing that cognitive score is not altered with Cbl supplementation (162). Another review identified a correlation between Hcy and Alzheimer disease but suggested this was due to diminished levels of vitamins B₁₂, B₆, and folate (163). Randomized control trials performed on elderly subjects treated with these B vitamins demonstrated a slower rate of brain atrophy, which could delay the onset of Alzheimer disease (164, 165). Cerebral atrophy in areas of the brain vulnerable to Alzheimer disease was also reduced in these subjects and was the result of lowered Hcy levels achieved through B vitamin supplementation (166).

1.4.4.3 Bone health, age-related macular degeneration, and frailty

There has been recent interest in determining if Cbl levels contribute to bone health. Hey levels may contribute to low bone mineral density resulting in an increased risk of fractures (167). Several studies have been performed on Cbl status and the risk of osteoporosis but results have been mixed (111). B vitamin supplementation had a positive effect on bone mineral density in a subgroup of osteoporotic patients with high levels of Hey (168) and stroke patients at risk for osteoporosis (169), but no effect was observed in a group of healthy older patients (170).

Cbl status has also been associated with development of age-related macular degeneration (AMD) and frailty, both major causes of disability in the elderly. AMD is the leading cause of vision loss in this population, with several studies demonstrating lower Cbl levels in patients with AMD (171, 172). A recent study analyzing a 10-year cohort indicated that Cbl deficiency in addition to elevated levels of Hcy and folate increased the risk of AMD in patients (173). These results complement a randomized control trial which demonstrated a significant reduction (34%) in AMD in a population at risk for vascular disease after supplementation with vitamins B_6 and B_{12} , and folate (174).

Frailty is characterized by muscle wasting and diminished strength and is associated with an increased vulnerability to stresses. This often causes longer and more complicated recoveries from illness or surgery (175). An increase in the risk of frailty has been associated with poor vitamin B status and elevated levels of MMA and Hcy (176, 177). Another study has associated the length of hospital stay to Cbl status, with increased lengths of stay for elderly patients with Cbl deficiencies (178).

1.5 Cobalamin and bacteria

1.5.0 Producing microorganisms

Vitamin B₁₂ is only synthesized by certain species of bacteria and archaea, whereas animals and protists require the cofactor but do not synthesize it (179). More than 30 genes are required for the *de novo* biosynthesis of cobalamin, corresponding to almost 1% of a typical bacterial genome (180). The following genera have been shown to produce vitamin B_{12} : Acetobacterium, Aerobacter, Agrobacterium, Alcaligenes, Azotobacter, Bacillus, Clostridium, Corynebacterium, Flavobacterium, Lactobacillus, Micromonospora, Mycobacterium, Norcardia, Propionibacterium, Protaminobacter, Proteus, Pseudomonas, Rhizobium, Salmonella, Serratia, Stretomyces, Streptococcus, and Xanthomonas (181). Two biosynthetic routes have been studied: an aerobic or oxygen-dependent pathway found in organisms like *Pseudomonas* denitrificans, and an anaerobic or oxygen-independent pathway found in organisms like Bacillus megaterium, Propionibacterium shermanii and Salmonella typhimurium. Genes involved in the aerobic pathway have the prefix "cob" for cobalamin biosynthesis whereas genes involved in the anaerobic pathway have the prefix "cbi" for cobinamide biosynthesis. The major differences in these pathways relate primarily to the requirement of molecular oxygen and the timing of cobalt insertion.

1.5.1 Biosynthesis

Elucidation of the aerobic cobalamin biosynthetic pathway in *P. denitrificans* was first described in 1993 after a 25-year collaborative effort between the groups of Blanche, Battersby and Scott in Texas (182-185). The aerobic *cob* genes were identified and isolated from an industrial strain of *P. denitrificans* SC510 (186-188). Most genes associated with the anaerobic pathway have significant homology (20-40% sequence identity) to genes in the aerobic pathway

(189). The *de novo* production of Cbl is one of the most complex pathways in nature, and can be classified into three distinct processes: (1) biosynthesis of precorrin-2; (2) conversion of precorrin-2 to adenosylcobyric acid; (3) attachment of the lower nucleotide loop to generate adenosylcobalamin. An overview of the biosynthetic pathway is described below.

1.5.1.0 Production of precorrin-2

The first step in Cbl biosynthesis is production of 5-aminolevulinic acid (ALA), the first general precursor to all known tetrapyrroles and the first committed intermediate (190, 191).

ALA is most commonly synthesized from the intact carbon skeleton of glutamic acid via the C-5 pathway (Fig 1.2). This involves the charging of tRNA with glutamate by glutamyl-tRNA synthetase (GluRS) in a step identical to protein synthesis and requiring ATP, glutamate, and tRNA. The product of this reaction, glutamyl-tRNA, is converted to glutamate-1-semialdehyde via NADPH-dependent glutamyl-tRNA reductase (GluTR) (192) which is followed by a transamination reaction catalyzed by glutamate-1-semialdehyde aminotransferase (GSA-AT) that generates ALA.

ALA is converted into uroporphyrinogen III by three enzymes: ALA dehydratase (ALAD), porphobilinogen deaminase (PBGD), and uroporphyrinogen III synthase (UROS). ALAD catalyzes a condensation reaction between two molecules of ALA to generate porphobilinogen (PBG), a pyrrolic building block. This reaction is metal-dependent, requiring magnesium for *P. aeruginosa* (193) and *B. japonicum* (194), and both zinc and magnesium for *E. coli* (195). Four molecules of PBG are then polymerized into a linear tetrapyrrole in a reaction catalyzed by PBGD (196) and requiring a unique dipyrromethane cofactor derived from PBG (197). The tetrapyrrole product is produced in an ordered fashion by initial attachment of the first PBG molecule to the cofactor, followed by sequential attachment of the remaining PBG

units to the growing chain. The link between cofactor and the first pyrrole ring of the product is severed to yield preuroporphyrinogen and reactivated enzyme. The last pyrrole unit of preuroporphyrinogen is inverted and linked to the first unit via UROS generating the large macrocyclic structure of uroporphyrinogen III. Uroporphyrinogen III can enter the heme and chlorophyll biosynthetic pathway by side chain decarboxylation to corproporphyrinogen.

Figure 1.2. C-5 pathway of precorrin-2 biosynthesis. Glutamyl-tRNA synthetase (GluRS) catalyzes formation of glutamyl-tRNA from tRNA, glutamate, and ATP. Glu-tRNA is converted to 5-aminolevulinic acid (ALA) by glutamyl-tRNA reductase (GluTR) and glutamate-1-semialdehyde aminotransferase (GSA-AT). ALA dehydratase condenses two ALA molecules to form porphobilinogen (PBG). Four PBG molecules are linked by PBG deaminase (PGBD) and uroporphyrinogen III synthase (UROS) to generate the macrocyclic structure of uroporphyrinogen III. This product is methylated by S-adenosyl-L-methionine-dependent uroporphyrinogen III methyltransferase (SUMT) to form precorrin-2, the common precursor to the aerobic and anaerobic cobalamin biosynthetic pathways.

For biosynthesis of Cbl, uroporphyrinogen III is converted to precorrin-2 by the enzyme uroporphyrinogen III methyltransferase (SUMT), encoded by *cobA* in aerobes and *cysG* in anaerobes (198, 199). SUMT uses S-adenosyl-L-methionine (SAM) as methyl donor to methylate uroporphyrinogen III at C2 and C7. For reference, the number associated with

precorrin represents the number of methyl groups which have been added to the tetrapyrrole framework (196). Precorrin-2 is the last common intermediate between the aerobic and anaerobic pathways before the synthesis of adenosylcobyric acid.

1.5.1.1 Conversion to adenosylcobyric acid

In the aerobic pathway (Fig. 1.3), precorrin-2 undergoes methylation at C20 by the SAMdependent methyltransferase CobI, producing precorrin-3A (200-202). The following ring contraction step is mediated by CobG and CobJ (182, 203). CobG acts as a monooxygenase and hydroxylates C20 of precorrin-3A to generate a γ-lactone with the acetate side chain of ring A, yielding precorrin-3B (204). Precorrin-3B undergoes ring contraction during C17 methylation by CobJ, resulting in precorrin-4 that contains a methylketone at C1 (182). Precorrin-4 undergoes additional methylation by CobM at C11 to yield precorrin-5 (205). In the next step, the acyl group at C1 is removed and replaced with a methyl group through the activity of CobF, which generates precorrin-6A (196). Precorrin-6A is reduced via the NADPH-dependent reductase CobK to yield precorrin-6B (206, 207). CobL decarboxylates the acetic acid side chain at C12 on ring C and methylates C5 and C15 to generate precorrin 8 (208). Precorrin-8 is converted into hydrogenobyrinic acid (HBA) by CobH, which catalyzes the migration of the C11 methyl group to C12 (209). HBA and cob(II)yrinic acid, the product of early anaerobic corrin synthesis, differ only in the coordination of cobalt which occurs much earlier in the anaerobic pathway.

CobB then amidates the acetate side chains on rings A and B of HBA using glutamine as donor to generate HBA a,c-diamide (210). HBA a,c-diamide is a substrate for the cobalt chelatase made of three subunits: CobN, CobS, and CobT (211). CobS and CobT form a chaperone-like ring complex characteristic of AAA(+) superfamily class of proteins and are

structurally similar to magnesium chelatase (212). Cobalt chelation requires ATP hydrolysis but the stoichiometry of ATP hydrolysis to cobalt insertion has yet to be determined (211). To give an idea of the energy requirement for this process, the magnesium chelatase utilizes ~ 15 ATP molecules per magnesium insertion event (213). CobS is the active ATPase in the complex (214). The resulting product of the CobNST-catalyzed reaction, cob(II)yrinic acid a,c-diamide, is reduced to the cob(I)yrinic acid a,c-diamide by the cobalt reductase CobR (214). The reduced cobalt is then adenosylated by CobO (215), after which the remaining side chains are amidated by CobQ which utilizes glutamine as substrate (216). The resulting product is adenosylcobyric acid.

In the anaerobic pathway (Fig. 1.3), precorrin-2 is oxidized to factor II by precorrin-2 dehydrogenase (SirC) which requires NAD⁺ as cofactor. The term "factor" is used to represent an oxidized version of the corresponding precorrin; factor II represents oxidized precorrin-2. Factor II is favoured over precorrin-2 for metal insertion early in the pathway because of its planar shape (189). CbiK or CbiX are the cobaltochelatases that insert cobalt into factor II to generate cobalt(II)-factor II. Both are homologous to a ferrochelatase involved in heme synthesis. Structures of CbiK and CbiX have recently been solved, allowing identification of critical tetrapyrrole and cobalt binding sites (217). The proposed mechanism for cobalt insertion involves manipulation of factor II by CbiK/CbiX such that the ring structure is placed proximal to the cobalt-binding site, allowing efficient insertion of the metal. Cobalt(II)-factor II undergoes methylation at C20 by the SAM-dependent methylase CbiL to produce cobalt(II)-factor III.

Ring contraction is the next step and this event is catalyzed by the SAM-dependent enzyme CbiH. CbiH methylates cobalt(II)-factor III at C17 and removes a methyl group at C20,

which results in the formation of a δ-lactone ring. The product of this reaction, cobalt-precorrin-4, is extremely unstable and rapidly oxidizes to cobalt-factor IV (218). Following this, CbiF methylates cobalt-precorrin-4 at C11 to produce cobalt-precorrin-5A (219). CbiG catalyzes the opening of the δ-lactone ring to produce cobalt-precorrin-5B (219, 220). In a recent landmark publication (221), a mixture of recombinant CbiH, CbiF, and CbiG resulted in synergistic production of cobalt-precorrin-5B from cobalt-factor III providing evidence for substrate channeling.

CbiD methylates cobalt-precorrin-5B at C1 to form cobalt-precorrin-6A based on genetic deletion studies and *in vitro* assays using recombinant CbiD (221, 222). CbiG and CbiD are unique to the anaerobic pathway (189), with CbiG having only weak similarity to an uncharacterized but essential CobE protein from the aerobic pathway (223). CbiJ, CbiE, CbiT, and CbiC then convert cobalt-precorrin-6A into cob(II)yrinic acid. CbiJ drives the production of cobalt-precorrin-6B from cobalt-precorrin-6A in an NADPH-dependent reduction of the C18/C19 double bond (221). CbiE and CbiT mediate cobalt-precorrin-8 synthesis from cobalt-precorrin-6B; CbiE methylates C5 and CbiT couples methylation of C15 to decarboxylation of an acetate side chain in ring C. Recombinant forms of CbiE and CbiT convert cobalt-precorrin-6B to a product consistent in mass with cobalt-precorrin-8 (221). Lastly, CbiC catalyzes the migration of a C11 methyl group to C12, generating cob(II)yrinic acid (221).

Cob(II)yrinic acid is amidated to cob(II)yrinic acid a,c-diamide by CbiA, which then undergoes reduction to accommodate adenosylation. An NADP⁺ flavodoxin reductase (Fdr) in conjunction with flavodoxin (FldA) may perform this reaction in *S. typhimurium* (224). The adenosyltransferase enzyme CobA (no similarity with the aerobic enzyme CobA) acts with FldA

and Fdr to produce adenosylcobyrinic acid a,c-diamide, which undergoes further amidation by CbiP at propionic acid side chains to generate adenosylcobyric acid.

1.5.1.2 Generation of adenosylcobalamin

The pathway to attach the lower nucleotide loop converges at adenosylcobyric acid in aerobes and anaerobes (Fig. 1.3). Adenosylcobinamide is generated from adenosylcobyric acid by attachment of 1-amino-2-propanol in a reaction that involves ATP/Mg²⁺, 1-amino-2-propanol, and two proteins (α and β). CobC and CobD are subunits for protein β , whereas the identity of protein α is unknown. Adenosyl-GDP-cobinamide is synthesized by the bifunctional proteins CobP (aerobic) or CobU (anaerobic) which function as kinases and nucleotidyl transferases (225, 226). In the kinase reaction CobP and CobU catalyze the ATP-dependent phosphorylation of adenosylcobinamide. The following nucleotidyl transferase reaction attaches a GMP to adenosylcobinamide phosphate forming adenosylcobinamide-GDP. The final step of cobalamin synthesis is catalyzed by the adenosylcobalamin synthases CobV (aerobes) or CobS (anaerobes). Here, the GMP moiety of adenosylcobinamide-GDP is substituted with an α -ribazole to generate adenosylcobalamin (227). α -ribazole is derived from α -ribazole phosphate, synthesized by CobU (aerobes) or CobT (anaerobes) from dimethylbenzimidazole (DMB) and nicotinic acid mononucleotide (227). α -ribazole phosphate is dephosphorylated by CobC to yield the α ribazole required by CobV/S. DMB in both aerobes and anaerobes is generated from its substrate flavin mononucleotide (228, 229). In an alternative pathway, CobV/S can use αribazole phosphate as substrate in a reaction that yields adenosylcobalamin-5'-phosphate (227). This product can undergo dephosphorylation by CobC to generate adenosylcobalamin (230).

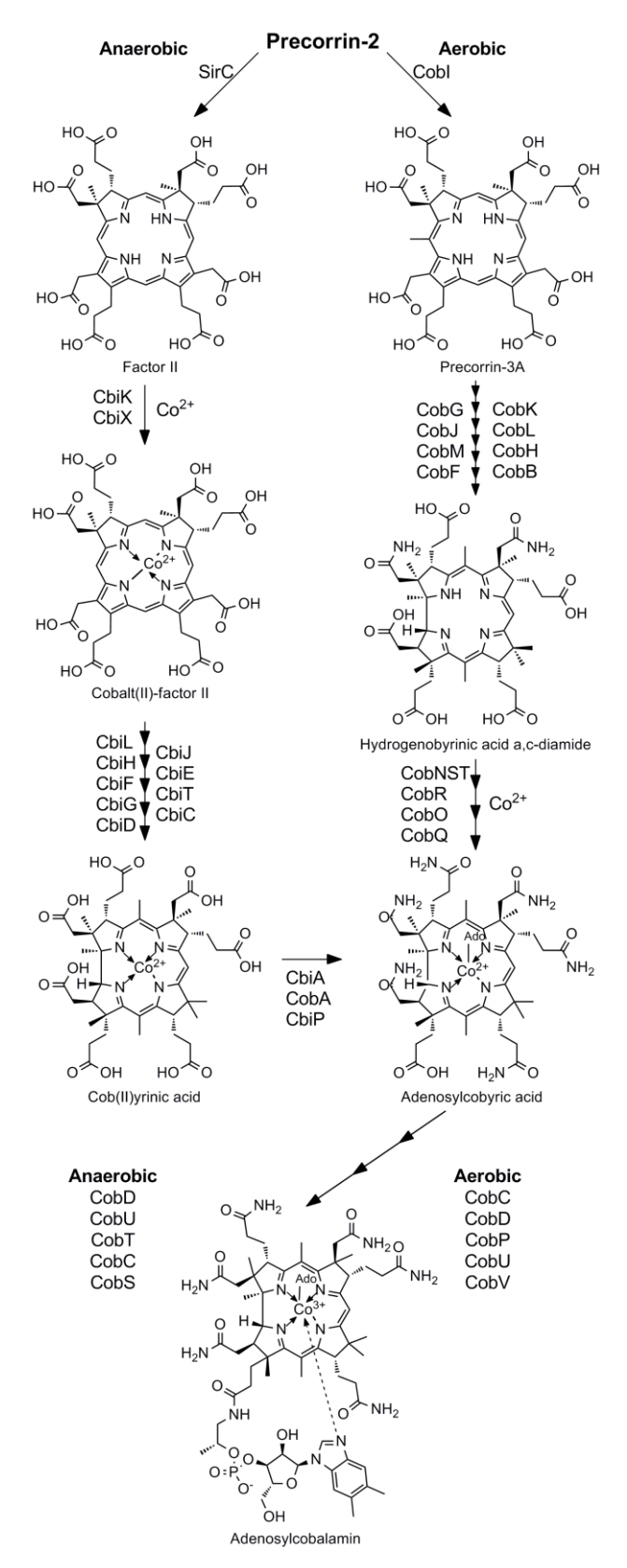


Figure 1.3. Biosynthesis of adenosylcobalamin from precorrin-2. Mechanistic details are described in sections *1.5.1.1* and *1.5.1.2*. Figure adapted from the pathway presented in (231).

1.5.2 Industrial production

Industrial production of Cbl relies exclusively on biosynthetic fermentation processes using genetically engineered bacteria from the *Propionibacterium* genus or *Pseudomonas denitrificans* (179). The *Propionibacterium* genus have the "Generally Regarded As Safe", or GRAS status, accorded by the US FDA, and *Propionibacterium shermanii* and *Propionibacterium freudenreichii* are most commonly used from this genus (179). Cbl production from microaerophilic *Propionibacterium* ranges from 60 – 200 mg of Cbl per L of fermented culture depending on the species and strain used (179). As described in the biosynthetic pathway (*section 1.5.1.2*), the substrate DMB is required for Cbl production. Since oxygen is necessary for DMB biosynthesis, production of Cbl in *Propionibacterium* is divided into stages. In the first 3 days of fermentation bacteria are grown anaerobically to produce the Cbl precursor, adenosylcobamide. Cbl biosynthesis is finalized by aeration of the culture for an additional 1-3 days which allows the DMB production and the generation of adenosylcobalamin.

P. denitrificans is almost exclusively used in industrial production of Cbl. Genetically engineered strains of P. denitrificans from Sanofi account for over 80% of the world production of Cbl, producing over 300 mg of Cbl per L of fermented culture (179). Amplification of cob genes through use of multicopy plasmids, manipulation of transcriptional or translational elements to increase Cob protein expression, heterologous protein expression, and supplementation of fermentation media with substrates such as DMB all contribute to the effective production of Cbl (179). Cultures of P. denitrificans are grown in oxygen-rich conditions during the entire fermentation process (2-3 days) (179). Harvested bacteria are then extensively heated to extract adenosylcobalamin. AdoCbl is converted to CNCbl by treatment of the heated cell suspension with cyanide or thiocyanate (179). After filtration, CNCbl is

precipitated using auxiliaries like tannic acid or cresol. CNCbl is further purified via extraction steps, chromatography, and crystallization using organic solvents to generate the necessary purity required for food and pharmaceutical applications (179).

1.5.3 Riboswitches

Riboswitches are RNA elements located at the 5' end of mRNAs that bind specific ligands such as vitamins, amino acids, or nucleotides (232). Riboswitches consist of an aptamer domain responsible for ligand binding and an expression platform that triggers the genetic response (232). Structural changes in the expression platform, induced by ligand binding at the aptamer domain, regulate the transcription or translation of downstream genes. Genes controlled by riboswitches are commonly involved in the uptake or metabolism of the corresponding ligand. The AdoCbl, or coenzyme B_{12} , riboswitch exists in most prokaryotic genomes and controls AdoCbl levels by regulating the expression of genes involved in Cbl import and synthesis (233). The vitamin B_{12} transporter of E. coli, BtuB, is regulated by the coenzyme B_{12} riboswitch; expression is repressed in Cbl-rich conditions (234). Likewise, mutant strains that are unable to synthesize AdoCbl constitutively express btuB mRNA (235). Mapping the 5' end of btuB mRNA revealed an untranslated leader sequence corresponding to the AdoCbl riboswitch (236). AdoCbl binds to the riboswitch and induces a structural rearrangement that inhibits translation by preventing ribosome binding (233). Studies by Gallo et al. (237, 238) have shown that the axial ligands and corrin ring of AdoCbl interact with the btuB aptamer. Affinity to the btuB riboswitch is mediated via the axial ligands, as AdoCbl demonstrates 1000-fold higher affinity than CNCbl or adenosylcobinamide. Despite this, elevated concentrations of either corrinoid can stimulate the riboswitch, indicating that the corrin ring is the minimal element required. The

amide group of side chain c, which points towards the upper axial side of the corrin ring, is critical to this interaction.

Molecular insights into Cbl riboswitches have been facilitated recently through the elucidation of their three-dimensional structure (239, 240). Unexpectedly, Cbl riboswitches isolated from certain marine bacteria had greater affinity towards MeCbl/OHCbl compared to AdoCbl (239). Cbl riboswitches are now subdivided into two classes: MeCbl/OHCbl-sensitive, and AdoCbl-sensitive. Both classes possess a core built around an evolutionary conserved four-way junction responsible for Cbl recognition. They also use a "kissing-loop" interaction between loop 5 (L5) of the aptamer domain and loop 13 (L13) of the expression platform; the latter contains a ribosome binding site that controls translation of genes involved in Cbl biosynthesis. Peripheral extensions of the aptamer domain define AdoCbl-sensitive riboswitches; these extensions are absent or condensed in the MeCbl/OHCbl class.

1.5.4 *Uptake*

The model system for bacterial uptake of Cbl is the TonB-dependent transport system of *E. coli* (Fig. 1.4). *E. coli*, like many bacteria, cannot fully synthesize Cbl *de novo*. Rather, Cbl and cobinamides (Cbi) are obtained from the environment to be converted into physiological MeCbl and AdoCbl (241). Due to the nature of the Gram-negative cell envelope, the outer membrane (OM) serves as a barrier to large nutrients (>600 Da). To circumvent this, TonB-dependent transporters (TBDTs) import large molecules, including iron chelating siderophores and Cbl, across the OM. In the absence of ATP-hydrolyzing proteins and a proton gradient, no source of energy exists at the OM (242). TBDTs bind substrate with high affinity and couple transport to an energy transduction complex embedded within the cytoplasmic membrane (CM). Energy for this process is derived from the chemiosmotic gradient maintained across the CM.

TonB, in complex with ExbB and ExbD, harnesses this potential by contacting and perturbing OM receptors which permits nutrient passage into the periplasm. Cbl transport in *E. coli* depends on the B-twelve-uptake (Btu) system, consisting of the TBDT BtuB, a periplasmic binding protein (PBP) BtuF, and an inner membrane ATP-binding cassette (ABC) transporter BtuC₂D₂ (243).

BtuB in the OM binds "base-on" Cbl with high affinity ($K_d \sim 0.3$ nM) in the presence of calcium and with 50-100 fold lower affinity in the absence of calcium (244). BtuB is composed of 22 anti-parallel β -strands that form a β -barrel. These β -strands are connected by 11 long loops of variable length (4-50 residues) at the extracellular interface and 10 short turns at the periplasmic side. A plug domain composed of roughly 150 N-terminal residues resides within the β -barrel. This plug, or cork, occludes the β -barrel and prevents nutrient passage in the absence of substrate. All TBDTs have an ordered conserved motif ("Ton-box") that is exposed to the periplasm upon substrate binding. Periplasmic accessibility of the Ton-box causes TonB recruitment. Deletion of the Ton-box abrogates transport but does not affect substrate binding (245).

Structures of BtuB in apo (246), holo (246) and TonB-bound (247) forms have been solved by X-ray crystallography. While structural details of Cbl and TonB-binding have been elucidated, the mechanism of Cbl passage through the β -barrel of BtuB remains poorly understood. It is unknown whether the plug domain is ejected from the β -barrel or whether it undergoes conformation rearrangements within the β -barrel to allow ligand passage. Simulations suggest that the force imparted by mechanical pulling of the Ton-box by TonB is substantial enough to unfold the plug domain leading to Cbl permeation (248).

Within the periplasm Cbl binds to the periplasmic binding protein BtuF. BtuF binds Cbl in the "base-on" form within a large cleft formed between two α/β sandwich domains linked by a α -helix (249). This high affinity interaction ($K_d \sim 15$ nM) (250) is mediated through hydrogen bonds between BtuF and the corrin ring side chains in addition to hydrophobic interactions between aromatic residues surrounding the lower axial DMB. BtuF and the siderophore-binding PBP FhuD demonstrate nanomolar affinity to TonB (251, 252). These PBP–TonB interactions are hypothesized to promote efficient unidirectional substrate transfer by coordinating the delivery of incoming cargo from TBDTs.

The next step involves delivery of Cbl by BtuF to the CM-embedded ABC transporter BtuC₂D₂. BtuC₂D₂ consists of two transmembrane subunits (BtuC) and two cytoplasmic ATP-hydrolyzing nucleotide binding domains (BtuD). Each BtuC subunit is composed of ten transmembrane α -helices and the interface between BtuC subunits forms a V-shaped cavity that is open to the periplasm but occluded to the cytoplasm (253). BtuD subunits are composed of conserved motifs responsible for binding and hydrolyzing ATP. These include Walker A and B motifs, signature and switch regions, and the Q-loop. The Walker A motif forms a loop that encloses the phosphate residues of ATP and ADP, and the signature/switch motifs act as a γ -phosphate sensor. Conserved residues from the Q-loop, Walker B motif, and switch region coordinate Mg²⁺ required for ATP hydrolysis. Apart from the signature sequence which is unique to the ABC transporter family, these motifs are conserved across numerous prokaryotic and eukaryotic ATP-hydrolyzing subunits (254). The ATP binding pocket is created at the homodimerization interface of BtuD from the Walker A motif of a BtuD subunit and the signature sequence of the partner BtuD subunit. Structures of BtuC₂D₂ alone without ATP (253),

BtuC₂D₂ complexed with apo-BtuF without ATP (255), and BtuC₂D₂ complexed with apo-BtuF and bound non-hydrolyzable ATP-analog AMP-PNP (256) have all been solved.

The proposed mechanism for Cbl transport across BtuC₂D₂ is based on the snapshots obtained of this transporter through structural studies (256). This first step involves docking of holo-BtuF to the outward-facing V-shaped transmembrane domains formed by BtuC subunits.

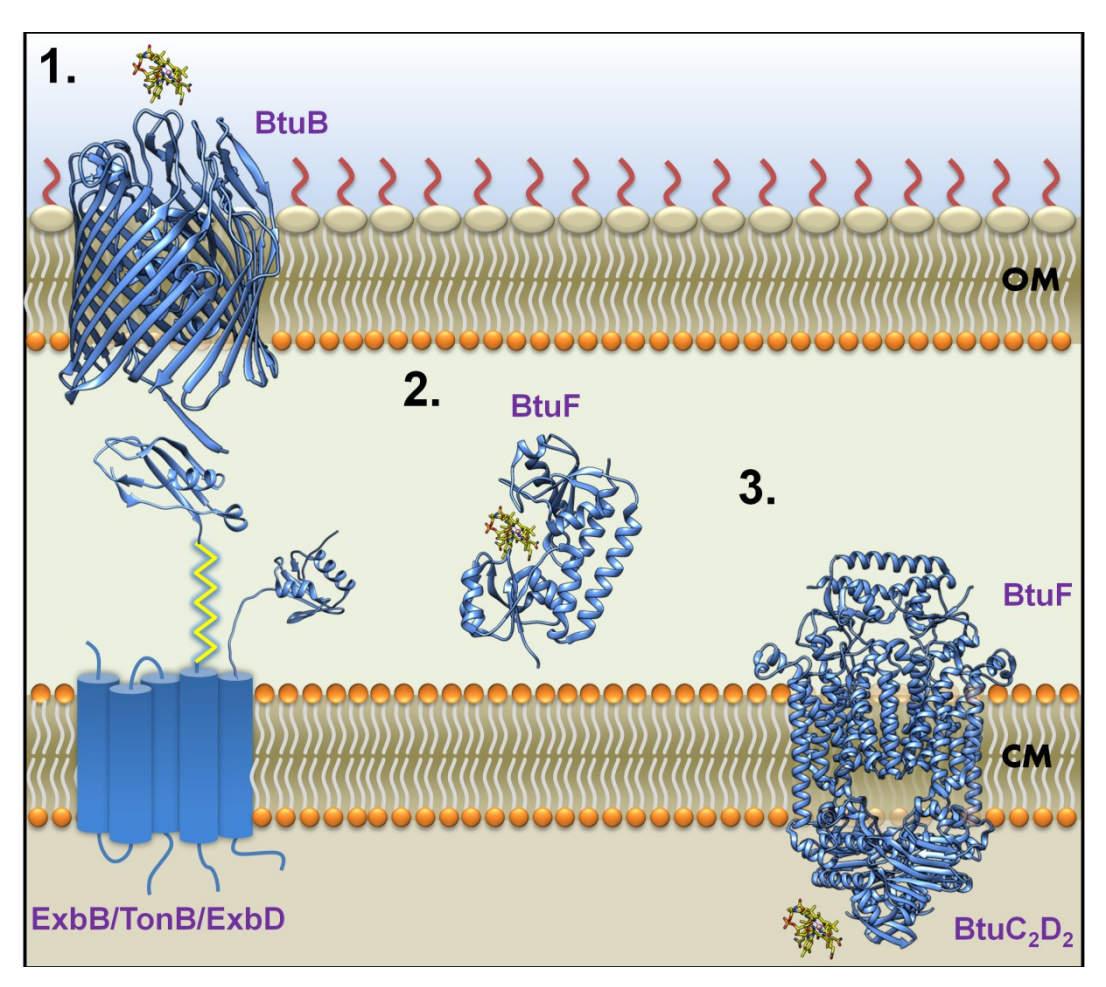


Figure 1.4. Vitamin B_{12} import by the B-twelve uptake (Btu) system of E. coli. 1. Binding of extracellular vitamin B_{12} to the outer membrane (OM) TonB-dependent transporter BtuB results in expulsion of the Ton box into the periplasm. TonB, in complex with ExbB and ExbD within the cytoplasmic membrane (CM), binds the Ton box and transduces energy derived from the proton motive force to transport vitamin B_{12} across the OM. 2. Vitamin B_{12} binds its cognate periplasmic binding protein BtuF; BtuF delivers its cargo to the ATP-binding cassette transporter BtuC₂D₂. 3. BtuC₂D₂ imports vitamin B_{12} into the cytoplasm through a mechanism involving ATP binding and hydrolysis.

Subsequent binding of ATP to the nucleotide binding domain (NBD) of BtuD subunits result in conformational rearrangements within BtuC₂ that trap Cbl within a translocation cavity. Cbl is released from BtuF by periplasmic loops of BtuC which occupy the Cbl-binding pocket of BtuF in the BtuC₂D₂F complex. ATP hydrolysis and displacement of the hydrolytic products from BtuD₂ is presumed to shift the transmembrane domains to an inward-facing conformation that permits Cbl egress into the cytoplasm.

1.5.5 Cobalamin-dependent enzymes

Enzymes that utilize Cbl as cofactor are divided into three major classes: reductive dehalogenases, methyltransferases, and AdoCbl-dependent enzymes (257). Methionine synthase and methylmalonyl-CoA mutase, present in humans and microorganisms, are part of the methyltransferase and AdoCbl-dependent enzyme classes, respectively. Corrinoid dehalogenases, however, are restricted to microorganisms. In most of these Cbl-dependent enzymes, Cbl binds the enzyme in the "base-off", or "base-off/His-on" state (*section 1.2.1*).

1.5.5.0 Reductive halogenases

Some anaerobic bacteria are able to dechlorinate aromatic and aliphatic organics such as chlorinated phenols and ethenes for use in energy metabolism (258). Exposure to these compounds induces the expression of genes involved in removing the chloride ion including Cbl-dependent reductive dehalogenases. The first dehalogenating anaerobe identified was *Desulfomonile tiedjei* (259), and over 20 species of dehalogenating microorganisms have been isolated to date, including the genera *Desulfomonile*, *Desulfitobacterium*, *Dehalobacter*, *Dehalospirillum* and *Dehalococcoides* (257, 260, 261). Most Cbl-dependent reductive dehalogenases contain one bound corrinoid and two Fe/S clusters (262).

1.5.5.1 Methyltransferases

Cbl-dependent methyltransferases are integral in human, animal, and bacterial metabolism and are involved in multiple pathways including the methylation of homocysteine to methionine (263), the formation of methane in methanogenic bacteria (264), and the fixation of carbon dioxide via the acetyl-coenzyme A pathway (265). Forms of Cbl that act as cofactor for these reactions include methyl-Co(III)-corrins, such as MeCbl, and Co(I)-corrins such as cob(I)alamin (243). Methyl group transfer occurs in nucleophilic substitution reactions, whereby the Co-C bond of the bound methylcorrinoid is heterolytically cleaved and re-formed at the end of the catalytic cycle. The mechanism for corrinoid-dependent methyl transfer involves an "ordered sequential mechanism" of two steps. In the first step, protein-bound Co(I)-corrin abstracts a methyl group from a substrate methyl donor, forming a methylated Co(III)-corrin. Subsequently, the methyl group of methylated Co(III)-corrin is transferred to a methyl-acceptor, forming the desired methylated product. These steps are performed by distinct modules (methyldonating, methyl-accepting, corrin-binding) within separate domains of a single polypeptide chain as in methionine synthase, or by separate proteins such as the enzymes involved in acetogenesis and methanogenesis. As Co(I)-corrins easily undergo oxidation to Co(II)-corrins, an additional activation module (often associated with the Co(I)-corrin binding module) restores methylated Co(III)-corrin by reductive methylation.

The formation of methionine by homocysteine methylation is mediated by MS and is important in human, animal, and bacterial metabolism (263). The most studied cobalamindependent MS is MetH from *E. coli*, which catalyzes the transfer of the methyl group from methyl-THF to homocysteine (Hcy) to form methionine (Met) and tetrahydrofolate (THF). MetH is a modular enzyme containing separate binding domains for homocysteine (methyl

acceptor), methyl-THF (methyl donor), Cbl, and SAM (activation). The functional properties of MetH are retained if each binding module is expressed individually (266). Structures of the Cbl-binding domain and activation domain of *E. coli* MetH have been determined (46, 267-269). MetH binds MeCbl in a "base-off/His-on" state in which the lower axial DMB is replaced by a histidine residue. Heterolytic cleavage of the MeCbl Co-C bond results in the formation of Met from Hcy and cob(I)alamin-bound MetH. Nucleophilic cob(I)alamin abstracts a methyl group from methyl-THF to re-form MeCbl. A regulatory triad of three conserved residues (Ser-Asp-His) are integral to this process, with the His residue coordinating the "base-off/His-on" state.

Methyl transfer from methyl-Co(III)-corrinoids is central to methanogenesis in certain anaerobic bacteria and archaea (243). These cofactors are required for the transfer of methyl groups from methanogenic substrates including methanol, methylamines, and acetate to a thiol group on coenzyme M (179). Alternatively, methyl groups can be transferred from methyltetrahydromethanopterin, an analog of methyl-THF, to a thiol group of coenzyme M using MeCbl as cofactor (179). Methylcoenzyme M reductase catalyzes the reduction of methylcoenzyme M to form methane in the final step of methanogenesis.

Methyl corrinoids are also used in the process of acetate formation in acetogenic, methanogenic, sulfur, and sulfate reducing bacteria via the Wood/Ljungdahl pathway. This pathway involves the synthesis of acetyl-CoA from two molecules of carbon monoxide (179). A complex formed between a methyltransferase and a corrinoid iron-sulfur protein (CoFeSP) mediates methyl transfer from methyl-THF to carbon monoxide (CO) dehydrogenase. The process involves abstraction of a methyl group from methyl-THF by a CoFeSP-bound corrinoid to form a methyl-Co(III)-corrinoid. This methyl group is subsequently transferred to CO dehydrogenase for synthesis of acetyl-CoA from CO and coenzyme A. Phosphorylation of

acetyl-CoA to acetylphosphate and subsequent phosphate transfer to ADP results in the production of ATP and acetic acid. The structure of a methyltransferase complex from the acetogenic bacteria *Moorella thermoacetica* was recently elucidated (270).

1.5.5.2 Adenosylcobalamin-dependent enzymes

AdoCbl-dependent enzymes catalyze processes that result in 1,2-isomerizations of protein-bound radicals. The common step in all reactions catalyzed by these enzymes is the homolytic cleavage of the Co-C bond of AdoCbl which yields cob(II)alamin and a 5'-deoxyadenosyl radical. This radical catalyzes the isomerization reactions by abstracting hydrogen directly from the substrate or indirectly through an enzyme-bound thyil radical as in the case of ribonucleotide reductase. The substrate radical then undergoes a rapid 1,2-rearrangement to form the product radical, which in turn re-abstracts a hydrogen from 5'-deoxyadenosine to give the rearranged product and a 5'-deoxyadenosyl radical. This radical combines with cob(II)alamin in the catalytic site, regenerating AdoCbl (243). Carbon skeleton mutases, diol dehydratases, ethanolamine ammonia lyase, aminomutases, and Cbl-dependent ribonucleotide reductases are all classified as AdoCbl-dependent enzymes (243).

The only carbon skeleton mutase found in mammals is MCM (*section 1.6.2.2*), which is also conserved across certain bacteria. In *Clostridia*, glutamate mutase (GLM) plays a central role in glutamate degradation by catalyzing the reversible inter-conversion of L-glutamate and L-threo-3-methylaspartate. GLM was the first enzyme for which corrinoid requirement was demonstrated (38) and has become the model for carbon skeleton mutases due to availability of multiple structures (271, 272). GLM is a heterotetramer made up of 2 smaller σ -subunits that form the Cbl-binding domain and two larger ε -subunits. Binding of two AdoCbl molecules occurs at the interface between the σ - and ε -subunits in a "base-off/His-on" mode.

Diol dehydratases, ethanolamine ammonia lyases, and aminomutases all catalyze rearrangements in which the migrating group is an amino or a hydroxy (243). The diol dehydratase (DDH) of *Klebsiella* catalyzes the conversion of 1,2-propanediol to propanal. DDH is a hetero-hexamer formed of two copies each of α , β , and γ subunits; the interface of the β subunits bind AdoCbl in a "base-on" form since contacts are formed predominantly between the lower face and nucleotide loop (273). Similarly, ethanolamine ammonia lyase of *E. coli* binds AdoCbl in a "base-on" form (274). In both reactions substrate is coordinated proximal to the corrin ring through hydrogen bonding with the corresponding enzyme. The structure of two aminomutases from *Clostridium stricklandii*, lysine 5,6-aminomutase (275) and ornithine-4,5-aminomutase (276), have also been elucidated. Binding of AdoCbl for aminomutases occurs in the "base-off/His-on" state similar to methionine synthase and carbon skeleton mutases.

Ribonucleotide reductases (RNRs) are found in all living cells and catalyze the conversion of ribonucleotides to deoxyribonucleotides required for DNA synthesis. Class II RNRs, found primarily in microorganisms, use AdoCbl as cofactor (243). Homolytic cleavage of the Co-C bond of AdoCbl generates a thiyl radical derived from a cysteine residue of the RNR which reacts with the substrate ribonucleotide. Structures of AdoCbl-dependent RNRs from *Lactobacillus leichmannii* (277) and *Thermotoga maritima* (278) have been determined. Class II RNRs bind AdoCbl in a "base-on" state.

1.6 Mammalian cobalamin metabolism

1.6.0 Assessment of enzyme activity and complementation groups

Our understanding of intracellular mammalian Cbl metabolism has largely been influenced by studying patients with inborn errors in this pathway. Accumulation of two metabolites defines these disorders; Hey is indicative of defects in the cytoplasmic MS pathway,

whereas MMA reflects errors in the mitochondrial MCM pathway. Inborn Cbl disorders result in elevated levels of either or both substrates in blood and urine. Following detection of homocystinuria and/or methylmalonic aciduria in patients, assessment of MS and MCM function is performed on patient fibroblasts followed by complementation analysis.

The assessment of MS and MCM function is performed through label incorporation assays on patient and control fibroblast cell lines. Measurement of MS function in fibroblasts has historically been performed in two ways, with both measuring incorporation of ¹⁴C from the methyl group of methyl-THF. The first is through direct incubation with [¹⁴C]methyl-THF and measuring incorporation into macromolecules (279). The alternate is through incubation with [¹⁴C]formate, which is converted to [¹⁴C]methyl-THF, and measuring specific incorporation into methionine (280). Since MS catalyzes the only cellular reaction capable of removing the methyl group from methyl-THF, radioactive counts are markedly decreased in patients with disorders in the MS pathway. Assessment of MCM function is performed through incorporation of label from [¹⁴C]propionate, the precursor to methylmalonic acid (281). Similarly, patients with defects in the MCM pathway demonstrate a decreased ability to incorporate label from propionate compared to healthy cell lines. Patients are subsequently categorized into three groups; impaired propionate incorporation, impaired methyl-THF incorporation, or combined impairment.

Somatic cell complementation is then utilized to define complementation groups. This technique involves the fusion of cultured cell lines from two patients using polyethylene glycol (282, 283). Fused cell lines that carry defects in the same gene are unable to complement one another. Alternatively, complementation between patient cell lines carrying defects in different genes occurs resulting in increased label incorporation based on the biochemical assays

described above. To date, nine complementation groups for Cbl metabolism have been established, designated *cblA-cblG*, *cblJ*, and *mut*.

1.6.1 Methionine synthase pathway

Inborn errors in genes involved in the MS pathway (Fig. 1.5) belong to the *cblG* and *cblE* complementation groups and lead to an isolated homocystinuria phenotype.

1.6.1.0 cblG

The *cblG* group results from mutations in the gene MTR, encoding the enzyme methionine synthase (MS) (284). Patients have elevated levels of homocysteine without evidence of methylmalonic aciduria. Biochemical analyses on fibroblasts show diminished incorporation of radiolabel from methyl-THF. Patients typically present in the first few months of life with vomiting, poor feeding, lethargy, megaloblastic anemia and developmental delay (285, 286). To date, 22 unique mutations have been identified in roughly 40 patients with the *cblG* disorder; the most common mutation is c.3518C \rightarrow T (p.P1173L) (287).

Human MS is a 140 kDa monomeric protein that catalyzes methyl transfer from methyl-THF to homocysteine utilizing MeCbl as cofactor (288). The reaction mechanism has been previously described for methyltransferases and *E. coli* MetH (*section 1.5.5.1*) and the human MS pathway is shown in Fig. 1.5. Human MS is 55% identical in sequence to *E. coli* MetH (289) and is predicted to have a similar modular arrangement of separate domains that coordinate binding of Cbl, methyl-THF, SAM, and Hcy (266). Briefly, a methyl group from methyl-THF is transferred to MS-bound cob(I)alamin to form MeCbl. This methyl group is then transferred to homocysteine to form methionine and regenerate cob(I)alamin. Because MS is the only known mammalian enzyme to use methyl-THF as methyl donor, the MS pathway also regulates the folate cycle. In patients with MS deficiency, accumulation of methyl-THF results in the

impairment of folate-dependent reactions such as purine synthesis and methylation which can lead to anemia. Further, MS is a key enzyme of the Met cycle and regulates cellular levels of SAM which is used as methyl donor for methylation of DNA, RNA, and proteins (286).

1.6.1.1 cblE

The *cblE* group arises from mutations in the gene *MTRR*, encoding the enzyme methionine synthase reductase (MSR) (284). There are roughly 20 known *cblE* patients in the world (285), and the clinical presentation is indistinguishable from the *cblG* defect (286).

The cob(I)alamin intermediate bound to MS oxidizes to cob(II)alamin every 200-1000 catalytic cycles which effectively inactivates MS. MSR encodes a 78 kDa protein containing FMN- and FAD/NADPH-binding sites (290) that reductively methylates MS-bound cob(II)alamin to yield MeCbl using SAM as a methyl source (Fig. 1.5) (291, 292). The FMN-binding domain of MSR interacts with the SAM-binding domain of MS with an affinity of 4.5 µM (293). Additionally, MSR catalyzes the reduction of free OHCbl to cob(II)alamin in the cytoplasm making it an aquocobalamin reductase (294).

Treatment of *cblG* and *cblE* patients with OHCbl improves biochemical and hematological abnormalities though neurological symptoms often linger (60). Betaine, a substrate used by betaine homocysteine methyltransferase in a Cbl-independent pathway for Hcy methylation, is often included with OHCbl to reduce Hcy levels and alleviate symptoms.

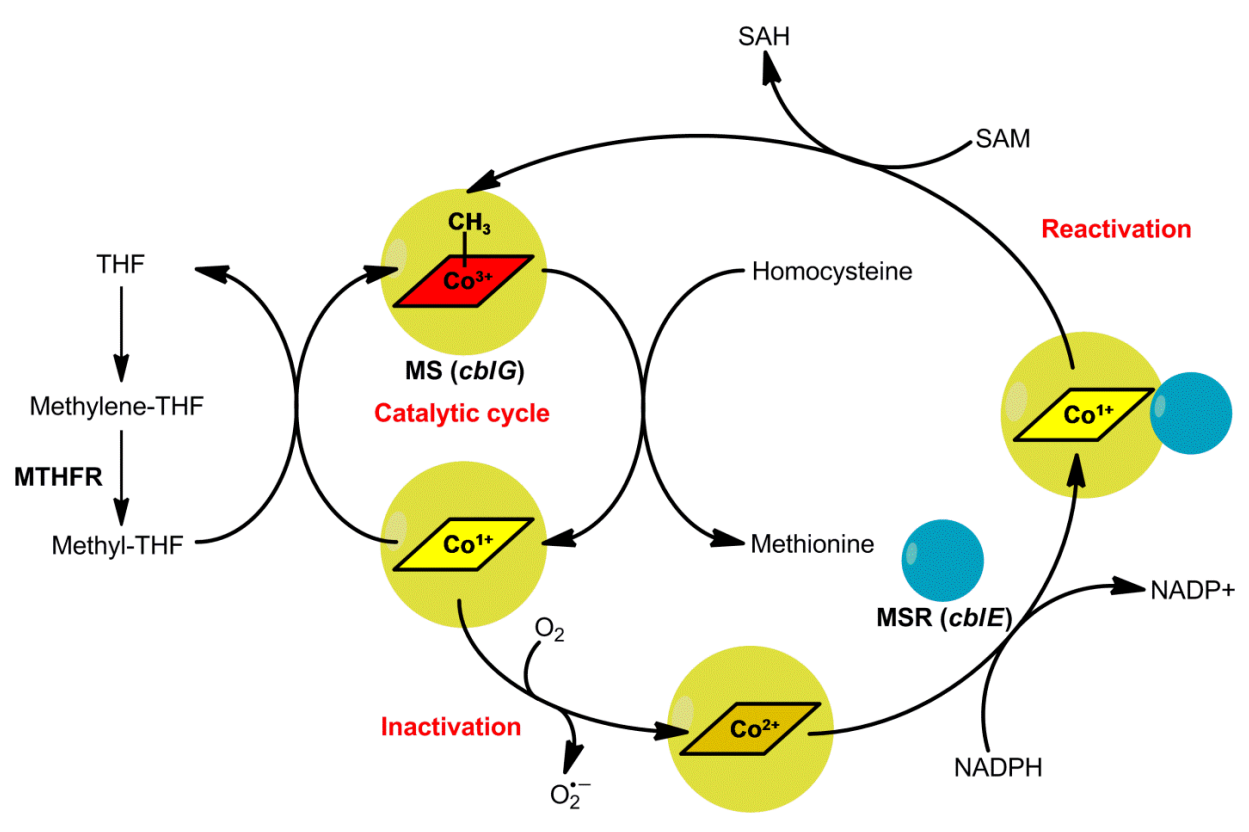


Figure 1.5. Mammalian pathway for the synthesis of methionine from homocysteine by methionine synthase. During the catalytic cycle, methionine synthase (MS; yellow circle) uses methylcobalamin (MeCbl) as methyl donor to generate methionine (Met) from homocysteine (Hcy). This mechanism involves the heterolytic cleavage of the Co-C bond from MeCbl to generate the Met product and cob(I)alamin. MeCbl is regenerated from cob(I)alamin through the transfer of a methyl group from methyl-THF, derived from THF by a reaction catalyzed by methylenetetrahydrofolate reductase (MTHFR). The occasional oxidation of cob(I)alamin to cob(II)alamin results in MS inactivation. Methionine synthase reductase (MSR) regenerates MeCbl through a coupled pathway which involves reduction of cob(II)alamin to cob(I)alamin using NADPH followed by methyl transfer from S-adenosylmethionine (SAM) to form reactivated MeCbl. Defects in MS are associated with the *cblG* complementation group whereas the *cblE* group results from defects in MSR. Figure adapted from the mechanism presented in (288).

1.6.2 Methylmalonyl-CoA mutase pathway

Inborn errors of the MCM pathway (Fig. 1.6) give the *cblA*, *cblB*, and *mut* complementation groups and lead to an isolated methylmalonic aciduria phenotype.

1.6.2.0 cblA

The *cblA* defect was first observed in patients with methylmalonic acidemia with diminished levels of AdoCbl. Despite normal levels of MeCbl, cells from *cblA* patients could not convert [57Co]OHCbl to [57Co]AdoCbl (295, 296). AdoCbl synthesis was restored when cell-free extracts of *cblA* patient fibroblasts were incubated with [57Co]OHCbl, ATP, and a reducing system (297). Because an external reducing system was able to alleviate this metabolic block, the *cblA* defect was hypothesized to correspond to a mitochondrial cob(II)alamin reductase. The human gene *MMAA* was identified through homology searching for genes proximal to bacterial MCM and mutations in this gene gave rise to the *cblA* defect (298). To date over 30 *cblA* patient mutations have been reported with over one-third corresponding to nonsense mutations. Patients typically present early in life with methylmalonic aciduria but respond well to Cbl therapy (299).

The product of the *MMAA* gene (methylmalonic aciduria type A) belongs to the P-loop GTPase family, traditionally involved in metalloenzyme assembly and function (298). MMAA is orthologous to the well-studied bacterial protein MeaB from *Methylobacterium extorquens*. MeaB exhibits nanomolar affinity for MCM and this affinity is modulated by ligand and substrate binding to either protein (300). Further, the activities of MeaB and MCM are influenced by one another; MeaB demonstrates ~100-fold greater GTPase activity in the presence of MCM (300, 301). Conversely, the catalytic activity of MCM is enhanced 2-fold in the presence of MeaB. Further, the ligand-bound state of MeaB (apo, GDP, or GTP bound)

modulates the affinity of MCM for AdoCbl (302). The current model proposes that AdoCbl bound to MCM periodically becomes inactivated during the catalytic turnover by escape of the 5'-deoxyadenosyl radical, which inactivates MCM (Fig. 1.6). MeaB is involved in restoring MCM activity by ejecting inactivated cob(II)alamin from MCM and gating the transfer of AdoCbl to MCM using its inherent GTPase activity (303). A similar model is proposed for human MMAA, which also forms a complex with MCM though its activity may (304) or may not be (305) modulated by MCM. Human MMAA and *M. extorquens* MeaB are homodimeric and structurally similar though MMAA dimers form a more open "U-shaped" conformation compared to the closed orientation formed by MeaB (304).

1.6.2.1 cblB

Patients with the *cblB* defect are deficient in AdoCbl synthesis and are metabolically similar to *cblA* patients. However, the *cblB* phenotype is more severe with patients presenting earlier in life and responding poorly to Cbl therapy. Symptoms include failure to thrive, developmental delay, lethargy, and encephalopathy. Patients with the *cblB* defect were originally differentiated from *cblA* patients based on cell free extracts failing to synthesize AdoCbl in the presence of a reducing system (297). Based on this work, the *cblB* defect was postulated to correspond to errors in a cob(I)alamin adenosyltransferase responsible for generating AdoCbl from cob(I)alamin. The gene *MMAB* was identified in similar fashion as *MMAA* by surveying MCM-containing bacterial operons (306). More than 20 unique mutations in the *MMAB* gene have been reported in patients with the *cblB* disorder, most of which are missense (13 of 23) and occur within the active site (307).

The gene *MMAB* encodes a 250-amino acid protein that is a member of the PduO family of cob(I)alamin adenosyltransferases (306, 308). MMAB, or ATR, is a bifunctional

mitochondrial enzyme involved in rescuing inactivated MCM by formation and delivery of AdoCbl. MMAB catalyzes the formation of AdoCbl by transfer of a 5'-deoxyadenosyl group from ATP to cob(I)alamin. It subsequently transfers AdoCbl to the active site of MCM (Fig. 1.6) (309). Spectroscopy studies have indicated that MMAB binds cob(II)alamin in a novel four-coordinate "base-off" state (310, 311). This alleviates the energy requirement and permits reduction to cob(I)alamin by a reductase or an electron transfer protein. Reduction to cob(I)alamin is required for adenosylation by MMAB, but it is currently not known if a reductase couples to MMAB. Flavoprotein oxidoreductases such as methionine synthase reductase (MSR), ferredoxin, and flavodoxin have been shown to complex with MMAB (312, 313).

MMAB forms a trimer with active sites situated at the subunit interfaces (314). In the *M. extorquens* MMAB homolog AdoCbl and ATP bind with negative cooperativity with only two of the three active sites available at a given time (309, 315). Following reductive adenosylation, ATP binding triggers ejection and delivery of AdoCbl from MMAB to the active site of MCM, which is mediated through protein-protein interactions between MMAB and MCM (309). Chaperoned Cbl delivery is a common theme in this metabolic pathway to prevent loss of the cofactor to the cellular milieu and avert conversion to the "base-on" state (50, 288, 309). A C-terminal truncation of MMAB, reflective of the c.700C>T (p.Q234X) mutation found in some *cblB* patients, compromises its ability to bind and release AdoCbl (316). Other mutations in *MMAB* alter substrate or cofactor binding, active site function or protein dynamics (314, 317-320). *cblB* patients with R186W or E193K mutations lack detectable MMAB, indicating a loss in protein stability (321).

1.6.2.2 mut

The *mut* complementation group arises from a defect in MCM, encoded by the gene MUT. MCM catalyzes the reversible isomerization of L-methylmalonyl-CoA to L-succinyl-CoA for entry into the tricarboxylic acid (TCA) cycle in the mitochondria (Fig. 1.6). Methylmalonyl-CoA is derived from propionyl-CoA, a metabolic product of branched-chain amino acids (methionine, threonine, valine, and isoleucine), cholesterol, and odd-chain fatty acids (286). Patients in the *mut* complementation group display similar symptoms to those in the *cblA* and cblB group (285) but synthesis of AdoCbl may not be compromised. Patients with the mut disorder are further subdivided into two groups, mut^0 and mut^- . Patient fibroblasts from the mut^0 class produce no detectable levels of MCM and MCM activity is not stimulated by supplementation with OHCbl. Conversely, MCM is immunologically detectable and MCM function is stimulated by supplementation with OHCbl in cultured fibroblasts of *mut*⁻ patients. The more severe phenotype occurs in mut^0 patients with a higher occurrence of morbidity, mortality, and neurological complications. Further, patients within the mut⁰ group are less responsive to OHCbl treatment compared to mut (299). Approximately 200 disease-causing mutations in MUT have been identified, the majority of which give the mut⁰ phenotype (322).

Structures of human MCM with or without Cbl and substrate have been solved (304) in addition to the homologous MCM from *P. shermanii* (323-325). Despite strong sequence identity (60%), the structural configuration of MCM from *P. shermanii* (psMCM) differs from human MCM (MCM); psMCM is a heterodimer of a catalytic (α) and an acatalytic subunit (β) (326) whereas MCM is homodimeric with two catalytic α subunits per dimer (327). Each monomer features a two-domain structure similar to the α subunit of psMCM; an N-terminal substrate binding domain connected to an AdoCbl-binding C-terminal domain by ~100 aa inter-

domain linker. The active site is formed at the domain interface. Because of the differences in overall enzyme architecture, MCM contains two active sites per dimer whereas psMCM has only one (304, 323). MCM binds its cofactor in the "base-off/His-on" state.

Treatment of patients within the *cblA*, *cblB*, and *mut* groups involves protein restriction or feeding with formula deficient in valine, isoleucine, methionine, and threonine as these amino acids are metabolized into methylmalonyl-CoA. Supplementation with OHCbl or CNCbl is a viable therapy for patients with the *cblA* defect but its usefulness in treating *cblB* and *mut* patients is limited (60). Administration of carnitine, which effectively removes propionyl-CoA from cells, has also been advocated (328), as has antibiotic treatment to reduce the number of gut bacteria producing propionate (60). Despite various treatment options, patient outcomes may remain poor.

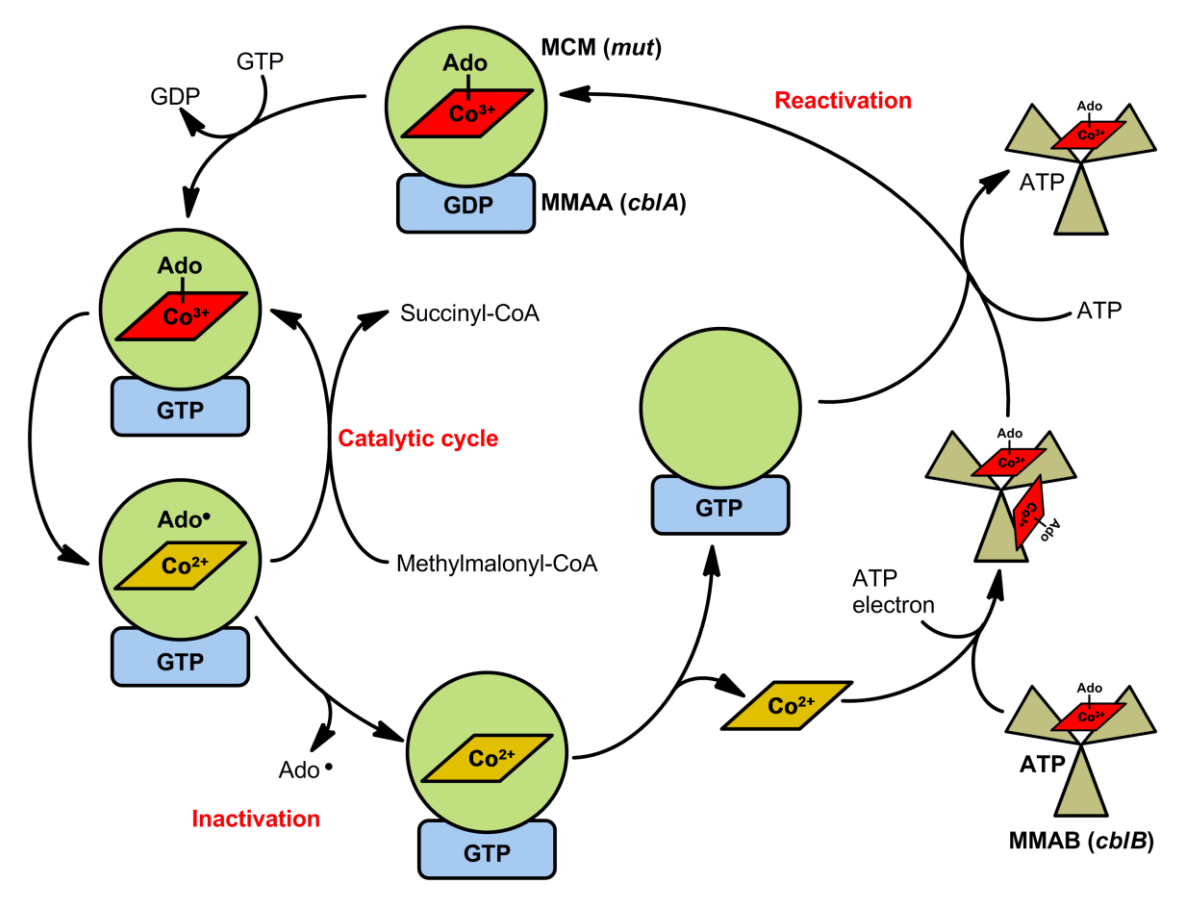


Figure 1.6. Mammalian pathway for the conversion of methylmalonyl-CoA to succinyl-CoA by methylmalonyl-CoA mutase. During the catalytic cycle methylmalonyl-CoA mutase (MCM; green circle) catalyzes the homolytic cleavage of the weak Co-C bond in adenosylcobalamin (AdoCbl) to generate a 5'-deoxyadenosyl (Ado) radical. This radical abstracts a hydrogen from methylmalonyl-CoA, resulting in a carbon skeleton rearrangement and the formation of succinyl-CoA and regenerated AdoCbl. Inactivation of MCM through loss of the Ado radical necessitates cofactor ejection from the active site of MCM by MMAA (blue rectangle, associated with MCM). Inactivated cob(II)alamin is converted to active AdoCbl via an ATP-dependent reaction catalyzed by the adenosyl transferase MMAB (brown triangles) that also requires reduction of cob(II)alamin by an unknown electron donor. MMAB can transfer AdoCbl back to MCM in a reaction that is gated by the GTPase activity of MMAA. The reactivation cycle is completed by substitution of MMAA-bound GDP with GTP. The complementation groups associated with each enzyme in this pathway are denoted in parentheses beside the enzyme abbreviation. Figure adapted from the mechanism presented in (288).

1.6.3 Combined defects of MeCbl and AdoCbl metabolism

A combined homocystinuria and methylmalonic aciduria phenotype is observed with the *cblF*, *cblJ*, *cblC* and *cblD* complementation groups.

1.6.3.0 cblF

The *cblF* defect was first described in an infant with developmental delay and mild methylmalonic aciduria that was responsive to Cbl treatment (329). Patient fibroblasts demonstrated an accumulation of unmetabolized, nonprotein-bound Cbl in lysosomes (329). Through quantitative electron microscopy radioautography using [57Co]CNCbl, control cell lines demonstrated a distribution of cobalamin as follows: 47% in the cytoplasm, 23.4% in the mitochondria, and 4.7% in the lysosome (330). In contrast, *cblF* fibroblasts had significant Cbl retention in the lysosome (60%) with reduced levels in the cytoplasm (12.6%) and mitochondria (1.2%) (330). Complementation analysis confirmed the genetically distinct disorder (331). Because *cblF* patients accumulate Cbl in the lysosome, the gene responsible for this defect was proposed to encode a lysosomal Cbl transporter.

As of today, there have been 16 reported cases of *cblF* (332-335). Patients with the *cblF* defect present early in life with symptoms that include being small for gestational age, failure to thrive, feeding difficulties, and persistent stomatitis (285). Some patients have congenital heart defects, facial abnormalities, macrocytic anemia, and neutropenia (285). Despite the original *cblF* patient suffering from only methylmalonic aciduria, patients typically demonstrate a combined methylmalonic aciduria and homocystinuria phenotype resulting from diminished AdoCbl and MeCbl levels that impair MCM and MS function (329). The gene responsible for this defect, *LMBRD1*, was recently identified and encodes the putative lysosomal cobalamin transporter LMBD1 (332). Eleven mutations in *LMBRD1* have been identified, the majority of

which are terminating frameshift mutations with c.1056delG (p.L352fsX18) being predominant (332, 333), though several splice-site mutations (334, 335) and a large deletion (334, 336) have also been identified. The *cblF* defect can be treated through intramuscular injection of milligram amounts of OHCbl, and this typically resolves hematological abnormalities and improves the biochemical profile despite remaining neurological conditions (337).

LMBD1 is a 61.4 kDa membrane protein consisting of 540 amino acids with six predicted N-glycosylation sites (332). LMBD1 localizes primarily to the lysosome in humans (332) and rats (338) but also appears to be present within the plasma membrane (339) and perinuclear region (332). Based on topology programs, predicted glycosylation pattern and freeze-fracture replica immunolabeling experiments (332), LMBD1 spans the lysosomal membrane via nine transmembrane helices with a lysosomal N-terminus and cytoplasmic C-terminus. LMBD1 demonstrates homology to the lipocalin-1 interacting membrane receptor (LIMR). LIMR internalizes proteins called lipocalins that bind small hydrophobic molecules like steroids and lipids (332). To date, a lipocalin-like molecule that binds Cbl within the lysosome has not been identified.

Because *LMBRD1* was only recently implicated in intracellular Cbl metabolism, limited studies have focused on the function of its gene product. Transfection of *LMBRD1* cDNA into *cblF* fibroblasts rescued AdoCbl and MeCbl synthesis as well as MS and MCM function implicating its involvement in the lysosomal export of cobalamin (332). A truncated isoform of LMBD1 lacking 73 N-terminal amino acids and its first two transmembrane helices has been detected in human liver tissue. Termed nuclear export signal-interacting protein (NESI), it has been implicated in the assembly of the hepatitis delta virus (340). NESI is glycosylated and localizes to the nuclear envelope where it interacts with nucleoporins and other components of

the nuclear pore complex (341). Unexpectedly, LMBD1 was recently implicated in regulating the endocytosis of the insulin receptor at the plasma membrane (339).

1.6.3.1 cblJ

A novel *cblJ* defect was identified in two patients that presented with methylmalonic aciduria and hyperhomocysteinemia (342). These patients had clinical symptoms similar to cblF that included hypotonia, lethargy, poor feeding, bone marrow suppression, macrocytic anemia and heart defects (342). Cultured fibroblasts from both patients demonstrated reduced AdoCbl and MeCbl synthesis in conjunction with impaired MCM and MS activity. Fibroblasts incubated with exogenous CNCbl accumulated large amounts of unmetabolized CNCbl (342, 343). A combined approach of microcell-mediated chromosome transfer and exome sequencing led to the identification of the ABCD4 gene as being responsible for the cblJ defect (342). Transfection of wild-type ABCD4 cDNA into cblJ fibroblasts rescued the biochemical phenotype (342). Biochemical rescue was not observed when LMBRD1 cDNA was transfected into cblJ fibroblasts, but transfection of ABCD4 cDNA into cblF fibroblasts resulted in partial rescue. To date, three patients exist with this defect and all have unique mutations in ABCD4 (342, 343). While long-term treatment outcomes have yet to be reported, the responsiveness of *cblJ* patient fibroblasts to OHCbl supplementation and the similar phenotype to cblF patients proposes that a similar treatment regimen.

ABCD4 encodes a non-glycosylated protein of 606 amino acids with molecular mass of 68.6 kDa (344, 345). ABCD4 is a member of the D subfamily of ABC half transporters and is also referred to as P70R, PMP69, or PXMP1-L (346). ABC half transporters dimerize to form an active, full transporter (347, 348). The three other members of this subfamily, ABCD1 or ALDP, ABCD2 or ALDR, ABCD3 or PMP70, localize to the peroxisomal membrane and

transport very-long-chain fatty acids from the cytoplasm into peroxisomes (349). ABCD4 has significant amino acid identity (25-27%) with these other members but is the most divergent member and lacks a hydrophilic N-terminal tail that mediates localization to the peroxisome (345). Despite originally identified as peroxisomal (346), studies aimed at identifying all peroxisomal proteins in rats and mice failed to detect ABCD4 but were able to identify the other three members of the family (350-352). In addition, cell lines with severe defects in peroxisome biogenesis synthesized normal levels of MeCbl and AdoCbl, arguing against peroxisome involvement in Cbl metabolism (342). ABCD4 was shown to localize to the endoplasmic reticulum (345), though two recent studies have demonstrated its presence solely within the lysosome of humans (342) and rats (338). Furthermore, expression of LMBD1 and ABCD4 in fibroblasts resulted in colocalization at the lysosomal membrane (342). Compounded with the fact that *ABCD4* cDNA can partially rescue *cblF* defects, a current model proposes that ABCD4 and LMBD1 form a complex responsible for Cbl export from the lysosome (342).

ABCD4 consists of two domains: an N-terminal transmembrane domain and a C-terminal nucleotide binding domain (NBD) (342). The topology of ABCD4 has both the N- and C-termini exposed to the cytoplasm based on bioinformatics predictions and loop directed glycosylation experiments (342, 345). The transmembrane domain has six predicted transmembrane helices (342, 345) whereas the NBD contains highly conserved motifs involved in ATP and Mg²⁺ binding, including Walker A and B motifs plus a modified ABC signature motif (342). Of the five mutations detected in ABCD4, three occur within the transmembrane domain (p.N141K, p.D143_S181del, p.Y319C) while the remaining two occur within the NBD (p.G443_S485del and p.E583LfsX9) (342, 343). Point mutations within the Walker A or Walker B motifs or in the putative catalytic site in *cblJ* fibroblasts reduced synthesis of both MeCbl and

AdoCbl implying that ATPase activity of ABCD4 is involved in cofactor transport (342).

ABCD4 is a close homolog to a newly identified *M. tuberculosis* vitamin B₁₂ transporter (Rv1819c) which diverges from the traditional BtuC₂D₂-type transporters found in most other bacteria (353).

1.6.3.2 cblC

The *cblC* disorder is the most common inborn error of Cbl metabolism with over 550 patients identified (354-359). Patients come to medical attention early in life and demonstrate failure to thrive, feeding difficulties, and developmental delay (60). Megaloblastic anemia is present in the majority of cases in addition to other hematological abnormalities. Patients may display prominent neurological issues that may include seizures, cerebral atrophy, ventriculomegaly and white matter disease, in addition to ocular impairment. The appearance of structural heart defects in cblC patients has also been reported (360). The cblC defect can be differentiated into two distinct phenotypes: early-onset and late-onset (361). Early-onset patients present within the first year of life with severe disease and respond poorly to treatment. Lateonset patients are rarer and present between childhood to adulthood, have less severe symptoms, and usually respond better to treatment (361). Fibroblasts from cblC patients have impaired AdoCbl and MeCbl synthesis with decreased activity from MS and MCM resulting in a combined methylmalonic aciduria and homocystinuria phenotype. Furthermore, cblC fibroblasts take up exogenous CNCbl but cannot convert this form into AdoCbl or MeCbl. Rather, only exogenous OHCbl stimulates the activity of MS and MCM in some late-onset *cblC* fibroblasts (361-363). The two *cblC* phenotypes can be attributed to specific mutations in the *MMACHC* gene (354).

Over 70 different mutations in MMACHC have been identified in cblC patients (60). The most frequent mutation is c.271dupA (p.R91KfsX14), a frameshift mutation that accounts for more than 40% of disease-causing alleles in European populations (307, 354, 355, 364). This mutation is rare in Chinese populations, but the c.609G>A (p.W203X) nonsense mutation is extremely common (358). Patients with early-onset cblC typically have the c.271dupA mutation or a c.331C>T (p.R111X) nonsense mutation in the homozygous or compound heterozygote state. Patients with late-onset *cblC* typically have the c.394C>T (p.R132X) nonsense mutation or the c.482G>A (p.R161Q) missense mutation (354, 356, 364). Patient treatment involves intramuscular administration of OHCbl often in conjunction with betaine to aid in controlling Hcy levels (60). As many as one third of early-onset *cblC* patients have died, while most others have permanent neurological impairment. Recent analysis of 18 cblC patients with no discernible mutations in MMACHC led to the identification of a novel complementation group termed cblX (365). Patients in the cblX group have an X-linked form of combined methylmalonic acidemia and hyperhomocysteinemia caused by missense mutations in HCFC1, a coregulator of the transcription factor THAP11. Patients have drastically reduced levels of MMACHC mRNA and MMACHC protein indicating that HCFC1, in complex with THAP11, is responsible for the transcriptional activation of MMACHC expression (365). Due to its X-linked inheritance, all currently identified *cblX* patients are male.

The gene product of *MMACHC* is a 282 amino acid protein with molecular mass of 32.0 kDa. MMACHC has high sequence identity to the Cbl-binding domain of MCM from *Streptomyces avermitilis* but lacks the consensus "DXHXXG" motif (354). The ~40 most C-terminal residues of MMACHC are homologous (>40 % identity) to a disordered proline-rich domain of bacterial TonB, involved in the uptake of Cbl in Gram-negative bacteria (*section*

1.5.4) (354). These C-terminal residues of MMACHC appear to be a recent evolutionary addition as they are not conserved in eukaryotes outside mammals (354). Alternative splicing of *MMACHC* is thought to generate both a full-length MMACHC and a truncated version that lacks these ~40 C-terminal residues (366). This shorter MMACHC variant appears to be the predominant, if not only, form in mice (366). The importance of these C-terminal residues is not well understood; no disease-causing mutations have identified within this region and recombinant truncated MMACHC is more thermostable than full length MMACHC (366).

MMACHC exhibits broad specificity for the upper axial ligand of Cbl and can bind CNCbl, OHCbl, MeCbl, AdoCbl in addition to several other alkylated forms (366-371).

MMACHC-bound Cbl exists in a five-coordinate "base-off" state where neither DMB nor histidine coordinates the central cobalt (366, 369, 372). In the two structures of MMACHC with bound AdoCbl (372) or MeCbl (366), DMB is separated from the corrin ring via hydrophobic interactions. This "base-off", five-coordinate state of Cbl has a lower energy barrier for cleavage of the Co-C bond compared to "base-on" Cbl (372). MMACHC is thus implicated in processing Cbl by removing the upper axial ligand. MMACHC catalyzes the glutathione-dependent dealkylation of MeCbl, AdoCbl, and C2-C6 alkane forms of Cbl (371, 373). MMACHC also catalyzes the decyanation of CNCbl in the presence of an electron donor (370). The cob(II)alamin product generated from removal of the upper axial ligand is necessary for the downstream MCM and MS reactions. The R161Q mutation is associated with late-onset *cblC*, and reduces the affinity of MMACHC to CNCbl but not OHCbl (368, 369). This arginine is proximal to the Cbl-binding site but does not directly contact the upper axial ligand (366).

While Cbl processing is a major function of MMACHC, it has been shown to complex with other proteins involved in the Cbl metabolic pathway. In very rare cases of the *cblG* defect

(termed *cblG*-variant), patient fibroblasts have undetectable levels of MS along with decreased conversion of CNCbl to OHCbl typical of the *cblC* defect (374). Fofou-Caillierez *et al.* (375) recently demonstrated that MS and MMACHC interact and that MMACHC mutants (including MMACHC-R161Q) have reduced affinity towards MS. In addition, our group was the first to characterize an interaction between MMACHC and the downstream adapter protein MMADHC (367). Protein-protein interactions involving MMACHC are proposed to mediate Cbl channeling to the Cbl-dependent enzymes; the importance of protein-protein interactions in this pathway is described in *section 1.8*.

1.6.3.3 cblD

The *cblD* defect was detected over 25 years ago in brothers with deficient MCM and MS activities resulting in combined methylmalonic aciduria and homocystinuria (376, 377). Both patients had symptoms similar to the *cblC* group but with decreased severity (362). Since the identification of several new *cblD* patients, the heterogeneity in their clinical phenotypes has resulted in the classification into three distinct subclasses. Patients with isolated homocystinuria resulting from defects in MeCbl synthesis and MS activity were classified as *cblD*-variant 1, or *cblD*-HC. Patients with isolated methylmalonic aciduria resulting from defects in AdoCbl synthesis and MCM activity were classified as *cblD*-variant 2, or *cblD*-MMA. Patients demonstrating a combined homocystinuria and methylmalonic aciduria phenotype resulting from defects in both MeCbl and AdoCbl synthesis with MCM and MS deficiency were classified as *cblD*-classic or "combined" (378). Because of this heterogeneity, the gene product causing the *cblD* defect was hypothesized to be involved at a branch point in the Cbl metabolic pathway after processing by MMACHC whereby cobalamin is distributed to MS in the cytoplasm or MCM in the mitochondria (378). The gene responsible for the *cblD* defect was recently identified as

MMADHC (379). A clear genotype-phenotype relationship exists: truncation mutations in the 5' region of MMADHC result in isolated methylmalonic aciduria (cblD-MMA), truncation mutations in the middle and 3' regions result in combined methylmalonic aciduria and homocystinuria (cblD-classic) and missense mutations in the 3' region cause only isolated homocystinuria (cblD-HC) (379, 380).

To date 17 *cblD* patients have been reported in the literature and 15 disease-causing mutations have been identified (379-381) with the following distribution; six patients are *cblD*-HC, six patients are *cblD*-MMA, and five patients are *cblD*-classic. Because of the heterogeneity in the *cblD* defect, symptoms are clinically variable, with patients presenting from early in life to adolescence. Symptoms for patients with *cblD*-HC include respiratory infection, hydrocephalus, nystagmus, dystonia, spastic ataxia, vena cava clot, and autistic features. Patients with *cblD*-MMA present with poor feeding, developmental delay, vomiting, lethargy, ketoacidotic coma and necrotizing enterocolitis. Patients with *cblD*-combined generally have symptoms from both subclasses in addition to macrocytosis, mental retardation, encephalopathy and reduced myelination. Seizures and convulsions have been described in patients with either forms of the disease. Treatment comprises of administration of CNCbl or OHCbl in addition to betaine, folic acid and carnitine, but neurological symptoms often linger (378, 381).

The MMADHC protein is 296 residues with molecular mass of 32.9 kDa (379). Features of MMADHC include a putative Cbl binding motif "DXHXXG" (residues 81-86) and a region homologous to an ATPase component of a putative ABC transporter in *Salmonella enterica* (379). However, MMADHC lacks critical motifs for ATP-binding including the Walker A, Walker B, and ABC signature domains found in all ABC transporters. Based on signal sequence predictions the 12 N-terminal residues of MMADHC encode a mitochondrial targeting sequence

(MTS) (379). Strong Kozak consensus motifs indicate possible alternate translation start codons at Met₆₂ or Met₁₁₆ that would produce shorter isoforms of the protein (379, 380). These isoforms would lack the putative MTS, which would result in cytoplasmic localization. MMADHC is detected in full length within control fibroblasts, indicating that translation reinitiation at downstream methionines does not occur in healthy subjects (380). In contrast, two shorter isoforms (26.5 kDa and 20.5 kDa) were identified in *cblD*-MMA fibroblasts containing truncation mutations N-terminal to Met₆₂, and only the shortest isoform (20.5 kDa) was detected in *cblD*-MMA fibroblasts containing a truncation mutation (p.N77EfsX5) between Met₆₂ and Met₁₁₆. These molecular masses correspond to the theoretical molecular masses of the Met₆₂ and Met₁₁₆ isoforms, suggesting that reinitiation of translation occurs in patients within the *cblD*-MMA subclass. Fibroblasts of patients with truncation mutations C-terminal to Met₁₁₆ have little to no detectable MMADHC levels resulting in the *cblD*-combined defect (380). Lastly, patients with the *cblD*-HC defect have missense mutations within a C-terminal stretch of 14 amino acids that diminishes only MS activity and MeCbl production.

Based on *cblD* patient phenotypes the current model proposes that MMADHC dual-localizes to both the mitochondria and cytoplasm, whereas the shorter MMADHC isoforms lacking a MTS, found in *cblD*-MMA patients, localize only to the cytoplasm (380). The mechanism for dual localization of MMADHC is currently unknown, but various mechanisms for other proteins have been described in the literature (382). Replacing the MTS of MMADHC with the stronger leader sequence of a mitochondrial aldehyde dehydrogenase significantly increases AdoCbl formation but reduces MeCbl levels, indicating that the subcellular distribution of MMADHC is finely balanced (380). Further, the coexpression of MMACHC and MMADHC

in *cblD*-MMA/HC or *cblD*-MMA cell lines significantly increased AdoCbl levels indicating a modulatory role for MMACHC in the activity or subcellular distribution of MMADHC (380).

Our group was the first to describe the interaction between MMADHC and MMACHC (367). Using surface plasmon resonance, we demonstrated specific, dose-dependent binding between MMACHC and a maltose-binding protein (MBP) fusion of MMADHC (MBP-MMADHC). We complemented these analyses with phage display technology and mapped five putative MMACHC-binding sites onto the sequence of MMADHC. These binding regions were C-terminal to Met₁₁₆ implying that the 115 N-terminal residues of MMADHC do not recruit MMACHC for complex formation. Two MMACHC-binding regions mapped to the putative ABC-transporter homology domain. An additional region encompassed the stretch of residues for which missense mutations were discovered in *cblD*-HC patients. These mutations may disrupt the MMACHC–MMADHC interaction, which may play an essential role in the distribution of Cbl to the Cbl-dependent enzymes (367, 380).

1.7 Model for intracellular metabolism

With the recent identification of the *cblJ* complementation group (342, 343), there are currently nine gene products known to participate in the intracellular Cbl metabolic pathway (Fig. 1.7); the following is a proposed model for this pathway based on reports from the literature. The first step in Cbl entry occurs when TC-Cbl is internalized by its cognate receptor, TCblR. Within the lysosome TC is digested and Cbl, typically as CNCbl or OHCbl, is released. Lysosomal Cbl is transported into the cytoplasm via the lysosomal membrane transporters LMBD1 and ABCD4; both are proposed to act in complex with ABCD4 providing energy through ATP hydrolysis and LMBD1 forming the substrate channel (342). MMACHC binds cytoplasmic Cbl and converts the cofactor to the "base-off" state which enables removal of the

upper axial ligand to form cob(II)alamin. The function of MMADHC is not well understood, but is postulated to act as an adapter protein by interacting with apo- or holo-MMACHC for Cbl partitioning to cytoplasmic MS and mitochondrial MCM.

In the cytoplasm, cob(II)alamin may be delivered directly to MS through interactions with MMACHC (375); the role of MMADHC in this process is unclear. In the cytoplasm, cob(II)alamin is reductively methylated by MSR using NADPH as electron donor to generate the active cofactor for MS, MeCbl. Cob(II)alamin is also partitioned to the mitochondria, though the mechanism for Cbl entry is unclear as a specific mitochondrial transporter has not yet been identified. MMAB binds cob(II)alamin in the mitochondrial matrix, and with the aid of an electron transfer protein, generates AdoCbl to serve as cofactor for the mitochondrial MCM reaction.

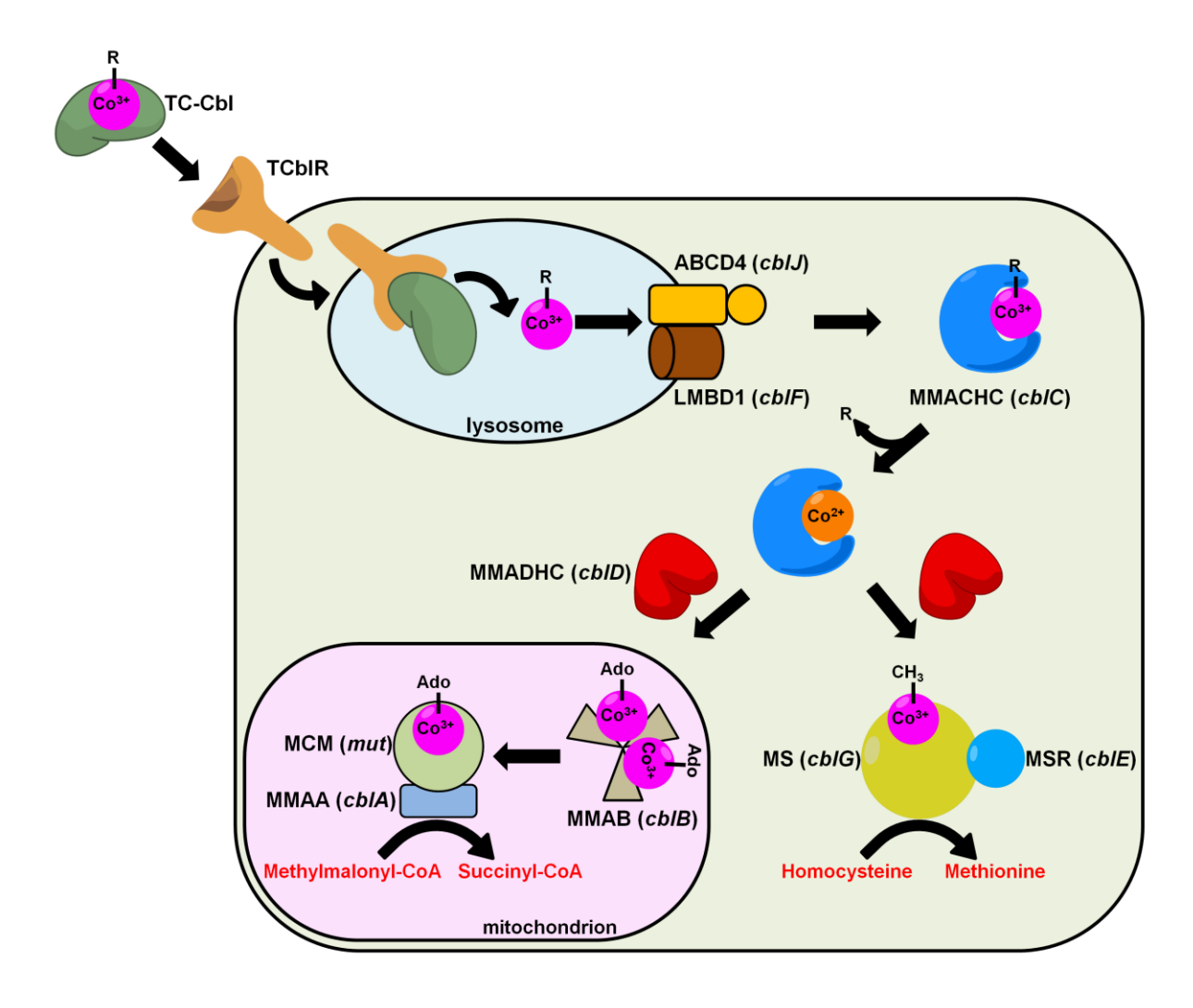


Figure 1.7. Intracellular metabolism of cobalamin in mammals. Holo-transcobalamin (TC-Cbl) engages the transcobalamin receptor (TCblR) and undergoes receptor-mediated endocytosis. Cobalamin (Cbl) is released from TC in the lysosome, where it is exported presumably by a complex formed between LMBD1 and ABCD4. Cytoplasmic Cbl binds MMACHC and is processed into cob(II)alamin by removal of the upper axial ligand ("R"). MMADHC forms a complex with MMACHC that partitions cob(II)alamin to the Cbl-dependent enzymes methionine synthase (MS) and methylmalonyl-CoA mutase (MCM). In the cytoplasm, cob(II)alamin is converted to MeCbl by methionine synthase reductase (MSR), which is then used as cofactor in the formation of methionine from homocysteine in a reaction catalyzed by MS. In the mitochondrion, cob(II)alamin is converted into AdoCbl by MMAB, which also delivers the cofactor to the active site of MCM in a process that involves MMAA. AdoCbl is subsequently used as cofactor for the MCM-dependent conversion of methylmalonyl-CoA to succinyl-CoA. Complementation groups resulting from inborn errors of Cbl metabolism are listed in parentheses beside the protein names.

1.8 Protein-protein interactions

Many cellular processes depend on the efficient delivery of rare and often reactive cofactors to target enzymes. This poses a challenge in a crowded cellular milieu. As opposed to a collision-based delivery system, the current hypothesis regarding delivery of reactive molecules including cofactors and coenzymes involves a chaperone-dependent system that shelters the molecule from unwanted side reactions and escorts them to the dependent enzymes (50, 288). This strategy is used in metabolic pathways whereby protein complexes mediate substrate transfer in a mechanism termed substrate channeling. The intracellular processing and transport of Cbl is proposed to follow a similar mechanism due to the following inherent challenges associated with the cellular utilization of Cbl (50, 288).

First, the abundance of intracellular Cbl is low, with reports estimating the concentration to be between 30-700 nM with variable tissue distribution (44). Compounded with this low abundance is that intracellular Cbl exists in different oxidation states, has variable upper axial ligands and is distributed to several cellular compartments including the lysosome, mitochondria, and cytoplasm. The next reason is the reactivity of Cbl. Free Cbl is stable in the cob(III)alamin form, but for the generation of AdoCbl and MeCbl reduction is necessary. Cob(I)alamin and cob(II)alamin are highly reactive and unstable when exposed to the cellular environment. The last reason pertains to the state of the lower axial ligand of Cbl. Under physiological conditions (neutral pH), free cobalamin exists in the "base-on" state. However, the Cbl-dependent enzymes MS and MCM require Cbl in the "His-on/base-off" form whereby an active site histidine replaces the lower axial DMB.

Given its low abundance and reactivity, Cbl is found almost exclusively (>95%) in a protein-bound state within the cell (383, 384). Because of this sequestration, the channeling of

Cbl occurs via protein-protein interactions that maintain the cofactor in the correct oxidation and coordination state by protecting from loss to the cellular milieu and inadvertent oxidation.

Protein-protein interactions between the Cbl-dependent enzymes and their accessory proteins are integral to Cbl metabolism. These include complexes formed between MMAA and MCM (300, 301) in addition to MS and MSR, with both complexes required for pathway reactivation (293). Further, the adenosyltransferase MMAB mediates the reactivation of the MCM pathway through the gated delivery of AdoCbl to MCM via protein-protein interactions (309).

While studies have reported protein complexes from MCM and MS, few have focused on the proteins involved in early Cbl uptake and processing, including MMACHC, MMADHC, LMBD1 and ABCD4. These proteins are promising targets for research due to their critical nature, with mutations responsible for defects in both the MS and MCM pathway. Limited functional studies have been performed on these proteins given only their recent identification. MMACHC remains the most well studied, with its roles in Cbl processing previously described (section 1.6.3.2). While MMACHC catalyzes the conversion to "base-off" and production of cob(II)alamin, how is this processed cofactor transferred to the corresponding enzymes? For MS this may be modulated by interactions with MMACHC in the cytoplasm (375). For MCM, the mechanism may involve MMACHC binding to the adapter protein MMADHC (367), whose function is not clearly understood but mediates cofactor partitioning to the cytoplasm and mitochondria (379). Protein-protein interactions between LMBD1 and ABCD4 are also postulated to mediate the lysosomal egress of Cbl (332, 342). But how is the lysosomal export of Cbl coupled to cytoplasmic effectors? These studies set out to uncover the protein-protein interactions involved in early Cbl substrate channeling.

1.9 Introduction to techniques used in this thesis

A combination of genetic, cellular and molecular biology and biophysical analyses were used in this work to characterize protein-protein interactions and delineate structural features of recombinant proteins involved in early Cbl metabolism. The following section briefly describes each major technique used in these studies.

1.9.0 Phage display

Phage display is a molecular genetics technique used to predict and localize binding determinants between two macromolecules. Applications of phage display include epitope mapping (385, 386), identification of small molecule binding sites on drug targets (387, 388), and mapping of protein-protein contacts (251, 252, 389, 390). This latter application has been used extensively in chapters 2 and 4 of this study. The phage display process to map protein-protein interfaces utilizes an in-house or commercially available combinatorial bacteriophage M13 library. These libraries are engineered to display random peptide sequences on their coat proteins; in our studies up to five copies each of a random peptide sequence are fused to the N-terminus of the pIII coat protein of bacteriophage M13. The diversity of the combinatorial phage library is up to one billion unique sequences, with each unique sequence displayed on the surface of a single phage.

An iterative process termed phage panning is used to predict and localize protein-protein interactions. This process involves immobilizing a purified bait protein onto a microtitre plate and incubating with the combinatorial phage library. Non-specific or weak interactions between bait and phage are minimized through stringent washing. Phages with affinity towards the bait protein are recovered and amplified by infecting an *E. coli* host strain. This enriched phage

population undergoes additional rounds of panning with increasingly stringent wash conditions to further enrich for a phage population with strong affinity for the bait protein.

DNA from these high-affinity bait-binding phages is harvested and sequenced to identify the displayed peptide. These phage-derived sequences are then aligned to the sequence of known or putative bait-binding proteins and scored based on an alignment matrix. Sequences that score above the threshold values are considered to align significantly with the target protein sequence. Many phage-derived sequences may align within a region of the target protein; clusters of aligned peptides are indicative of specific regions of interaction between the bait and target protein.

Phage panning can be used to refine regions of interaction between proteins known to interact, or can identify novel protein-protein interactions. Complementary analyses can also be performed reversing protein immobilization followed by phage panning. These activities allow for the prediction of interacting regions between two proteins and guide further experimental strategies to refine these complementary interaction surfaces.

1.9.1 Surface Plasmon Resonance

Surface plasmon resonance (SPR) is a leading-edge biophysical technique to characterize protein-protein and protein-ligand interactions in real-time without intrusive labeling. Compared to other techniques that only provide an overall measure of affinity (such as fluorescence spectroscopy or isothermal titration calorimetry), SPR can determine the individual kinetics of binding (i.e. association and dissociation rate constants) using only minimal amounts of recombinant protein - a distinct advantage when working with membrane proteins. Based upon observed versus predicted binding responses, SPR can also help to determine interaction stoichiometries.

As an injected protein or "analyte" binds and then dissociates from an immobilized binding partner, or "ligand", the real-time changes in bulk refractive indices are measured and quantified. Immobilization of the ligand commonly occurs through covalent linkage to dextrancoated sensor chips. Amine-coupling randomly orients a ligand over a sensor chip surface by activating the surface to couple with ε-amino groups of lysines. In contrast, thiol-coupling is typically used to specifically orient ligands onto the sensor chip surface through disulfide bridge formation (e.g. cysteine site-directed mutagenesis of ligands containing no intrinsic cysteine residues or with proteins that have low cysteine content).

Coordinated by a microfluidics system, the analyte is injected over reference and ligandimmobilized surfaces in tandem. Interaction between the analyte and ligand results in an accumulation of mass over the sensor chip surfaces which is detected as a bulk refractive index change through an optics system. The responses are recorded in values of resonance units (RU), whereby 1 RU represents a surface density of 1 pg/mm². Thus, the more mass that accumulates over the sensor chip surface, the larger the signal response that is observed during the initial association phase. Following the analyte injection, the flow of running buffer initiates dissociation of the ligand-analyte complex, thus decreasing the accumulated mass with a concomitant decrease in signal response. Throughout the entire process (of association and dissociation) the changes in response units are recorded and fit to an appropriately selected model to determine binding kinetics/affinity and stoichiometry of the ligand-analyte interaction. In the single-cycle and multi-cycle kinetic models, the rates of association and dissociation are determined based upon the reference-subtracted SPR profiles or "sensorgrams" (overlay of association/dissociation binding responses for multiple analyte concentrations as a function of time). In the steady-state model, equilibrium binding responses near the end of the association

phase are plotted against the analyte concentration and the equilibrium dissociation constant is determined by non-linear regression analysis.

1.9.2 Dynamic light scattering

Dynamic light scattering (DLS) is an optical technique used to characterize particles in solution based on their ability to scatter light. In our studies, a protein sample is placed within a cell and a laser emits light upon the sample. Incident light scattered by the protein is measured by a detector at an angle of 90° over short time intervals of 100 ns to 30 ms. The magnitude of scattered light intensity fluctuates with time due to Brownian motion of the suspended protein. This rate of fluctuation is directly related to the rate of diffusion of the protein through the solvent, termed the translational diffusion coefficient; this coefficient is related to the hydrodynamic radius of the protein, which can be used to estimate the molecular mass if the protein is globular. Thus, DLS allows the direct determination of the translation diffusion coefficient and hydrodynamic radius of a protein, which in turn can be used to estimate molecular mass. Protein applications of DLS include monitoring protein hydrodynamic radius upon addition of an external ligand (251, 367) or protein (251, 252), which monitors proteinligand or protein-protein formation. DLS has also been demonstrated to be an efficient way of determining the thermostability of protein samples by measuring the total scattering intensity or hydrodynamic radius as a function of temperature (391, 392).

1.9.3 Static light scattering

Molecular mass estimations using DLS are influenced significantly by the conformation and shape of a protein. Unlike DLS, static light scattering is an optical technique that can directly measure the average molecular mass of a particle in solution without determination of the translational diffusion coefficient. Multiple detectors are often used to measure intensities at

several different scattering angles; the technique is therefore referred to as multi angle light scattering (MALS). A scattering curve is made from this information (scattering intensity vs angle), and from this curve the size, shape, and molecular mass of a protein can be accurately determined. Because MALS calculates weight-averaged molecular masses which is influenced by sample heterogeneity (impurities, aggregates, etc), chromatographic separation by protein size is performed inline by size exclusion chromatography (SEC). SEC-MALS is a powerful tool for the study of membrane proteins. For solution studies, membrane proteins necessitate solubilization in detergents. Detergent-solubilized membrane proteins exist as protein-detergent complexes (PDC), whereby the detergent contributes significantly to the molecular mass of the PDC. Thus, it is inherently difficult to assess the molecular mass of a membrane protein in detergent using SEC and DLS since the contribution of detergent to the molecular mass can not be accurately calculated using these traditional techniques. This is exacerbated in cases where membrane proteins form oligomers. By coupling SEC-MALS with an absorbance spectrometer and a differential refractometer, the contribution of detergents to these PDCs can be elucidated, particularly if the detergents poorly absorb light at 280 nm (393). This technique allows for direct molecular mass calculation of the protein component of the PDC, allowing identification of the stoichiometry for oligomeric membrane proteins.

1.9.4 Analytical ultracentrifugation

Analytical ultracentrifugation (AUC) is a complementary technique to MALS and DLS analyses and provides protein hydrodynamic properties. Similar to these techniques, AUC can determine the molecular mass of proteins and protein complexes, in addition to providing information on the overall shape of the molecule in solution through elucidation of its frictional ratio. These analyses are obtained by fitting protein sedimentation profiles. The application of a

centrifugal force to a protein results in sedimentation that is dependent on the hydrodynamic shape and size of the protein (394). Protein sample is placed within a clear sample cell that is housed within a centrifuge rotor. Application of a strong centrifugal forge to the sample results in protein sedimentation towards the bottom of the sample cell. Radial UV-vis absorbance measurements are taken throughout the run by an optics system to monitor sedimentation.

Sedimentation profiles are then fit to the Lamm equation, which describes sedimentation behavior of a particle in solution. Fits to this equation yield information on the sedimentation coefficient of the protein, which is directly proportional to its molecular mass (395). Additional parameters that are fit include the frictional ratio, a measure of a protein's hydrodynamic shape. The frictional ratio measures deviation a protein hydrodynamic shape relative to that of a perfect sphere; globular proteins possess frictional ratios between 1.2-1.3, whereas elongated proteins possess values of 1.8 and greater (396).

1.9.5 Far UV Circular dichroism

Far UV circular dichroism (CD) is a technique used to monitor and estimate protein secondary structure content. The circular dichroism effect refers to the differential absorption of circularly polarized light. Circularly polarized light is made of 2 components of equal magnitude; one rotating counter-clockwise (left-handed), and one rotating clockwise (right-handed. When left-handed and right-handed light is differentially absorbed by a chiral molecule such as a protein, the resulting combined radiation possesses elliptical polarization as opposed to circular polarization. CD instruments measure the differential absorbance between the left-handed and right-handed circularly polarized components and reports these values in terms of ellipticity. The CD spectrum of a protein is obtained when ellipticity is measured as a function of wavelength, particularly between 240 and 180 nm (far UV) where absorption is principally

due to the peptide bond. Different types of secondary structure found in proteins give rise to characteristic spectra within this region. Using datasets of CD spectra from various proteins whose structure has been elucidated by X-ray crystallography, secondary structure content of uncharacterized proteins can be estimated with considerable accuracy using CD spectroscopy.

1.10 Rationale and thesis objectives

Cbl is a water soluble vitamin required as cofactor for two mammalian processes: methionine regeneration in the cytoplasm by MS, and fatty acid/amino acid metabolism in the mitochondria by MCM. To date, nine genes have been implicated in the intracellular Cbl metabolic pathway. Mutations in *MMACHC*, *MMADHC*, *LMBRD1* and *ABCD4* cause defects in early intracellular Cbl transport and processing. As a result, MCM and MS reactions are compromised resulting in substrate accumulation and leading to a combined methylmalonic aciduria and homocystinuria phenotype. Apart from limited phenotypic studies, few studies have examined the molecular nature of intracellular Cbl transport in mammals. Given current knowledge on Cbl levels and reactivity within the cell we hypothesize that the intracellular chaperoning of Cbl is a highly coordinated process involving protein-protein interactions between MMACHC, MMADHC, LMBD1 and ABCD4. The underlying objective throughout this project was to characterize protein-protein interactions involved in the early intracellular transport and processing of Cbl in mammals.

Our first aim was to examine the interaction between soluble proteins MMACHC and MMADHC, described in chapter 2. MMACHC is involved in the early processing of Cbl, whereas the function of MMADHC has not been elucidated. Recombinant isoforms of MMADHC were produced in *E. coli* and low-resolution structural features were determined to gain insight into function. MMADHC was monomeric and adopted an extended conformation in

solution, with regions of disorder identified at the N-terminal domain. Unlike MMACHC, we found no involvement of MMADHC in Cbl binding or processing. Panning combinatorial phage libraries against recombinant MMACHC and MMADHC allowed the mapping of putative sites of interaction on each protein. Kinetic analyses using surface plasmon resonance confirmed a sub-micromolar affinity for the MMACHC–MMADHC interaction. Based on these studies, we propose that the function of MMADHC is exerted through its structured C-terminal domain via interactions with MMACHC in the cytoplasm.

The next aim was to determine the subcellular location of MMACHC and MMADHC, discussed in chapter 3. Clinical phenotypes and subcellular location of MS and MCM dictate that MMACHC functions in the cytoplasm while MMADHC functions at a branch point in the pathway in both the cytoplasm and the mitochondrion. Using subcellular fractionation and immunofluorescence we confirmed that MMACHC is cytoplasmic while MMADHC is dual-localized to the cytoplasm and mitochondria.

The final aim was to identify interactions between the lysosomal membrane transporters LMBD1 and ABCD4, discussed in chapter 4. Recombinant LMBD1 and ABCD4 were purified to homogeneity using a eukaryotic expression system. Detergent-solubilized LMBD1 and ABCD4 formed homodimers in solution. We demonstrated that LMBD1 and ABCD4 interact with low nanomolar affinity by SPR. By phage display, we mapped regions on LMBD1 and ABCD4 predicted to recruit MMACHC and complemented these predictions with SPR analyses. We propose a model whereby LMBD1 and ABCD4 facilitate the vectorial delivery of lysosomal cobalamin to cytoplasmic MMACHC, preventing cofactor dilution to the cytoplasmic milieu and protecting from inactivating side reactions.

Preface to chapter 2

The function of many recently identified gene products involved in early cobalamin metabolism have yet to be elucidated, due in large part to the lack of purified recombinant forms. Chapter 2 describes the first reported purification of two physiologically relevant MMADHC isoforms. Recombinant production of MMADHC alongside MMACHC permitted the identification of endogenous proteins in human cell lines. Purified MMADHCs were subjected to biophysical analyses whereby hydrodynamic properties, oligomeric state, and secondary structure were elucidated. Cobalamin binding to MMADHC was assayed but we found no such function for this protein. By aligning affinity-selected peptides obtained from panning against MMADHC, we identified regions on MMACHC proposed to be involved in recruiting MMADHC. Using a similar analysis we discovered regions on MMACHC that implicate its self-association. To confirm our predictions, we performed interaction analyses using surface plasmon resonance and uncovered low micromolar affinities. Based on our phage display and SPR analyses, we propose that MMACHC interacts with the structured C-terminal domain of MMADHC.

Chapter 2

Structural features of	recombinant M	MADHC isoforms	and their i	interactions
with MMACH	C, proteins of ma	nmalian vitamin	B ₁₂ metabo	olism

Justin C. Deme, Isabelle R. Miousse, Maria Plesa, Jaeseung C. Kim, Mark A. Hancock, Wayne Mah, David S. Rosenblatt, James W. Coulton

Molecular Genetics and Metabolism (2012). 107(3): 352-362

Copyright © 2012, Elsevier Ltd All rights reserved

2.0 Summary

The genes MMACHC and MMADHC encode critical proteins involved in the intracellular metabolism of cobalamin. Two clinical features, homocystinuria and methylmalonic aciduria, define inborn errors of these genes. Based on disease phenotypes, MMADHC acts at a branch point for cobalamin delivery, apparently exerting its function through interaction with MMACHC that demonstrates dealkylase and decyanase activities. Here we present biophysical analyses of MMADHC to identify structural features and to further characterize its interaction with MMACHC. Two recombinant tag-less isoforms of MMADHC (MMADHCΔ1-12 and MMADHC Δ 1-61) were expressed and purified. Full length MMACHC and full length MMADHC were detected in whole cell lysates of human cells; by Western blotting, their molecular masses corresponded to purified recombinant proteins. By clear-native PAGE and by dynamic light scattering, recombinant MMADHCs were stable and monodisperse. Both species were monomeric, adopting extended conformations in solution. Circular dichroism and secondary structure predictions correlated with significant regions of disorder within the Nterminal domain of MMADHC. We found no evidence that MMADHC binds cobalamin. Phage panning against MMADHC predicted four binding regions on MMACHC, two of which overlap with predicted sites on MMACHC at which it may self-associate. Specific, concentrationdependent responses were observed for MMACHC binding to itself and to both MMADHC constructs. As estimated in the sub-micromolar range, the binding of MMACHC to itself was weaker compared to its interaction with either of the MMADHC isoforms. We propose that the function of MMADHC is exerted through its structured C-terminal domain via interactions with MMACHC.

2.1 Introduction

Vitamin B₁₂, or cobalamin (Cbl), is a water soluble vitamin required by all mammals. Because mammals lack the enzymes required for *de novo* synthesis, Cbl is acquired through dietary intake (50, 286). The physiologically relevant Cbl forms in mammals are methylcobalamin (MeCbl) and deoxyadenosylcobalamin (AdoCbl), utilized by methionine synthase (MS) and methylmalonyl-CoA mutase (MCM), respectively. MS is a cytoplasmic enzyme that catalyzes methionine regeneration through remethylation of homocysteine, whereas MCM resides in the mitochondrion and is responsible for the terminal metabolism of odd carbon number fatty acids and the amino acids valine, methionine, isoleucine and threonine, for entry into the tricarboxylic acid cycle.

Based on somatic complementation assays, nine inherited defects of intracellular cobalamin metabolism have been discovered, designated *cblA* to *cblJ* and *mut* (284, 331, 342, 377, 397-399). These defects are characterized by increased production of methylmalonic acid and/or homocysteine, with symptoms that may include lethargy, hypotonia, developmental delay, seizures, and megaloblastic anemia. Four of these defects (*cblC*, *cblD*, *cblF*, *cblJ*) can cause combined homocystinuria and methylmalonic aciduria. The *cblC* class of cobalamin disorders correspond to mutations in the *MMACHC* (methylmalonic aciduria type \underline{C} and homocystinuria) gene (354) and are the most frequent inborn errors of vitamin B_{12} metabolism with \sim 500 known cases and over 70 different causal mutations (285, 356, 400). *MMACHC* encodes a protein of 282 amino acids (31.7 kDa), and based on disease phenotype is predicted to localize to the cytoplasm. Recent evidence suggests possible localization to the mitochondrion (401) despite its lacking a predicted mitochondrial targeting sequence (MTS). MMACHC binds Cbl (367-369) in a "base-off" conformation (366). The recently solved structure of MMACHC revealed two

structurally distinct modules: N-terminal (residues 1-172) and C-terminal (residues 183-244) (366). MMACHC uses FMN or FAD as prosthetic group for reductive decyanation of cyanocobalamin (CNCbl) (370), likely through its N-terminal core module which displays fold homology to the NADP oxidase/flavin reductase family (366). The C-terminal module is made of four helices that cap the core module, with cobalamin binding in the large cavity formed between both modules. MMACHC also catalyzes the dealkylation of alkylcobalamins through glutathione transferase activity (366, 371).

The MMADHC (methylmalonic aciduria type \underline{D} and homocystinuria) gene corresponds to the cblD complementation group (379). There are 17 patients in this group that may have combined homocystinuria and methylmalonic aciduria, isolated homocystinuria, or isolated methylmalonic aciduria (379-381). MMADHC encodes a 296-amino acid protein (32.9 kDa) that is highly conserved across mammalian species (379). The MMADHC gene encodes a strong Nterminal MTS and a conserved vitamin B_{12} -binding motif (residues 81–86) (379). Given different subcellular locations of MS and MCM, MMADHC is postulated to have functions in both the cytoplasmic and mitochondrial pathways for vitamin B_{12} processing and assimilation. At the protein level, healthy patients produce full length MMADHC (380), predicted to be localized to both compartments through mechanisms still not well understood. However, the leader sequence appears to play a role in dictating production of the two active cobalamin forms, MeCbl and AdoCbl (380). Premature translation termination at early residues gives only the methylmalonic aciduria (cblD-MMA, cblD-variant 2) phenotype in the mitochondrion due to reinitiation of translation occurring at Met₆₂ or Met₁₁₆ and resulting in production of wild-type levels of MeCbl in the cytoplasm (379, 380). Missense mutations at C-terminal residues of MMADHC cause homocystinuria (cblD-HC, cblD-variant 1) in the cytoplasm, indicating that

function in the mitochondrion is not compromised. The combined defect (cblD-combined) is caused by genetic mutations that compromise polypeptide length after Met₁₁₆ (379-381).

While the physiological function of MMADHC remains to be elucidated, our group adopted phage display to predict regions on MMADHC that bind to MMACHC (367). Five regions were mapped onto MMADHC, all corresponding to residues C-terminal to Met₁₁₆. The interaction between MMADHC and MMACHC was validated *in vitro* using surface plasmon resonance (SPR) and *in vivo* using a bacterial two hybrid assay. Because MMADHC was produced as a fusion with maltose binding protein (MBP) resulting in a heterogeneous sample that contained MBP–MMADHC in addition to free MBP, binding affinities could only be estimated as nanomolar for the MMACHC–MMADHC interaction by SPR.

In this study, we describe two recombinant tag-less putative isoforms of MMADHC: MMADHCΔ1-12, corresponding to MMADHC after cleavage of the predicted MTS according to MitoprotII (379); and MMADHCΔ1-61, an N-terminally truncated isoform found in some patients with the *cblD*-MMA defect (380). When purified to near homogeneity (>95%), both constructs were monodisperse by dynamic light scattering (DLS) and were stable in solution at high concentrations by clear native-PAGE (CN-PAGE). MMADHCΔ1-12 and MMADHCΔ1-61 were monomeric and adopted an extended conformation in solution. Circular dichroism (CD) and secondary structure predictions identified N-terminal residues of MMADHC as being unstructured. Neither form of MMADHC bound cobalamin, indicating MMADHC function is not dependent on this cofactor. Phage display performed on purified MMADHCΔ1-12 predicted four binding regions on MMACHC; conversely, three regions were also predicted at which MMACHC may form multimers. SPR demonstrated specific, concentration-dependent

responses for MMACHC binding to itself (K_D of 520 nM) and to both MMADHC constructs: MMADHC Δ 1-12, K_D of 220 nM; MMADHC Δ 1-61, K_D of 175nM.

2.2 Materials and methods

2.2.0 Cloning, expression and purification of MMADHC∆1-12 and MMADHC∆1-61

cDNA corresponding to the MMADHC gene was codon-optimized for expression in E. coli and subcloned into a pUC19 plasmid (Genscript). Two derivatives, corresponding to MMADHC Δ 1-12 and MMADHC Δ 1-61 at the protein level, were subcloned into pETM-41. Briefly, coding sequences were PCR-amplified by primers that incorporated an NcoI restriction site (underlined) at the 5' end (forward primer for MMADHC Δ 1-12: 5'-TTAACCATGGCTTCCTATCTGCCGGGCTTCT-3'; forward primer for MMADHCΔ1-61: 5'- TTTATCCATGGGCCCGTTTGGTCCGCAG-3') and a BamHI site (underlined) at the 3' end (reverse primer for both constructs: 5'-CGCGGATCCTCAGTTGCCCGACAGTTTT-3'). Trimmed PCR products were ligated in-frame to the pETM-41 vector using NcoI/BamHI cut sites. The pETM-41 vector encodes, in the following order, a hexahistine tag (His₆), maltose binding protein (MBP), and a tobacco etch virus (TEV) NIa protease site all upstream of the ligated inserts. Plasmids pETM-41-MMADHCΔ1-12 and pETM-41-MMADHCΔ1-61 were sequenced-confirmed (McGill University and Genome Quebec Innovation Center, Montreal). Upon transforming these plasmids into E. coli BL21 (DE3) pLysS, cells were grown in Luria broth (LB) supplemented with 0.2% glucose, kanamycin (30 μg/ml) and chloramphenicol (35 μ g/ml) to an OD₆₀₀ of 0.6 and then induced by addition of 0.5 mM isopropyl β -D-1thiogalactopyranoside (IPTG; BioVectra) for 4 h at 25°C. Cells were collected by centrifugation (7,000 x g at 4°C, 30 min) and stored at -20°C.

Cell pellets were resuspended in ice cold lysis buffer containing 50 mM Tris pH 8.0, 300 mM NaCl, 5 mM imidazole, 0.2 mM tris(2-carboxyethyl)phosphine (TCEP; BioVectra). Resuspended cells, supplemented with 5 mM MgCl₂, lysozyme (200 µg/ml; Roche), DNase (60 μg/ml; Roche), RNase (60 μg/ml; Roche), 175 μM phenylmethylsulfonyl fluoride (PMSF; Sigma), and a Complete EDTA-free protease inhibitor cocktail tablet (Roche), were subjected to two passages through an Emulsiflex-C5 homogenizer (Avestin) at 15,000 psi. Supernatant collected after centrifugation of the lysate (34,000 x g at 4°C, 1 h) was clarified by filtration (0.45 µm) and loaded onto a freshly regenerated Ni-NTA Superflow resin (Qiagen) preequilibrated with lysis buffer. Following extensive washing (lysis buffer + 20 mM imidazole), recombinant proteins were eluted with lysis buffer containing 100 mM imidazole. Fractions corresponding to the eluted peak were pooled and concentration determined by Bradford assay (Bio-Rad) using bovine serum albumin (BSA) as standard. TEV NIa protease was added to pooled eluate in 1:10 mass ratio (TEV:sample) and dialyzed in 50 mM Tris pH 8.0, 250 mM NaCl, 0.2 mM TCEP, 10% glycerol for 16 h. Subsequent dialysis in 50 mM Tris pH 8.0, 250 mM NaCl, 0.2 mM TCEP was followed by loading onto a second Ni-NTA Superflow column (Qiagen). Flowthrough was pooled and concentrated using a stirred cell with molecular weight cut-off (MWCO) ultrafiltration disc of 10,000 Da (Millipore). Concentrated material was subjected to size exclusion chromatography (SEC) using a pre-calibrated Superdex 75 (HiLoad 16/60) column (GE Healthcare Bio-Sciences) equilibrated with 50 mM Tris pH 8.0, 250 mM NaCl and 0.5 mM TCEP. Concentrations following SEC were verified by Bradford assay (Bio-Rad).

2.2.1 Protein purity and analyses

In addition to MMADHC that was purified as described above, MMACHC was also cloned, expressed, and purified as we previously described (367). Protein assays were performed in SEC buffer (unless otherwise stated) and purity was assessed by sodium dodecyl sulfate polyacrylamide gel electrophoresis (SDS-PAGE) and clear-native PAGE (CN-PAGE). For SDS-PAGE, 1 µg of protein sample was diluted in reducing Laemmli sample buffer to 1X and loaded onto a precast Mini-PROTEAN TGX 4-15% gradient gel (Bio-Rad). Samples were run using a standard Tris-glycine-SDS buffer system followed by silver staining. Molecular masses of MMADHC Δ 1-12 and MMADHC Δ 1-61 were estimated from SDS-PAGE by comparison to a molecular weight ladder (Pageruler; Fermentas). For CN-PAGE, 5 µg of protein sample was diluted in native sample buffer (30 mM Tris pH 6.8, 20% glycerol, 0.005% bromophenol blue) and loaded onto a precast Mini-PROTEAN TGX 4-15% gradient gel (Bio-Rad). CN-PAGE was performed using a Tris-glycine buffering system at 200 V for 60 min with electrophoresis tank submerged in ice, followed by silver staining. To confirm identity and purity, MMADHCΔ1-12 and MMADHCΔ1-61 were subjected to Western blotting and to mass spectrometry (Sheldon Biotechnology Centre, McGill University).

2.2.2 Western blotting

Human embryonic kidney cell line 293 (HEK293) and fibroblast cell lines MCH46 and WG3646 (genetically identical to WG3583) were used to detect endogenous MMACHC and MMADHC. Briefly, cells were grown to confluence in Dulbecco's Modified Eagle Medium (DMEM) supplemented with 10 % fetal bovine serum, followed by washing in PBS, trypsinization (0.25 % trypsin) and centrifugation at 500 x g (5 min at 25°C) to collect cells. After washing, cells were lysed in PBS containing 1.5% n-dodecyl-β-d-maltoside (DDM) and a

Complete EDTA-free protease inhibitor cocktail tablet (Roche) for 1 h on ice. Samples were centrifuged at 12,000 x *g* for 20 min at 4°C and Bradford assay was performed on supernatants to quantify protein concentration in soluble lysates. Soluble lysates (75 μg) were run along with recombinant MMACHC (5 ng) or MMADHCΔ1-12 (1 ng) and MMADHCΔ1-61 (5 ng) on SDS-PAGE. Protein was transferred to a 0.45 μm PVDF membrane (Immobilon P, Millipore) using a semi dry transfer system (Bio-Rad) according to manufacturer's protocols. Membranes were blocked overnight in blocking buffer (2% casein in TBS containing 0.1% v/v Tween-20; TBST). Membranes were washed five times in TBST, followed by 1 h incubation with mouse monoclonal antibodies (mAb) against human MMACHC (NeuroMab UC Davis) or against human MMADHC (ImmunoK) diluted (1:3,000 mAb MMACHC; 1:1,000 mAb MMADHC) in blocking buffer. After another five washes in TBST, membranes were incubated for 1 h with goat anti-mouse IgG1 conjugated to horseradish peroxidase (HRP; Abcam) for detection of MMACHC (1:20,000 in blocking buffer) and MMADHC (1:10,000 in blocking buffer). Immunodetection was performed using chemiluminescent HRP substrate (Millipore).

2.2.3 Dynamic light scattering (DLS)

For analyses of polydispersity and hydrodynamic radius, MMADHCΔ1-12 and MMADHCΔ1-61 in SEC buffer were concentrated to 9.0 mg/ml and 9.3 mg/ml, respectively and tested in the absence and presence of 10-fold molar excesses of CNCbl, MeCbl, hydroxocobalamin (OHCbl), and AdoCbl. Prior to each measurement, samples (20 μl) were centrifuged at 12,000 x g for 10 min, 4°C, added to freshly cleaned DLS cuvettes and left to equilibrate for 5 min at the recording temperature of 20°C. Readings were recorded on a DynaPro-99-E-50 instrument (Protein Solutions) running Dynamics version 6.3.18 software. A total of 20 acquisitions were recorded with an average time of 10 s per acquisition at a laser

power of 100% and wavelength of 825 nm. Data were filtered to select for amplitudes of 1.000 ± 0.001 and to exclude sum of square (SOS) values above 15. Molecular masses were estimated based on hydrodynamic radii calculated by Dynamics using the globular proteins model.

For thermal curves, ten acquisitions (10 s each) of MMADHC Δ 1-12 (25 μ M; 0.67 mg/ml) or MMADHC Δ 1-61 (25 μ M; 0.8 mg/ml) \pm cobalamins (250 μ M) in size exclusion buffer were taken after incubation for 5 min at 20°C, 25°C, 30°C and five acquisitions (10 s each) were then taken at each 2°C increment above 30°C. A slow 2 min thermal ramping allowed the sample to equilibrate to each temperature point; this was followed by a 1 min equilibration once the temperature was achieved. To ensure proper sample equilibration, the first and last acquisitions of each measurement were monitored with no significant differences in scattering intensity or hydrodynamic radius. Scattering intensity, hydrodynamic radius, and sample molecular mass were monitored over a temperature range of 20-60°C and error values were calculated from acquisitions for each measurement.

2.2.4 Analytical ultracentrifugation (AUC)

Sedimentation velocity experiments were conducted on a Beckman XL-I analytical ultracentrifuge at a rotor speed of 40,000 rpm and at 20°C. Sample and reference sectors (1.2 cm path length) were filled with 400 μl of protein (MMADHCΔ1-12 at OD₂₈₀ of 1.0; MMADHCΔ1-61 at OD₂₈₀ of 0.7) and 425 μl of buffer, respectively. Two hundred continuous scans were taken from 5.9 - 7.2 cm at absorbance wavelength of 280 nm. Data were analyzed using the program Sedfit (394). SEDNTERP (http://bitcwiki.sr.unh.edu/index.php/Downloads) was used to calculate buffer viscosity and density values (402). Sedimentation profiles were obtained by fitting the data to a continuous c(s) model, using a root mean square deviation (rmsd) of 0.007 as

threshold value, and allowing for direct determination of sedimentation coefficient (s), frictional ratio (f/f_0), and molecular mass.

2.2.5 Circular dichroism (CD)

Prior to measurements, MMADHC Δ 1-12 and MMADHC Δ 1-61 samples underwent exhaustive dialysis in 10 mM sodium phosphate pH 7.5 and 150 mM NaF. After dialysis, samples were eluted from a Superdex 75 column (GE Healthcare Bio-Sciences) pre-equilibrated with dialysis buffer. Samples (0.1 mg/ml) were centrifuged for 10 min at 12,000 x g and analyzed by DLS to ensure sample monodispersity prior to data collection. Far-UV CD spectra were recorded from 180 to 260 nm at 25°C using a Jasco J-815 spectropolarimeter and a quartz cuvette with an optical path length of 1 mm. Spectra were acquired at 1 nm bandwidth, 1 sec response time, 1 nm step size and 100 nm/min scan speed. Each spectrum was calculated as the average of 10 accumulations and corrected by subtracting buffer baseline. Secondary structure estimations were performed by the DICHROWEB server (403) using a mean residue weight of 111.25 Da for MMADHC Δ 1-12 and 112.74 Da for MMADHC Δ 1-61. Data were fit using the CDSSTR (404) method with reference set 6 (optimized for 185-240 nm), giving nRMSD values <0.02 and a total secondary motif content of 1.00 \pm 0.01.

2.2.6 Secondary structure (PSI-PRED) and disorder (DISOPRED2) predictions

The amino acid sequence of full length MMADHC (UniProt ID: Q9H3L0) was input to PSIPRED (405) (http://bioinf.cs.ucl.ac.uk/psipred/) and DISOPRED2 (406) (http://bioinf.cs.ucl.ac.uk/disopred/) web servers. PSIPRED generated secondary structure predictions based on position specific iterated BLASTs (PSI-BLAST) outputs. DISOPRED2 predicted intrinsically disordered regions based on a non-redundant set of high resolution X-ray structures by identifying residues appearing in sequence records but with missing coordinates in

electron density maps. Both techniques are complementary and are used to identify unstructured or disordered regions on proteins based on primary sequence analysis. A false positive threshold of 5% was used for DISOPRED2 analysis. Results from analyses were compiled onto a diagram using the protein sequence alignment editor ALINE (407).

2.2.7 Phage display

Phage display was performed on MMADHC Δ 1-12 using two commercially available libraries: Ph.D.-12 and Ph.D.-C7C (New England Biolabs). MMADHC Δ 1-12 was diluted to 100 μ g/ml in 0.1 M NaHCO₃, pH 8.6; 150 μ l of protein was adsorbed to a polystyrene microtiter plate by incubation overnight at 4°C. Wells were blocked with 5 mg/ml BSA in 0.1 M NaHCO₃ pH 8.6 for 2 h at 4°C, followed by washing vigorously with TBST. A solution of 10 μ l of each phage library corresponding to 1.5 x 10¹¹ plaque forming units (pfu) diluted in 90 μ l of TBST was added to the wells and gently rocked for 1 h at 25°C. Phage panning, clone isolation, and DNA sequencing were performed as previously described (251, 252).

Pair-wise alignments of affinity-selected peptides from phage panning against MMADHCΔ1-12 or against MMACHC (367) were performed against MMACHC using the REceptor LIgand Contacts (RELIC) server MATCH program (408). This program uses a default scoring window of five; the threshold score requires at minimum three identities and one similarity between selected peptides and alignment sequence based on a modified BLOSUM62 amino acid substitution matrix. Identities are given a score of +4, whereas similarities are given a score of +1. Alignment mismatches are given a score of either −1 or 0. For a window size of 5 residues, the threshold for MATCH is a score of 13. Improvements to the pair-wise alignments were obtained by using the program MatchScan (P.D. Pawelek, unpublished data) that calculates alignment scores for a range of scoring windows. For MatchScan, the minimum scoring

threshold is increased or decreased by 1 for each residue added or subtracted to the default scoring window, respectively. Predicted regions of interaction were mapped to the 3-D structure of MMACHC (PDB ID: 3SC0) using the molecular viewer UCSF Chimera (409).

2.2.8 Surface plasmon resonance (SPR)

Label-free, real-time binding between recombinant MMACHC and MMADHC was examined using a Biacore 3000 system (GE Healthcare Bio-Sciences AB, Uppsala, Sweden; BIAcontrol v4.1 control software). Experiments were performed on research-grade CM4 sensors (Biacore) at 25°C using filtered (0.2 μm) and degassed HBS-ET running buffer (10 mM HEPES pH 7.4, 150 mM NaCl, 3 mM EDTA, and 0.05% v/v Tween-20). Proteins were amine-coupled (Biacore kit; 20 μg/ml in 10 mM sodium acetate pH 4.0) at low density (~ 300 RU each of MMADHCΔ1-12, MMADHCΔ1-61 and MMACHC); corresponding references surfaces were prepared in the absence of protein.

Single-cycle kinetic experiments were performed in which MMACHC (0–500 nM; 4-fold dilution series) was titrated over reference and protein-immobilized surfaces at 50 μl/min (60 sec association and 30-300 sec dissociation). In addition, multi-cycle kinetic experiments were performed in which MMACHC (0-200 nM; 2-fold dilution series) was titrated over reference and protein-immobilized surfaces at 25 μl/min (480 sec association and 900 sec dissociation). In all cases, sensor surfaces were regenerated at 50 μl/min using two 30-sec pulses of HBS-ET containing 1 M NaCl, 5 mM NaOH, and 0.1% (v/v) Empigen. As negative binding controls, BSA and MBP were injected at high concentration (500 nM) in a similar manner. Multi-cycle titration series were analyzed using the "Steady-state affinity" model (i.e. nonlinear regression of equilibrium amounts bound, R_{eq}, *versus* analyte concentration, C; BIAevaluation software v4.1) to predict apparent equilibrium dissociation constants (*K*_D). Theoretical binding maxima were

predicted for each surface using the following equation: $R_{max} = (M_A/M_L)(R_L)(n)$ where R_{max} is the maximal binding response (RU) at saturation; M_A is the molecular mass (kDa) of the injected analyte; M_L is the molecular mass (kDa) of the immobilized ligand; R_L is the amount (RU) of immobilized ligand; and n is the predicted binding stoichiometry. All SPR data were double referenced (410) and are representative of duplicate injections acquired from three independent trials.

2.3 Results

2.3.0 Purification of recombinant MMADHC

A construct of MMADHC corresponding to the predicted mitochondrial form after removal of the leader sequence (MMADHC Δ 1-12) and a shorter cytoplasmic isoform representing an alternatively translated polypeptide beginning at Met₆₂ (MMADHCΔ1-61) were codon-optimized and expressed in *E.coli* as MBP-fusions to improve solubility and yield. MBP was separated from MMADHC constructs by cleavage with TEV NIa protease followed by affinity and size exclusion chromatography. Both constructs were purified to >95% as assessed by SDS-PAGE (Fig. 2.0A). MMADHCΔ1-12 and MMADHCΔ1-61 migrated to molecular masses of 33 kDa and 28 kDa, respectively, values similar to those calculated from primary sequence (31.9 kDa and 26.6 kDa, respectively). Identity and purity was confirmed by mass spectrometry (sequence coverage >80%). A yield of 25 mg per 3 L of bacterial cell culture was achieved for each purified protein. Clear-native PAGE (CN-PAGE), a technique that separates proteins based on intrinsic protein charge, was used to assess sample monodispersity under native (non-denaturing) conditions (Fig. 2.0B). Although molecular masses using a protein ladder could not be deduced from CN-PAGE due to inherent limitations of the technique, MMADHCΔ1-12 and MMADHCΔ1-61 migrated as single bands under native conditions,

indicating that the recombinant proteins were stable and homogeneous in solution with no detectable aggregates.

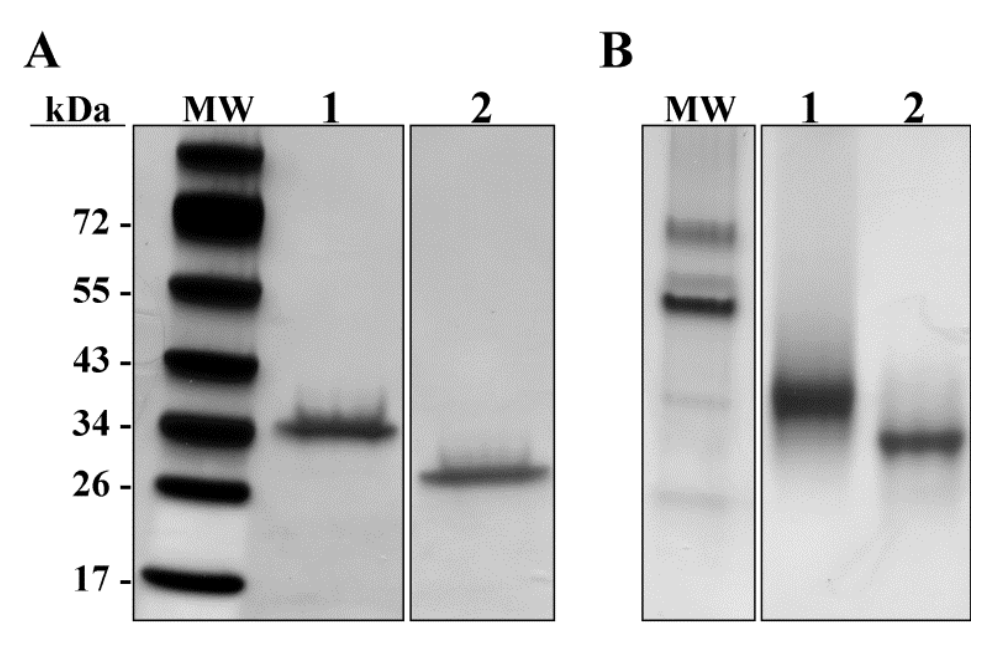


Figure 2.0. Recombinant MMADHC Δ 1-12 and MMADHC Δ 1-61 following size exclusion chromatography. A. SDS-PAGE of MMADHC Δ 1-12 (lane 1) and MMADHC Δ 1-61 (lane 2). B. CN-PAGE of MMADHC Δ 1-12 (lane 1) and MMADHC Δ 1-61 (lane 2).

2.3.1 Immunodetection of MMACHC and MMADHC in human cell lines

A previous study (366) determined that MMACHC in murine tissues exists predominantly as a C-terminally truncated form. In mammals, the final ~40 residues of MMACHC are predicted to be highly disordered; in non-mammalian species, this region is apparently missing (366). Using a monoclonal antibody (mAb) raised against recombinant human MMACHC, we performed immunodetection by Western blotting against human cell lines. Endogenous MMACHC was detected in lysates from whole cells of Human Embryonic Kidney 293 (HEK293), as well as the human fibroblast cell line MCH46 (Fig. 2.1A).

MMACHC migrated to molecular mass of 32 kDa, in agreement with recombinant full-length MMACHC lacking a purification tag (31.9 kDa). These results confirm that human MMACHC

is expressed as a full-length form in HEK and fibroblast cell lines, different from the truncated form previously identified in murine tissue (366).

We also identified the presence of endogenous MMADHC in HEK293 and MCH46 fibroblasts cell lysates using Western blotting with a monoclonal antibody generated against human MMADHC (Fig. 2.1B). MMADHC detected in HEK293 and MCH46 migrated to a molecular mass of 33 kDa, corresponding to purified MMADHCΔ1-12. Endogenous MMADHC could not be detected in *cblD*-combined patient line WG3646 (p.S228X) (380, 381) indicating the absence of full length MMADHC polypeptide. We were unable to detect the presence of smaller MMADHC isoforms in both control fibroblast and HEK293 cell lines and demonstrated that endogenous MMADHC exists only in full-length, in agreement with a report by Stucki *et al.* (380).

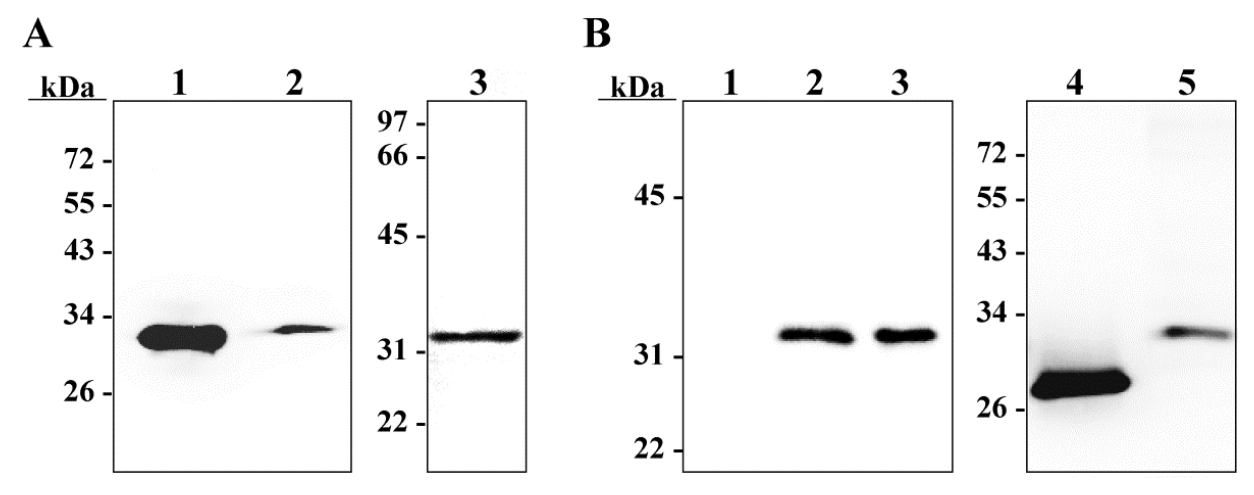


Figure 2.1. Immunodetection of endogenous MMACHC and MMADHC. A. Western blotting against MMACHC; lane 1, recombinant MMACHC; lane 2, soluble HEK lysate; lane 3, soluble MCH46 fibroblast lysate **B.** Western blotting against MMADHC; lane 1, soluble WG3646 fibroblast lysate; lane 2, recombinant MMADHCΔ1-12; lane 3, soluble MCH46 fibroblast lysate; lane 4, recombinant MMADHCΔ1-61; lane 5, soluble HEK lysate.

2.3.2 MMADHC is stable, monomeric, and elongated in solution

Stability and conformational homogeneity of MMADHCΔ1-12 and MMADHCΔ1-61 were quantitatively assessed in solution at high concentrations using dynamic light scattering

(DLS). Hydrodynamic radii (R_H) were 3.5 nm \pm 0.1 nm for MMADHC Δ 1-12 and 3.3 nm \pm 0.1 nm for MMADHC Δ 1-61 (Fig. 2.2A). Scattering intensity derived from these major species corresponded to >90% of total sample intensity and represented >99% of total mass in solution. Furthermore, sample polydispersity (Pd) <25%, sum of squares (SOS) values below 15, and baseline values of 1.000 indicated that both MMADHC proteins were monomodal and conformationally homogeneous (monodisperse) in solution (411). Molecular mass estimations based on R_H calculated for both MMADHC constructs using a globular protein model indicated 74 kDa and 60 kDa for MMADHC Δ 1-12 and MMADHC Δ 1-61, respectively. These values were significantly above the molecular masses for both proteins as calculated from primary sequence and by SDS-PAGE, yet they agreed with values obtained by subjecting each species to size-exclusion chromatography calibrated with globular molecular mass standards (data not shown).

Analytical ultracentrifugation (AUC) was performed to determine oligomeric state. MMADHC Δ 1-12 sedimented to 2.15 S, with frictional ratio (f/f₀) of 1.6 and R_H of 3.5 nm; MMADHC Δ 1-61 sedimented to 1.98 S, with f/f₀ of 1.5 and R_H of 3.1 nm (Fig. 2.2B). Both constructs were >98% monomeric by mass with a calculated molecular mass of 33.0 kDa for MMADHC Δ 1-12 and 26.9 kDa for MMADHC Δ 1-61. Hydrodynamic radii obtained by AUC were consistent with DLS results. The f/f₀ values determined for both constructs were slightly higher than for globular proteins (f/f₀ 1.2-1.3), indicating a more elongated shape (396). These results explained the higher-than-anticipated molecular mass estimations by DLS and SEC, whose models or calibrations are based on globular proteins. In comparison, MMADHC Δ 1-61 was significantly less elongated than MMADHC Δ 1-12, an indication that the N-terminus of MMADHC contributes to this extended shape.

Deviation from globularity in proteins is often an indicator of unstructured/disordered regions. Using secondary structure (PSI-PRED) prediction software (405), MMADHC was assessed as containing significant regions lacking secondary structure, most notably from Nterminal residues 26-109 which correspond to ~30% of all residues (Fig. 2.3). Disorder predictions using DISOPRED2 (406) complemented these findings and identified three intrinsically disordered regions (28-48, 83-106, 124-139) on MMADHC. The presence of regions lacking secondary structure on MMADHCΔ1-12 and MMADHCΔ1-61 was estimated using circular dichroism (CD) spectroscopy (Fig. 2.2C). Both constructs displayed strong positive ellipticity at 193 nm and negative ellipticity at 208 and 222 nm, indicative of α-helical content (412, 413). Spectrum deconvolution using CDSSTR (404) estimated an α -helical content of 33% and 43% for MMADHCΔ1-12 and MMADHCΔ1-61, respectively. Contributions from β-strands were similar for both constructs (10-11%), as was turn content (21%). Unordered content was also estimated in both MMADHCΔ1-12 (36%) and MMADHCΔ1-61 (25%). While accurate estimation of disordered content by CD is inherently difficult, the difference in unordered content between MMADHCΔ1-12 and MMADHCΔ1-61 could be effectively estimated given that our constructs were derived from the same protein and were subjected to identical analyses using the same reference dataset. MMADHCΔ1-61 demonstrated greater total secondary structure (74%) compared to MMADHCΔ1-12 (65%) and, in turn, approximately 11% less unordered content. These results are in agreement with our secondary structure predictions and identify N-terminal residues of MMADHC as contributing to overall disorder.

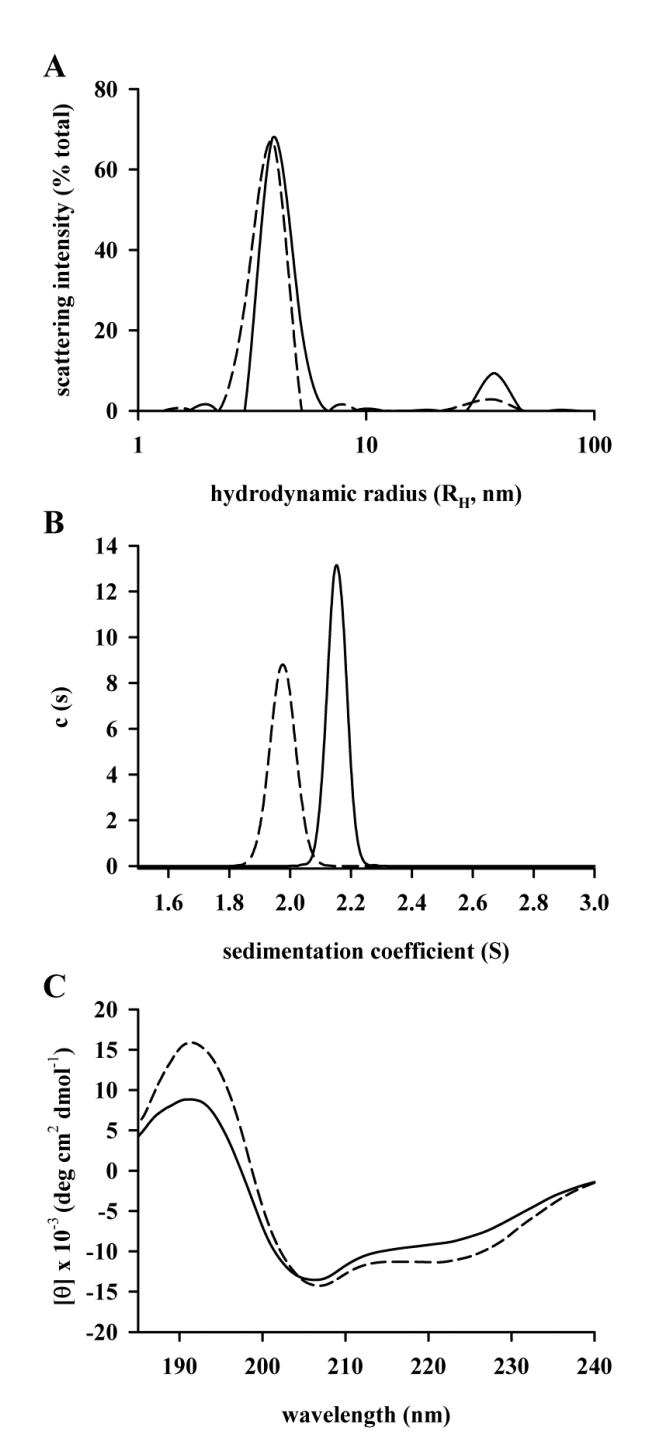


Figure 2.2. Biophysical characterization of MMADHCΔ1-12 and MMADHCΔ1-61. Biophysical characterization of MMADHCΔ1-12 and MMADHCΔ1-61. **A.** By dynamic light scattering (DLS), MMADHCΔ1-12 (solid trace) had an average hydrodynamic radius (R_H) of 3.5 nm \pm 0.1 and MMADHCΔ1-61 (dashed trace) had an average R_H of 3.3 nm \pm 0.1. **B.** Fitting the sedimentation profile of MMADHCΔ1-12 and MMADHCΔ1-61 using the continuous c(s) model in SEDFIT. MMADHCΔ1-12 (solid trace) sedimented to 2.15 S, corresponding to a frictional ratio (f/f_0) of 1.6, a R_H of 3.5 nm, and a molecular mass of 33.0 kDa. MMADHCΔ1-61 (dashed trace) sedimented to 1.98 S, corresponding to a frictional ratio (f/f_0) of 1.5, a R_H of 3.1 nm, and a molecular mass of 26.9 kDa. **C.** CD spectrum of MMADHCΔ1-12 (solid trace) and MMADHCΔ1-61 (dashed trace).

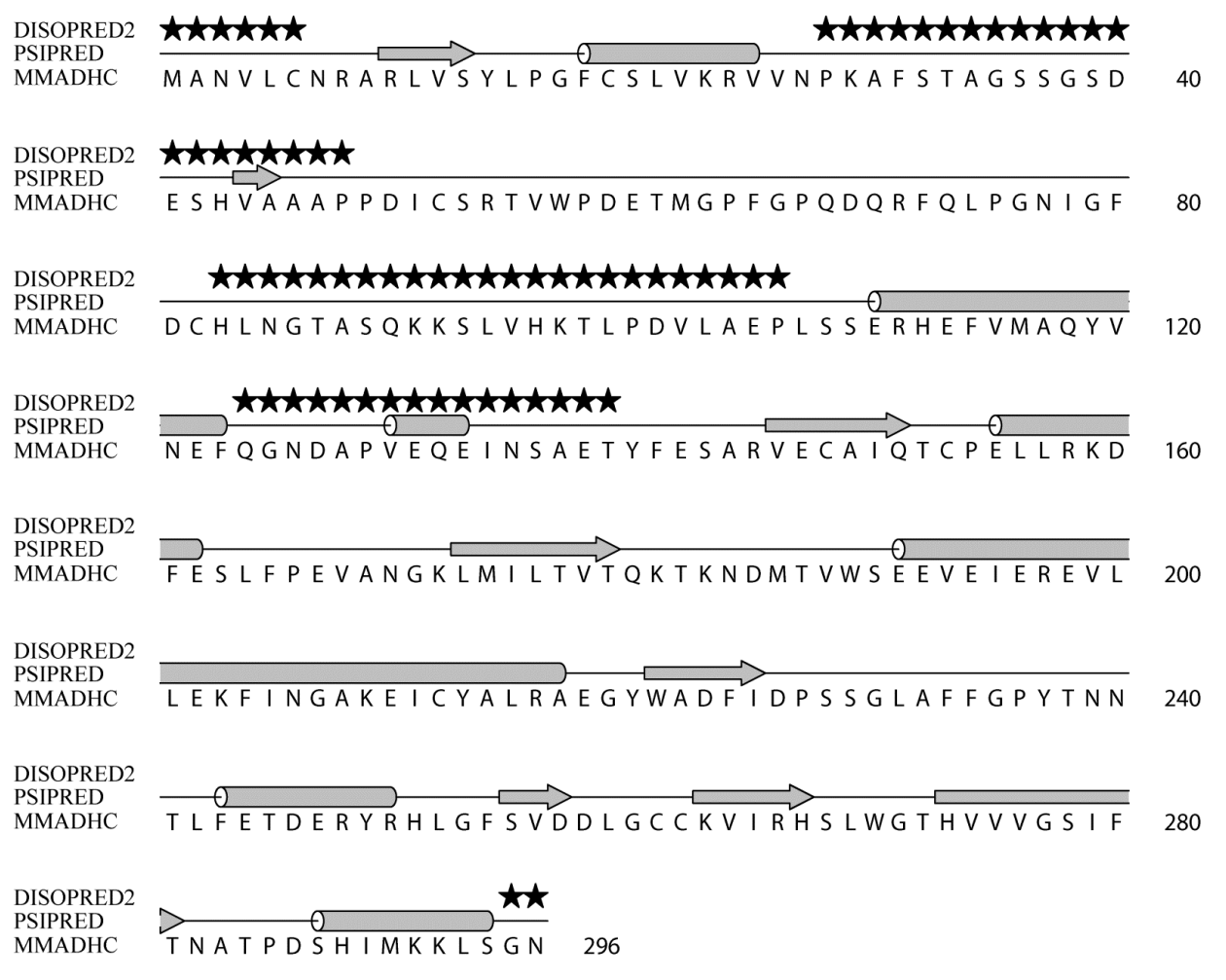


Figure 2.3. Alignment of predicted structural features to sequence of MMADHC. Structural features of MMADHC (UniProt ID: Q9H3L0) were predicted using the secondary structure prediction program PSIPRED (405) and the disorder prediction program DISOPRED2 (406). Black stars correspond to disordered residues by DISOPRED2 using a false positive threshold of 5%. Secondary structure is depicted as β-strands (grey arrows), α-helices (grey cylinders), and random coils (black line) as defined by high-confidence predictions from PSIPRED. Raw data from program output were used to create alignment in the program ALINE (407).

2.3.3 MMADHC does not bind cobalamin

Primary sequence analysis indicated a putative B₁₂-binding motif (81-DXHXXG-86) for MMADHC (379); hence, the ability of MMADHC to bind cobalamin *in vitro* was tested. Addition of a 10-fold molar excess of the four cobalamin derivatives (CNCbl, OHCbl, MeCbl, AdoCbl) to MMADHCΔ1-12 did not significantly alter the R_H by DLS, signifying either that MMADHCΔ1-12 did not bind cobalamin or that binding resulted in only minor changes to the conformation and overall size of the protein (data not shown). This was in contrast to MMACHC, which showed (367) significant R_H changes by DLS upon addition of 10-fold molar excesses of cobalamins, most noticeably AdoCbl and MeCbl.

The stabilization by cobalamins on the melting temperature (T_m) of MMADHC Δ 1-12 was tested by generating thermal curves from DLS data. Protein unfolding by heat results in solvent exposure of hydrophobic groups leading to aggregation with neighboring molecules and successive increase in size. Aggregate formation was monitored by measuring the scattering intensity of protein samples at increasing temperatures, as size is exponentially correlated with scattering intensity. Samples of MMADHC Δ 1-12 and MMADHC Δ 1-61 alone or in the presence of 10-fold molar excess of cobalamins were heated and temperature plotted against total scattering intensity (Fig. 2.4). Baseline values from 20-35°C corresponded well with the previously determined R_H of both MMADHC constructs alone or with cobalamins. In the absence of cobalamins, total scattering intensity increased exponentially above 48°C for MMADHC Δ 1-12 and above 52°C for MMADHC Δ 1-61, a transition point reflecting the melting temperature (T_m) for proteins (391, 392). These values are significantly higher than that reported for full length MMACHC (~40°C) (366, 369). Furthermore, the addition of 10-fold molar excesses of the four cobalamins to either MMADHC construct did not shift the transition points

to a higher temperature, indicating no apparent stabilization by cobalamin. Rather, cobalamin addition decreased thermostability of both constructs: OHCbl by 8-10°C, and CNCbl, AdoCbl, or MeCbl by 4°C. These results contrast greatly with an MMACHC study that demonstrated cobalamin-induced thermostabilization by up to 18°C (369). To complement these data, limited trypsin proteolysis experiments were performed with both MMADHCΔ1-12 and MMADHCΔ1-61. Both constructs were proteolyzed to a similar extent in the absence or presence of cobalamin, indicating no apparent stabilization by cobalamin in solution (data not shown). These results again contrast with a publication (414) demonstrating cobalamin-induced stability for bovine MMACHC.

Confirmation that MMADHC did not bind cobalamin involved incubating samples of MMADHCΔ1-12 or MMADHCΔ1-61 with molar excesses of cobalamins followed by application onto a Superdex 75 size exclusion resin. Elution volumes corresponding to monomeric MMADHCΔ1-12 or MMADHCΔ1-61 were consistent despite addition of cobalamins, indicating no significant conformational changes (data not shown). UV-vis spectroscopy (300-600 nm) failed to detect the presence of cobalamins on eluted monomers, indicating MMADHC constructs did not coelute with bound ligand. Binding isotherms of MMADHCΔ1-12 with cobalamin could not be generated by isothermal titration calorimetry, again indicating MMADHC did not bind or had very low affinity for cobalamin.

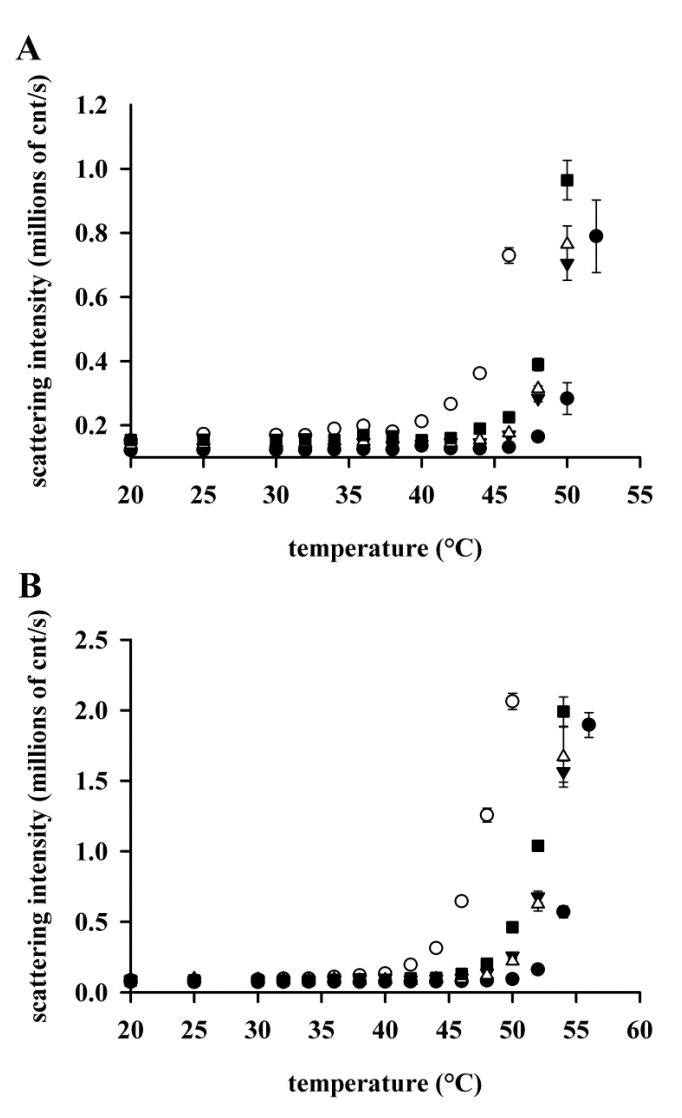


Figure 2.4. Thermostability of recombinant MMADHCs in solution by DLS. A. Thermal profiles of MMADHCΔ1-12 (25 μM) in the absence or presence of 10-fold molar excesses of cobalamin (250 μM) were obtained by monitoring scattering intensity as a function of temperature. Inflection point of MMADHCΔ1-12 alone (•) was determined to be 48°C. Addition of 10x molar excess of CNCbl (Δ), OHCbl (\circ), MeCbl (\blacktriangledown) or AdoCbl (\blacksquare) did not stabilize MMADHCΔ1-12. **B.** Thermal profiles of MMADHCΔ1-61 (25 μM) in the absence or presence of 10-fold molar excesses of cobalamin (250 μM). Inflection point of MMADHCΔ1-61 alone (•) was determined to be 52°C. CNCbl (Δ), OHCbl (\circ), MeCbl (\blacktriangledown) or AdoCbl (\blacksquare) also did not stabilize MMADHCΔ1-61. Scattering intensity was measured as an average of ten (20-30°C) or five (32-60°C) acquisitions for each temperature point; error bars represent % error as determined by Dynamics v6.3.18 software.

2.3.4 Identification of MMADHC- and MMACHC-binding sites on MMACHC by phage display

Thirty five MMADHC-affinity selected peptides were aligned to the primary sequence of MMACHC (Table 2.0), producing clusters at four distinct regions (Fig. 2.5A). Eleven peptides aligned to residues 34-57 (region I). Another eleven aligned to residues 221-238 (region II), and six peptides aligned to residues 236-250 (region III); these regions may be separate or they may form a contiguous region of interaction. Seven peptides aligned to residues 261-280 (region IV). Regions I and II were mapped onto the structure of MMACHC (PDB ID: 3SC0; Fig. 2.5B,C). Region I spanned helix H_C and strand β_2 of the core module of MMACHC. Region II mapped to C-terminal helices H_K and H_L, part of the cap module. These helices undergo major conformational changes when MMACHC binds to cobalamin (366). Both predicted regions show significant surface exposure, except for strand β_2 of region I that forms part of the antiparallel β-sheet buried within the hydrophobic core. Several surface-exposed residues of region I contribute to the crevice involved in coordinating the cofactor tail although they do not directly interact with cobalamin. While regions III and IV could not be mapped to a three dimensional model, these regions are likely extensions of region II and predicted to be part of the 48-residue stretch of disorder at the C-terminus of human MMACHC (366). Disordered residues often indicate regions of protein interactions (415-417).

Table 2.0. MATCH/MatchScan identification of MMADHC affinity-selected Ph.D.-12 and Ph.D.-

C7C peptides aligned to sequence of MMACHC

Peptide ^a	Peptide MATCH	Scoring window	Region	Alignment
	$Score^b$	(residues)		position ^c
TLLSPAQ	15	5	I	34
TLPGTKL	14	6	I	43
G GPILPF	14	6	I	45
Q ppsiyl esyqr	14	6	I	36
DLTRV lppngp r	14	6	I	41
VI lpsmgp hpap	14	6	I	41
GF PLVTLA SKPQ	14	6	I	44
SLPTNA PGLKFL	14	6	I	46
SPNSI PTLA AAR	16	4	I	46
ALPIDYM listp	14	5	I	52
SQHR VLAVPS AN	14	5	I	52
S SHLPAQ	14	6	II	224
P STVPA V	15	5	II	224
TLLSPAQ	15	6	II	234
AYFTS MSHDPRA	14	5	II	221
YMSSP DRQPTLT	13	5	II	222
WHNWL ywsfpp r	16	6	II	222
AATDSP FSSPIA	16	6	II	223
TN tppsqr vhls	21	6	II	225
TWVPYN PGQRL P	16	5	II	227
QSTALL WTHQTL	14	6	II	229
ALLEL PRQIRTS	15	5	II	232
HSSKPFS	15	6	III	240
LPT TSPS	13	4	III	244
SQHRV LAVPS AN	15	5	III	236
DLLPLTH ekps h	16	4	III	241
H SMPSP PSNSIK	15	5	III	244
QTFKANH SPDL V	16	6	III	245
HHS GNPSR NNTG	20	5	IV	261
SSLNPR SLFPHT	16	6	IV	268
QYQMNH SPAVRP	14	6	IV	271
H PRHWPP QINPH	14	6	IV	272
DLT rvlpp ngpr	15	5	IV	272
QYPALPL rvshp	15	5	IV	273
TKLYPAL ppasp	20	5	IV	276

 ^a Scoring window residues in **bold**.
 ^b Score of aligned residues based on modified BLOSUM62 matrix.
 ^c First residue of scoring window aligned to protein sequence.

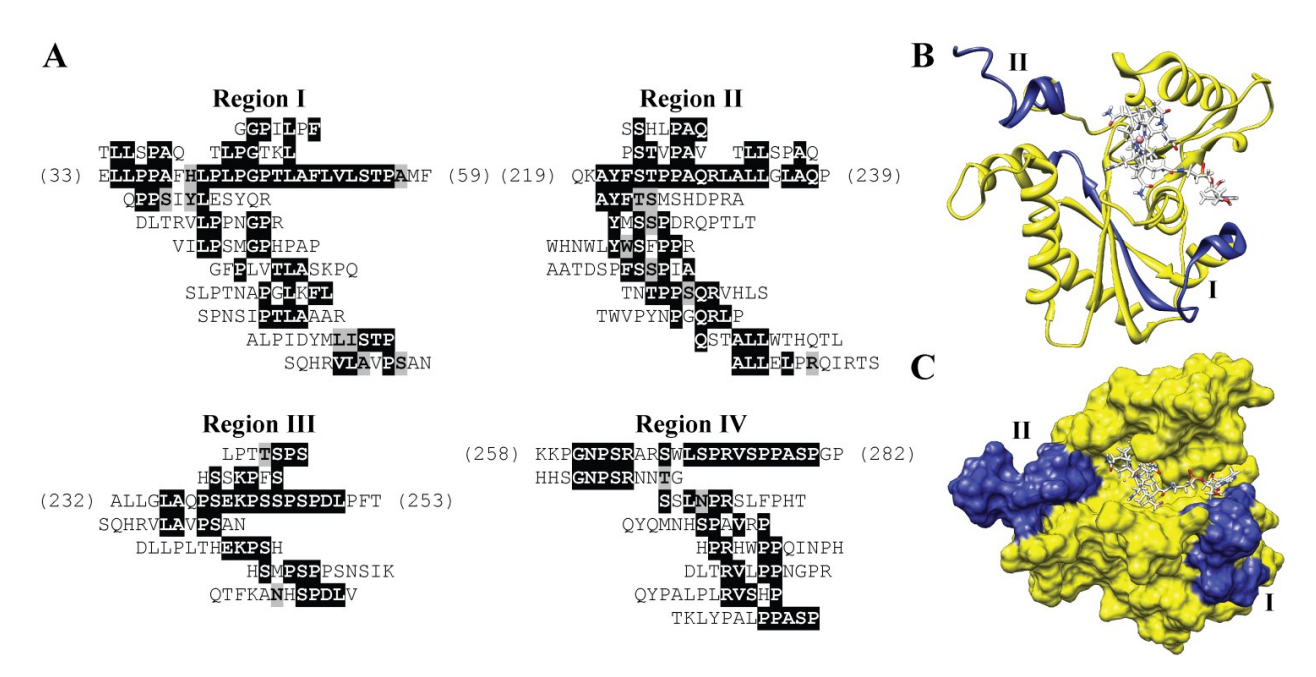


Figure 2.5. Phage display identifies putative MMADHC binding sites on MMACHC. A. MMADHC affinity-selected Ph.D.-C7C and Ph.D.-12 peptides aligned to the primary sequence of MMACHC at four distinct regions (I-IV). Exact sequence matches are highlighted in black; conservative matches are highlighted in gray. **B.** Ribbon representation of MMACHC (yellow) with predicted MMADHC-binding regions shaded blue. **C.** Molecular surface representation of MMACHC (yellow) with predicted MMADHC-binding regions shaded blue. Methylcobalamin bound to MMACHC (PDB ID: 3SC0) is shown in stick representation and colored by atoms (cobalt, pink; carbon, white; nitrogen, blue; oxygen, red; phosphorus, orange).

Phage display was also used to predict regions on MMACHC that may contribute to its forming oligomers. Ensembles of 129 Ph.D.-C7C peptides and 149 Ph.D.-12 peptides previously isolated from MMACHC-binding phages (367) were aligned against the primary sequence of MMACHC using RELIC/MATCH and MatchScan. Twenty unique affinity-selected peptides aligned to the primary sequence of MMACHC (Table 2.1), producing clusters at three distinct regions (Fig. 2.6A). Eight peptides aligned to residues 32-46 (region I) and seven aligned to residues 52-60 (region II). Five peptides aligned to the disordered C-terminus of MMACHC (region III; residues 267-278). Regions I and II mapped to the core module of MMACHC (Fig. 2.6B,C); region I corresponded to helix H_C and region II mapped to residues bordering strand β_2 and helix H_D . Region I is surface-exposed with several residues forming the crevice involved in cofactor binding, whereas region II is buried within the hydrophobic core. These predicted regions border or are incorporated within a region on MMACHC that may be involved in binding MMADHC (region I; Fig. 2.6D). Residues 34-46 of MMACHC appear to form a continuous surface involved in recruiting MMADHC or MMACHC.

Table 2.1. MATCH/MatchScan identification of MMACHC affinity-selected Ph.D.-12 and Ph.D.-C7C peptides aligned to sequence of MMACHC

Peptide ^a	Peptide MATCH	Scoring window	Region	Alignment
_	$Score^b$	(residues)	-	position ^c
LLPPDLS	16	4	I	34
NGM WHLP	13	4	I	39
$ ext{TW}\mathbf{PLPMP}$	15	5	I	42
nvllp sgllstq	15	5	I	32
YVHNP YHLPNP P	16	6	I	39
SMWH ylpl yrdg	13	4	I	40
VFTT LPLPHP NQ	19	6	I	41
HSLRPEWR mpgp	13	4	I	43
VSTPTFY	13	4	II	52
NVLLPSG llst Q	13	4	II	52
AFAKVW ILGTP H	13	5	II	52
KHVPRTE lssp r	13	4	II	53
STPSLHWALHQT	14	5	II	54
STPS AQLGPAPT	13	4	II	54
HWA PSMYD YVSW	14	5	II	56
QTGLSPR	17	7	III	267
\perp RNSPP T	15	5	III	273
SWRSEQLSLPQM	16	8	III	268
HL lspel kllar	13	5	III	270
FQTIP PHISPP F	17	6	III	272

 ^a Scoring window residues in **bold**.
 ^b Score of aligned residues based on modified BLOSUM62 matrix.
 ^c First residue of scoring window aligned to protein sequence.

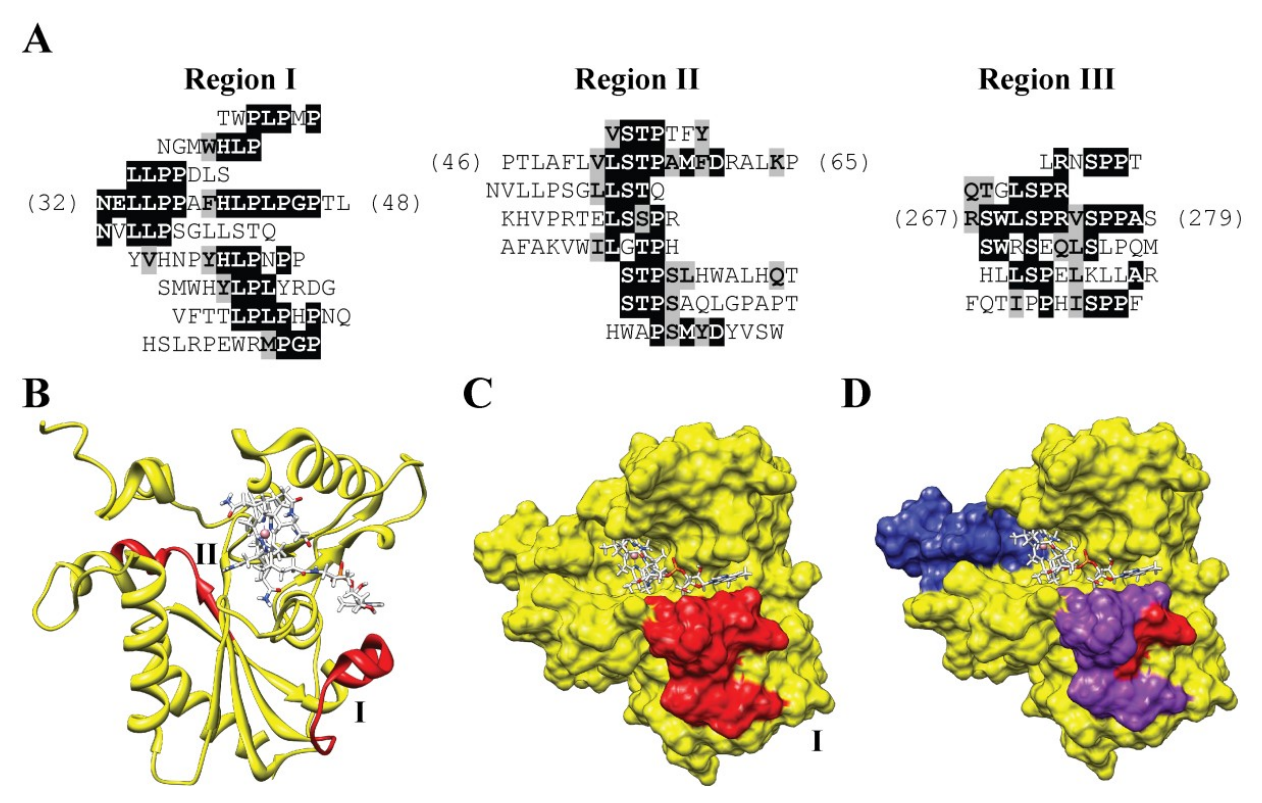


Figure 2.6. Phage display predicts self-binding regions on MMACHC. A. MMACHC affinity-selected Ph.D.-C7C and Ph.D.-12 peptides aligned to the primary sequence of MMACHC at three distinct regions (I-III). Exact sequence matches are highlighted in black; conservative matches are highlighted in gray. **B.** Ribbon representation of MMACHC (yellow) with predicted MMACHC-binding regions shaded red. **C.** Molecular surface representation of MMACHC (yellow) with predicted MMACHC-binding regions shaded red. Methylcobalamin bound to MMACHC (PDB ID: 3SC0) is shown in stick representation and colored by atoms (cobalt, pink; carbon, white; nitrogen, blue; oxygen, red; phosphorus, orange). **D.** Molecular surface representation of MMACHC (yellow) with predicted MMADHC- and MMACHC-binding regions shaded blue and red, respectively. Shared predicted regions of interaction are displayed in purple.

2.3.5 MMADHC∆1-12 and MMADHC∆1-61 bind to MMACHC with similar affinity

Using label-free, real-time surface plasmon resonance (SPR), we investigated binding between solution-phase MMACHC and low density, amine-coupled MMADHC Δ 1-12 (235 RU) and MMADHC Δ 1-61 (220 RU) surfaces. In single-cycle experiments, specific and dose-dependent binding of MMACHC (0-500 nM) to the MMADHC Δ 1-12 and MMADHC Δ 1-61 surfaces was detected (Fig. 2.7). The overall binding responses with MMADHC Δ 1-12 (i.e. $R_{obs} \sim 230$ RU of MMACHC bound at 500 nM) correlated with a 1:1 stoichiometry (i.e. $R_{max} = 257$ RU) and indicated that the amine-coupled MMADHC Δ 1-12 surfaces were active (>90%). Over the identical titration range and similar surface density, the overall binding responses with MMADHC Δ 1-61 were lower (i.e. $R_{obs} \sim 150$ RU vs R_{max} of 296 RU = $\sim 50\%$ surface activity with random amine-coupling procedure). As negative binding controls (data not shown) (i) there was little or no binding of 500 nM BSA or MBP to the immobilized MMADHC surfaces; (ii) there was no non-specific binding of MMACHC to the amine-coupled reference surfaces; and (iii) there were no MMADHC Δ 1-12 or MMADHC Δ 1-61 self-associations when they were flowed over both MMADHC-immobilized surfaces.

Multi-cycle titrations (Fig. 2.8A,B) showed biphasic association phases in the binding profiles. While there were no major differences between titration series with either MMADHC construct, the data deviated from a simple 1:1 kinetics and therefore were analyzed according to the steady-state amounts of MMACHC bound at the end of each association phase (Fig. 2.9A,B). The apparent K_D values indicated that both MMADHC isoforms share similar sub-micromolar binding affinities for MMACHC (217 ± 49 nM and 175 ± 42 nM, respectively).

Because these binding profiles and phage display data implicate MMACHC's selfassociation, we examined solution-phase MMACHC binding to low density, amine-coupled

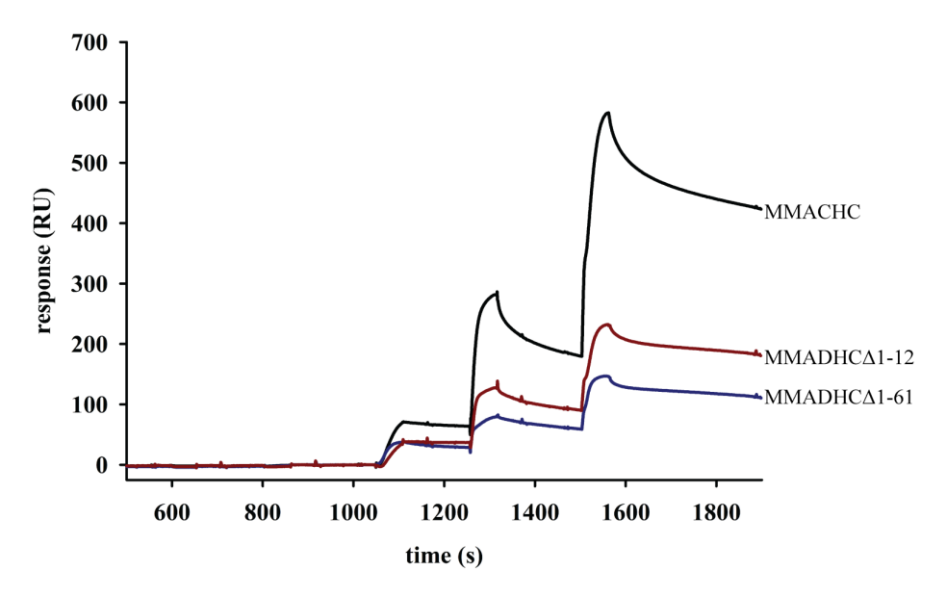


Figure. 2.7 Real-time single-cycle kinetics of MMACHC binding to low-density MMADHCΔ1-12, MMADHCΔ1-61, and MMACHC. Representative single-cycle SPR of MMACHC (0-500 nM; 4-fold dilution series) titrated over amine-coupled surfaces (*red trace*, 235 RU MMADHCΔ1-12; *blue trace*, 220 RU MMADHCΔ1-61; *black trace*, 340 RU MMACHC) at 50 μl/min (60 s association and 30-300 s dissociation).

MMACHC (340 RU) by SPR. Without regeneration until the end of the titration sequence, single-cycle experiments (Fig. 2.7) identified MMACHC–MMACHC signal responses that exceeded 1:1 stoichiometry predictions (i.e. $R_{obs} \sim 580$ RU at 500 nM MMACHC vs. $R_{max} = 340$ RU). With regeneration between sample injections in the multi-cycle titration series (Fig. 2.8C), the overall MMACHC binding responses were less than R_{max} but biphasic association phases were again apparent. The self-association of MMACHC (K_D 525 \pm 270 nM; Fig. 2.9C) likely explains why the MMADHC Δ 1-12 and MMADHC Δ 1-61 titration series exhibited complex kinetics: biphasic association and slow dissociation.

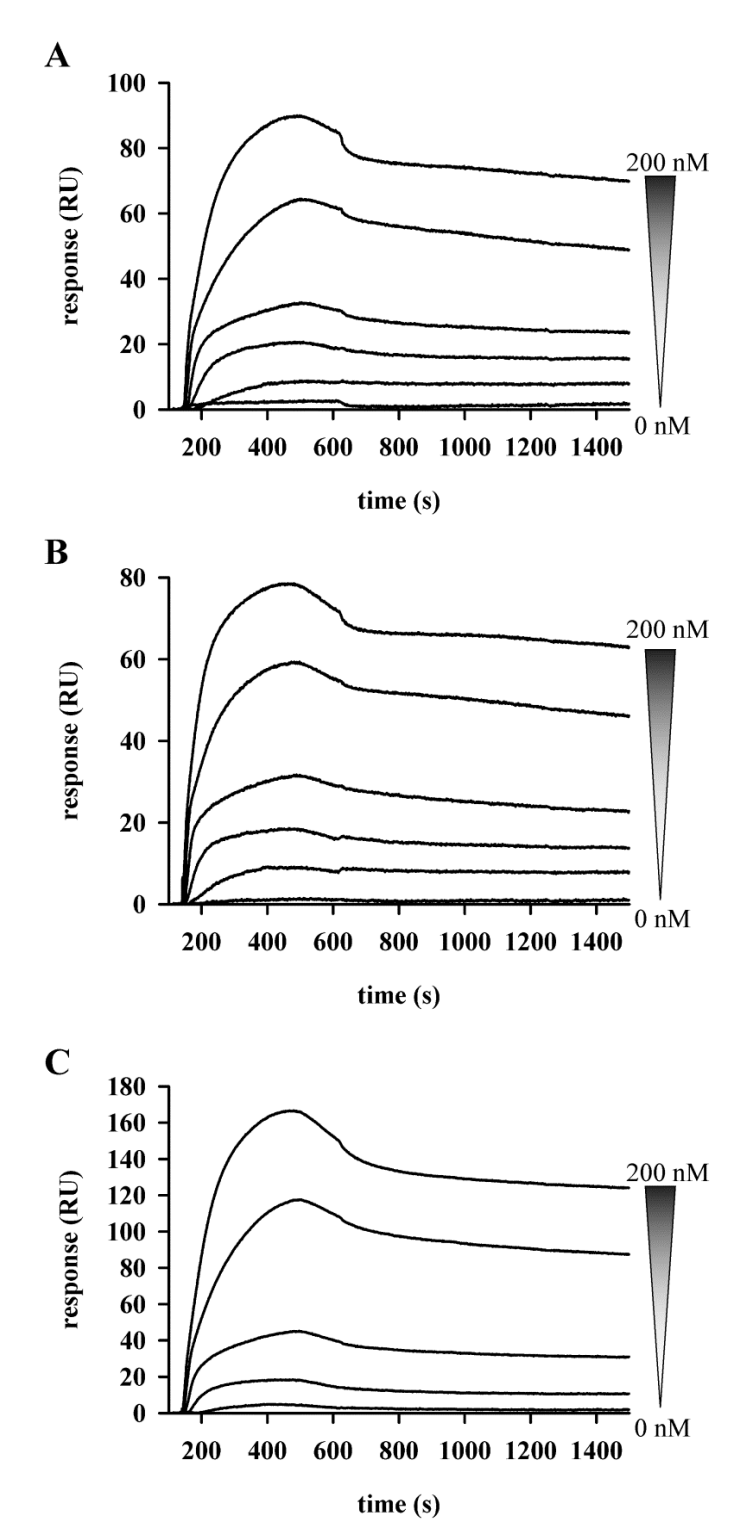


Figure. 2.8. Real-time multi-cycle kinetics of MMACHC binding to low-density MMADHCΔ1-12, MMADHCΔ1-61, and MMACHC. Representative multi-cycle SPR of MMACHC (0-200 nM; 2-fold dilution series) titrated over amine-coupled surfaces (A, 235 RU MMADHCΔ1-12; B, 220 RU MMADHCΔ1-61; C, 340 RU MMACHC) at 25 μl/min (8 min association and 15 min dissociation).

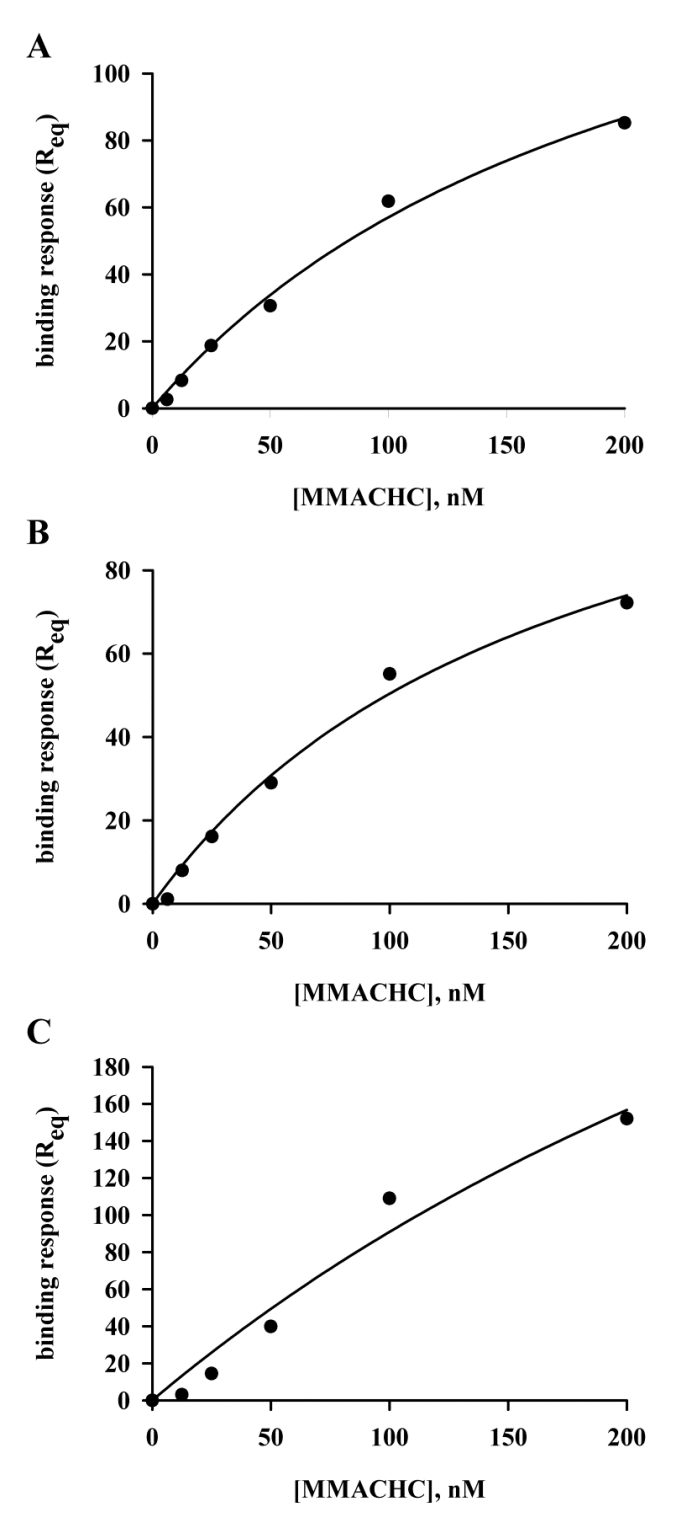


Figure. 2.9. Representative fitting of SPR data to steady-state affinity model. Non-linear regression analysis for equilibrium amounts of MMACHC bound (R_{eq}) as a function of concentration. Over each amine-coupled surface (\mathbf{A} , 235 RU MMADHC Δ 1-12; \mathbf{B} , 220 RU MMADHC Δ 1-61; \mathbf{C} , 340 RU MMACHC), the apparent equilibrium dissociation constants represent the average of duplicate injections acquired from three independent trials.

2.4 Discussion

Though the gene encoding MMADHC was recently identified (379), there have been few studies that elucidate its function. Our study provides new insights into the intracellular cobalamin metabolic pathway by characterizing recombinant MMADHC. From mutant phenotypes that result in either isolated methylmalonic aciduria type D or homocystinuria (379-381), MMADHC is proposed to be bifunctional. Since methylmalonic aciduria is associated with defects in the mitochondrial cobalamin pathway and homocystinuria is associated with deficiencies in the cytoplasmic cobalamin pathway, MMADHC may function in both subcellular compartments through mechanisms still poorly understood, though the involvement of the MTS has been implicated (380). Here, we report purification of two recombinant MMADHC constructs, MMADHC Δ 1-12 and MMADHC Δ 1-61. As predicted by Mitoprot II (418), MMADHC Δ 1-12 corresponds to the form of MMADHC localized to the mitochondrion (379) after processing of the MTS. This proposed isoform was also selected over full length MMADHC previously used by Plesa et al. (367), because cleavage and removal of the MBP fusion partner by TEV protease was greatly enhanced. MMADHCΔ1-61 corresponds to a cytoplasmic form detected in some *cblD*-MMA patients (380). Both constructs were highly pure (>95%), monodisperse, stable in solution, and monomeric as assessed by SDS-PAGE, CN-PAGE, DLS and AUC.

From primary sequence analysis, the unstructured N-terminal domain of MMADHC includes a predicted cobalamin-binding motif (81-DXHXXG-86). Our data indicate that MMADHC was not stabilized by cobalamin nor binds cobalamin *in vitro*. Notably, our thermostability assay demonstrated reduced stability for both MMADHC constructs when 10-fold molar excesses of cobalamin were added to either construct. We attribute this to non-

specific interactions between cofactor and protein since destabilization was only observed at substantial cobalamin concentrations. The non-specific reactivity of cobalamins with MMADHC was likely caused by the presence of the reducing agent TCEP in our buffers, which can generate reactive cob(II)alamins (419, 420). Proportional decreases in thermostability were detected when cobalamin was added in 10-100 fold molar excesses, indicative of non-saturable binding. Cobalamin concentrations used in this assay (250 µM) attempted to saturate the predicted ligand-binding site and did not reflect physiological values in human tissues (30–700 nM) (44). Removal of TCEP from our buffers made both MMADHC constructs significantly more thermolabile and addition of cobalamins had no apparent effect on thermostability. Lastly, titrating lower concentrations of cobalamin against MMADHCΔ1-12 did not produce binding isotherms using a calorimetry-based technique, indicating cobalamin does not specifically bind MMADHC even at reduced concentrations. Overall, these results are in direct contrast to MMACHC, previously shown to bind all cobalamin derivatives with low micromolar affinity (367-369) and resulting in stabilization by up to 18°C (369). They also agree with a complementation study in which a derivative of MMADHC lacking the first 115 residues stimulated MeCbl synthesis equally well in cblD-combined patient fibroblasts compared to wildtype (380). The authors concluded that residues N-terminal to Met₁₁₆, including the predicted cobalamin binding site, are dispensable for MeCbl synthesis in the cytoplasm. While the possibility exists that MMADHC uses cobalamin for the mitochondrial reaction, our in vitro results suggest otherwise.

We detected full-length endogenous MMACHC and MMADHC in two human cell lines using Western blotting. Readily available, patient and control fibroblast lines provided clinically-relevant cells for study, whereas HEK cells expressed MMACHC and MMADHC in

greater abundance; both cell lines gave complementary results. Immunoblotting of endogenous MMACHC in HEK and fibroblast cell lines corresponded to a full length version that migrated as our recombinant full-length MMACHC lacking a purification tag. Our study could not detect a smaller (27 kDa) MMACHC derivative previously identified in murine tissue (366). Based on our results, MMACHC is expressed as a full-length form in human cell lines. While endogenous MMADHC migrated to a molecular mass that corresponded with our recombinant MMADHC Δ 1-12, we could not confirm the removal of the predicted mitochondrial targeting sequence in endogenous MMADHC given only the ~1 kDa difference in theoretical molecular mass between endogenous and our recombinant form. Despite using a monoclonal anti-MMADHC antibody that targeted C-terminal residues (239-253) of MMADHC, we failed to detect smaller isoforms of MMADHC in our control fibroblast and HEK cell lines. We detected MMADHC as full-length in healthy patients; smaller isoforms are restricted to cblD-MMA patients, as previously identified (380). Given three *cblD* phenotypes, it is hypothesized that MMADHC exists in both the mitochondrion and the cytoplasm. Our results indicate that MMADHC exists only in full-length and is likely targeted to both compartments within the cell, in agreement with a previous report (380).

Biophysical characterization of MMADHC Δ 1-12 and MMADHC Δ 1-61 provided contrast into structural features. From thermal scattering curves, melting temperatures of 48°C and 52°C were deduced for MMADHC Δ 1-12 and MMADHC Δ 1-61, values greater than those reported for MMACHC (~ 40°C) (366, 369) and MMACHC lacking ~ 40 C-terminal residues (46.6°C) (366). The increased stability of MMADHC Δ 1-61 in solution compared to MMADHC Δ 1-12 was likely the result of greater secondary structure content and fewer disordered regions as estimated by circular dichroism spectroscopy. These results were in

agreement with PSI-PRED and DISOPRED predictions in demonstrating that the N-terminus of MMADHC is poorly structured. These disordered regions contributed to the overall shape of the protein as MMADHCΔ1-61 was more globular than MMADHCΔ1-12 by analytical ultracentrifugation (396). Overall, our biophysical results indicate that MMADHC may contain two structurally distinct domains. The N-terminal domain is largely unstructured and contributes to the overall asymmetric shape of MMADHC; this region likely encompasses residues 1-140 based on our predictions. The C-terminal domain, residues 141-296, has significantly greater secondary and tertiary structure which results in a well-folded region consistent with most globular proteins. This hypothesis is in agreement with a previous report (380) proposing MMADHC has two functional domains: an N-terminal domain that interacts with mitochondrial targets, and C-terminal domain that interacts with MMACHC or other cytoplasmic targets. Expectedly, regions on MMADHC predicted to interact with MMACHC (367) all localize to this proposed C-terminal domain.

Complementing these results are phage display predictions of MMADHC-interacting sites on MMACHC and regions on MMACHC that may contribute to its forming multimers. Overall, our results identify multiple recruitment sites on MMACHC. Two sites are involved in uniquely docking MMADHC (Fig. 2.5A, regions II and III); these may be separate docking regions or may form a continuous surface. The other regions appear to bind either MMADHC (Fig. 2.5A, regions I, IV) or MMACHC (Fig. 2.6A, regions I, II, III). Mapped onto the three dimensional structure, these shared regions of interaction corresponded to residues on the surface of MMACHC that likely play a structural role not directly involved in binding cobalamin, as well as residues buried deep within the hydrophobic core. Because phage display results are predictive and not absolute, these solvent-inaccessible residues may represent false positives

associated with the methodology. However, our predictions are strengthened by high-scoring peptides that align only to surface-exposed regions on MMACHC. For instance, a unique MMADHC-binding site not involved in docking MMACHC was mapped to H_K and H_L of the cap module, corresponding to helices thought to undergo major conformational changes upon binding of cobalamin and/or glutathione (366). We hypothesize that ligand binding may signal dissociation from MMACHC or recruitment of MMADHC.

Our SPR titrations complement the phage display data (367) in that the N-terminus of MMADHC (residues 1-61) is not essential for binding to MMACHC. This result builds upon our previous preliminary identification and characterization of the MMACHC-MMADHC interaction (367) in which solution-phase MBP-MMADHC was titrated over thiol-coupled MMACHC. Specific and dose-dependent binding responses were observed at that time, but heterogeneous, MBP-tagged MMADHC preparations complicated the estimates of binding constants. In the present study, we validated MMACHC-MMADHC interactions by reversing the ligand-analyte orientation, utilizing a different coupling strategy, and employing homogeneous, tag-free MMADHC. Overall, our SPR results demonstrate that the C-terminal regions of MMADHC are important for binding to MMACHC. Removing the first 61 amino acids at the N-terminus of MMADHC had no effect on the binding kinetics, in agreement with the five MMACHC-binding sites (all C-terminal to Met₆₂) that we previously identified on MMADHC (367). Our SPR results also complement the phage display data in that MMACHC can self-associate, but we were unable to assess its multimeric status by AUC because of limited solubility (µg/ml) compared to MMADHC preparations (mg/ml). In contrast, no binding responses were observed when both MMADHC constructs were flowed over MMADHCΔ1-12 or over MMADHC Δ 1-61 surfaces. The lack of self-association within or between the

MMADHC species agrees with DLS, SEC and AUC results indicating that MMADHC Δ 1-12 and MMADHC Δ 1-61 are monomeric in solution.

We conclude that the function of MMADHC is exerted through C-terminal residues that mediate its interaction with MMACHC, as opposed to binding cobalamin directly. In contrast, we cannot attribute any function to the unstructured N-terminal residues. Based on our phage display data, it is tempting to speculate that MMACHC may be involved in recruiting subunits of both MMACHC and MMADHC. This would contribute to a larger complex that would sequester and protect this reactive cofactor from its entry point into the cytoplasm through the lysosome until its delivery to target enzymes.

2.5 Acknowledgments

Research was supported by operating grants to J.W.C. from the Natural Sciences and Engineering Research Council (NSERC; RGPIN 7289-06-07) and to D.S.R. from the Canadian Institutes of Health Research (CIHR; MOP-15078). Sheldon Biotechnology Centre is supported by a Research Resource Grant from CIHR (200610PRG-165657-PRG-CFAA-11449). Canada Foundation for Innovation provided infrastructure for surface plasmon resonance to the Montreal Integrated Genomics Group for Research on Infectious Pathogens. J.C.D. is recipient of a Canada Graduate Scholarship from NSERC and doctoral research award B2 from the Fonds Québécois de la Recherche sur la Nature et les Technologies (FQRNT). The authors wish to thank David Coelho for generously providing the monoclonal anti-MMADHC antibody, Bernard F. Gibbs (Sheldon Biotechnology Centre) for mass spectrometry services, Valentin Dan Nelea and Dieter Reinhardt (McGill University) for training and use of the circular dichroism spectrometer, Nadeem Siddiqui (McGill University) for training and use of the analytical

ultracentrifugation hosted at the Institute for Research in Immunology and Cancer (IRIC, Université de Montréal) and James Féthière (IRIC) for the pETM-41 plasmid.

Preface to chapter 3

In chapter 2 we described the recombinant production and characterization of MMADHC isoforms. Additionally, we described an *in vitro* interaction between MMACHC and MMADHC. The range of phenotypes associated with *MMADHC* mutations has given rise to the hypothesis that intracellular MMADHC localizes to both the mitochondria and cytoplasm. In chapter 3, we set out to determine the subcellular location of MMADHC using a combinatory approach of immunofluorescence microscopy and subcellular fractionation. We demonstrate that MMADHC is found exclusively as a full-length protein in both the cytoplasm and mitochondria, indicating a mechanism for dual localization of the protein. Further, we demonstrate that a truncated isoform found in *cblD*-MMA patients localizes exclusively to the cytoplasm. Based on conflicting reports for MMACHC, we determine that MMACHC localizes to the cytoplasm. Localization of both MMACHC and MMADHC to the cytoplasm extends our understanding of the MMACHC–MMADHC interaction and proposes that MMACHC may play a role in the dual localization of MMADHC.

Chapter 3

Subcellular location of MMACHC and MMADHC, two human proteins $central\ to\ intracellular\ vitamin\ B_{12}\ metabolism$

Wayne Mah, Justin C. Deme, David Watkins, Stephen Fung, Alexandre Janer, Eric A. Shoubridge, David S. Rosenblatt, James W. Coulton

Molecular Genetics and Metabolism (2013). 108(2): 112-118

Copyright © 2013, Elsevier Ltd All rights reserved

3.0 Summary

MMACHC and MMADHC are the genes responsible for cblC and cblD defects of vitamin B₁₂ metabolism, respectively. Patients with *cblC* and *cblD* defects present with various combinations of methylmalonic aciduria (MMA) and homocystinuria (HC). Those with cblC mutations have both MMA and HC whereas cblD patients can present with one of three distinct biochemical phenotypes: isolated MMA, isolated HC, or combined MMA and HC. Based on the subcellular localization of these enzymatic pathways it is thought that MMACHC functions in the cytoplasm while MMADHC functions downstream of MMACHC in both the cytoplasm and the mitochondrion. In this study we determined the subcellular location of MMACHC and MMADHC by immunofluorescence and subcellular fractionation. We show that MMACHC is cytoplasmic while MMADHC is both mitochondrial and cytoplasmic, consistent with the proposal that MMADHC acts as a branch point for vitamin B₁₂ delivery to the cytoplasm and mitochondria. The factors that determine the distribution of MMADHC between the cytoplasm and mitochondria remain unknown. Functional complementation experiments showed that retroviral expression of the GFP tagged constructs rescued all biochemical defects in cblC and cblD fibroblasts except propionate incorporation in cblD-MMA cells, suggesting that the endogenous mutant protein interferes with the function of the transduced wild type construct.

3.1 Introduction

Vitamins are essential nutrients required for normal growth, development, and function in mammals. Acquired from the diet, vitamin B₁₂ (cobalamin) is metabolized within the cell into two physiologically relevant forms, methylcobalamin (MeCbl) and adenosylcobalamin (AdoCbl) (421). Defects in intracellular vitamin B₁₂ metabolism were originally identified by studying patients with rare, inherited defects in this pathway, resulting in the identification of nine

complementation groups: *cblA-cblG*, *cblJ*, and *mut* (286, 342). Inborn errors affecting synthesis of AdoCbl result in a decreased function of the mitochondrial enzyme methylmalonyl-CoA mutase (MUT or MCM) and accumulation of its substrate, methylmalonic acid. Inborn errors affecting methylcobalamin result in a decreased activity of the cytoplasmic enzyme methionine synthase (MS or MTR) and accumulation of its substrate homocysteine. Defects in early steps of the pathway that are common to the synthesis of both cobalamin coenzymes result in accumulation of methylmalonic acid and homocysteine. Methylmalonic acidemia/aciduria (MMA) is associated with episodes of life-threatening metabolic acidemia and long-term development of neurologic and renal problems. Hyperhomocysteinemia and homocystinuria (HC) are associated with megaloblastic anemia and a variety of neurologic defects (285). Inborn errors of cobalamin metabolism may present with isolated MMA, isolated HC, or combined MMA and HC depending upon which step in the pathway is affected.

The subcellular locations of MS and MCM play important roles in the metabolism and dispersion of vitamin B₁₂ throughout the cell. MS functions in the cytoplasm, whereas MCM resides in the mitochondrion (422, 423). The *cblC* and *cblD* complementation groups exhibit unique biochemical phenotypes. *cblC* presents exclusively as combined MMA and HC whereas *cblD* patients can have three distinct phenotypes: isolated homocystinuria (*cblD*-HC), isolated methylmalonic aciduria (*cblD*-MMA), or combined homocystinuria and methylmalonic aciduria (*cblD*-MMA/HC) (354, 379). Based on phenotypic presentation and the known subcellular localization of MS and MCM, it is thought that MMACHC functions in the cytoplasm upstream of MMADHC. MMADHC would then act as a branch point for vitamin B₁₂ delivery between the cytoplasm and mitochondria. Further, MMACHC and MMADHC have been shown to complex *in vivo* and *in vitro* (367, 424). Genotype–phenotype correlation

analysis of the three *cblD* variants suggests that the N- and C-termini of MMADHC have specific functions in the mitochondrion and cytoplasm, respectively (379-381). Mutations in *cblD*-MMA patients result in premature translation termination at the protein level before Met₆₂ or Met₁₁₆. Reinitiation of translation at one of these residues could produce truncated versions of MMADHC lacking the N-terminal residues. These MMADHC isoforms would permit cytoplasmic MS function but lack mitochondrial MCM function. In contrast, *cblD*-HC patients have mutations at conserved residues at the C-terminus but retain integrity of N-terminal residues proposed to be involved in mitochondrial MCM function. Finally, *cblD*-MMA/HC patients have mutations after Met₁₁₆, creating severely truncated proteins. In summary, *cblD*-MMA retains cytoplasmic function due to translation of an error-free C-terminus facilitated by downstream reinitiation; *cblD*-HC retains mitochondrial function with a full-length protein which harbors only C-terminal missense mutations in conserved residues; and in *cblD*-MMA/HC complete loss of functionality occurs with nonsense or splicing mutations that are localized downstream of Met₁₁₆.

Here we report the subcellular location of MMACHC and MMADHC as determined from overexpressing GFP (green fluorescent protein)-fusions in transduced fibroblasts and from endogenous protein in control fibroblasts. To study the localization of proposed MMADHC isoforms, truncated MMADHC corresponding to translation initiation at Met₆₂ (MMADHCΔ1-61) was also studied. Subcellular localization was determined by immunofluorescence imaging and subcellular fractionation with immunoblotting, and the functionality of the fusion proteins was determined by biochemical complementation analysis.

3.2 Materials and Methods

3.2.0 Cloning

cDNA sequences of *MMACHC* and *MMADHC* were cloned into the pEGFP-N1 vector (Clontech) via restriction digestion and ligation using XhoI and BamHI restriction sites to incorporate a C-terminal GFP. *MMACHC-GFP*, *MMADHC-GFP* and *MMADHCΔ1-61-GFP* were subsequently PCR amplified to incorporate *attB1* and *attB2* recombination sites for Gateway cloning (Invitrogen). Oligonucleotide primers are shown in Table 3.0. Gene fusions were then cloned into the Gateway-modified retroviral mammalian expression vectors pBabe (MMACHC-GFP) or pLXSH (MMADHC-GFP and MMADHCΔ1-61-GFP) following manufacturer's protocols.

Table 3.0. Primers used to produce MMACHC and MMADHC constructs

Name Sequence				
Restriction Digestion-Ligation into pEGFP-N1				
MMACHC XhoI forward	CCGCTCGAGATGGAGCCGAAAGTCGCA			
MMACHC BamHI reverse	CCGCTCGAGATGGCCAATGTGCTTTGT			
MMADHC XhoI forward	CGCGGATCCCGAGGGCCAGGGGATGC			
MMADHC BamHI reverse	CGCGGATCCCGATTTCCACTTAATTTCTTCATAAT			
Gateway				
MMACHC forward	GGGGACAAGTTTGTACAAAAAAGCAGGCTTCACCATGGAGCCGAAAGTCGCA			
MMADHC forward	GGGGACAAGTTTGTACAAAAAAGCAGGCTTCACCATGGCCAATGTGCTTTGT			
MMADHCΔ1-61 forward	GGGGACAAGTTTGTACAAAAAAGCAGGCTTCACCATGGGACCCTTTGGACCT			
EGFP reverse	GGGGACCACTTTGTACAAGAAAGCTGGGTTTTACTTGTACAGCTCGTC			

3.2.1 Gene transduction

Retroviral constructs were transiently transfected into a Phoenix packaging cell line with the HBS/Ca₃(PO₄) method (425). Patient and control fibroblasts were infected 48 h later by exposure to viral media in the presence of 4 mg/ml polybrene for 24 h followed by removal of viral media and growth in selective media for 2–4 weeks. Patient genotypes are detailed in Table 3.1.

Table 3.1. Genotypes of transduced patient fibroblasts

cblD	Allele 1		Allele 2	
<u>Phenotype</u>	Nucleotide change	Protein (predicted)	Nucleotide change	Protein (predicted)
MMA / HC	c.683>T	p.S228X	c.683>T	p.S228X
MMA	c.60insAT	p.L20fsX21	c.455dupC	p.T152fsX162
НС	c.737A>G	p.D246G	c.737A>G	p.D246G
cblC	Allele 1		Allele 2	
<u>Phenotype</u>	Nucleotide change	Protein (predicted)	Nucleotide change	Protein (predicted)
MMA / HC	c.394C>T	p.R132X	c.394C>T	p.R132X

3.2.2. Cell culture

Cultured skin fibroblasts were grown in Dulbecco's modified Eagle's medium supplemented with 10% fetal calf serum at 37°C in an atmosphere of 5% CO₂ in air. Antibiotics (200 units/ml hygromycin or 2.5 µg/ml puromycin) were added to media propagating transduced fibroblast cell lines. Control fibroblasts were propagated in media free of antibiotics.

3.2.3 Mitochondrial isolation

Fibroblasts were grown to confluence (10-15 x 150 mm plates) and pelleted by centrifugation for 5 min at $600 \times g$. Cells were washed twice with PBS and resuspended in ice-cold isolation buffer (220 mM mannitol, 20 mM sucrose, 5 mM HEPES-KOH, pH 7.5, 1 mM EGTA, 1 x Complete protease inhibitor) and lysed by 10 passes through an ice-cold Potter Elvehjem zero-clearance homogenizer (Kimble/Kontes, Vineland, NJ). All subsequent centrifugation steps were carried out at 4° C and cell solutions were kept on ice at all times. Cellular debris was pelleted and removed by centrifugation of the homogenate 3-4 times for 10 min at $600 \times g$ until a pellet was no longer observed. The supernatant was retained and crude mitochondria were collected by centrifugation for 10 min at $7000 \times g$. Supernatant was retained as the soluble fraction containing cytoplasmic contents including lysosomes, microsomes and ER. The pellet was gently washed with isolation buffer and then resuspended in isolation buffer and centrifuged for 10 min at $10,000 \times g$. Pure mitochondria were obtained by differential

centrifugation through a stepwise Percoll density gradient: 0.5 ml 80%, 1 ml 52% and 1.5 ml 26% Percoll in a 4 ml centrifuge tube (Ultra-Clear, Beckman Coulter) at 59,000 x g for 45 min (Beckman SW 60 Ti rotor). Mitochondria were collected at the 26%/52% Percoll interface (401). Mitochondrial fractions were resuspended in 5 ml isolation buffer and pelleted by centrifugation in 1.5 ml Eppendorf tubes for 10 min at 7000 x g. The mitochondrial pellet was solubilised in 1.5% n-dodecyl- β -d-maltoside (DDM) and incubated for 1 h on ice to harvest proteins. The suspension was then pelleted by centrifugation at 12,000 x g for 20 min, retaining the soluble fraction. Cytoplasmic components collected earlier were additionally purified from trace mitochondria by centrifugation at 7000 x g for 10 min. To achieve quantities sufficient for visualization by Western blotting, this fraction was concentrated to half-initial volume using a Vacufuge (Eppendorf) at 30°C. Whole cell lysates were obtained by solubilization of harvested fibroblasts in 1.5% DDM.

3.2.4 Immunoblotting

Isolated protein samples were resolved by SDS-PAGE through 10% or 12% acrylamide or 4%-10% acrylamide gradient gels (Bio-Rad) followed by semi-dry transfer (Bio-Rad) onto polyvinylidene fluoride membrane (Millipore). After blocking in TBS containing 0.1% Tween-20 (Sigma) (TBST) with 5% non-fat dry milk (Rockland Immunochemicals Inc.), membranes were probed with monoclonal antibodies: anti-MMACHC (Neuromab, Berkeley, USA), anti-MMADHC (AMSBio, Lugano, Switzerland), anti-GFP (Allele Biotech), anti-SDHA (Abcam); or with polyclonal anti-SOD1 (Stressgen). Following washing in TBST and incubation of secondary HRP antibodies (Jackson Immunoresearch), immunoreactive proteins were visualized with Immobilon Western Chemiluminescent HRP substrate (Millipore) on a FluorChem FC2 fluorescence imaging system (Alpha Innotech) utilizing a chemiluminescence imaging filter.

3.2.5 Immunofluorescence

Coverslips were coated with 0.01% polylysine (Sigma) in PBS for 10 min at 37°C followed by rinsing with PBS. Cells grown on coverslips were rinsed with PBS and fixed with 4% formaldehyde (Sigma) in PBS for 10 min at 37°C. All subsequent incubations were conducted at 25°C and were preceded by multiple washes with PBS. Cells were permeabilized with 0.1% Triton X-100 (Fisher) in PBS for 15 min. Blocking of non-specific antigenic sites was carried out using a blocking solution containing 4% BSA (Fisher) in PBS for 30 min and then cells were incubated with primary antibody in blocking solution for 2 h at 25°C. Secondary antibody in blocking solution was applied for 1 h followed by coverslip mounting in Geltol mounting medium (Thermo). Antibodies used for staining included mouse monoclonal anti-GFP antibody (1:500) to stain GFP-fusion proteins, and rabbit polyclonal anti-SLIRP antibody (1:300) (Abcam) to stain mitochondria. Fluorescent secondary antibodies (1:1000) were goat anti-mouse Alexa488 and goat anti-rabbit Alexa594 (Invitrogen). Immunofluorescence images were obtained using a wide-field fluorescence microscope (Imager A1, Zeiss) using a 60x oil immersion objective and filter sets selecting for the excitation and emission of Alexa488 (Filter Set 10, Zeiss) and Alexa594 (Filter Set 20, Zeiss). In the absence of laser-based illumination, samples were imaged in the presence and absence of mitochondrial staining to ensure that coincidental excitation of Alexa594-stained mitochondria did not contribute to target immunofluorescence. By imaging a control fibroblast cell line subjected to identical staining procedures and imaged using identical exposure times, background fluorescence was determined.

3.2.6 Biochemical studies

Incorporation of label from [14C]propionate and [5-14C]methyl-THF into trichloroacetic acid precipitable cellular macromolecules was performed as previously described (426).

Fibroblasts were plated in 35 mm tissue culture dishes at a density of 400,000 cells per dish. Cultures were incubated for 18 h in medium supplemented with either [14C]propionate (Perkin Elmer) or [5-14C]methyl-THF (Quotient Bioresearch) at 37°C in 5% CO₂. After incubation, cultures were washed with PBS and cellular macromolecules were precipitated by exposure to 5% (w/v) trichloroacetic acid at 5 °C. Precipitated material was dissolved in 0.2 N NaOH and incorporated radioactivity was determined by liquid scintillation counting.

3.3 Results

3.3.0 Subcellular location of MMACHC and of MMADHC isoforms by immunofluorescence

To investigate the subcellular distribution of MMACHC and MMADHC we first constructed retroviral vectors expressing GFP-fusion proteins and verified their expression by immunoblot analysis using an anti-GFP antibody (Fig. 3.0). The molecular masses of the GFPfusions were consistent with values calculated from amino acid sequence: MMACHC-GFP: 59.4 kDa; MMADHC-GFP: 60.6 kDa; MMADHCΔ1-61-GFP: 54.2 kDa. Free GFP was not detected in the lysates of the cells expressing the fusion constructs. We transduced immortalized primary human fibroblasts with each of these constructs and investigated the subcellular distribution by immunofluorescence (Fig. 3.1A). Mitochondria were visualized using an antibody against the mitochondrial stem-loop RNA binding protein (SLIRP) (427). To eliminate optical interference in the absence of laser-based illumination, cells were also imaged without mitochondrial staining (Fig. 3.1B). MMADHC-GFP fluorescence exhibited specific mitochondrial localization in addition to diffuse fluorescence throughout the cytoplasm. A similar mitochondrial network was observed in cells that were not counterstained with the mitochondrial marker, demonstrating that the co-localization was not due to fluorescence bleedthrough from the SLIRP fluorescence. These results suggest that MMADHC is a dual-localized

protein, found in both the mitochondrion and cytoplasm. Immunofluorescence of MMADHCΔ1-61-GFP and MMACHC-GFP showed a diffuse cytoplasmic signal lacking specific colocalization with stained mitochondria, suggesting that both are confined to the cytoplasm. The cytoplasmic localization of MMACHC was confirmed by additional experiments with MMACHC epitope-tagged on the C-terminus with HA or FLAG (Fig. 3.2).

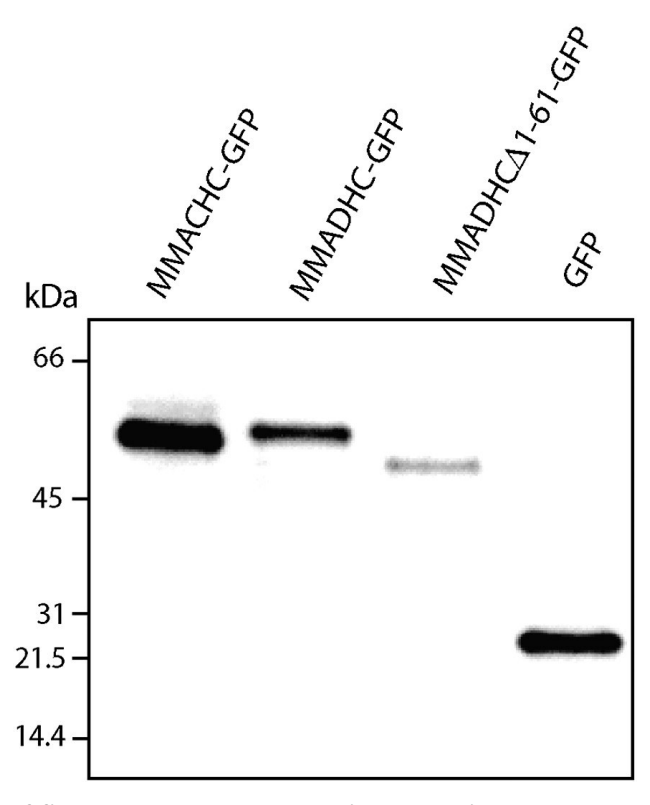


Figure 3.0. Immunoblot of fibroblasts transduced with retroviral constructs expressing MMACHC-GFP or MMADHC-GFP isoforms. Whole cell lysates were immunoblotted with anti-GFP antibodies to verify expression of MMACHC-GFP (lane 1), MMADHC-GFP (lane 2) and MMADHCΔ1-61-GFP (lane 3). Native GFP (lane 4) was produced by transient transfection of HEK293 cells with pEGFP-N1 vector.

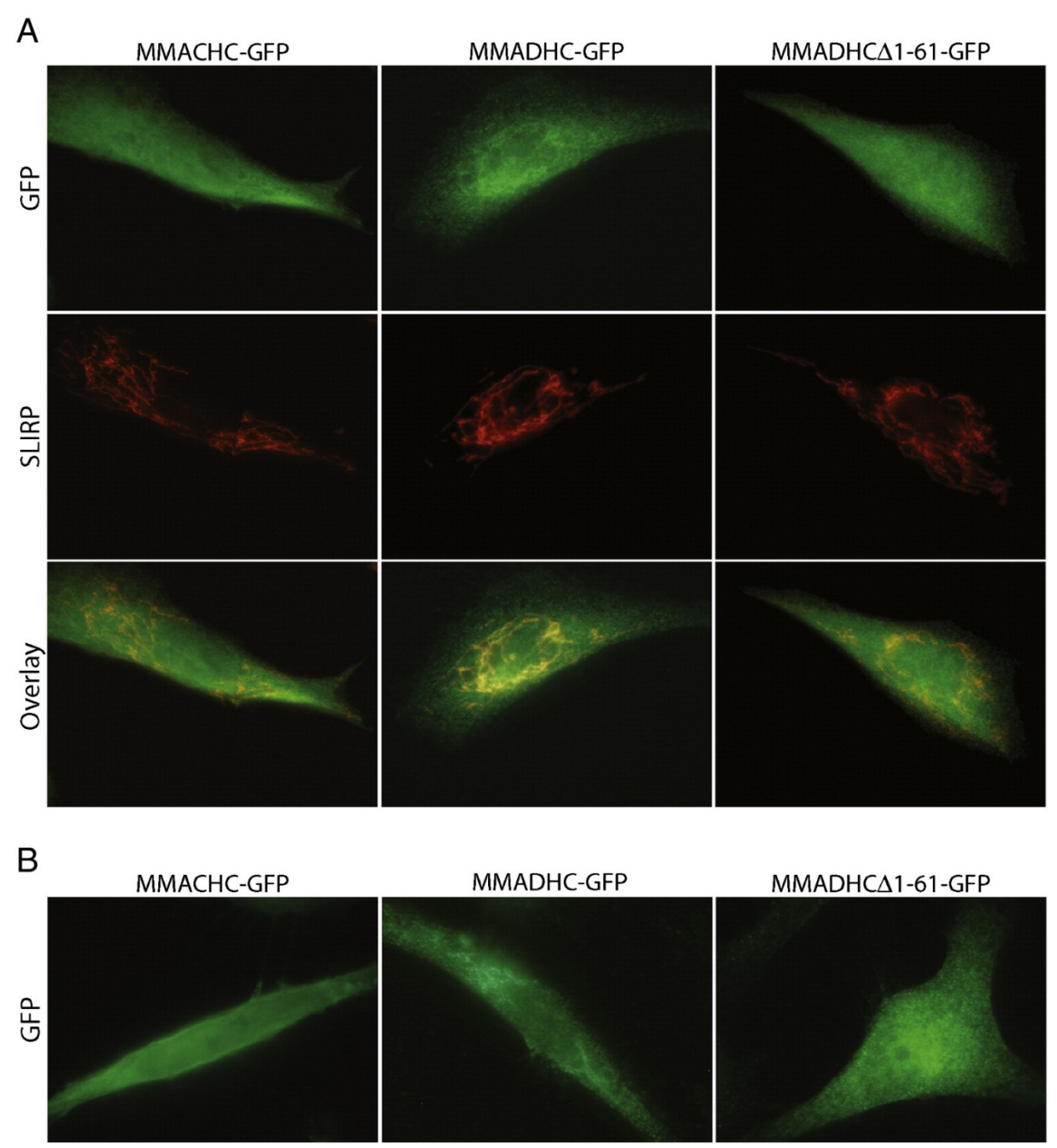


Figure 3.1. Immunofluorescence of fibroblasts transduced with retroviral constructs expressing MMACHC-GFP or MMADHC-GFP isoforms. A. An anti-GFP antibody was used to detect the GFP-tagged proteins (top panels); mitochondria were visualized with an anti-SLIRP antibody (middle panels). Images were overlayed to identify mitochondrial localization (bottom panels), observed only for MMADHC-GFP. **B.** Cells stained with anti-GFP antibody, omitting mitochondrial staining in order to minimize optical interference.

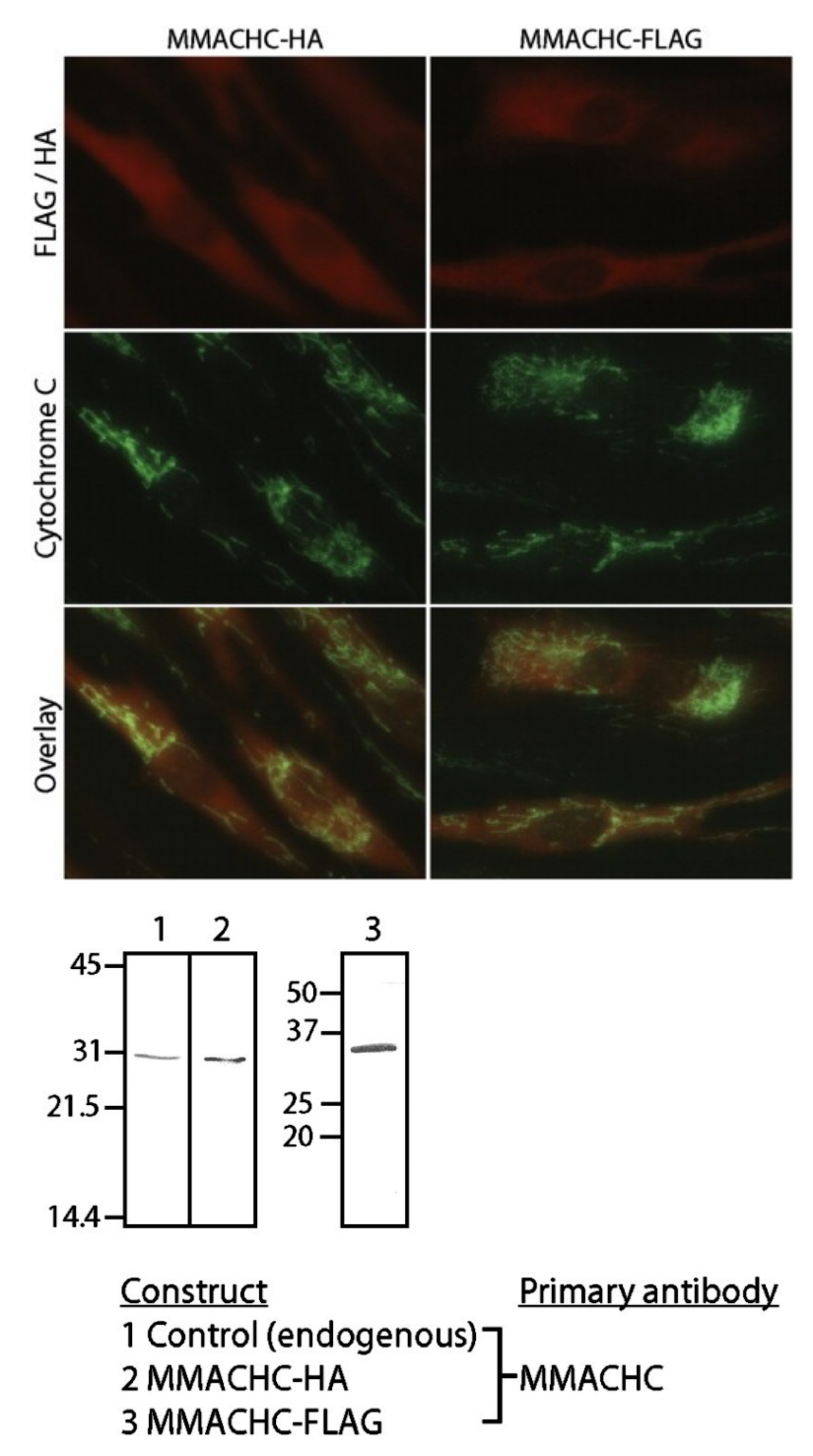


Figure 3.2. Immunofluorescence and immunoblot of fibroblasts transduced with retroviral constructs expressing C-terminal HA or FLAG-tagged MMACHC. A. Anti-HA (left panels) or anti-FLAG (right panels) antibody was used to detect tagged MMACHC (top panels); mitochondria were visualized with an anti-cytochrome C antibody (middle panels). Images were overlayed to identify mitochondrial localization (bottom panels), which was not observed. **B.** Whole cell lysates were immunoblotted using anti-MMACHC antibody to verify expression.

3.3.1 Subcellular location of MMACHC and of MMADHC isoforms by subcellular fractionation

After carrying out the mitochondrial isolation procedure (401) on transduced and control fibroblasts used for immunofluorescence imaging, the presence of MMACHC and MMADHC proteins in mitochondrial and soluble fractions (containing cytoplasm, lysosomes, and endoplasmic reticulum) was determined by SDS-PAGE followed by immunoblotting using appropriate antibodies. The location of all proteins as determined by subcellular fractionation with immunoblotting was in agreement with the results of the immunofluorescence experiments (Figs. 3.3A and B): MMACHC-GFP and MMADHCΔ1-61-GFP were detected only in the soluble fraction, whereas MMADHC-GFP was detected in both soluble and mitochondrial fractions. Results from probing control fibroblasts for endogenous MMACHC and MMADHC were also concordant with results obtained with GFP fusion proteins (Figs. 3.3A and B). To confirm the qualities of the highly purified mitochondria and soluble material, control mitochondrial (SDHA; (428)) and cytoplasmic (SOD1; (429)) proteins were probed by immunoblotting (Fig. 3.3C). Results of our isolation procedure showed negligible presence of SOD1 in isolated mitochondrial fractions.

Endogenous and transduced MMADHC were concurrently detected in transduced fibroblasts due to the low expression level of MMADHC-GFP constructs (Fig. 3.3B). In both MMADHC-expressing fibroblasts, endogenous MMADHC showed clear localization to the soluble and mitochondrial fractions, in agreement with data for MMADHC-GFP. In contrast, MMADHCΔ1-61-GFP was not detected in the mitochondrial fraction. Endogenous MMACHC could not be detected when probing transduced MMACHC-GFP fibroblasts due to its low relative abundance. These results indicate that the subcellular targeting of the GFP fusion proteins is not altered by the presence of a C-terminal GFP.

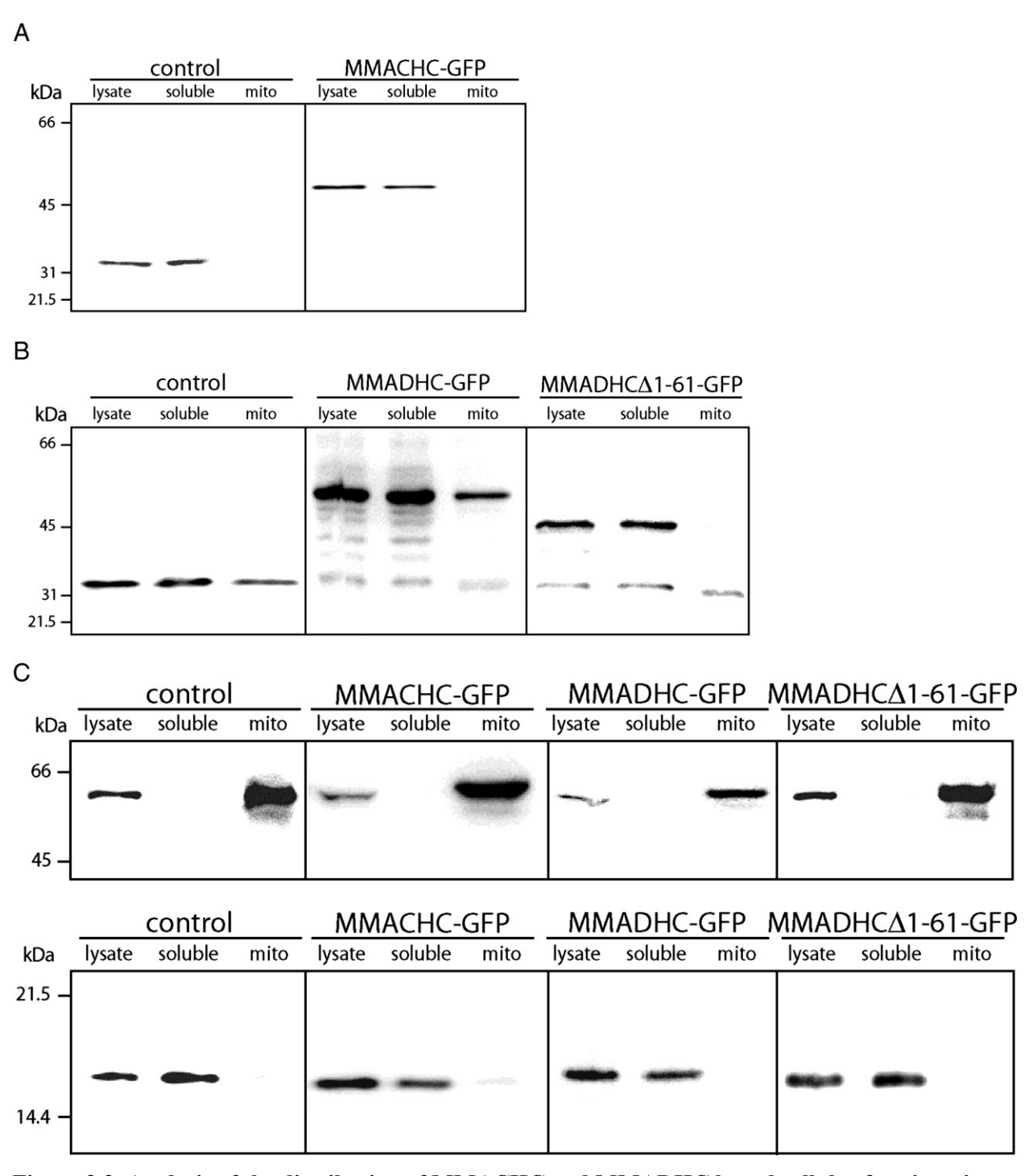


Figure 3.3. Analysis of the distribution of MMACHC and MMADHC by subcellular fractionation. A. Immunoblot using an anti-MMACHC antibody showing that endogenous MMACHC and MMACHC-GFP are found exclusively in the soluble fraction. B. Immunoblot using an anti-MMADHC antibody showing that endogenous MMADHC and MMADHC-GFP are found in both the soluble and mitochondrial fractions, whereas MMADHC Δ 1-61-GFP is found only in the soluble fraction. C. Control immunoblots using antibodies against SDHA, a mitochondrial marker (top panels); and against SOD1, a cytoplasmic marker (bottom panels) demonstrating the purity of the subcellular fractions.

3.3.2 Biochemical studies

To assess functionality of the GFP-tagged constructs, we measured incorporation of label from [14C]propionate and [5-14C] methyl-THF into cellular macromolecules, measures of the function of MCM and MS respectively (426). Immortalized *cblC* fibroblasts showed decreased incorporation of both propionate and methyl-THF, which was normalized after transduction with MMACHC-GFP (Figs. 3.4A and B). Three immortalized cell lines, *cblD*-MMA, *cblD*-HC and *cblD*-MMA/HC, showed propionate and methyl-THF incorporation values (Figs. 3.4A and B) that are typical for these disorders. Transduction of MMADHC-GFP or MMADHCΔ1-61-GFP constructs corrected methyl-THF incorporation in *cblD*-HC and *cblD*-MMA/HC cells (Fig. 3.4A). On the other hand, propionate incorporation was not corrected in *cblD*-MMA immortalized fibroblasts after transduction with either the MMADHC-GFP or the MMADHCΔ1-61-GFP constructs. There was a small but statistically significant increase in propionate incorporation in *cblD*-MMA/HC immortalized fibroblasts transduced with the full-length MMADHC construct but not with the MMADHCΔ1-61 construct (Fig. 3.4B).

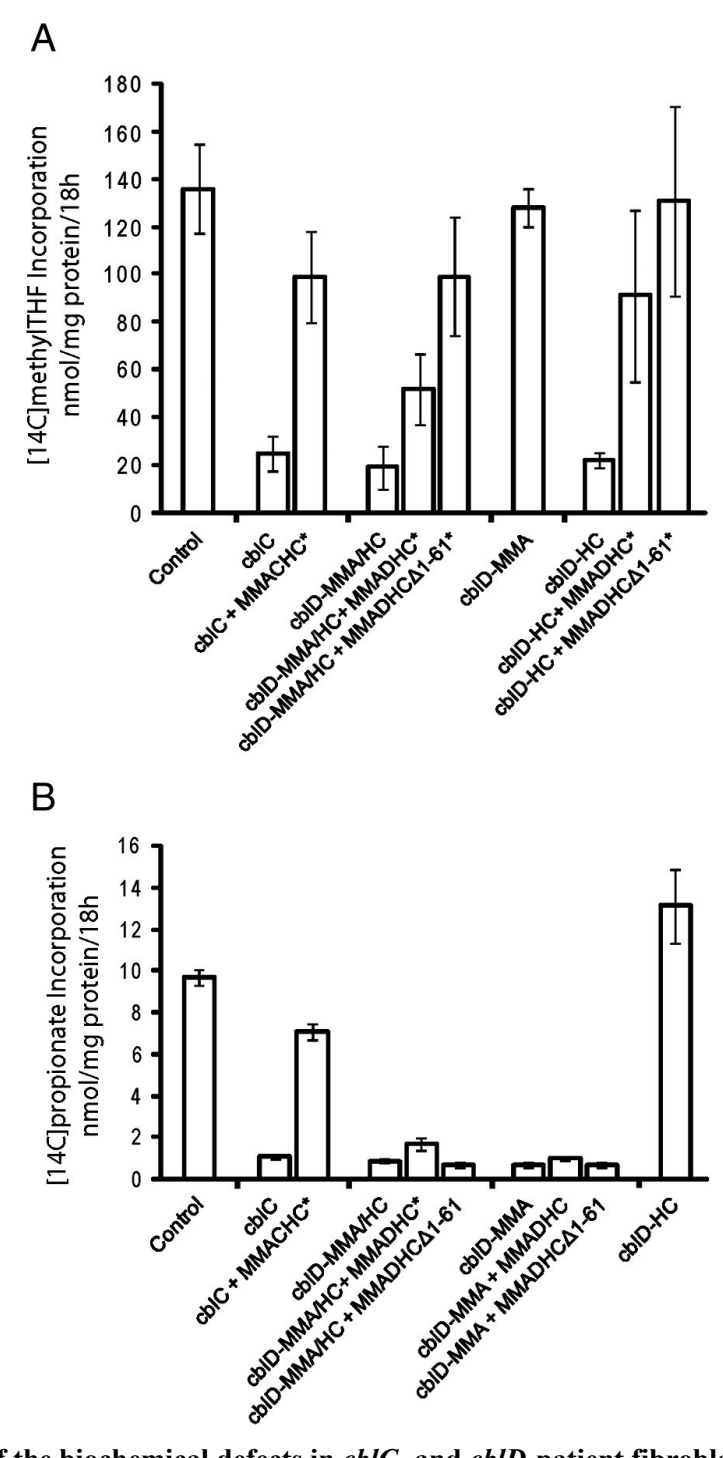


Figure 3.4. Rescue of the biochemical defects in *cblC*- and *cblD*-patient fibroblasts transduced with retroviral vectors expressing MMACHC-GFP or MMADHC-GFP isoforms. A. Incorporation of label from $[5^{-14}C]$ methyl-THF into cellular macromolecules measures the function of MS. B. Incorporation of label from $[^{14}C]$ propionate into cellular macromolecules measures the function of MCM. Error measurements for each sample represent the standard deviation of six replicates. (*) indicates values that are significantly increased relative to untransduced patient fibroblasts (p < 0.01).

3.4 Discussion

Reports of the subcellular localization of the MMACHC protein have been equivocal. On the basis of the *cblC* cellular phenotype, it is recognized as a cytoplasmic protein. Functionally, MMACHC lies downstream of the LMBD1 and ABCD4 proteins that apparently mediate transfer of endocytosed cobalamin across the lysosomal membrane and into the cytoplasm (286). MMACHC lies upstream of the MMADHC protein, proposed to partition internalized cobalamin between the cytoplasmic MS and mitochondrial MCM enzymes. MMACHC also lacks a mitochondrial targeting sequence. The results of our study unambiguously demonstrate localization of both endogenous MMACHC and of transduced GFPtagged MMACHC to the cytoplasm, with no evidence of mitochondrial localization. Transduction of the GFP-tagged MMACHC was also shown to correct function of both cobalamin-dependent enzymes in cblC patient fibroblasts, confirming that the GFP-tagged enzyme was metabolically active. On the other hand, an analysis of the mouse mitochondrial proteome identified Mmachc among 1098 proteins expressed in that organelle, and a GFP-tagged MMACHC construct expressed in HeLa cells was reported to localize to mitochondria (401). In light of our identification of MMACHC as a cytoplasmic protein, it was subsequently acknowledged (D. J. Pagliarini, personal communication) that the transfected cDNA (BC006122) in their immunofluorescence assay did not encompass the entire MMACHC sequence but lacked 57 N-terminal residues. MitoprotII analysis of this truncated MMACHC variant indicated a significant increase in probability of mitochondrial targeting and thus we speculate that removal of these N-terminal residues on MMACHC resulted in the production of a mitochondrial targeting sequence (MTS) that would localize MMACHC to the mitochondria. That MMACHC functions as a cytoplasmic protein is now conclusively shown.

Our immunofluorescence and subcellular fractionation studies using endogenous MMADHC and GFP-tagged MMADHC established that this protein localizes both to mitochondria and to cytoplasm, consistent with the heterogeneous *cblD* biochemical phenotype. Immunoblot analysis of endogenous or GFP-tagged MMADHC using an anti-MMADHC antibody identified a single band that corresponded in mass to full-length MMADHC in all instances, indicating that the molecular basis for dual-localization of MMADHC is a single fulllength protein targeted to both subcellular compartments. It had been suggested that the dual localization of MMADHC could arise from either a single protein or from expression of multiple isoforms due to translation reinitiation at strong downstream Kozak sequences starting at residues Met₆₂ or Met₁₁₆ (379). Credence for downstream reinitiation is provided by genotype– phenotype correlation analysis of the isolated *cblD*-MMA disorder; patients with mutations that lead to pre-emptive translation termination preceding Met₆₂ or Met₁₁₆ retain cytoplasmic MS function. This suggests that translation reinitiation results in production of truncated MMADHC and supports provision of cobalamin necessary for MS function in *cblD*-MMA patients. Identification of these isoforms was confirmed (380) by immunoblot analysis of cblD-MMA patients in which bands corresponding in molecular mass to translation reinitiation at both Met₆₂ and Met₁₁₆ were detected.

The phenomenon of dual-localization of proteins is not uncommon; over 100 mitochondrial proteins are predicted to be dual-localized as the result of multiple targeting signals (430), inefficient translocation (431), retrograde translocation (432), changes in targeting sequence accessibility (433), or multiple translation products (434). Our data confirm the molecular basis for dual-localization of MMADHC, in agreement with a recent study (380) that used multiple transfection assays in *cblD* patient fibroblasts, measuring formation of AdoCbl and

MeCbl. Transfection experiments with MMADHC constructs lacking both downstream methionines showed that MeCbl synthesis was recovered to varying degrees. Our experiments confirm dual-localization of full-length MMADHC through direct immunofluorescence visualization and subcellular fractionation, in contrast to the transfection studies that, while providing conclusive resolution to the molecular basis of dual-localization, did not directly investigate the dual-localized nature of MMADHC. MMADHC is predicted (by Mitoprot) to have a conventional matrix-targeted mitochondrial leader sequence, and the factors that determine the fractional distribution to the mitochondrial and cytoplasmic compartments, while crucial to function, remain unknown.

By transduction of MMADHC Δ 1-61-GFP into control fibroblasts, we mimic one of the potential isoforms arising from downstream reinitiation. We found that this isoform, lacking a putative MTS, was localized exclusively to the cytoplasm, in agreement with genotype—phenotype correlation of *cblD* patient cells. As a measure of MS function, incorporation of label from [14 C]methyl-THF into cellular macromolecules in *cblD* fibroblasts transduced with the full-length or the truncated MMADHC construct showed rescue of MS function in both *cblD*-HC and *cblD*-MMA/HC lines. The presence of the C-terminal domain of MMADHC is thus sufficient to support provision of cobalamin to MS, again in agreement with genotype—phenotype correlation in *cblD* patients.

As a measure of MCM function, incorporation of label from [¹⁴C]propionate into cellular macromolecules showed that transduction of neither MMADHC isoform was able to correct MCM function in *cblD*-MMA or *cblD*-MMA/HC cells. This outcome extends results of previous studies (379) showing that correction of MCM function could not be achieved by transfection of wild type MMADHC into *cblD* cells unless a C-terminal V5-polypeptide was

added to the MMADHC construct. A subsequent study (380) found an inverse correlation between recovery of AdoCbl synthesis and endogenous MMADHC mRNA levels in *cblD*-MMA fibroblasts transiently transfected with wild type MMADHC, suggesting that endogenous patient MMADHC might influence AdoCbl rescue by transfected MMADHC, but this awaits further investigation.

In summary, through direct visualization of GFP-tagged constructs and by immunoblot analysis of over-expressed GFP-tagged and endogenous protein, we determined the subcellular location of MMACHC and MMADHC. Our identification of MMACHC as a cytoplasmic protein resolves a report that identified MMACHC as a mitochondrial protein. Confirming the localization of MMACHC, MMADHC and a potential MMADHC isoform provides clearer understanding of the role of MMACHC and MMADHC within the intracellular vitamin B₁₂ metabolic pathway. Further studies will probe demonstrated interactions between MMADHC and MMACHC using fluorescence-based microscopy to elucidate the biological role of this interaction, which may be, at least in part to retain some MMADHC in the cytoplasmic compartment.

3.5 Acknowledgments

This research was supported by operating grants to J.W.C. from the Natural Sciences and Engineering Research Council (NSERC; RGPIN 7289-06-07), to D.S.R. from the Canadian Institutes of Health Research (CIHR; MOP-15078), and to E.A.S. from the Canadian Institutes of Health Research (CIHR; Mt-15460). We thank Timothy Johns for cell-line immortalizations and imaging of MMACHC-HA and MMACHC-FLAG. Tamiko Nishimura provided tissue culture training. Jaeseung Kim contributed to the initial project planning. David Coelho generously provided monoclonal anti-human MMADHC antibody.

Preface to chapter 4

In chapters 2 and 3 we described the interaction between MMACHC and MMADHC and suggested that this interaction occurs within the cytoplasm. To extend our detailed protein interaction analyses, we describe the recombinant production of the lysosomal membrane proteins LMBD1 and ABCD4 in chapter 4. Both putative cobalamin transporters were expressed from a baculovirus expression system, and purified, detergent-solubilized LMBD1 and ABCD4 formed homodimers. Using surface plasmon resonance we demonstrate a high-affinity interaction between LMBD1 and ABCD4. Extending these studies to soluble components of the pathway, we demonstrate that both membrane proteins interact with MMACHC. With our MMACHC affinity-selected peptides we mapped regions on LMBD1 and ABCD4 predicted to recruit MMACHC. We propose a model consisting of a multiprotein complex formed between soluble (MMACHC) and lysosomal membrane (LMBD1, ABCD4) proteins that mediate the vectorial delivery of cobalamin effectively preventing inadvertent dilution of the cofactor into the cytoplasmic milieu and protecting the cofactor from inactivation by side reactions.

Chapter 4

The putative human lysosomal vitamin B_{12} transporters LMBD1 and ABCD4 interact *in vitro*

Justin C. Deme, Mark A. Hancock, Xiaobing Xia, Maria Plesa, Jaeseung C. Kim, Elisabeth P. Carpenter, David S. Rosenblatt, James W. Coulton

In preparation (2013)

4.0 Summary

Mutations in the LMBRD1 and ABCD4 genes result in the failure to export lysosomal vitamin B₁₂ to the cytoplasm which impairs the two vitamin B₁₂-dependent enzymes methionine synthase and methylmalonyl-CoA mutase. The gene products of *LMBRD1* and *ABCD4* are proposed to mediate vitamin B₁₂ transport at the lysosome through complex formation. Here we present protein-protein interactions analyses on LMBD1 and ABCD4; these clarify the mechanism for lysosomal vitamin B₁₂ transport. We describe the recombinant production of LMBD1 and ABCD4 for detailed biophysical analyses. Using techniques including blue native-PAGE, chemical crosslinking, and size exclusion chromatography coupled to multi angle light scattering (SEC-MALS), we show that detergent-solubilized LMBD1 and ABCD4 form homodimers. To examine the functional properties of these proteins, surface plasmon resonance (SPR) provided direct in vitro binding data to support the following predictions: (i) LMBD1 and ABCD4 can interact with each other according to low nanomolar affinity; (ii) the cytoplasmic vitamin B₁₂-processing protein MMACHC can interact with LMBD1 and ABCD4 with high affinity. We propose a model whereby membrane-bound LMBD1 and ABCD4 facilitate the vectorial delivery of lysosomal vitamin B₁₂ to cytoplasmic MMACHC, thus preventing cofactor dilution to the cytoplasmic milieu and protecting from inactivating side reactions.

4.1 Introduction

Dubbed nature's most beautiful cofactor (1), cobalamin (Cbl or vitamin B_{12}) is the largest of all vitamins and the most structurally complex (30). This cofactor is composed of a central cobalt atom that is coordinated by a tetrapyrrole framework termed the corrin ring and by two axial ligands. The lower axial ligand is in a "base-on" state when the pendant dimethylbenzimidazole (DMB) base connected to the corrin ring coordinates cobalt. Protonation

of DMB or histidine substitution results in the "base-off" or "base-off/His-on" forms of Cbl, respectively. Cbl diversity is provided by its upper axial ligand which covalently attaches to the central cobalt. Methyl, 5'-deoxyadenosyl, hydroxyl, or cyano groups can serve as upper axial ligand and give rise to several forms of Cbl: methylcobalamin (MeCbl), 5'-adenosylcobalamin (AdoCbl), hydroxocobalamin (OHCbl), and cyanocobalamin (CNCbl). Methylmalonyl-CoA mutase (MCM) and methionine synthase (MS) use Cbl as cofactor to catalyze chemically unique reactions. Methionine is generated from homocysteine by cytoplasmic MS and MeCbl. AdoCbl is used by mitochondrial MCM for the isomerization of methylmalonyl-CoA to succinyl-CoA for entry into the tricarboxylic acid (TCA) cycle.

Nine inherited defects of intracellular Cbl metabolism, designated *cblA* to *cblJ* and *mut*, have been discovered through somatic complementation assays (286, 342). Defects in this pathway result in MCM and MS substrate accumulation and the resultant methylmalonic aciduria and/or homocystinuria can give rise to severe hematological and neurological conditions. Patients within the *cblF* (329, 331) or *cblJ* (342, 343) groups have similar clinical phenotypes: hypotonia, lethargy, poor feeding, bone marrow suppression, macrocytic anemia and heart defects. Cultured fibroblasts from *cblF* patients accumulate nonprotein-bound Cbl in lysosomes (329, 330). The accumulation of unprocessed, nonprotein-bound Cbl within the cell has also been reported for *cblJ* patients (342, 343) who mimic the *cblF* phenotype (329). Mutations in *LMBRD1* (332) and *ABCD4* (342) were recently identified as the cause of the *cblF* and *cblJ* defects, respectively. Transfection of *LMBRD1* into *cblF* fibroblasts or *ABCD4* into *cblJ* fibroblasts rescues AdoCbl and MeCbl synthesis and restores MCM and MS function, implicating these gene products in the lysosomal export of Cbl (332, 342).

LMBRD1 encodes LMBD1, a 61.4 kDa membrane protein of 540 residues and six predicted lysosomal N-glycosylation sites (332). LMBD1 localizes primarily to the lysosome (332, 338) but also appears in the plasma membrane (339) and perinuclear region (332). Based on topology modeling programs, predicted glycosylation pattern and freeze-fracture replica immunolabeling experiments (332), LMBD1 spans the lysosomal membrane via nine transmembrane helices with a lysosomal N-terminus and cytoplasmic C-terminus. LMBD1 demonstrates homology to the lipocalin-1 interacting membrane receptor (LIMR) involved in the internalization of lipocalins, which bind small hydrophobic molecules like steroids and lipids (332, 435).

ABCD4 encodes ABCD4, a non-glycosylated protein of 606 residues with molecular mass of 68.6 kDa (344, 345). Originally identified as peroxisomal (346), two recent studies have demonstrated its presence solely within the lysosome of humans (342) and rats (338). ABCD4 consists of two domains: an N-terminal transmembrane domain and a C-terminal nucleotide binding domain (NBD) (342). The transmembrane domain has six predicted transmembrane helices (342, 345) whereas the NBD contains highly conserved motifs involved in ATP and Mg²⁺ binding, including Walker A and B motifs plus a modified ABC signature motif (342). The topology of ABCD4 has both the N- and C-termini exposed to the cytoplasm, based on bioinformatics predictions and loop directed glycosylation experiments (342, 345). ABCD4 is a member of the D subfamily of ABC half transporters that dimerize to form active, full transporters (347, 348). ABCD4 has significant amino acid identity (25-27%) with these other members, but lacks a hydrophilic N-terminal tail that mediates localization to the peroxisome (345).

The functional interplay between LMBD1 and ABCD4 is supported by a fluorescence microscopy study that demonstrated colocalization of both proteins to the lysosomal membrane (342). In addition, AdoCbl/MeCbl synthesis and MCM/MS function can be partially rescued by transfection of *ABCD4* cDNA into cultured *cblF* fibroblasts (342). It is suggested that ABCD4 and LMBD1 form a complex that is critical to the export of lysosomal Cbl to the cytoplasm; LMBD1 forms the substrate channel and ABCD4 alleviates the energy requirements through its proposed ATPase activity (342). These lysosomal membrane proteins are also proposed to mediate the directional transfer of Cbl to the cytoplasmic Cbl-processing protein MMACHC (286, 435).

In this study, we set out to characterize protein-protein interactions involved in Cbl egress from the lysosome. We describe the recombinant production of the lysosomal membrane proteins LMBD1 and ABCD4 using the baculovirus expression system. Using blue native-PAGE, chemical crosslinking, and SEC-MALS, detergent-solubilized LMBD1 and ABCD4 formed homodimers in solution. Using label-free, real-time SPR, LMBD1 and ABCD4 interacted with low nanomolar affinity. As predicted by phage display, MMACHC interacted with both LMBD1 and ABCD4 according to low nanomolar affinities. Our results are consistent with the current hypothesis in the literature that implicates LMBD1 and ABCD4 in the vectorial delivery of lysosomal Cbl to cytoplasmic MMACHC. Direct evidence for the protein interactions involved in egress of lysosomal Cbl (and their detailed characterizations) advances our basic understanding of early intracellular Cbl metabolism which has largely been limited to phenotypic studies to date.

4.2 Materials and methods

4.2.0 Protein purification

cDNA corresponding to *LMBRD1* or *ABCD4* were cloned into the pFB-CT10HF-LIC transfer vector which encodes downstream, in the following order: a TEV cleavage site (ENL YFQS); a decahistidine tag (His₁₀); and, a FLAG (DYKDDDDK) tag. Baculoviruses were constructed according to the Bac-to-Bac system (Life Technologies). *Spodoptera frugiperda* (Sf9) insect cells were grown in shaker flasks in I-MAX (Wisent) or Sf-900 II SFM media (Life Technologies) at 27°C and infected with amplified recombinant baculovirus (MOI of 0.25-0.5) for 72 h. Following infection, cells were collected by centrifugation (1,000 x g for 10 min), washed in phosphate-buffered saline (PBS), flash frozen in liquid nitrogen, and stored at -80°C until use.

Infected cells were resuspended (25 ml/L of cells) in cold lysis buffer (50 mM HEPES pH 7.5 plus a Complete EDTA-free protease inhibitor cocktail tablet (Roche)) and lysed by three passes through an EmulsiFlex-C5 homogenizer (Avestin) at 15,000 psi. Cell debris was removed by centrifugation (10,000 x g at 4°C, 10 min) and NaCl was added to supernatants to a final concentration of 1 M. Supernatants were then centrifuged (100,000 x g at 4°C, 75 min) to collect membranes. Salt-washed membranes were resuspended in lysis buffer plus 1 M NaCl using a Dounce homogenizer, and subjected to an additional round of ultracentrifugation (100,000 x g at 4°C, 75 min). Membranes expressing LMBD1 were resuspended in extraction buffer (50 mM HEPES pH 7.5, 200 mM NaCl, 5 % glycerol, 1% (w/v) n-dodecyl-β-D-maltoside (DDM) and 0.1% (w/v) cholesteryl hemisuccinate (CHS)) while membranes expressing ABCD4 were extracted in extraction buffer plus 0.5 mM tris(2-carboxyethyl)phosphine (TCEP) and 1 mM MgCl₂ for 16 h at 4°C by slow mixing on a rotating mixer.

Detergent-extracted membranes were collected by ultracentrifugation (100,000 x g at 4°C, 45 min) and supplemented with 10 mM imidazole. Ni-NTA Superflow (Qiagen), preequilibrated in purification buffer (50 mM HEPES pH 7.5, 200 mM NaCl, 5% glycerol, 0.03% DDM, 0.003% CHS, plus 0.5 mM TCEP and 1 mM MgCl₂ for ABCD4 preparations) with 10 mM imidazole, was added to detergent-extracted membranes, followed by gentle mixing for 1 h at 4°C. Resin was captured through a gravity column and washed with 15 column volumes (CV) of purification buffer plus 20 mM imidazole, followed by stringent washing using 15 CV of purification buffer supplemented with 40 mM imidazole. Protein was eluted by addition of purification buffer containing 300 mM imidazole and exchanged into gel filtration buffer (20 mM HEPES pH 7.5, 200 mM NaCl, 0.02% DDM, 0.002% CHS, plus 0.5 mM TCEP and 1 mM MgCl₂ for ABCD4), using a PD Minitrap G-25 desalting column (GE Healthcare Life Sciences). TEV protease was added to each sample in a 1:2 mass ratio of TEV:protein, and Peptide-N-Glycosidase F (PNGase F) was concurrently added to LMBD1 samples in a 1:30 mass ratio of PNGaseF:LMBD1 and incubated for 72 h at 4°C. TEV protease and PNGase F were prepared in house.

Cleaved LMBD1 and ABCD4 were separated from the His₆-tagged TEV protease and PNGase F by incubation for 1 h with Ni-NTA Superflow resin at 4°C. Resin was collected in a gravity column and flowthrough was pooled and concentrated to ~ 1 mg/ml using a centrifugal filter (Millipore; Amicon 100 kDa MWCO). MMACHC and MMADHC were cloned, expressed, and purified as previously described (367, 424). Protein concentrations were derived from A₂₈₀ measurements using the theoretical extinction coefficients and molecular masses for LMBD1 (106,230 M⁻¹cm⁻¹; 62.2 kDa), ABCD4 (92,250 M⁻¹cm⁻¹; 69.4 kDa), MMACHC (47,900 M⁻¹cm⁻¹; 31.9 kDa), and MMADHC (32,430 M⁻¹cm⁻¹; 31.9 kDa).

Purity of LMBD1 and ABCD4 was assessed by SDS-PAGE using 8% polyacrylamide gels followed by silver staining. Apparent protein molecular masses derived from SDS-PAGE were estimated using molecular mass standards. Monodispersity of LMBD1 and ABCD4 protein-detergent complexes (PDCs) were assessed using analytical size exclusion chromatography (aSEC). Briefly, samples (50 µg) were applied onto a Superdex 200 10/300 GL column (GE Healthcare Life Sciences) equilibrated in gel filtration buffer and apparent molecular masses were derived from soluble protein standards (Biorad). Purified LMBD1 and ABCD4 were subjected to Western blotting using anti-FLAG and anti-His6 antibodies and to mass spectrometry (Structural Genomics Consortium, University of Oxford) to confirm primary sequence fidelity.

4.2.1 BN-PAGE analysis

Blue-native PAGE was performed using 4-20% polyacrylamide gradient gels generated in-house. The buffering components of the gel included 50 mM Bis-tris and 500 mM aminocaproic acid, pH 7.0. Protein samples (8 µg) were incubated in the presence or absence of SDS (1%) for 10 min prior to loading. Samples and unstained protein standards (NativeMark; Life Technologies) were run in cold anode (50 mM Bis-tris pH 7.0) and deep blue cathode buffers (50 mM Tricine, 15 mM Bis-tris, 0.02% Coomassie G-250, pH 7.0) for 1 h at 100 V, whereupon the cathode buffer was replaced with slightly blue cathode buffer (50 mM Tricine, 15 mM Bis-tris, 0.002% Coomassie G-250, pH 7.0) and electrophoresis continued for 2-3 h at 180 V. Following electrophoresis, gels were stained with Coomassie brilliant blue (R-250).

4.2.2 Chemical crosslinking

Prior to crosslinking LMBD1 was diluted to 2.5 μ M (0.15 mg/ml) and ABCD4 was diluted to 1.2 μ M (0.08 mg/ml) in gel filtration buffer. For LMBD1 crosslinking, ultrapure

electron microscopy (EM) grade glutaraldehyde (EM sciences) was mixed with samples to a final concentration of 0.025% (w/w). Aliquots of LMBD1 were removed from the reaction mixture following incubation for 10, 30, and 60 min at 25°C. To ensure specific crosslinking with glutaraldehyde, a control reaction of LMBD1 preincubated with 1% SDS followed by glutaraldehyde treatment (0.025%) for 1 h was performed concurrently. For ABCD4, formaldehyde (Pierce) was added to a final concentration of 0.075% (w/v) to initiate crosslinking; aliquots were removed following incubation for 30 min, 1 h, and 4 h at 25°C. To terminate crosslinking for all reactions, aliquots were treated with SDS-PAGE sample buffer for 10 min prior to loading onto a 4-12% polyacrylamide gel prepared in-house. Following electrophoresis by SDS-PAGE, crosslinked samples were visualized by silver staining.

4.2.3 SEC-MALS

For molecular mass determination of protein-detergent complexes (PDCs) size exclusion chromatography was coupled to multi angle light scattering, refractive index, and UV detection. Both LMBD1 and ABCD4 were applied to a Superdex 200 10/300 GL column (GE Healthcare Life Sciences) connected to a Waters 2695 HPLC system at 20°C at a flow rate of 0.25 ml/min using gel filtration buffer. Elution was monitored inline by absorption at 280 nm (Waters 2489 UV/Vis detector), by refractive index at 658.0 nm using an Optilab rEX detector (Wyatt Technology), and by multi angle light scattering at 656.0 nm using the three detectors (49°, 90°, 131°) of the miniDAWN TREOS (Wyatt Technology). Data were analyzed using ASTRA 5.3.4.16 software (Wyatt Technology), using a standard template for determination of PDC molecular masses and the "protein conjugate" module for protein and detergent contributions to the PDC, according to Slotboom *et al.* (393). Rabbit muscle aldolase (GE Healthcare Life Sciences; 158 kDa) was used as internal standard for detector normalization. For protein

conjugate analyses, a (dn/dc)_{protein} value of 0.192 ml/mg was used for LMBD1 based on SEDFIT estimations (394). The (dn/dc)_{detergent} of DDM-CHS, 0.185 ml/mg, was calculated offline in batch mode using a standard curve of known detergent concentrations in gel filtration buffer. The extinction coefficient of LMBD1 at 280 nm (1.707 ml mg⁻¹cm⁻¹) was calculated from primary sequence whereas the contribution of DDM-CHS at 280 nm was considered negligible (393).

4.2.4 Surface plasmon resonance

Interactions between ABCD4 (310 kDa), LMBD1 (220 kDa), MMACHC (32 kDa), and/or MMADHC (32 kDa) were examined using label-free, real-time BIACORE 3000 instrumentation (GE Healthcare Bio-Sciences AB, Uppsala, Sweden). Experiments were performed on research-grade CM4 sensor chips at 25°C using filtered (0.2 μm) and degassed HBS-ED running buffer (10 mM HEPES pH 7.4, 150 mM NaCl, 3.4 mM EDTA, 0.02% (w/v) DDM). Fatty acid free bovine serum albumin (BSA, 66 kDa) was from Sigma (#A8806), Pierce Gentle Elution (PGE) was from Thermo Scientific (#21027), and Anatrace detergents were from Affymetrix (DDM #D310 and Empigen #D350); all other chemicals were reagent-grade quality.

Low- (100 RU), medium- (400 RU), and high-density (1000 RU) ABCD4 surfaces were immobilized using the Biacore Amine Coupling kit (10 µg/ml ABCD4 in 10 mM sodium acetate pH 5.0 containing 0.02% (w/v) DDM); corresponding reference surfaces were prepared in the absence of any ABCD4 protein. To examine binding specificity, short injections of buffer (blank), BSA (negative control), ABCD4 (test self-association), and LMBD1 (test partner) were flowed over reference and ABCD4-immobilized surfaces using low flow rates (25 µl/min x 1 min association + 5 min dissocation). To examine binding affinity, LMBD1 (0-100 nM, 2-fold serial dilutions) was titrated to steady-state plateaus using low flow rates (10 µl/min x 10 min

association + 20 min dissociation); inherently slow dissociation phases were further characterized using Biacore's linked reaction test (i.e. repeated injection of fixed LMBD1 concentration at constant flow rate, but increasing contact time). To cross-validate our results in the reversed "ligand-analyte" orientation, amine-coupled LMBD1 surfaces were prepared and tested in the similar manner. MMACHC and MMADHC were also amine-coupled (200-700 RU each) in other experiments to test for their interaction with ABCD4 and LMBD1, as well as solution-phase MMACHC or MMADHC (positive controls). In all cases, sensor chip surfaces were regenerated between sample injections at 50 µl/min using two 30-second pulses of solution I (PGE containing 0.05% (v/v) Empigen), II (1 M imidazole containing 0.05% (v/v) Empigen), III (PGE containing 33 mM H₃PO₄, 1.5 M NaCl, and 0.05% (v/v) Empigen), IV (50 mM NaOH containing 1 M NaCl and 0.05% (v/v) Empigen), and V (HBS-ED) followed by 'EXTRACLEAN' and 'RINSE' procedures.

SPR data were doubled-referenced (410) and are representative of triplicate injections acquired from at least three independent trials. For each replicate series, a buffer blank was injected first, the highest titrant concentration second, and serial dilutions followed (from the lowest to the highest concentration repeated); comparing responses between the two highest titrant injections verified consistent immobilized surface activity throughout each assay. Apparent equilibrium dissociation constants (K_D) were determined by global fitting of the data (averaged responses at the end of each association phase (R_{eq}) plotted versus concentration) to a "steady-state affinity" model in the BIAevaluation software (v 4.1). In all cases, theoretical binding maxima were predicted using the following equation: $R_{max} = (M_A/M_L)(R_L)(n)$ where R_{max} is the maximal binding response (RU) at saturation; M_A is the molecular mass (kDa) of the

injected analyte; M_L is the molecular mass (kDa) of the immobilized ligand; R_L is the amount (RU) of immobilized ligand; and n is the predicted binding stoichiometry (e.g. 1:1).

4.2.5 Phage display

Phage display was performed for MMACHC as previously described (367). Briefly, MMACHC was diluted to 100 μg/ml in 0.1 M NaHCO₃, pH 8.6 and adsorbed to a polystyrene microtiter plate by incubation overnight at 4°C. Wells were subsequently blocked with 5 mg/ml BSA in 0.1 M NaHCO₃ pH 8.6, 0.02% w/v NaN₃ for 2 h at 4°C, followed by washing in trisbuffered saline plus 0.1% v/v Tween-20 (TBST). Phage (1.5 x 10¹¹ pfu) from two commercially available libraries, Ph.D.-12 and Ph.D.-C7C (New England Biolabs), were diluted in TBST, added to wells, and gently rocked for 1 h at 25°C. Phage panning, clone isolation, and DNA sequencing were performed as previously described (251, 252, 367, 424).

Pair-wise alignments of affinity-selected peptides against MMACHC were performed against LMBD1 and ABCD4 using the REceptor LIgand Contacts (RELIC) server MATCH (408) and the MatchScan program (P.D. Pawelek, unpublished data). MATCH uses a default scoring window of five and a minimum threshold score of three identities plus one similarity between selected peptides and alignment sequence based on a modified BLOSUM62 amino acid substitution matrix. Identities are given a score of +4, similarities are given a score of +1, and mismatches are given a score of either –1 or 0. For a window size of 5 residues, the threshold for MATCH is a score of 13. MatchScan improves pair-wise alignments by calculating alignment scores for a range of scoring windows. For MatchScan, the minimum scoring threshold is increased or decreased by 1 for each residue added or subtracted to the default scoring window, respectively.

4.3 Results

4.3.0 Purification of recombinant LMBD1 and ABCD4

After extensive preliminary screening with multiplicity of infection optimization, fulllength constructs of LMBD1 and ABCD4 (incorporating tandem C-terminal affinity tags (His₁₀-FLAG)) were expressed using the baculovirus expression vector system. LMBD1 and ABCD4 were extracted from Sf9 membranes by solubilization in n-dodecyl-β-D-maltoside (DDM) plus cholesteryl hemisuccinate (CHS) and subjected to Ni-NTA affinity chromatography (Fig. 4.0A). Affinity-purified LMBD1 (> 95% pure) exhibited smearing by SDS-PAGE, indicative of the six putative N-glycosylation sites that are predicted (332). Smearing was eliminated by adding Peptide-N-Glycosidase F (PNGase F) to samples prior to electrophoresis. Following affinity tag removal and extensive deglycosylation through incubation with TEV protease and PNGase F, LMBD1 migrated as two distinct species (55 kDa and 57 kDa). Continued SDS-PAGE heterogeneity was attributed to the incomplete deglycosylation of LMBD1 by PNGase F; only the lower band (55 kDa) was visualized following exogenous PNGase F addition. These results indicated that PNGase F was active in SDS and yielded complete deglycosylation only when LMBD1 was denatured – i.e. deglycosylated LMBD1 migrated to an apparent molecular weight of 55 kDa, whereas partially deglycosylated LMBD1 migrated to 57 kDa. Based on the marginal difference in mass, we propose that partially deglycosylated LMBD1 is detected because of a single N-glycosylation site that is inaccessible to PNGase F under native conditions; resistance to PNGase F treatment is a common outcome for detergent-solubilized membrane proteins (436). Extending PNGase F incubation times, screening other buffer conditions, and testing the activity of alternate deglycosylating enzymes (such as endoglycosidase H) did not alleviate this heterogeneity (data not shown). Regardless of the observed glycosylation heterogeneity,

LMBD1 was homogeneous and monodisperse based on analytical size exclusion chromatography (aSEC) (Fig. 4.0B).

ABCD4 was purified using a similar workflow. Following the preliminary Ni-NTA purification step, ABCD4 migrated at a molecular mass of 62 kDa and was >95% pure by SDS-PAGE (Fig. 4.0A). Subsequent TEV proteolysis (for affinity tag removal) then yielded two bands (62 kDa and 60 kDa). ABCD4 is not predicted to be glycosylated and, accordingly, we demonstrate that treatment with PNGase F does not shift its molecular mass by SDS-PAGE (Fig. 4.0A). Alternatively, immunoblotting (anti-His₁₀ or anti-FLAG) revealed that the 62 kDa band retained its affinity tag, whereas the 60 kDa did not, indicative of incomplete TEV proteolysis (data not shown). Extending TEV protease incubation times or altering the TEV:ABCD4 ratio did not reduce the presence of the 62 kDa band (data not shown). Notably, the observed molecular masses for both LMBD1 and ABCD4 deviated from the theoretical primary sequence calculations, a common occurrence for membrane proteins which bind more SDS compared to globular proteins (437). Primary sequence fidelity was confirmed by immunoblotting against affinity tags and by mass spectrometry (data not shown).

The high-quality purification results described above were obtained only after extensive detergent screening and assessment of sample monodispersity by aSEC. LMBD1 monodispersity was maintained in DDM, n-decyl-β-D-maltoside (DM), n-undecyl-β-D-maltoside (UDM), and decyl maltose neopentyl glycol (DMNG) with the latter three detergents (DM, UDM, DMNG) requiring supplementation with CHS at a 10:1 detergent:CHS mass ratio (data not shown). For ABCD4, DDM plus CHS yielded aSEC profiles with the least polydispersity (C. Shintre, personal communication). LMBD1 and ABCD4 solubilized in DDM plus CHS were subjected to aSEC to assess hydrodynamic properties of protein-detergent

complexes (PDCs) (Fig. 4.0B). LMBD1 was monodisperse in solution, yielding a peak corresponding to a PDC molecular mass of 230 kDa based on molecular mass standards.

ABCD4 yielded a polydisperse profile with 3 apparent peaks; a ~600 kDa minor leading peak, a ~350 kDa major peak, and a ~220 kDa minor trailing peak.

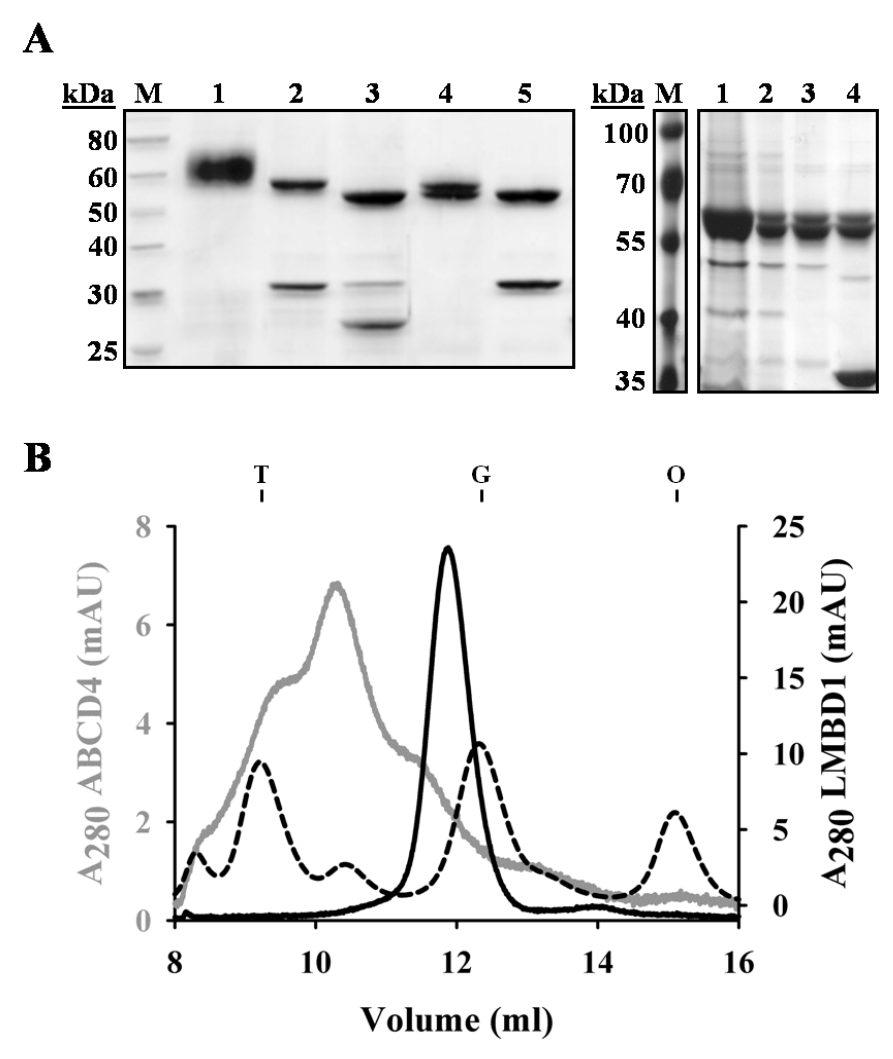


Figure 4.0. Purified, detergent-solubilized LMBD1 and ABCD4. A. *Left*, SDS-PAGE of recombinant LMBD1; lane M, molecular mass standards; lane 1, affinity-purified LMBD1; lane 2, affinity-purified LMBD1 plus PNGase F; lane 3, LMBD1 following proteolysis by TEV protease and deglycosylation by PNGase F; lane 4, cleaved LMBD1 following reverse affinity purification; lane 5, cleaved LMBD1 following reverse affinity purification; lane 5, cleaved LMBD1 following reverse affinity purification; lane 5, cleaved LMBD1 following reverse affinity purified ABCD4; lane 2, ABCD4 following TEV proteolysis; lane 3, ABCD4 following reverse affinity purification; lane 4, ABCD4 following reverse purification plus exogenous PNGase F. **B.** Analytical size exclusion chromatogram of LMBD1 (black), ABCD4 (grey), and molecular weight standards (dashed); T, thyroglobulin (670 kDa); G, γ-globulin (158 kDa); O, ovalbumin (44 kDa).

4.3.1 Oligomerization of LMBD1 and ABCD4

Due to the inherent difficulties in elucidating membrane protein oligomerization by aSEC, an alternative series of techniques was used. Blue-native PAGE (BN-PAGE) allows for the assessment of membrane protein complexes by native electrophoresis such that negatively charged Coomassie G-250 exchanges with the protein-bound detergent, thereby allowing the membrane protein to migrate through an electric field. This technique has widely been utilized in combination with SDS-mediated complex dissociation to analyze purified components of bacterial secretion systems (438-440). LMBD1 subjected to BN-PAGE yielded a homogeneous band with apparent molecular mass of 180-200 kDa, when compared to a molecular weight ladder derived from soluble proteins (Fig. 4.1A). Treatment of LMBD1 with SDS prior to electrophoresis resulted in increased migration to an apparent molecular mass of 90-100 kDa. While elucidation of the molecular masses of membrane protein complexes using soluble standards is inherently difficult due to the differential Coomassie binding properties of soluble and membrane proteins, our results suggest that subunit dissociation through SDS treatment yields monomeric LMBD1 and that native LMBD1 is dimeric. BN-PAGE profiles of ABCD4 were heterogeneous, similar to its aSEC profiles, with visible bands corresponding to molecular masses of ~300 and ~600 kDa (Fig. 4.1A). SDS-treated ABCD4 migrated to a single species with apparent molecular mass of 90 kDa, again suggesting that ABCD4 exists as a higher-order oligomeric complex.

To further assess oligomerization, chemical crosslinking was performed on purified LMBD1 or ABCD4 followed by separation by SDS-PAGE and visualization by silver staining. Untreated LMBD1 migrated to a molecular mass of 55 kDa, whereas 1 h treatment of LMBD1 with glutaraldehyde (0.025 %) resulted in the formation of a protein adduct with molecular mass

of 110 kDa, consistent with dimeric LMBD1 (Fig. 4.1B). To ascertain that this adduct did not arise from non-specific crosslinking, LMBD1 was treated with both SDS and glutaraldehyde which effectively prevented dimer formation. For ABCD4, treatment with formaldehyde (0.1%) over 4 h resulted in the formation of complexes consistent in mass with dimeric (120-150 kDa) and tetrameric (230 - 270 kDa) forms of ABCD4, compared to monomeric molecular masses of 60 and 62 kDa in untreated samples (Fig. 4.1C). The dimeric form predominated at 30 min and 1 h, with the tetrameric form occurring only after extended incubation (4 h).

To augment our BN-PAGE and crosslinking analyses, we then employed size exclusion chromatography with multi angle light scattering (SEC-MALS). SEC-MALS allows for direct molecular mass determination of PDCs (including contributions arising from the individual protein or detergent components) and does not require a calibration curve composed of molecular mass standards (393). Analysis of LMBD1 revealed a PDC molecular mass of 220 kDa (Fig. 4.1D), consistent with the 230 kDa estimation from our aSEC analyses (Fig. 4.0B); the LMBD1 protein component contributed 135 kDa, whereas the detergent-based DDM-CHS component contributed 85 kDa. Given the theoretical molecular mass of deglycosylated LMBD1 is 62.2 kDa, our SEC-MALS analyses indicated that LMBD1 was dimeric. LMBD1 was also determined to be dimeric in DM plus CHS, as was a ten residue C-terminal truncation of LMBD1 (LMBD1Δ531-540) in DM or DDM plus CHS (data not shown). While the heterogeneity of ABCD4 prevented elucidation of individual protein/detergent contributions to the PDC, we confirmed molecular masses of the three prominent PDCs observed in our aSEC profiles; a minor leading peak with molecular mass of 510 kDa, a minor trailing peak of 240 kDa and the prominent peak corresponding to 310 kDa (Fig. 4.1D). Based on the theoretical molecular mass of ABCD4 (69.5 kDa) and our chemical crosslinking results, we propose that

this major 310 kDa peak represents homodimeric ABCD4. Our findings are strengthened by previous literature indicating that ABC half transporters dimerize to reconstitute functional transporters (347, 348). While the 310 kDa peak may also correspond to trimeric ABCD4, the absence of literature to this effect combined with our inability to detect trimeric ABCD4 by formaldehyde crosslinking favours the dimeric proposal. ABC half transporters may also form tetramers (441), but we argue that the protein contribution of tetrameric ABCD4 (280 kDa) to the 310 kDa PDC would be too substantial to permit ABCD4 solubilization based upon the minor amount of bound detergent (30 kDa). Overall, we propose that the leading shoulder (500-600 kDa) is tetrameric ABCD4, and the trailing shoulder (220-240) is monomeric ABCD4.

Surface plasmon resonance was then employed to further test for the self-association of LMBD1 or ABCD4. Fixed concentration injections of LMBD1 or ABCD4 (100 nM each) over low density, amine-coupled LMBD1 and ABCD4 surfaces (100 RU each) elicited specific binding responses compared to BSA (Fig. 4.1E-F) or amine-coupled reference surfaces (no non-specific binding; data not shown). Not only were LMBD1-LMBD1 and ABCD4-ABCD4 self-associations detected, but LMBD1-ABCD4 binding was detected in both "ligand-analyte" orientations.

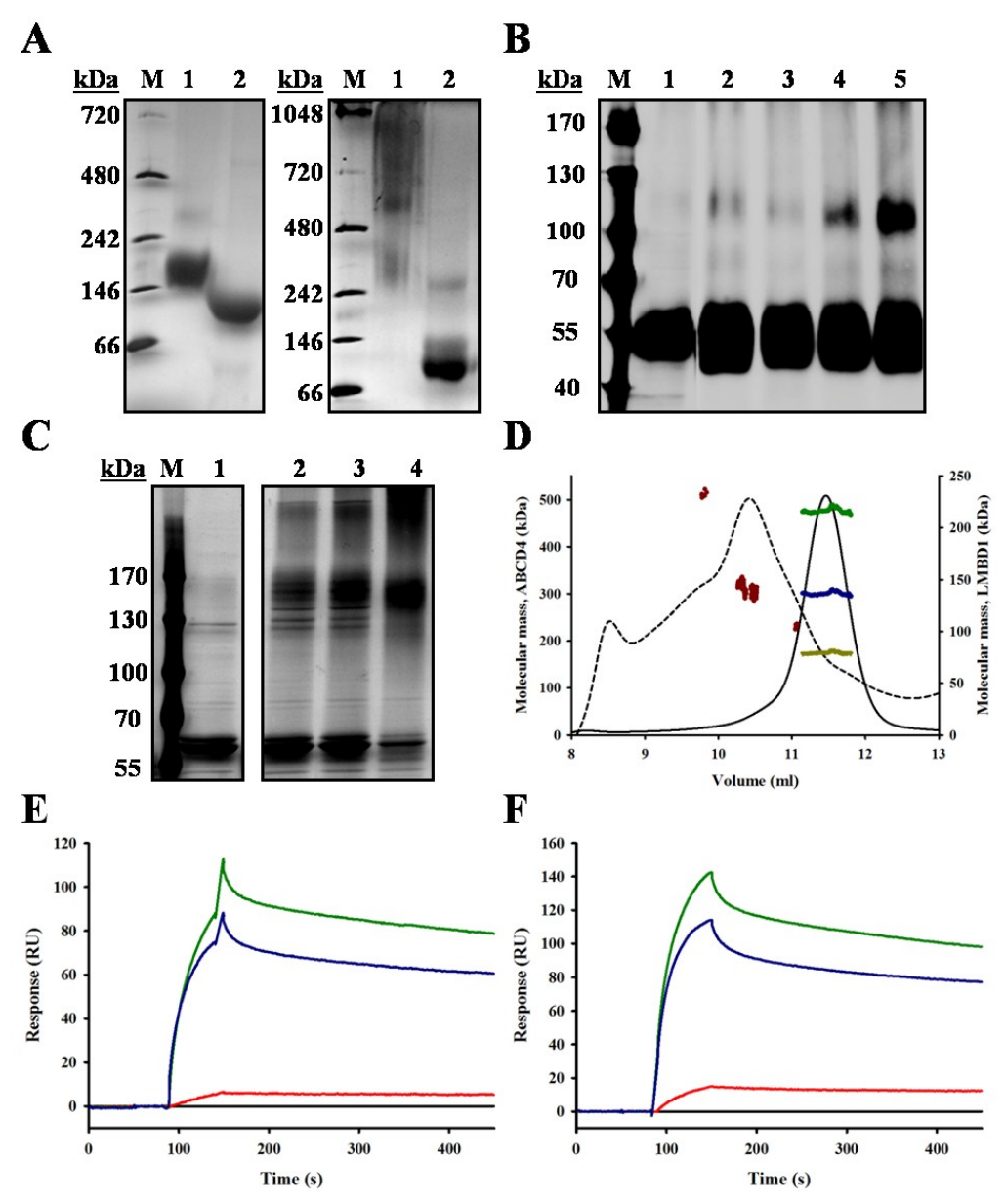


Figure 4.1. Self-association of LMBD1 and ABCD4. A. Blue-native PAGE (BN-PAGE) of purified LMBD1 (left) and ABCD4 (right). Lanes 1, DDMCHS-solubilized; lanes 2, SDS-solubilized (1%). **B.** Chemical crosslinking of LMBD1 with glutaraldehyde (0.025%) at 25°C for 10 min (lane 3), 30 min (lane 4), and 1 h (lane 5). Untreated LMBD1 (lane 1) or a 1 h glutaraldehyde-treated LMBD1 sample containing 1% SDS (lane 2) were used as controls. **C.** Chemical crosslinking of ABCD4 with formaldehyde (0.1%) at 25°C for 30 min (lane 2), 1 h (lane 3) and 4 h (lane 4). Untreated ABCD4 (lane 1) used as control. **D.** SEC-MALS analysis of LMBD1 (solid) and ABCD4 (dashed). The three major peaks of ABCD4, corresponding to PDCs, are indicated in red. For LMBD1, molecular mass contributions of protein (blue) and detergent (yellow) were deduced from the molecular mass of the PDC (green) using the ASTRA method (393). **E + F.** Representative SPR for fixed concentration screening (100 nM each) of buffer (black), BSA (red), ABCD4 (green), or LMBD1 (blue) binding to low-density LMBD1 (**E**, 100 RU) or ABCD4 (**F**, 100 RU) at 25 μl/min (1 min association + 5 min dissociation).

4.3.2 LMBD1 and ABCD4 interact by surface plasmon resonance (SPR)

From our preliminary screening (Fig. 4.1E-F), we detected specific LMBD1-ABCD4 binding when either protein was amine-coupled. To analyze the kinetics in greater detail, LMBD1 was then titrated over medium-density, amine-coupled ABCD4 surfaces (Fig. 4.2A). The saturable, dose-dependent LMBD1 binding observed (i.e. R_{obs} ~200 RU of LMBD1 bound at 100 nM) correlated well with a 1:1 PDC:PDC stoichiometry, based upon the PDC molecular masses calculated by SEC-MALS (i.e. 220 kDa LMBD1 / 310 kDa ABCD4 x 350 RU ABCD4 immobilized x 1:1 = 250 RU R_{max} predicted) and indicated that amine-coupled ABCD4 was functional (i.e. 200 RU R_{obs} / 250 RU R_{max} = ~80% surface activity). Slow dissociation rates (<10 %) did not permit fitting of the data using the simple 1:1 kinetics model. Alternatively, the multi-cycle titrations were analyzed according to the steady-state amounts of LMBD1 bound at the end of each association phase (Fig. 4.2B). Independent of mass transport effects, steady-state analyses for LMBD1 over low- (100 RU) and high-density (1150 RU) ABCD4 surfaces matched the medium-density outcomes in terms of (i) specific, dose-dependent binding characterized by slow dissociation kinetics, and (ii) low nanomolar binding affinities predicted. In the reversed orientation, steady-state analyses for ABCD4 (0-100 nM) titrated over multidensity LMBD1 surfaces (100, 200, 300 RU) yielded consistent outcomes. Taken together, our SPR data indicate that the specific, dose-dependent interaction between LMBD1 and ABCD4 is stable (i.e. slow dissociation rate kinetics) and high-affinity (i.e. apparent equilibrium dissociation constant (K_D) of 23 ± 4 nM; n = 7).

Given that binding between LMBD1 and ABCD4 was specific (i.e. minimal non-specific binding with 100 nM BSA or amine-coupled reference surfaces at 10 or 25 µl/min), a "linked reaction test" was performed to further investigate the slow dissociation rates consistently

observed across our multi-density, multi-orientation SPR experiments. Using the same flow rate, a fixed concentration of LMBD1 was repeatedly injected over immobilized ABCD4 with increasing contact time (Fig 4.2C). Using the "Fit separate k_a/k_d " tool (at beginning of dissociation phase to minimize potential rebinding effects), a 7-fold decrease in the rate of dissociation was detected as the contact time increased from 1 min ($k_d = 1.34 \times 10^{-3} \text{ s}^{-1}$) to 9 min ($k_d = 2.01 \times 10^{-4} \text{ s}^{-1}$). These findings suggest that LMBD1–ABCD4 binding may involve a conformational rearrangement – i.e. as evidenced during the linked reaction test, extended contact times prolong the time needed for LMBD1 and ABCD4 to dissociate (indicative of slower k_d rate during linked reaction test).

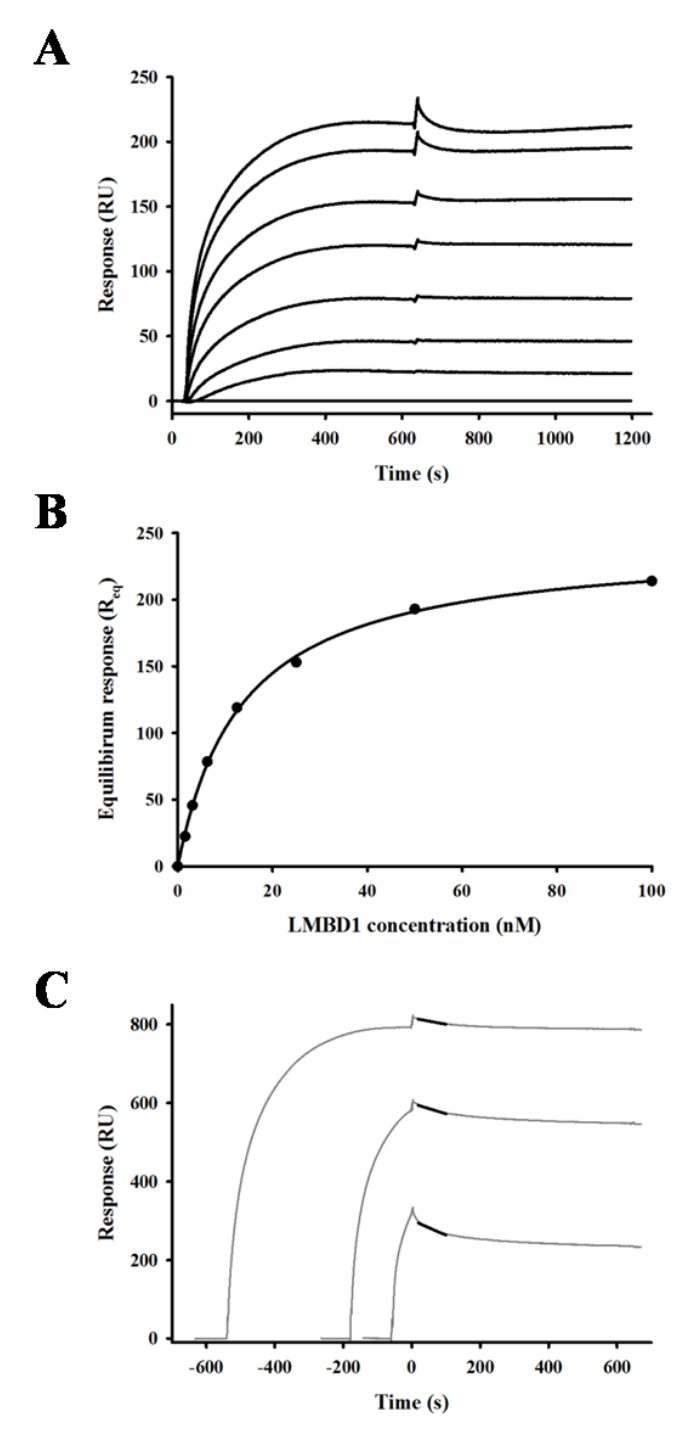


Figure 4.2. Representative SPR analyses for LMBD1 binding to amine-coupled ABCD4. A. Kinetics of LMBD1 (0-100 nM, 2-fold serial) binding to amine-coupled ABCD4 (350 RU) at 10 μ l/min (10 min association + 20 min dissociation). **B.** Steady-state binding responses were plotted versus LMBD1 concentration (circles) and fit to the "steady-state affinity" model in BIAevaluation (line). **C.** Under similar assay conditions, linked reaction test for LMBD1 (25 nM; grey) binding to ABCD4 (1100 RU) for 1, 3, and 9 min contact times (corresponding black bars reflect dissociation rate constants determined using "Fit separate k_a/k_d " tool in BIAevaluation).

4.3.3 Identification of MMACHC-binding sites on LMBD1 and ABCD4 by phage display

Phage display was used to predict regions on LMBD1 that may interact with MMACHC. Ensembles of 129 Ph.D.-C7C peptides and 149 Ph.D.-12 peptides previously isolated from MMACHC-binding phages (367) were aligned against the primary sequence of LMBD1, using RELIC/MATCH and MatchScan. Thirty four MMACHC-affinity selected peptides aligned to cytoplasmic loops (Table 4.0) based on the proposed topology of LMBD1 (UNIPROT: Q9NUN5), producing three distinct clusters (Fig. 4.3). Eight peptides aligned to residues 135-145 (region I), the loop between transmembrane helices (TM) 3 and 4. The largest cluster consisted of twenty aligned peptides (region II), aligning to residues 215-225 within the largest cytoplasmic segment of LMBD1 between TM5 and TM6. The remaining six peptides mapped within this same loop but to residues 260-267 (region III).

The same procedure was used to predict regions on ABCD4 that may interact with MMACHC. Affinity-selected peptides against MMACHC (367) were mapped to the primary sequence of ABCD4. Fourty three affinity-selected peptides aligned to ABCD4 and formed distinct clusters (Fig. 4.4; Table 4.1). All four predicted MMACHC-binding regions (I-IV) localized to the proposed cytoplasmic C-terminal nucleotide binding domain of ABCD4 (UNIPROT: O14678). Region I (residues 392-404) was N-terminal to the proposed Walker A motif (residues 421-428). Regions II (residues 456-464) and III (residues 501-511) mapped between the Walker A motif and proposed ABC signature (residues 524-530), Walker B motifs (544-549), and D-loop (548-555). The last region (IV; residues 584-592) mapped to the C-terminus of the NBD.

Table 4.0. MatchScan identification of MMACHC affinity-selected Ph.D.-12 and Ph.D.-C7C peptides aligned to sequence of LMBD1

Peptide	Peptide MATCH	Scoring window	Region	Alignment
	Score ¹	(residues) ²		position ³
TTLPYTH	15	6	I	139
L diksa h	13	5	I	136
H TALS AE	12	4	I	139
ATQVSTTFKILR	17	8	I	135
HSL talpwll ar	15	7	I	139
SPWSLTW THIKS	13	5	I	135
TL dmkta TGEMQ	13	5	I	136
HYSHWHNH RTAL	13	4	I	138
MKSLTLN	16	7	II	216
SALPNKM	16	4	II	217
TWSRLPL	15	5	II	217
N GMWHLP	14	6	II	215
MPLHL KC	14	5	II	218
AFPIN PT	13	5	II	219
LEF PLRL	12	4	II	220
D lplt rg	12	4	II	219
RP stlp y	12	4	ΙΙ	217
HS ltalpwll ar	16	8	II	216
TINKIKWTVHPL	15	7	II	221
KLW mwappl paq	14	6	II	216
GKANFAS LNLLR	14	5	II	221
VF TTLPL PHPNQ	13	5	II	217
KCCYPQ mssl vh	13	4	II	216
QSQLYPQ lpld W	13	4	II	219
SPKIIS sglp ty	12	4	II	217
VGATMQ stlp sy	12	4	II	217
GMNTNFS PLTL R	12	4	II	220
HD PLKL WQKWRH	12	4	II	220
PVPA ASY	13	4	III	260
QTH PLPS	13	4	III	260
KLWMWAP PLPAQ	17	5	III	260
QM RDKQ THWHVS	13	4	III	264
D FPAR LMPYGFL	12	4	III	261
HWWQMHPS FPAR	12	4	III	261

¹ Scoring window residues in **bold**.
² Score of comparison residues based on modified BLOSUM 62 matrix.
³ First residue of scoring window aligned to protein sequence.

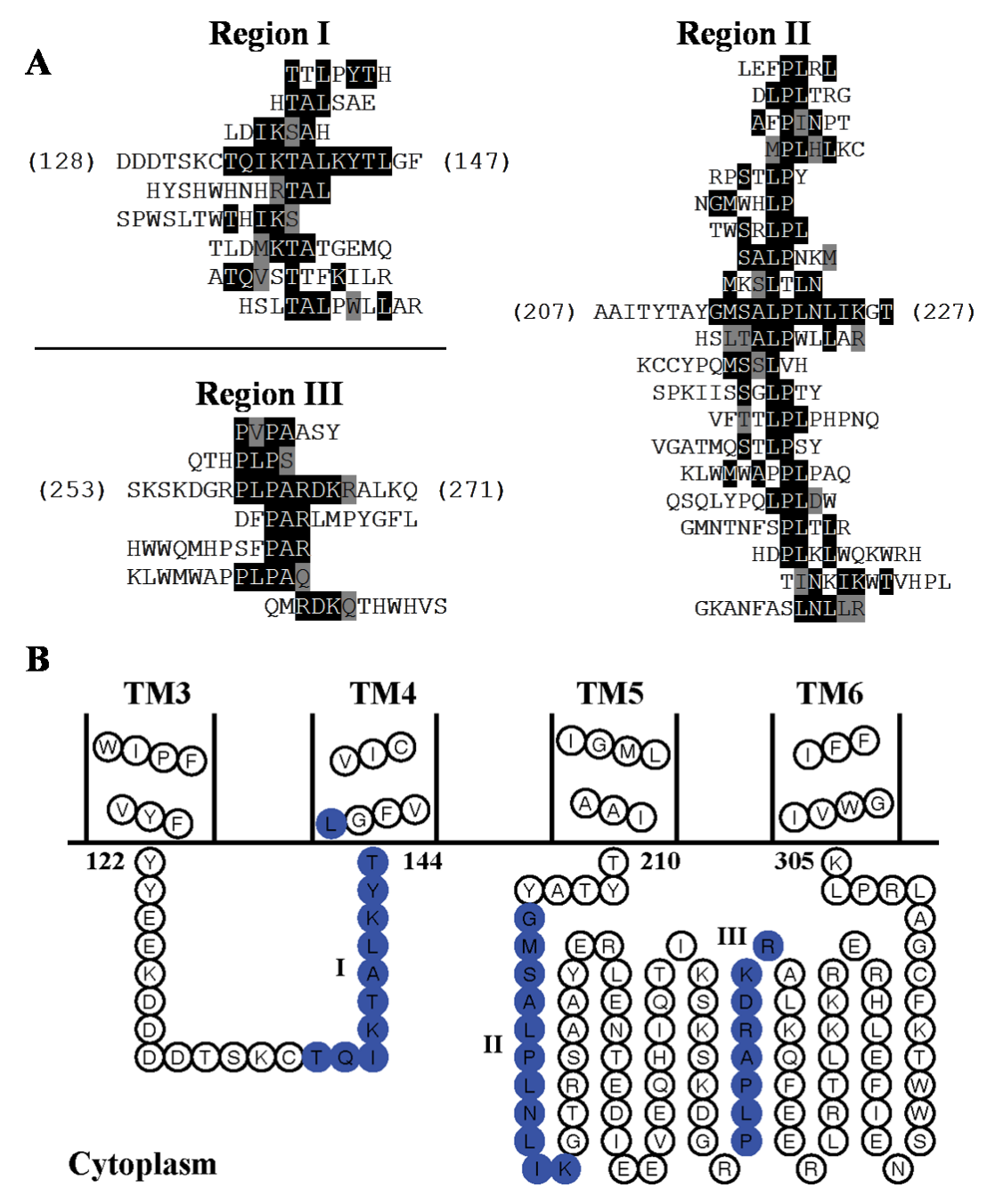


Figure 4.3. Phage display identifies putative MMACHC binding sites on LMBD1. A. MMACHC affinity-selected peptides aligned to three regions within cytoplasmic loops of LMBD1. Exact sequence matches are highlighted in black; conservative matches are highlighted in gray. **B.** Topology diagram of TM helices 3-6 of LMBD1 using boundaries from UniProt (Q9NUN5) and visualization with TOPO2. MMACHC-binding regions displayed in blue and denoted by roman numerals.

Table 4.1. MatchScan identification of MMACHC affinity-selected Ph.D.-12 and Ph.D.-C7C

peptides aligned to sequence of ABCD4

Peptide	Peptide MATCH	Scoring window	Region	Alignment
	Score ¹	(residues) ²		position ³
NSPKPLL	17	7	I	398
TPSSNRF	14	5	I	397
GD MKAPS	13	5	I	394
IDAPTWT	13	5	I	394
APST YLS	13	4	I	396
SP spss r	13	4	I	396
SKPLTAL	12	4	I	400
KCCYYL TSDKP G	17	5	I	398
HTSPW PSSQK HY	16	5	I	397
KCC VPISHP PLH	14	6	I	392
STPSA QLGPAPT	13	5	I	395
TFS SVSVP PPHI	13	5	I	393
YNNHQHNK SPSS	13	4	I	396
AGHDRLAV TPSS	12	4	I	396
STPSLHWALHQT	12	4	I	395
SA lpnk M	12	4	ΙΙ	459
LELPKEPW TRLP	18	8	ΙΙ	457
K iwmlpqqp elw	17	8	II	456
SYLHLRP LFLPN	16	5	II	457
SWRSEQ lslpq M	15	5	II	457
HDP LKLWQK WRH	14	6	II	457
Q TGLS PR	12	4	III	500
H nlvprhlg TVL	17	8	III	504
HSLTA LPWLLAR	15	7	III	502
KH vprte lsspr	15	5	III	506
YHEQDW LWAPTE	14	6	III	505
KCCYPQ msslv h	14	5	III	502
HLLSPELK LLAR	13	4	III	505
KCCFYQD NLLA N	13	4	III	504
HT LSDL YSPNLT	13	4	III	502
KIMPPNW LVAK L	13	4	III	505
VSNL PNSMYGTS	13	4	III	502
AQMPTEK LVGR W	12	4	III	505
LNN VLNL	12	4	IV	589
MK SLTL N	12	4	IV	587
P NFHS HN	12	4	IV	584
KIMPP NWLVAKL	15	7	IV	586
GKAN FASLNL LR	14	6	IV	585
HLL spelkl lar	14	6	IV	584
HNLVPRHLGTVL	13	4	IV	586
YSLRQDV LVLE E	13	4	IV	588
SYS KLHS STSLF	12	4	IV	584
HSLT ALPWLLAR	12	4	IV	586

⁷ Scoring window residues in **bold**.
² Score of comparison residues based on modified BLOSUM 62 matrix.
³ First residue of scoring window aligned to protein sequence.

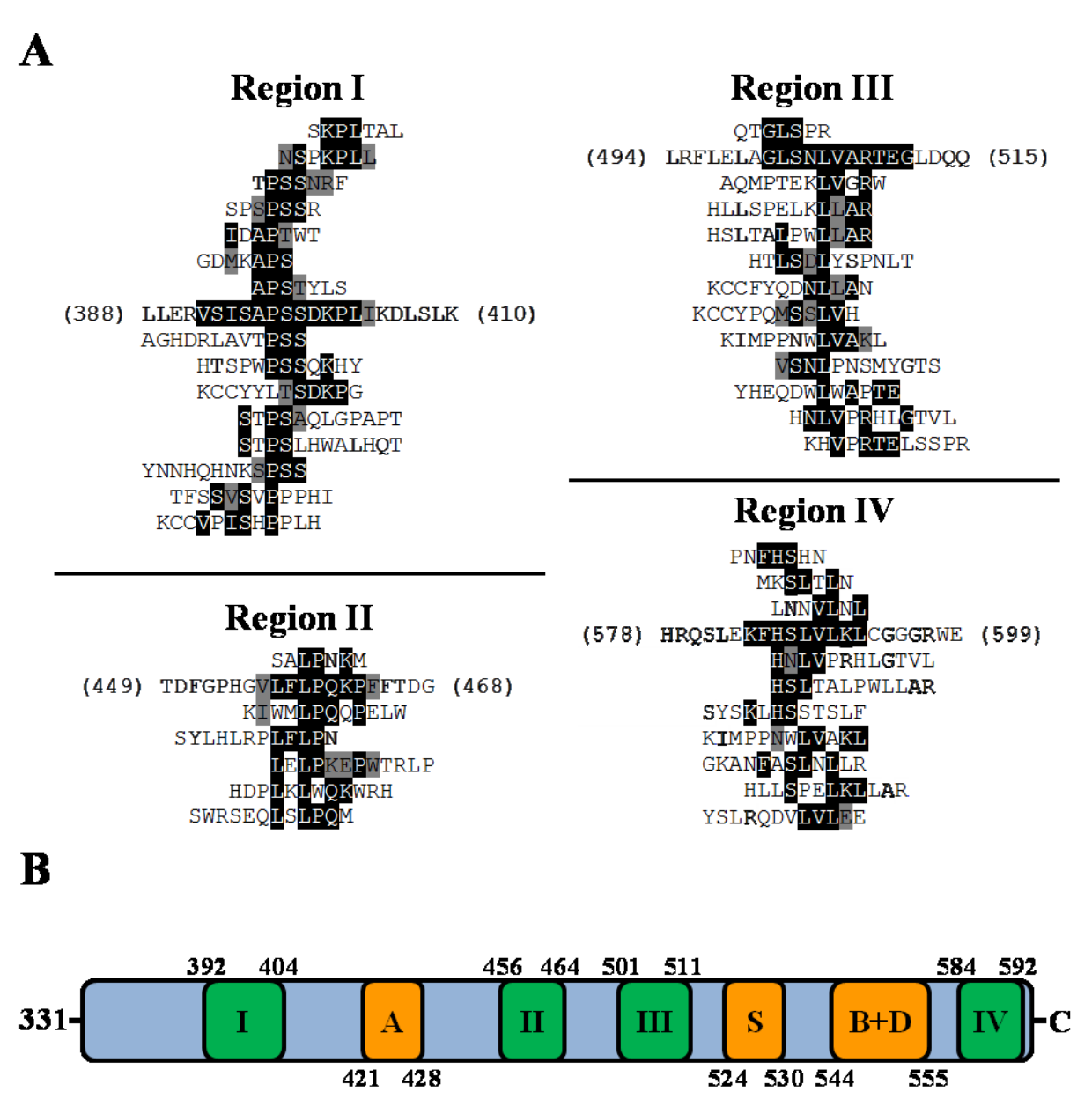


Figure 4.4. Phage display identifies putative MMACHC binding sites on ABCD4. A. MMACHC affinity-selected peptides aligned to four regions within the C-terminal nucleotide binding domain (NBD) of ABCD4 (I-IV). Exact sequence matches are highlighted in black; conservative matches are highlighted in grey. **B.** Linear representation of the NBD of ABCD4 with proposed catalytic motifs highlighted in orange: A, Walker A; S, ABC signature; B+D, Walker B and D-loop. MMACHC-binding regions are annotated in roman numerals and displayed in green.

4.3.4 Binary interactions of LMBD1 or ABCD4 with MMACHC or MMADHC by SPR

To supplement our phage display predictions, additional SPR analyses favoured the immobilization of MMACHC and MMADHC (32 kDa each) to maximize the signal range with the significantly larger LMBD1 (220 kDa) and ABCD4 (310 kDa) membrane proteins. Fixed concentration injections of LMBD1 and ABCD4 (100 nM each) yielded specific binding responses (1500-2000 RU) against immobilized MMACHC as compared to BSA (50 RU; Fig. 4.5A); even with normalization for the 3-5 fold difference in molecular mass between the PDCs and BSA, the binding responses with LMBD1 and ABCD4 were still significantly larger compared to BSA (e.g. 50 RU observed, as compared to 4-fold scale up = \sim 200 RU). In contrast, LMBD1 and ABCD4 yielded minor binding responses (20-30 RU) against immobilized MMADHC as compared to BSA (5 RU; 4-fold scale up = \sim 20 RU; Fig. 4.5B). Even with normalization for the 3.5-fold difference in the amine-coupled densities between MMACHC (700 RU) and MMADHC (200 RU), the LMBD1 and ABCD4 binding responses were still extremely low with MMADHC when compared to the theoretical R_{max} values (signal range of 1300-1900 RU anticipated, as readily achieved with MMACHC). While these results do not support a definitive role for MMADHC interacting with LMBD1 and ABCD4, we crossvalidated the integrity of our cytoplasmic protein preparations by titrating MMACHC with MMADHC (Fig. 4.5C); consistent with our previous publications (367, 424), MMACHC titrated over amine-coupled MMADHC surfaces yielded comparable, sub-micromolar affinity (Fig. 4.5D; $K_D = 360 \pm 23$ nM).

To examine their binding specificity with MMACHC in greater detail, detergent-solubilized ABCD4 (Fig. 4.6A) and LMBD1 (Fig. 4.6C) were then titrated over amine-coupled MMACHC surfaces. ABCD4 (Fig. 4.6B) and LMBD1 (Fig. 4.6D) exhibited saturable, dose-

dependent binding to MMACHC and similar affinities were detected (K_D of 50 ± 9 nM versus 31 \pm 6 nM, respectively). As a positive control, we also titrated MMACHC over the same immobilized MMACHC surfaces; similar to our previous publication (424), the association phase deviated from simple 1:1 kinetics (i.e. multi-phasic MMACHC-MMACHC interaction) and weak, sub-micromolar affinity was detected ($K_D = 798 \pm 42$ nM, n=3; see Fig. 4.6E-F for representative titration).

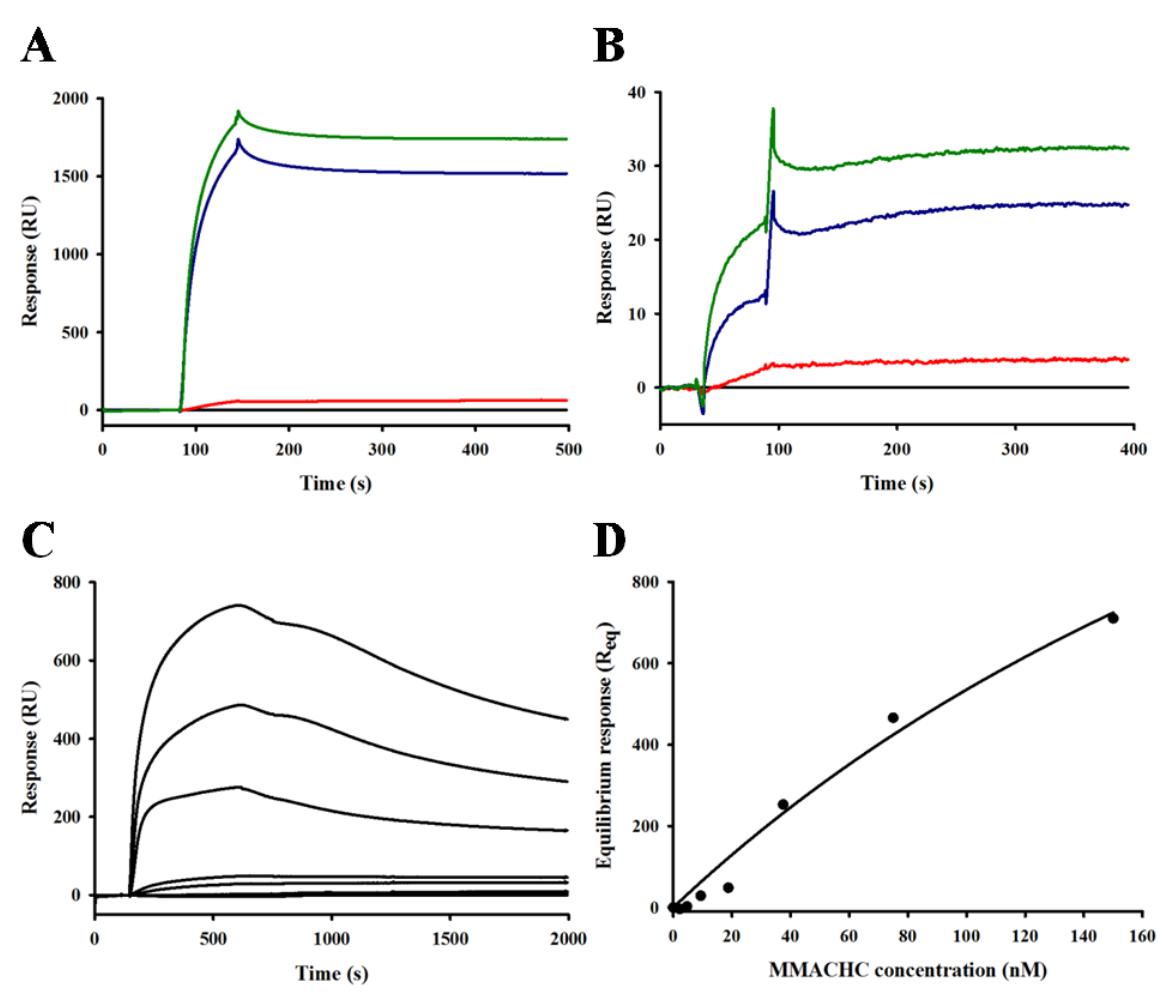


Figure 4.5. Representative SPR for LMBD1 and ABCD4 binding to amine-coupled MMACHC and MMADHC. Kinetics of buffer (black), BSA (red), ABCD4 (green), or LMBD1 (blue), each at 100 nM, binding to amine-coupled MMACHC (A, 700 RU) or MMADHC (B, 200 RU) at 25 μ l/min (1 min association + 5 min dissociation). C. Kinetics of MMACHC (0-150 nM, 2-fold serial) binding to MMADHC (700 RU) at 25 μ l/min (10 min association + 20 min dissociation). D. Steady state binding responses from C were plotted versus MMACHC concentration (circles) and fit to the "steady-state affinity" model in BIAevaluation (line).

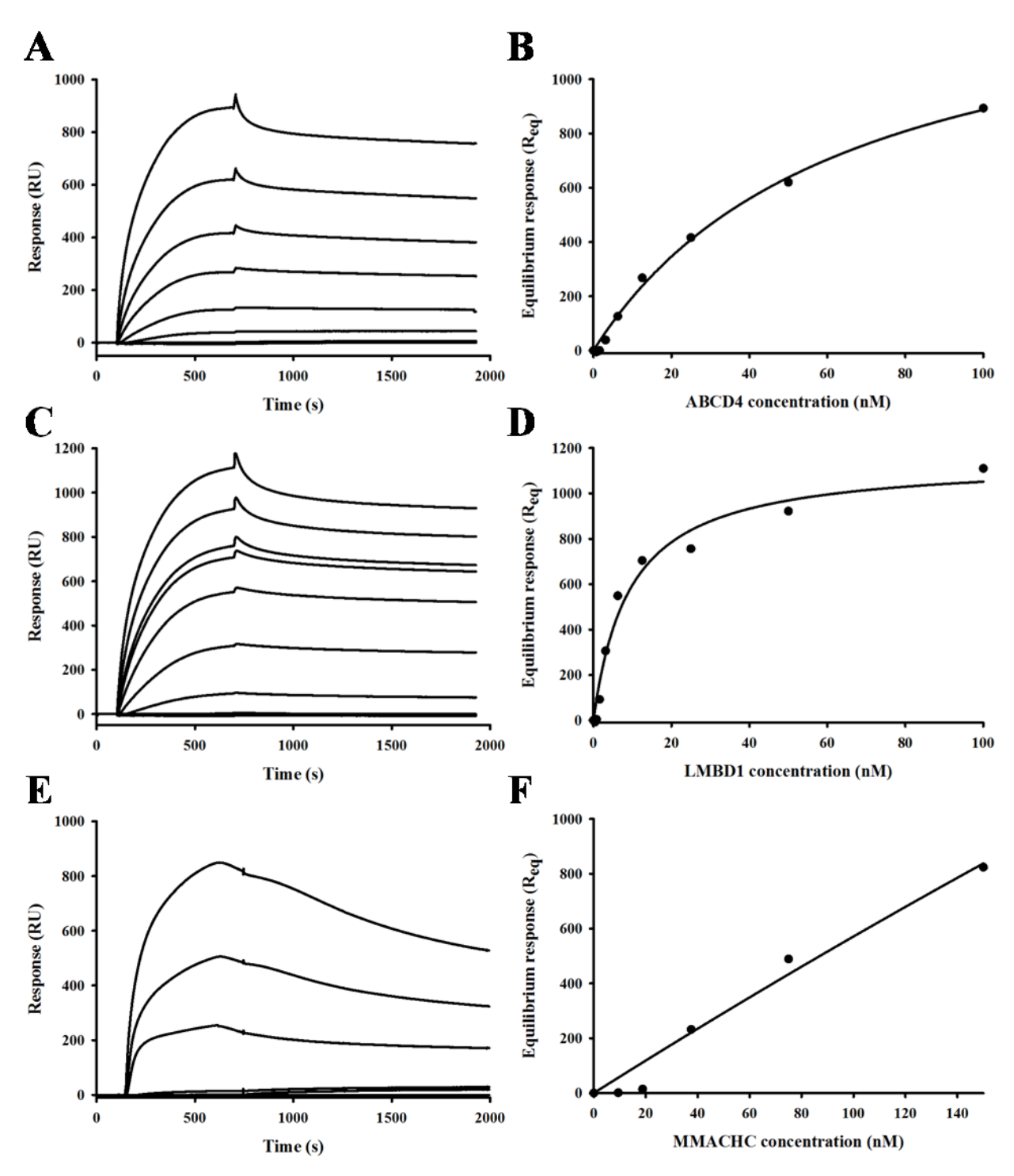


Figure 4.6. Representative SPR for ABCD4, LMBD1, and MMACHC binding to amine-coupled MMACHC. Kinetics of ABCD4 (A), LMBD1 (C), and MMACHC (E) binding (0-100 nM for LMBD1 and ABCD4, 0-150 nM for MMACHC, all 2-fold serial) to immobilized MMACHC (700 RU) at 25 μl/min (10 min association + 20 min dissociation). Corresponding binding isotherms in which steady-state binding responses were plotted versus analyte concentrations (circles; **B**, ABCD4; **D**, LMBD1; **F**, MMACHC) and fit to the "steady-state affinity" model in BIAevaluation (lines).

4.4 Discussion

The molecular bases of the *cblF* and *cblJ* defects were recently solved when *LMBRD1* and *ABCD4* were identified to encode putative lysosomal exporters of Cbl (332, 342). Mutations in their encoded gene products, LMBD1 and ABCD4, prevent the lysosomal release of Cbl to the cytoplasm. We have now reported the recombinant production of LMBD1 and ABCD4 and, although the overall yields of these membrane proteins were fairly limited (despite extensive optimization), both were highly pure (> 95%) and stable in solution – essential criteria for the biophysical analyses performed. LMBD1 was monodisperse by size exclusion chromatography, despite the presence of heterogeneous glycosylation by SDS-PAGE. ABCD4 was more polydisperse than LMBD1 and also heterogeneous at the protein level, due to solvent inaccessibility of the affinity tag.

Because of limited structure-function studies, our understanding of LMBD1 and ABCD4 has been primarily derived from homologous proteins to date. LMBD1 shares homology (13.7% identity, 27.8% similarity) with the lipocalin-1 interacting membrane receptor (LIMR). LIMR is widely expressed across tissues and localizes to the plasma membrane (442), in contrast to LMBD1 which demonstrates only minor localization to the plasma membrane (339). Consistent with LMBD1, LIMR contains nine putative transmembrane helices. LIMR binds and internalizes lipocalins via receptor-mediated endocytosis; lipocalins are small extracellular carriers of hydrophobic molecules. Recombinant production of human LIMR in a *Drosophila* expression system was recently demonstrated by Hesselink and co-workers (443). Consistent with our LMBD1 results, their migration of LIMR by SDS-PAGE was aberrant, despite immunoblotting and mass spectrometry that identified a complete protein. More importantly, the authors demonstrated that DDM-solubilized LIMR forms dimers in solution. Our BN-PAGE,

crosslinking, and SEC-MALS results for LMBD1 are consistent with those for LIMR, in that LMBD1 predominantly forms dimers in solution.

Recombinant ABCD4 demonstrates heterogeneity in its oligomeric state, but our results indicate that dimeric ABCD4 is the predominant form when solubilized in mixed DDM and CHS micelles. ABCD4 is part of the D subfamily of peroxisomal ABC half transporters and shares homology (25-27% sequence identity) with the other members; ABCD1, ABCD2, and ABCD3 (349). Interaction analyses performed on other members of this subfamily support our conclusions that ABCD4 forms homodimers. Using yeast two-hybrid approaches, Liu and coworkers (347) showed that the cytoplasmic C-terminal nucleotide binding domain of ABCD1, ABCD2, and ABCD3 mediates homo- and heterodimerization in all possible combinations. In another study, ABCD1 and ABCD3, isolated from mouse liver, formed homodimers (444). Live cell FRET microscopy recently identified homodimerization of ABCD1 and ABCD3 in addition to the formation of an ABCD1-ABCD3 heterodimer complex (348). This study also concluded that the extreme C-terminal residues mediate dimerization. The c.1746 1747insCT (p.E583LfsX9) frameshift mutation in ABCD4 that gives rise to the cblJ defect (342) may therefore reflect the inability of ABCD4 to form a functional ABC transporter by preventing homodimerization. Homodimerization of ABCD4 via C-terminal residues buried within this interface may explain the heterogeneity of our ABCD4 preparations at the affinity tag.

Following our BN-PAGE, crosslinking, and SEC-MALS experiments, the SPR analyses validated the ABCD4 and LMBD1 self-associations, as well as LMBD1–ABCD4 binding kinetics. Amine-coupled sensor surfaces were selected over Ni-NTA due to the lower sample consumption, and previous reports that indicated similar membrane protein outcomes using either surface (445). The high-affinity interaction that we detected between ABCD4 and

LMBD1 (i.e. $K_D \sim 23$ nM by SPR) suggests that their interaction is physiologically relevant. Moreover, the slow dissociation rate indicates that they form a very stable complex. Based on our linked reaction test results, we suggest that the slow dissociation between ABCD4 and LMBD1 may result from conformational rearrangements that predominate with increasing contact time. For example, the ABC transporter BtuC₂D₂ mediates Cbl import into the cytoplasm of E. coli by forming a complex with the periplasmic Cbl-binding protein BtuF. Similar to our ABCD4–LMBD1 outcomes, BtuF binds BtuC₂D₂ with high affinity and their interaction is characterized by a slow dissociation rate (446). Slow dissociation may be an inherent feature for protein-protein interactions involving Cbl-binding proteins, as we also observed poor dissociation when assessing the MMACHC–MMADHC interaction (367, 424). On its own, BtuC₂D₂ has poor affinity for Cbl which necessitates the delivery of Cbl by BtuF. In mammalian Cbl metabolism, a BtuF-like lysosomal Cbl binding protein has not yet been identified. Cultured cblF or cblJ fibroblasts accumulate non-protein bound Cbl, which argues against the presence of a lysosomal Cbl-binding protein. Instead, we propose that Cbl transport across the lysosome is mediated by tight complex formed between LMBD1 and ABCD4; in accordance with a previously proposed hypothesis (342), it is likely that LMBD1 forms the substrate channel and ABCD4 provides the energy for transport.

Our phage display predictions indicate that cytoplasmic regions of LMBD1 and ABCD4 can recruit MMACHC. We identified three cytoplasmic loop regions on LMBD1 that localized between TM helices 3-4 and 5-6, with the latter loop containing two predicted MMACHC recruitment sites. There are no known point mutations within these regions in patients with the *cblF* defect. Rather, all known mutations in *LMBRD1* result in protein truncation (332, 334, 335). For ABCD4, we identified four regions within the cytoplasmic C-terminal nucleotide

binding domain. These regions did not overlap with the putative motifs required for ATP hydrolysis, but two overlapped with known mutations in *ABCD4* (p.G443_S485del and p.E583LfsX9) that would effectively abrogate the proposed binding residues.

The predictive power of phage display is illustrated in our previous work where we proposed binding interfaces between MMACHC and MMADHC and then followed up with SPR (*in vitro*) and bacterial two hybrid (*in vivo*) analyses to provide direct evidence for their interaction (367, 424). Five MMACHC-binding regions were proposed that localized to residues C-terminal to Glu₁₄₂ on MMADHC (367). An independent group (447) recently corroborated our findings by demonstrating that MMACHC can bind to an MMADHC variant lacking 115 N-terminal residues. Further, phage display has also been used to uncover putative protein recruitment regions on solvent-exposed regions of membrane proteins. This technique was used to identify regions on ferrichrome or Cbl TonB-dependent transporters (TBDT) (448) which were later confirmed by structures of TBDT-TonB complexes (247, 449). Thus, the utility of phage display to predict protein-protein interactions has been validated.

We now communicate phage display results that predict MMACHC-binding sites on ABCD4 and LMBD1. Importantly, our SPR analyses have provided convincing, direct evidence that both of these membrane proteins can interact with MMACHC in a specific, dose-dependent manner. While the same analyses do not provide convincing evidence that MMADHC is a partner protein for ABCD4 or LMBD1, we did perform control titrations to cross-validate our previously published SPR data for MMACHC–MMACHC and MMACHC–MMADHC (367, 424). Given that the functional integrity of our MMACHC and MMADHC preparations was intact, it is interesting to note that the affinity of MMACHC for ABCD4 or LMBD1 ($K_D \sim 50$ nM and $K_D \sim 30$ nM, respectively) is stronger compared to MMADHC ($K_D \sim 360$ nM). Thus, the

interaction of MMACHC with these lysosomal exporters would be favoured over cytoplasmic MMADHC should they be mutually exclusive.

Our evidence for the recruitment of MMACHC to the cytoplasmic side of lysosomal exporters agrees with a model proposed by other groups (286, 435). In this model, recruitment of MMACHC to the lysosomal exporters permits the vectorial delivery of transported Cbl to MMACHC preventing exposure of the reactive cofactor to the cellular milieu. A similar model has been proposed for the transport of siderophores and Cbl across the OM of E. coli, whereby periplasmic binding proteins are recruited by TonB and oriented beneath the periplasmic face of TBDTs to allow for the efficient capture of incoming substrate (251, 252). MMACHC shows sequence homology to TonB, which interacts with periplasmic-accessible residues of TBDTs to mediate transport across the outer membrane. Our results suggest that MMACHC favours recruitment by LMBD1 ($K_D = 30 \text{ nM}$) over ABCD4 ($K_D = 50 \text{ nM}$). While this is plausible given that LMBD1 is speculated to be the transport channel of this process (342), we cannot discount that MMACHC interacts with both putative exporters. We also propose that Cbl-binding triggers dissociation of MMACHC from these exporters and recruitment of MMADHC to chaperone MMACHC-bound Cbl in the cytoplasm. The Cbl-dependence of the MMACHC-MMADHC interaction has recently been shown by an independent group (447).

Results from this study are consistent with the proposed channeling and chaperoning of Cbl that is mediated through protein-protein interactions (50, 288). Limited to phenotypic studies, to date, the identification and characterization of multiprotein complexes involved in the lysosomal transport of Cbl advances our basic understanding of early intracellular vitamin B_{12} metabolism.

4.5 Acknowledgments

Research was supported by operating grants to J.W.C. from the Natural Sciences and Engineering Research Council (NSERC; RGPIN 7289-06-07) and to D.S.R. from the Canadian Institutes of Health Research (CIHR; MOP-15078). The McGill SPR Facility thanks the Canada Foundation for Innovation (CFI grant to Montreal Integrated Genomics Group for Research on Infectious Pathogens) and Canadian Institutes of Health Research (CIHR Research Resource Grant 200610PRG-165657-PRG-CFAA-11449) for infrastructure support. The Structural Genomics Consortium (SGC) is a registered charity (no. 1097737) that receives funds from AbbVie, Canadian Institutes for Health Research, Genome Canada, GlaxoSmithKline, Eli Lilly Canada, the Novartis Research Foundation, Pfizer, Takeda, Canada Foundation for Innovation, the Ontario Ministry of Economic Development and Innovation, and the Wellcome Trust (092809/Z/10/Z). J.C.D. is recipient of a Canada Graduate Scholarship from NSERC and doctoral research award B2 from the Fonds Québécois de la Recherche sur la Nature et les Technologies (FQRNT). The authors wish to thank other members of the SGC, including L. Shrestha for baculovirus construction and initial detergent screening of LMBD1, C. Shintre for providing ABCD4 baculovirus and purification conditions, R. Chalk and G. Berridge for mass spectrometry services, and S. Mukhopadhyay for cell culture training.

Chapter 5

Conclusions and future directions

5.0 Completion of thesis objectives

Patients with mutations in *MMACHC*, *MMADHC*, *LMBRD1*, or *ABCD4* have severe hematological and neurological conditions caused by the impairment of the MCM and MS reactions. To date, few studies have examined the structural and functional properties of the MMACHC, MMADHC, LMBD1 and ABCD4 protein products as related to the molecular mechanisms of Cbl transport. Consistent with Cbl channeling models found in enzymes involved in Cbl biosynthesis (221) and the reactivation of MCM (309), we hypothesize that protein-protein interactions involving MMACHC, MMADHC, LMBD1 and ABCD4 mediate the vectorial delivery of Cbl to the downstream enzymes MCM and MS. The underlying objective of this thesis was to perform detailed characterizations of the protein interactions involved in early intracellular transport and processing of Cbl in mammals.

In chapter 2, we reported the recombinant production of two physiologically relevant isoforms of MMADHC. We demonstrated that N-terminal residues of MMADHC contribute to the overall disorder and conformation of the protein but are not involved in binding MMACHC. We further characterized this interaction by predicting regions on MMACHC that self-associate or bind MMADHC. Based on these analyses, we proposed that the function of MMADHC is exerted through C-terminal residues that mediate its interaction with MMACHC, as opposed to binding Cbl directly. Since our publication of these outcomes, a more recent report has validated these findings by demonstrating that an MMACHC–MMADHC complex can be formed using an MMADHC variant lacking its unstructured N-terminal domain (447).

To gain insight into the subcellular location for such a complex, immunofluorescence and fractionation studies were performed in chapter 3. Previous reports on the cellular distribution of MMACHC and MMADHC were ambiguous. We have now provided definitive evidence that

MMADHC is found exclusively as a full-length protein in both the cytoplasm and mitochondria, indicating a mechanism for dual localization of the protein. We also localized MMACHC exclusively to the cytoplasm. We therefore propose that the MMACHC–MMADHC complex is formed in the cytoplasm and that MMACHC may play a role in the dual localization of MMADHC.

In chapter 4 we extended our protein-protein interaction analyses by describing the recombinant production of the lysosomal membrane proteins LMBD1 and ABCD4. Detergent-solubilized LMBD1 and ABCD4 formed homodimers. We further demonstrated that LMBD1 and ABCD4 interacted with low nanomolar affinity, in addition to each membrane protein's binding MMACHC with slightly weaker affinity. Through phage display, putative MMACHC-binding regions on LMBD1 and ABCD4 were identified. These previously proposed interactions (286, 342, 435) are now supported by our direct experimental outcomes.

Overall, we have elucidated and characterized protein-protein interactions involved in early intracellular Cbl metabolism; our results support a model for the vectorial delivery of Cbl. In this model an LMBD1–ABCD4 complex mediates the efflux of lysosomal Cbl to the cytoplasm. The recruitment of MMACHC to cytoplasmic regions on LMBD1 and ABCD4 permits the efficient directional transfer of the cofactor to the Cbl-binding site of MMACHC, further sheltering Cbl from the cellular milieu. We propose that substrate transfer triggers the dissociation of MMACHC from LMBD1 and ABCD4 and signals recruitment by the adapter protein MMADHC. The cytoplasmic MMACHC–MMADHC complex could then be responsible for the processing and partitioning of Cbl between the cytoplasm and mitochondria and the delivery of this cofactor to the downstream enzymes MCM and MS.

The identification and characterization of protein-protein interactions involved in the escort of Cbl improves our basic understanding of early intracellular Cbl metabolism which to date has been limited to phenotypic studies. While our analyses support the model described above, many questions remain unanswered including the mechanism for the transport of Cbl by the LMBD1–ABCD4 complex. To this end, the next steps for this research program are proposed below.

5.1 Directions for future research

5.1.0 Detection of protein complexes in vivo

Our *in vitro* protein-protein analyses have characterized interactions between soluble cytoplasmic (MMACHC, MMADHC) and lysosomal membrane proteins (LMBD1, ABCD4). To corroborate these outcomes, we advocate the use of *in vivo* experimental strategies.

Detection of the MMACHC–MMADHC interaction by protein complex immunoprecipitation (Co-IP) would be feasible given the availability of anti-MMACHC or anti-MMADHC antibodies previously generated from our recombinant proteins. Immobilized antibodies on a Protein A/G support would be incubated with fibroblast lysates derived from control or patients in the *cblC* or *cblD* complementation group and precipitated via centrifugation. MMACHC and MMADHC complexes pulled down from the lysate would be eluted and separated by SDS-PAGE. Visualization of these proteins would necessitate Western blotting since MMACHC and MMADHC levels within fibroblasts are low (424). This strategy has recently been used to detect complex formation between MMACHC and MS in fibroblasts (375).

The use of chemical crosslinking agents to identify protein complexes *in vitro* has been reported in our work. This experimental strategy also shows prospects for *in vivo* studies, and

we propose a procedure for the detection of MMACHC and MMADHC complexes in vivo. The availability of commercial crosslinking agents with various spacer arm lengths and coupling chemistries enables us to probe for MMACHC and MMADHC complexes using several of these chemicals. Formaldehyde is a cell-permeable crosslinker with short cross-linking span (2-3 Å) that couples proteins with high specificity via primary amines. Homobifunctional amine-toamine crosslinkers, such as NHS and imidoesters, provide more variable spacer arm lengths (3.0-16.1 Å) and can be used to probe for these complexes. Other crosslinking chemistries include sulfhydryl groups found on cysteine residues, which can be crosslinked to other sulfhydryl or amine groups. The protocol for *in vivo* crosslinking involves incubation of the chemical crosslinker directly with intact fibroblasts, in which case the crosslinker must be permeable to the membrane, or with lysates derived from fibroblasts. Similar to co-IP experiments our cultured fibroblasts would consist of control lines and lines from cblC and/or cblD patients. Following crosslinking, samples would be subjected to SDS-PAGE followed by Western blotting using our anti-MMACHC and anti-MMADHC antibodies which would detect the presence of protein adduct of molecular mass consistent with an MMACHC–MMADHC complex.

The *in vivo* detection of complexes formed from LMBD1 or ABCD4 (i.e. LMBD1–LMBD1, ABCD4–ABCD4, LMBD1–ABCD4, LMBD1–MMACHC, ABCD4–MMACHC) will be more challenging given the lack of well-characterized antibodies targeting either membrane protein. Antibodies derived from LMBD1 or ABCD4 peptides have been described in the literature (339, 340, 345, 346), but their specificities have been brought into question, particularly for ABCD4 (345). Prior to embarking on co-IP and crosslinking studies similar to those described for MMACHC and MMADHC above, we advocate the generation of specific polyclonal antibodies targeting our native, recombinant forms of LMBD1 and ABCD4.

5.1.1 Refinement of protein interaction interfaces

To determine the regions or residues that specifically mediate these interactions we propose a standard mutagenesis approach. We have already begun delineating the MMACHC–MMADHC interaction (chapter 2) whereby we demonstrated that N-terminal residues of MMADHC are not necessary for binding MMACHC (424). We further proposed that structured C-terminal residues of MMADHC are critical for this interaction and mapped these residues by phage display (367, 424). A recent study corroborated our outcomes by demonstrating MMACHC binding to an MMADHC variant lacking 115 N-terminal residues (447).

The use of alanine-scanning mutagenesis to mutate the five predicted MMACHC-binding regions on MMADHC, or the four predicted MMADHC-binding regions on MMACHC, would elucidate the interaction interface. Mutated recombinant forms of MMACHC or MMADHC could be analyzed by SPR and binding kinetics reported. Alternatively, *in vivo* strategies similar to those outlined above could be used. For fibroblast studies, the use of *cblC* or *cblX* cell lines that lack MMACHC expression or *cblD* cell lines that lack MMADHC expression would be required to eliminate production of wild-type proteins. Corresponding cell lines would be transfected to express mutant MMACHC or MMADHC and complex formation monitored by co-IP or crosslinking analyses. The use of a bacterial coexpression system, whereby wild-type protein and mutant partner are produced simultaneously, would be easier to implement. This system would also allow for disulfide-scanning mutagenesis studies whereby residues within regions on MMACHC and MMADHC predicted to interact are converted to cysteine and complexation monitored after addition of an oxidizing agent (typically copper phenanthroline).

In chapter 4 we identified MMACHC-binding sites on cytoplasmic regions of LMBD1 and ABCD4. It would be desirable to perform complementary analyses to identify regions on

MMACHC predicted to bind LMBD1 and ABCD4. Unlike soluble proteins, the utilization of detergent-solubilized membrane proteins for combinatorial phage panning has not been widely reported in the literature. However, the use of a synthetic model membrane system, or nanodiscs, to support membrane proteins for phage panning has recently shown promise (450). Reconstitution of LMBD1 and ABCD4 into nanodiscs followed by phage panning would allow for the identification of residues involved in: (i) homodimerization, (ii) binding their partner membrane protein, and (iii) recruiting MMACHC. These outcomes would also open up similar avenues for mutagenesis experiments would elucidate the residues that mediate these protein-protein interactions.

5.1.2 Mechanism for the dual-localization of MMADHC

In chapter 3 we demonstrated the subcellular location of MMACHC and MMADHC. The mechanism for the dual localization of MMADHC to the cytoplasm and mitochondria is not well understood, with several mechanisms proposed for this process (382). Based on our results (451) and an additional study (380), it has been proposed that MMACHC influences the partitioning of MMADHC to its two known subcellular locations by complex formation. It would be desirable to understand the molecular mechanisms of the dual localization of MMADHC. We suggest an experimental strategy whereby MMADHC is isolated from cytoplasmic and mitochondrial fractions of cultured fibroblasts by subcellular fractionation, and pulled down using anti-MMADHC antibodies coupled to a protein A/G resin. Affinity-purified cytoplasmic and mitochondrial MMADHC would be subjected to SDS-PAGE followed by blotting onto a PVDF membrane and Coomassie staining. Stained blots would be sent for N-terminal sequencing (Edman degradation) which would identify the MTS. The absence of an MTS on cytoplasmic MMADHC would imply that MMADHC is processed in the mitochondria

and transported in retrograde fashion back into the cytoplasm. Alternatively, the presence of a MTS would signify that mitochondrial import of MMADHC is inhibited. To test the hypothesis that the interaction of MMADHC with MMACHC is the mitigating factor in mitochondrial import of MMADHC, the distribution of MMADHC could be determined in cultured fibroblasts from *cblC* or *cblX* patients that express mutated or reduced levels of MMACHC, respectively. This can be performed using subcellular fractionation as described in chapter 3 (451) followed by quantitative densitometry analyses that compare MMADHC cytoplasmic/mitochondria distributions from patient lines compared to control lines. Outcomes from these studies would determine the involvement of MMACHC in the dual-localization of MMADHC and provide mechanistic details for this process.

5.1.3 Assessment of LMBD1 and ABCD4 activity

Chapter 4 described the production of LMBD1 and ABCD4 necessary for our interaction analyses. The availability of recombinant LMBD1 and ABCD4 enables the pursuit of functional studies to determine the direct involvement of these proteins in Cbl binding and export across the lysosomal membrane. In the Cbl-uptake system of *E. coli*, the periplasmic Cbl-binding protein BtuF mediates delivery of Cbl to the cytoplasmic membrane ABC transporter BtuC₂D₂. BtuC₂D₂ has weak affinity for Cbl on its own and necessitates docking of holo-BtuF for cellular Cbl import (446). A homolog of BtuF or of lipocalin-like Cbl-binding proteins has not been detected in mammals, and may not exist given that the *cblF* and *cblJ* phenotypes are characterized by the accumulation of nonprotein-bound Cbl. Thus, LMBD1 and ABCD4 have been implicated in the transport of Cbl through direct binding of the cofactor, with LMBD1 forming a substrate channel and ABCD4 providing the energy for this process. The use of surface plasmon resonance (SPR) to study the binding of Cbl to LMBD1 or ABCD4 has been

advocated (452), and we have demonstrated success using this technique to characterize LMBD1 and ABCD4 interactions. To test for Cbl-binding, LMBD1 or ABCD4 would be immobilized to the surface of a sensor chip at very high densities (~10,000 RU), given the significantly large differences in molecular mass calculated for the protein-detergent complexes of LMBD1 (220 kDa) and ABCD4 (310 kDa) compared to injected Cbl analytes (1.3-1.5 kDa). Binding of all four Cbl derivatives (CNCbl, OHCbl, MeCbl, AdoCbl) to LMBD1 and/or ABCD4 would be assessed.

To assay the transport of Cbl across a membrane, we advocate the reconstitution of LMBD1 and/or ABCD4 into proteoliposomes. Proteoliposomes are formed by the insertion of membrane proteins into liposomes that are small vesicles composed of lipid bilayers.

Proteoliposome assays are advantageous because they directly monitor substrate transfer across a membrane. Furthermore, the function of ABC transporters is typically enhanced in proteoliposomes compared to detergents (453, 454). We advocate a protocol similar to that described by Borths *et al.* (455), whereupon the transport of radiolabeled Cbl and the rates of ATP hydrolysis were measured following reconstitution of the bacterial Cbl ABC transporter BtuC₂D₂ into proteoliposomes. Our studies would necessitate the reconstitution of LMBD1 and ABCD4 individually or together into proteoliposomes, followed by assessment of activity by assaying rates of Cbl transport and ATP hydrolysis. The modulatory effects of MMACHC, MMADHC, other Cbl derivatives, and acidification (pH 5.0) to reflect the lysosomal environment, on these rates could further be determined.

5.1.4 Structure determination of MMADHC, LMBD1, and ABCD4

While two structures of MMACHC were solved (366, 372) during the course of this thesis, structural details of MMADHC, LMBD1, and ABCD4 remain elusive. In chapter 2 we

describe the production of highly pure recombinant isoforms of MMADHC suitable for structural analyses. Apart from forming a complex with MMACHC (367, 424, 447), the function of MMADHC remains obscure; determination of the MMADHC structure could provide details into its function. As reported (424, 447), the N-terminal domain of MMADHC is unstructured making these residues intractable for X-ray crystallography or nuclear magnetic resonance (NMR) studies. As such, we were unable to generate crystals despite high-throughput screening of our MMADHC isoforms. Based on our disorder predictions (424) and proteolytic degradation studies (447), the C-terminal domain of MMADHC is stable, structured, and resistant to degradation. We therefore propose the generation of an N-terminal deletion variant of MMADHC (MMADHCΔ1-115) for crystal screening and structure determination. Given that MMADHCΔ1-115 still demonstrates affinity towards MMACHC (447), co-crystallization of an MMACHC–MMADHCΔ1-115 complex could also be initiated for elucidation of specific residues that mediate this interaction.

Given that membrane proteins account for 20-30% of the total proteome and represent major targets, they are greatly underrepresented in the Protein Data Bank (< 0.1% of total protein structures). This is largely due to the hydrophobicity of such proteins which require membrane mimetic environments such as detergents. For LMBD1 and ABCD4, these limitations are further influenced by (i) yields which impede further purification by preparative size exclusion chromatography, and (ii) inherent heterogeneity. Yields can be improved by the growth of larger scale cultures. For LMBD1, heterogeneity is imparted by glycosylation that is not alleviated through treatment with PNGase F. Given that heterogeneous glycosylation can inhibit crystallographic efforts, we propose the purification of an LMBD1 mutant lacking its six predicted N-glycosylation sites. For ABCD4, heterogeneity is the result of incomplete affinity-

tag cleavage, which we have not found a way to alleviate to date. To improve sample homogeneity, we propose not incorporating a cleavage and reverse purification step for structural studies on ABCD4. Rather, this step can be replaced by preparative size exclusion chromatography which would allow the isolation of monodisperse, homogeneous, ABCD4 with its affinity tag intact. Studies of structural biology on both membrane proteins will be difficult, but rewarding. Co-crystallization of an LMBD1–ABCD4 complex would also be an avenue worth pursuing as a long term goal for this project.

References

- 1. **Stubbe J.** 1994. Binding site revealed of nature's most beautiful cofactor. Science **266:**1663-1664.
- 2. **Addison T.** 1855. On the constitutional and local effects of disease of the suprarenal capsules. Highley, London.
- 3. **Scott JM, Molloy AM.** 2012. The discovery of vitamin B₁₂. Ann. Nutr. Metab. **61:**239-245.
- 4. **Ehrlich P.** 1880. Über regeneration und degeneration der rothen Blutschreiben bei Anäemien. Klin. Wochenschr. **117:**405.
- 5. **Fenwick S.** 1870. On atrophy of the stomach. Lancet **96:**78-80.
- 6. **Cahn A, Mering J.** 1886. Die Säuren des gesunden und kranken Magens. Deutsches Arch. Klin. Med. **39:**233-253.
- 7. **Faber K, Bloch C.** 1900. Über die pathologischen Veränderungen am digestion-stractus bei der perniciösen anämie und über die sogenannte Darmatrophie. Ztschr. Klin. Med. **40:**98-135.
- 8. **Whipple GH, Robscheit FS, Hooper CW.** 1920. Blood regeneration following simple anemia. IV. Influence of meat, liver and various extractives, alone or combined with standard diets. Am. J. Physiol. **53:**236-262.
- 9. **Minot GR, Murphy WP.** 1926. Treatment of pernicious anemia by a special diet. JAMA **87:**470-476.
- 10. **Cohn EJ, Minot GR, Fulton JB, Ulricks HF, Sargent FC, Weare JH, Murphy WP.** 1927. The nature of the material in liver effective in pernicious anemia. J. Biol. Chem. **7:**69-73.
- 11. **Wyckoff HA, Bloomfield AL.** 1929. Liver extract in pernicious anemia its effects: with report of cases. Cal. West. Med. **30:**225-231.
- 12. **Castle WB.** 1929. Observations on the etiologic relationship of achylia gastrica to pernicious anemia: I. Effect of administration to patients with pernicious anemia of contents of normal human stomach recovered after the ingestion of beef muscle. Am. J. Med. Sci. **178:**748-763.
- 13. **Castle WB, Townsend WC.** 1929. Observations on the etiologic relationship of achylia gastrica to pernicious anemia: II. The effect of the administration to patients with pernicious anemia of beef muscle after incubation with normal human gastric juice. Am. J. Med. Sci. **178:**764-777.

- 14. **Castle WB, Heath CW, Strauss MB, Heinle RW.** 1937. Observations on the etiologic relationship of achylia gatrica to pernicious anemia. VI. Site of interaction of food (extrinsic) and gastric (intrinsic) factors: failure of *in vitro* incubation to produce thermostable hematopoietic principle. Am. J. Med. Sci. **294:**618-625.
- 15. **Bethell FH, Swendseid ME.** 1949. Observations of the hemopoietic factors in hog stomach and duodenum, and the treatment of pernicious anemia by orally administered vitamin B₁₂ in combination with extracts of duodenal mucosa. Univ. Hosp. Bull. **15:**49-53.
- 16. **Schwartz M, Lous P, Meulengracht E.** 1957. Reduced effect of heterologous intrinsic factor after prolonged oral treatment in pernicious anaemia. Lancet **272:**751-753.
- 17. **Abels J, Bouma W, Jansz A, Woldring MG, Bakker A, Nieweg HO.** 1963. Experiments on the intrinsic factor antibody in serum from patients with pernicious anemia. J. Lab. Clin. Med. **61:**893-906.
- 18. **Jeffries GH, Hoskins DW, Sleisenger MH.** 1962. Antibody to intrinsic factor in serum from patients with pernicious anemia. J. Clin. Invest. **41:**1106-1115.
- 19. **Markson JL.** 1963. Pernicious anaemia as an auto-immune disease and the significance of this. Curr. Med. Drugs **3:**17-25.
- 20. **Taylor KB, Roitt IM, Doniach D, Couchman KG, Shapland C.** 1962. Autoimmune phenomena in pernicious anaemia: gastric antibodies. Br. Med. J. **2:**1347-1352.
- 21. **Hoedemaeker PJ, Abels J, Wachters JJ, Arends A, Nieweg HO.** 1964. Investigations about the site of production of Castle's gastric intrinsic factor. Lab. Invest. **13:**1394-1399.
- 22. **Rozendaal HM, Washburn RN.** 1938. Gastric secretion in cases of pernicious anemia. Ann. Intern. Med. **11:**1834-1837.
- 23. **Karlsson FA, Burman P, Loof L, Mardh S.** 1988. Major parietal cell antigen in autoimmune gastritis with pernicious anemia is the acid-producing H⁺,K⁺-adenosine triphosphatase of the stomach. J. Clin. Invest. **81:**475-479.
- 24. **Roitt IM, Doniach D, Shapland C.** 1965. Autoimmunity in pernicious anemia and atrophic gastritis. Ann. N. Y. Acad. Sci. **124**:644-656.
- 25. **Smith EL.** 1948. Purification of anti-pernicious anaemia factors from liver. Nature **161:**638.
- 26. **Rickes EL, Brink NG, Koniuszy FR, Wood TR, Folkers K.** 1948. Crystalline vitamin B₁₂. Science **107**:396-397.
- 27. **Shorb MS.** 1948. Activity of vitamin B₁₂ for the growth of *Lactobacillus lactis*. Science **107:**397-398.

- 28. **Brink NG, Kuehl FA, Jr., Folkers K.** 1950. Vitamin B_{12} : the identification of vitamin B_{12} as a cyano-cobalt coordination complex. Science **112:3**54.
- 29. **Berk L, Castle WB, Welch AD, Heinle RW, Anker R, Epstein M.** 1948. Observations on the etiologic relationship of achylia gastrica to pernicious anemia; activity of vitamin B₁₂ as food, extrinsic factor. N. Engl. J. Med. **239**:911-913.
- 30. **Hodgkin DC, Kamper J, Mackay M, Pickworth J, Trueblood KN, White JG.** 1956. Structure of vitamin B₁₂. Nature **178:**64-66.
- 31. **Lenhert PG, Hodgkin DC.** 1961. Structure of the 5,6-dimethyl-benzimidazolylcobamide coenzyme. Nature **192:**937-938.
- 32. **Woodward RB.** 1973. The total synthesis of vitamin B₁₂. Pure Appl. Chem. **33:**145-177.
- 33. **Schilling RF.** 1953. Intrinsic factor studies II. The effect of gastric juice on the urinary excretion of radioactivity after the oral administration of radioactive vitamin B₁₂. J. Lab. Clin. Med. **42:**860-866.
- 34. **Grasbeck R.** 1956. Studies on the vitamin B₁₂-binding principle and other biocolloids of human gastric juice. Acta Med. Scand. Suppl. **314:**1-87.
- 35. **Grasbeck R.** 1955. Fractionation of human gastric juice and saliva employing starch electrophoresis. Gastroenterologia **84:**99-102.
- 36. **Hall CA, Finkler AE.** 1962. *In vivo* plasma vitamin B₁₂ binding in B₁₂ deficient and nondeficient subjects. J. Lab. Clin. Med. **60:**765-776.
- 37. **Hall CA, Finkler AE.** 1963. A second vitamin B₁₂-binding substance in human plasma. Biochim. Biophys. Acta. **78:**234-236.
- 38. **Barker HA, Weissbach H, Smyth RD.** 1958. A coenzyme containing pseudovitamin B₁₂. Proc. Natl. Acad. Sci. U. S. A. **44:**1093-1097.
- **Toohey JI, Barker HA.** 1961. Isolation of coenzyme B₁₂ from liver. J. Biol. Chem. **236:**560-563.
- 40. **Smith EL, Mervyn L, Johnson AW, Shaw N.** 1962. Partial synthesis of vitamin B₁₂ coenzymes and analogues. Nature **194:**1175.
- 41. **Lindstrand K.** 1963. On vitamin B₁₂ forms in human plasma. Acta Med. Scand. **174:**665-669.
- 42. **Herbert V, Zalusky R.** 1962. Interrelations of vitamin B₁₂ and folic acid metabolism: folic acid clearance studies. J. Clin. Invest. **41:**1263-1276.
- 43. **Krautler B.** 2005. Vitamin B₁₂: chemistry and biochemistry. Biochem. Soc. Trans. **33:**806-810.

- 44. **Hsu JM, Kawin B, Minor P, Mitchell JA.** 1966. Vitamin B₁₂ concentrations in human tissues. Nature **210**:1264-1265.
- 45. **Brown KL, Hakimi JM.** 1986. Heteronuclear NMR studies of cobalamins. 4. .alpha.ribazole-3'-phosphate and the nucleotide loop of base-on cobalamins. J. Am. Chem. Soc. **108:**496-503.
- 46. **Drennan CL, Huang S, Drummond JT, Matthews RG, Lidwig ML.** 1994. How a protein binds B₁₂: A 3.0 Å X-ray structure of B₁₂-binding domains of methionine synthase. Science **266**:1669-1674.
- 47. **Marsh EN, Holloway DE.** 1992. Cloning and sequencing of glutamate mutase component S from *Clostridium tetanomorphum*. Homologies with other cobalamin-dependent enzymes. FEBS Lett. **310:**167-170.
- 48. **Brown KL, Zou X.** 1999. Thermolysis of coenzymes B₁₂ at physiological temperatures: activation parameters for cobalt-carbon bond homolysis and a quantitative analysis of the perturbation of the homolysis equilibrium by the ribonucleoside triphosphate reductase from *Lactobacillus leichmannii*. J. Inorg. Biochem. **77:**185-195.
- 49. **Schrauzer GN, Deutsch E.** 1969. Reactions of cobalt(I) supernucleophiles. The alkylation of vitamin B_{12s} cobaloximes(I), and related compounds. J. Am. Chem. Soc. **91:**3341-3350.
- 50. **Banerjee R.** 2006. B₁₂ trafficking in mammals: A for coenzyme escort service. ACS Chem. Biol. **1:**149-159.
- 51. **Fedosov SN, Berglund L, Fedosova NU, Nexo E, Petersen TE.** 2002. Comparative analysis of cobalamin binding kinetics and ligand protection for intrinsic factor, transcobalamin, and haptocorrin. J. Biol. Chem. **277:**9989-9996.
- 52. **Burger RL, Mehlman CS, Allen RH.** 1975. Human plasma R-type vitamin B₁₂-binding proteins. I. Isolation and characterization of transcobalamin I, transcobalamin III, and the normal granulocyte vitamin B₁₂-binding protein. J. Biol. Chem. **250:**7700-7706.
- 53. **Stupperich E, Nexo E.** 1991. Effect of the cobalt-N coordination on the cobamide recognition by the human vitamin B₁₂ binding proteins intrinsic factor, transcobalamin and haptocorrin. Eur. J. Biochem. **199:**299-303.
- 54. **Furger E, Frei DC, Schibli R, Fischer E, Prota AE.** 2013. Structural basis for universal corrinoid recognition by the cobalamin transport protein haptocorrin. J. Biol. Chem. **288**:25466-25476
- 55. **Carmel R.** 1983. R-binder deficiency. A clinically benign cause of cobalamin pseudodeficiency. JAMA **250**:1886-1890.
- 56. **Adcock BB, McKnight JT.** 2002. Cobalamin pseudodeficiency due to a transcobalamin I deficiency. South. Med. J. **95:**1060-1062.

- 57. **Carmel R.** 2003. Mild transcobalamin I (haptocorrin) deficiency and low serum cobalamin concentrations. Clin. Chem. **49:**1367-1374.
- 58. **Carmel R, Parker J, Kelman Z.** 2009. Genomic mutations associated with mild and severe deficiencies of transcobalamin I (haptocorrin) that cause mildly and severely low serum cobalamin levels. Br. J. Haematol. **147:**386-391.
- 59. **Sigal SH, Hall CA, Antel JP.** 1987. Plasma R binder deficiency and neurologic disease. N. Engl. J. Med. **317:**1330-1332.
- 60. **Watkins D, Rosenblatt DS.** 2011. Inborn errors of cobalamin absorption and metabolism. Am. J. Med. Genet. C Semin. Med. Genet. **157:**33-44.
- 61. **Allen RH.** 1975. Human vitamin B₁₂ transport proteins. Prog. Hematol. **9:**57-84.
- 62. **Hewitt JE, Gordon MM, Taggart RT, Mohandas TK, Alpers DH.** 1991. Human gastric intrinsic factor: characterization of cDNA and genomic clones and localization to human chromosome 11. Genomics **10:**432-440.
- 63. **Gueant JL, Kouvonen I, Michalski JC, Masson C, Grasbeck R, Nicolas JP.** 1985. Purification of human intrinsic factor using high-performance ion-exchange chromatography as the final step. FEBS Lett. **184:**14-19.
- 64. Mathews FS, Gordon MM, Chen Z, Rajashankar KR, Ealick SE, Alpers DH, Sukumar N. 2007. Crystal structure of human intrinsic factor: cobalamin complex at 2.6-Å resolution. Proc. Natl. Acad. Sci. U. S. A. 104:17311-17316.
- 65. **Kozyraki R, Kristiansen M, Silahtaroglu A, Hansen C, Jacobsen C, Tommerup N, Verroust PJ, Moestrup SK.** 1998. The human intrinsic factor-vitamin B₁₂ receptor, cubilin: molecular characterization and chromosomal mapping of the gene to 10p within the autosomal recessive megaloblastic anemia (MGA1) region. Blood **91:**3593-3600.
- 66. **Quadros EV.** 2010. Advances in the understanding of cobalamin assimilation and metabolism. Br. J. Haematol. **148:**195-204.
- 67. **Kristiansen M, Kozyraki R, Jacobsen C, Nexo E, Verroust PJ, Moestrup SK.** 1999. Molecular dissection of the intrinsic factor-vitamin B₁₂ receptor, cubilin, discloses regions important for membrane association and ligand binding. J. Biol. Chem. **274:**20540-20544.
- 68. **Andersen CB, Madsen M, Storm T, Moestrup SK, Andersen GR.** 2010. Structural basis for receptor recognition of vitamin-B₁₂-intrinsic factor complexes. Nature **464:**445-448.
- 69. **Strope S, Rivi R, Metzger T, Manova K, Lacy E.** 2004. Mouse amnionless, which is required for primitive streak assembly, mediates cell-surface localization and endocytic function of cubilin on visceral endoderm and kidney proximal tubules. Development **131:**4787-4795.

- 70. **Kozyraki R, Fyfe J, Verroust PJ, Jacobsen C, Dautry-Varsat A, Gburek J, Willnow TE, Christensen EI, Moestrup SK.** 2001. Megalin-dependent cubilin-mediated endocytosis is a major pathway for the apical uptake of transferrin in polarized epithelia. Proc. Natl. Acad. Sci. U. S. A. **98:**12491-12496.
- 71. **Kozyraki R, Cases O.** 2013. Vitamin B₁₂ absorption: mammalian physiology and acquired and inherited disorders. Biochimie **95:**1002-1007.
- 72. Kalantry S, Manning S, Haub O, Tomihara-Newberger C, Lee HG, Fangman J, Disteche CM, Manova K, Lacy E. 2001. The amnionless gene, essential for mouse gastrulation, encodes a visceral-endoderm-specific protein with an extracellular cysteinerich domain. Nat. Genet. 27:412-416.
- 73. He Q, Madsen M, Kilkenney A, Gregory B, Christensen EI, Vorum H, Hojrup P, Schaffer AA, Kirkness EF, Tanner SM, de la Chapelle A, Giger U, Moestrup SK, Fyfe JC. 2005. Amnionless function is required for cubilin brush-border expression and intrinsic factor-cobalamin (vitamin B₁₂) absorption *in vivo*. Blood 106:1447-1453.
- 74. **Verroust PJ, Kozyraki R, Hammond TG, Moestrup SK, Christensen EI.** 2000. Physiopathologic role of cubilin and megalin. Adv. Nephrol. Necker. Hosp. **30:**127-145.
- 75. Kantarci S, Al-Gazali L, Hill RS, Donnai D, Black GC, Bieth E, Chassaing N, Lacombe D, Devriendt K, Teebi A, Loscertales M, Robson C, Liu T, MacLaughlin DT, Noonan KM, Russell MK, Walsh CA, Donahoe PK, Pober BR. 2007. Mutations in *LRP2*, which encodes the multiligand receptor megalin, cause Donnai-Barrow and facio-oculo-acoustico-renal syndromes. Nat. Genet. **39:**957-959.
- 76. **Birn H, Willnow TE, Nielsen R, Norden AG, Bonsch C, Moestrup SK, Nexo E, Christensen EI.** 2002. Megalin is essential for renal proximal tubule reabsorption and accumulation of transcobalamin-B₁₂. Am. J. Physiol. Renal Physiol. **282:**408-416.
- 77. Tanner SM, Li Z, Perko JD, Oner C, Cetin M, Altay C, Yurtsever Z, David KL, Faivre L, Ismail EA, Grasbeck R, de la Chapelle A. 2005. Hereditary juvenile cobalamin deficiency caused by mutations in the intrinsic factor gene. Proc. Natl. Acad. Sci. U. S. A. 102:4130-4133.
- 78. **Kristiansen M, Aminoff M, Jacobsen C, de La Chapelle A, Krahe R, Verroust PJ, Moestrup SK.** 2000. Cubilin P1297L mutation associated with hereditary megaloblastic anemia 1 causes impaired recognition of intrinsic factor-vitamin B₁₂ by cubilin. Blood **96:**405-409.
- 79. Aminoff M, Carter JE, Chadwick RB, Johnson C, Grasbeck R, Abdelaal MA, Broch H, Jenner LB, Verroust PJ, Moestrup SK, de la Chapelle A, Krahe R. 1999. Mutations in *CUBN*, encoding the intrinsic factor-vitamin B₁₂ receptor, cubilin, cause hereditary megaloblastic anaemia 1. Nat. Genet. 21:309-313.

- 80. Yang YM, Ducos R, Rosenberg AJ, Catrou PG, Levine JS, Podell ER, Allen RH. 1985. Cobalamin malabsorption in three siblings due to an abnormal intrinsic factor that is markedly susceptible to acid and proteolysis. J. Clin. Invest. 76:2057-2065.
- 81. **Katz M, Lee SK, Cooper BA.** 1972. Vitamin B₁₂ malabsorption due to a biologically inert intrinsic factor. N. Engl. J. Med. **287:**425-429.
- 82. **Grasbeck R.** 2006. Imerslund-Gräsbeck syndrome (selective vitamin B₁₂ malabsorption with proteinuria). Orphanet J. Rare Dis. **1:**17.
- 83. **Laframboise R, Cooper BA, Rosenblatt DS.** 1992. Malabsorption of vitamin B₁₂ from the intestine in a child with *cblF* disease: evidence for lysosomal-mediated absorption. Blood **80:**291-292.
- 84. **Beedholm-Ebsen R, van de Wetering K, Hardlei T, Nexo E, Borst P, Moestrup SK.** 2010. Identification of multidrug resistance protein 1 (MRP1/ABCC1) as a molecular gate for cellular export of cobalamin. Blood **115:**1632-1639.
- 85. **Quadros EV, Regec AL, Khan KM, Quadros E, Rothenberg SP.** 1999. Transcobalamin II synthesized in the intestinal villi facilitates transfer of cobalamin to the portal blood. Am. J. Physiol. **277:**G161-166.
- 86. **Rothenberg SP, Quadros EV.** 1995. Transcobalamin II and the membrane receptor for the transcobalamin II-cobalamin complex. Baillieres Clin. Haematol. **8:**499-514.
- 87. **Quadros EV, Rothenberg SP, Jaffe EA.** 1989. Endothelial cells from human umbilical vein secrete functional transcobalamin II. Am. J. Physiol. **256:**C296-303.
- 88. **Regec A, Quadros EV, Platica O, Rothenberg SP.** 1995. The cloning and characterization of the human transcobalamin II gene. Blood **85:**2711-2719.
- 89. **Pathare PM, Wilbur DS, Heusser S, Quadros EV, McLoughlin P, Morgan AC.** 1996. Synthesis of cobalamin-biotin conjugates that vary in the position of cobalamin coupling. Evaluation of cobalamin derivative binding to transcobalamin II. Bioconjug. Chem. **7:**217-232.
- 90. Wuerges J, Garau G, Geremia S, Fedosov SN, Petersen TE, Randaccio L. 2006. Structural basis for mammalian vitamin B₁₂ transport by transcobalamin. Proc. Natl. Acad. Sci. U. S. A. **103**:4386-4391.
- 91. **Quadros EV, Rothenberg SP, McLoughlin P.** 1996. Characterization of monoclonal antibodies to epitopes of human transcobalamin II. Biochem. Biophys. Res. Commun. **222:**149-154.
- 92. Fedosov SN, Orning L, Lovli T, Quadros EV, Thompson K, Berglund L, Petersen TE. 2005. Mapping the functional domains of human transcobalamin using monoclonal antibodies. FEBS J. 272:3887-3898.

- 93. **Li N, Rosenblatt DS, Seetharam B.** 1994. Nonsense mutations in human transcobalamin II deficiency. Biochem. Biophys. Res. Commun. **204:**1111-1118.
- 94. **Qian L, Quadros EV, Regec A, Zittoun J, Rothenberg SP.** 2002. Congenital transcobalamin II deficiency due to errors in RNA editing. Blood Cells Mol. Dis. **28:**134-142.
- 95. Namour F, Helfer AC, Quadros EV, Alberto JM, Bibi HM, Orning L, Rosenblatt DS, Jean-Louis G. 2003. Transcobalamin deficiency due to activation of an intra exonic cryptic splice site. Br. J. Haematol. 123:915-920.
- 96. **Cooper BA, Rosenblatt DS.** 1987. Inherited defects of vitamin B₁₂ metabolism. Annu. Rev. Nutr. **7:**291-320.
- 97. **Meyers PA, Carmel R.** 1984. Hereditary transcobalamin II deficiency with subnormal serum cobalamin levels. Pediatrics **74:**866-871.
- 98. Schiff M, Ogier de Baulny H, Bard G, Barlogis V, Hamel C, Moat SJ, Odent S, Shortland G, Touati G, Giraudier S. 2010. Should transcobalamin deficiency be treated aggressively? J. Inherit. Metab. Dis. 33:223-229.
- 99. **Haurani FI, Hall CA, Rubin R.** 1979. Megaloblastic anemia as a result of an abnormal transcobalamin II (Cardeza). J. Clin. Invest. **64:**1253-1259.
- 100. **Seligman PA, Steiner LL, Allen RH.** 1980. Studies of a patient with megaloblastic anemia and an abnormal transcobalamin II. N. Engl. J. Med. **303:**1209-1212.
- 101. **DiGirolamo PM, Huennekens FM.** 1975. Transport of vitamin B₁₂ into mouse leukemia cells. Arch. Biochem. Biophys. **168:**386-393.
- 102. **Quadros EV, Nakayama Y, Sequeira JM.** 2009. The protein and the gene encoding the receptor for the cellular uptake of transcobalamin-bound cobalamin. Blood **113:**186-192.
- 103. **Jiang W, Nakayama Y, Sequeira JM, Quadros EV.** 2013. Mapping the functional domains of TCblR/CD320, the receptor for cellular uptake of transcobalamin-bound cobalamin. FASEB J. **27:**2988-2994.
- 104. **Amagasaki T, Green R, Jacobsen DW.** 1990. Expression of transcobalamin II receptors by human leukemia K562 and HL-60 cells. Blood **76:**1380-1386.
- 105. **Lindemans J, Kroes AC, van Geel J, van Kapel J, Schoester M, Abels J.** 1989. Uptake of transcobalamin II-bound cobalamin by HL-60 cells: effects of differentiation induction. Exp. Cell Res. **184:**449-460.
- 106. **Hall CA.** 1984. The uptake of vitamin B₁₂ by human lymphocytes and the relationships to the cell cycle. J. Lab. Clin. Med. **103:**70-81.

- 107. **Takahashi K, Tavassoli M, Jacobsen DW.** 1980. Receptor binding and internalization of immobilized transcobalamin II by mouse leukaemia cells. Nature **288:**713-715.
- 108. Quadros EV, Lai SC, Nakayama Y, Sequeira JM, Hannibal L, Wang S, Jacobsen DW, Fedosov S, Wright E, Gallagher RC, Anastasio N, Watkins D, Rosenblatt DS. 2010. Positive newborn screen for methylmalonic aciduria identifies the first mutation in TCblR/CD320, the gene for cellular uptake of transcobalamin-bound vitamin B₁₂. Hum. Mutat. 31:924-929.
- 109. Pangilinan F, Mitchell A, VanderMeer J, Molloy AM, Troendle J, Conley M, Kirke PN, Sutton M, Sequeira JM, Quadros EV, Scott JM, Mills JL, Brody LC. 2010. Transcobalamin II receptor polymorphisms are associated with increased risk for neural tube defects. J. Med. Genet. 47:677-685.
- 110. Lai SC, Nakayama Y, Sequeira JM, Wlodarczyk BJ, Cabrera RM, Finnell RH, Bottiglieri T, Quadros EV. 2013. The transcobalamin receptor knockout mouse: a model for vitamin B₁₂ deficiency in the central nervous system. FASEB J. 27:2468-2475.
- 111. **O'Leary F, Samman S.** 2010. Vitamin B₁₂ in health and disease. Nutrients **2:**299-316.
- 112. **Watanabe F.** 2007. Vitamin B₁₂ sources and bioavailability. Exp. Biol. Med. (Maywood) **232:**1266-1274.
- 113. **Bennink MR, Ono K.** 1982. Vitamin B₁₂, E and D content of raw and cooked beef. J. Food Sci. **47:**1786-1792.
- 114. Watanabe F, Abe K, Fujita T, Goto M, Hiemori M, Nakano Y. 1998. Effects of microwave heating on the loss of vitamin B₁₂ in foods. J. Agric. Food Chem. **46:**206-210.
- 115. **Mozafar A.** 1994. Enrichment of some B-vitamins in plants with application of organic fertilizers. Plant Soil **167:**305-311.
- 116. **Suzuki H.** 1995. Serum vitamin B₁₂ levels in young vegans who eat brown rice. J. Nutr. Sci. Vitaminol. **41:**587-594.
- 117. **Rauma AL, Torronen R, Hanninen O, Mykkanen H.** 1995. Vitamin B₁₂ status of long-term adherents of a strict uncooked vegan diet ("living food diet") is compromised. J. Nutr. **125:**2511-2515.
- 118. **Dagnelie PC, van Staveren WA, van den Berg H.** 1991. Vitamin B₁₂ from algae appears not to be bioavailable. Am. J. Clin. Nutr. **53:**695-697.
- 119. **Brandt LJ, Goldberg L, Bernstein LH, Greenberg G.** 1979. The effect of bacterially produced vitamin B₁₂ analogues (cobamides) on the *in vitro* absorption of cyanocobalamin. Am. J. Clin. Nutr. **32:**1832-1836.

- 120. Watanabe F, Katsura H, Takenaka S, Fujita T, Abe K, Tamura Y, Nakatsuka T, Nakano Y. 1999. Pseudovitamin B₁₂ is the predominant cobamide of an algal health food, spirulina tablets. J. Agric. Food Chem. 47:4736-4741.
- 121. **Doscherholmen A, McMahon J, Ripley D.** 1978. Vitamin B₁₂ assimilation from chicken meat. Am. J. Clin. Nutr. **31:**825-830.
- 122. **Heyssel RM, Bozian RC, Darby WJ, Bell MC.** 1966. Vitamin B₁₂ turnover in man. The assimilation of vitamin B₁₂ from natural foodstuff by man and estimates of minimal daily dietary requirements. Am. J. Clin. Nutr. **18:**176-184.
- 123. **Doscherholmen A, McMahon J, Ripley D.** 1975. Vitamin B₁₂ absorption from eggs. Proc. Soc. Exp. Biol. Med. **149**:987-990.
- 124. **Adams JF, Ross SK, Mervyn L, Boddy K, King P.** 1971. Absorption of cyanocobalamin, coenzyme B₁₂, methylcobalamin, and hydroxocobalamin at different dose levels. Scand. J. Gastroenterol. **6:**249-252.
- 125. **Berlin H, Berlin R, Brante G.** 1968. Oral treatment of pernicious anemia with high doses of vitamin B₁₂ without intrinsic factor. Acta Med. Scand. **184:**247-258.
- 126. Institute of Medicine (US) standing committee on the scientific evaluation of dietary reference intakes and its panel on folate, other B vitamins, and choline. 1998. Dietary reference intakes for thiamin, riboflavin, niacin, vitamin B₆, folate, vitamin B₁₂, pantothenic acid, biotin, and choline. National Academies Press, Washington, DC.
- 127. **Park S, Johnson MA.** 2006. What is an adequate dose of oral vitamin B₁₂ in older people with poor vitamin B₁₂ status? Nutr. Rev. **64:**373-378.
- 128. **Millet P, Guilland JC, Fuchs F, Klepping J.** 1989. Nutrient intake and vitamin status of healthy French vegetarians and nonvegetarians. Am. J. Clin. Nutr. **50:**718-727.
- 129. **Allen RH, Stabler SP, Lindenbaum J.** 1993. Serum betaine, N,N-dimethylglycine and N-methylglycine levels in patients with cobalamin and folate deficiency and related inborn errors of metabolism. Metabolism **42:**1448-1460.
- 130. **Miller JW, Garrod MG, Rockwood AL, Kushnir MM, Allen LH, Haan MN, Green R.** 2006. Measurement of total vitamin B₁₂ and holotranscobalamin, singly and in combination, in screening for metabolic vitamin B₁₂ deficiency. Clin. Chem. **52:**278-285.
- 131. **Pfeiffer CM, Caudill SP, Gunter EW, Osterloh J, Sampson EJ.** 2005. Biochemical indicators of B vitamin status in the US population after folic acid fortification: results from the National Health and Nutrition Examination Survey 1999-2000. Am. J. Clin. Nutr. **82:**442-450.
- 132. **Klee GG.** 2000. Cobalamin and folate evaluation: measurement of methylmalonic acid and homocysteine vs vitamin B_{12} and folate. Clin. Chem. **46:**1277-1283.

- 133. **Carmel R, Sarrai M.** 2006. Diagnosis and management of clinical and subclinical cobalamin deficiency: advances and controversies. Curr. Hematol. Rep. **5:**23-33.
- 134. **Healton EB, Savage DG, Brust JC, Garrett TJ, Lindenbaum J.** 1991. Neurologic aspects of cobalamin deficiency. Medicine (Baltimore) **70:**229-245.
- 135. Savage D, Gangaidzo I, Lindenbaum J, Kiire C, Mukiibi JM, Moyo A, Gwanzura C, Mudenge B, Bennie A, Sitima J, et al. 1994. Vitamin B₁₂ deficiency is the primary cause of megaloblastic anaemia in Zimbabwe. Br. J. Haematol. **86:**844-850.
- 136. **Briani C, Torre CD, Citton V, Manara R, Pompanin S, Binotto G, Adami F.** 2013. Cobalamin deficiency: clinical picture and radiological findings. Nutrients **5:**4521-4539.
- 137. **Allen LH.** 2009. How common is vitamin B₁₂ deficiency? Am. J. Clin. Nutr. **89:**693S-696S.
- 138. **den Elzen WP, Groeneveld Y, de Ruijter W, Souverijn JH, le Cessie S, Assendelft WJ, Gussekloo J.** 2008. Long-term use of proton pump inhibitors and vitamin B₁₂ status in elderly individuals. Aliment. Pharmacol. Ther. **27:**491-497.
- 139. **Dharmarajan TS, Kanagala MR, Murakonda P, Lebelt AS, Norkus EP.** 2008. Do acid-lowering agents affect vitamin B₁₂ status in older adults? J. Am. Med. Dir. Assoc. **9:**162-167.
- 140. **Valuck RJ, Ruscin JM.** 2004. A case-control study on adverse effects: H2 blocker or proton pump inhibitor use and risk of vitamin B₁₂ deficiency in older adults. J. Clin. Epidemiol. **57:**422-428.
- 141. **Bauman WA, Shaw S, Jayatilleke E, Spungen AM, Herbert V.** 2000. Increased intake of calcium reverses vitamin B₁₂ malabsorption induced by metformin. Diabetes Care **23**:1227-1231.
- 142. **Filioussi K, Bonovas S, Katsaros T.** 2003. Should we screen diabetic patients using biguanides for megaloblastic anaemia? Aust. Fam. Physician **32:**383-384.
- 143. **Greibe E, Miller JW, Foutouhi SH, Green R, Nexo E.** 2013. Metformin increases liver accumulation of vitamin B₁₂ an experimental study in rats. Biochimie **95:**1062-1065.
- 144. **Hathout L, El-Saden S.** 2011. Nitrous oxide-induced B₁₂ deficiency myelopathy: Perspectives on the clinical biochemistry of vitamin B₁₂. J. Neurol. Sci. **301:**1-8.
- 145. **Li F, Watkins D, Rosenblatt DS.** 2009. Vitamin B₁₂ and birth defects. Mol. Genet. Metab. **98:**166-172.
- 146. **Thompson MD, Cole DE, Ray JG.** 2009. Vitamin B₁₂ and neural tube defects: the Canadian experience. Am. J. Clin. Nutr. **89:**697S-701S.

- 147. De Wals P, Tairou F, Van Allen MI, Uh S-H, Lowry RB, Sibbald B, Evans JA, Van den Hof MC, Zimmer P, Crowley M, Fernandez B, Lee NS, Niyonsenga T. 2007. Reduction in neural-tube defects after folic acid fortification in Canada. N. Engl. J. Med. 357:135-142.
- 148. **Molloy AM, Kirke PN, Troendle JF, Burke H, Sutton M, Brody LC, Scott JM, Mills JL.** 2009. Maternal vitamin B₁₂ status and risk of neural tube defects in a population with high neural tube defect prevalence and no folic acid fortification. Pediatrics **123**:917-923.
- 149. Ray JG, Wyatt PR, Thompson MD, Vermeulen MJ, Meier C, Wong PY, Farrell SA, Cole DE. 2007. Vitamin B₁₂ and the risk of neural tube defects in a folic-acid-fortified population. Epidemiology **18:**362-366.
- 150. **Boushey CJ, Beresford SA, Omenn GS, Motulsky AG.** 1995. A quantitative assessment of plasma homocysteine as a risk factor for vascular disease. Probable benefits of increasing folic acid intakes. JAMA **274:**1049-1057.
- 151. **Homocysteine Studies Collaboration.** 2002. Homocysteine and risk of ischemic heart disease and stroke: a meta-analysis. JAMA **288:**2015-2022.
- 152. **Homocysteine Lowering Trialists' Collaboration.** 2005. Dose-dependent effects of folic acid on blood concentrations of homocysteine: a meta-analysis of the randomized trials. Am. J. Clin. Nutr. **82:**806-812.
- 153. **Spence JD, Bang H, Chambless LE, Stampfer MJ.** 2005. Vitamin Intervention For Stroke Prevention trial: an efficacy analysis. Stroke **36:**2404-2409.
- 154. Quinlivan EP, McPartlin J, McNulty H, Ward M, Strain JJ, Weir DG, Scott JM. 2002. Importance of both folic acid and vitamin B₁₂ in reduction of risk of vascular disease. Lancet **359**:227-228.
- 155. Loland KH, Bleie O, Blix AJ, Strand E, Ueland PM, Refsum H, Ebbing M, Nordrehaug JE, Nygard O. 2010. Effect of homocysteine-lowering B vitamin treatment on angiographic progression of coronary artery disease: a Western Norway B Vitamin Intervention Trial (WENBIT) substudy. Am. J. Cardiol. 105:1577-1584.
- 156. **Huang T, Chen Y, Yang B, Yang J, Wahlqvist ML, Li D.** 2012. Meta-analysis of B vitamin supplementation on plasma homocysteine, cardiovascular and all-cause mortality. Clin. Nutr. **31:**448-454.
- 157. **Smith AD, Refsum H.** 2009. Vitamin B₁₂ and cognition in the elderly. Am. J. Clin. Nutr. **89:**707S-711S.
- 158. **Lewis MS, Miller LS, Johnson MA, Dolce EB, Allen RH, Stabler SP.** 2005. Elevated methylmalonic acid is related to cognitive impairement in older adults enrolled in an elderly nutrition program. J. Nutr. Elder. **24:**47-65.

- 159. Hin H, Clarke R, Sherliker P, Atoyebi W, Emmens K, Birks J, Schneede J, Ueland PM, Nexo E, Scott J, Molloy A, Donaghy M, Frost C, Evans JG. 2006. Clinical relevance of low serum vitamin B₁₂ concentrations in older people: the Banbury B₁₂ study. Age Ageing **35**:416-422.
- 160. **Garrod MG, Green R, Allen LH, Mungas DM, Jagust WJ, Haan MN, Miller JW.** 2008. Fraction of total plasma vitamin B₁₂ bound to transcobalamin correlates with cognitive function in elderly Latinos with depressive symptoms. Clin. Chem. **54:**1210-1217.
- 161. **Morris MS, Jacques PF, Rosenberg IH, Selhub J.** 2007. Folate and vitamin B₁₂ status in relation to anemia, macrocytosis, and cognitive impairment in older Americans in the age of folic acid fortification. Am. J. Clin. Nutr. **85:**193-200.
- 162. **Malouf R, Areosa Sastre A.** 2003. Vitamin B₁₂ for cognition. Cochrane Database Syst. Rev. **3:**CD004326.
- 163. **Van Dam F, Van Gool WA.** 2009. Hyperhomocysteinemia and Alzheimer's disease: a systematic review. Arch. Gerontol. Geriatr. **48:**425-430.
- 164. Smith AD, Smith SM, de Jager CA, Whitbread P, Johnston C, Agacinski G, Oulhaj A, Bradley KM, Jacoby R, Refsum H. 2010. Homocysteine-lowering by B vitamins slows the rate of accelerated brain atrophy in mild cognitive impairment: a randomized controlled trial. PLoS One 5:e12244.
- de Jager CA, Oulhaj A, Jacoby R, Refsum H, Smith AD. 2012. Cognitive and clinical outcomes of homocysteine-lowering B-vitamin treatment in mild cognitive impairment: a randomized controlled trial. Int. J. Geriatr. Psychiatry 27:592-600.
- 166. **Douaud G, Refsum H, de Jager CA, Jacoby R, Nichols TE, Smith SM, Smith AD.** 2013. Preventing Alzheimer's disease-related gray matter atrophy by B-vitamin treatment. Proc. Natl. Acad. Sci. U. S. A. **110**:9523-9528.
- 167. Herrmann M, Peter Schmidt J, Umanskaya N, Wagner A, Taban-Shomal O, Widmann T, Colaianni G, Wildemann B, Herrmann W. 2007. The role of hyperhomocysteinemia as well as folate, vitamin B₆ and B₁₂ deficiencies in osteoporosis: a systematic review. Clin. Chem. Lab. Med. 45:1621-1632.
- 168. Herrmann M, Umanskaya N, Traber L, Schmidt-Gayk H, Menke W, Lanzer G, Lenhart M, Peter Schmidt J, Herrmann W. 2007. The effect of B-vitamins on biochemical bone turnover markers and bone mineral density in osteoporotic patients: a 1-year double blind placebo controlled trial. Clin. Chem. Lab. Med. 45:1785-1792.
- 169. **Sato Y, Honda Y, Iwamoto J, Kanoko T, Satoh K.** 2005. Effect of folate and mecobalamin on hip fractures in patients with stroke: a randomized controlled trial. JAMA **293**:1082-1088.

- 170. **Green TJ, McMahon JA, Skeaff CM, Williams SM, Whiting SJ.** 2007. Lowering homocysteine with B vitamins has no effect on biomarkers of bone turnover in older persons: a 2-y randomized controlled trial. Am. J. Clin. Nutr. **85:**460-464.
- 171. **Kamburoglu G, Gumus K, Kadayifcilar S, Eldem B.** 2006. Plasma homocysteine, vitamin B₁₂ and folate levels in age-related macular degeneration. Graefes Arch. Clin. Exp. Ophthalmol. **244:**565-569.
- 172. **Rochtchina E, Wang JJ, Flood VM, Mitchell P.** 2007. Elevated serum homocysteine, low serum vitamin B₁₂, folate, and age-related macular degeneration: the Blue Mountains Eye Study. Am. J. Ophthalmol. **143:**344-346.
- 173. **Gopinath B, Flood VM, Rochtchina E, Wang JJ, Mitchell P.** 2013. Homocysteine, folate, vitamin B₁₂, and 10-y incidence of age-related macular degeneration. Am. J. Clin. Nutr. **98:**129-135.
- 174. **Christen WG, Glynn RJ, Chew EY, Albert CM, Manson JE.** 2009. Folic acid, pyridoxine, and cyanocobalamin combination treatment and age-related macular degeneration in women: the Women's Antioxidant and Folic Acid Cardiovascular Study. Arch. Intern. Med. **169:**335-341.
- 175. **Fried LP, Ferrucci L, Darer J, Williamson JD, Anderson G.** 2004. Untangling the concepts of disability, frailty, and comorbidity: implications for improved targeting and care. J. Gerontol. A Biol. Sci. Med. Sci. **59:**255-263.
- 176. Bartali B, Semba RD, Frongillo EA, Varadhan R, Ricks MO, Blaum CS, Ferrucci L, Guralnik JM, Fried LP. 2006. Low micronutrient levels as a predictor of incident disability in older women. Arch. Intern. Med. 166:2335-2340.
- 177. Matteini AM, Walston JD, Fallin MD, Bandeen-Roche K, Kao WH, Semba RD, Allen RH, Guralnik J, Fried LP, Stabler SP. 2008. Markers of B-vitamin deficiency and frailty in older women. J. Nutr. Health Aging 12:303-308.
- 178. **O'Leary F, Flood VM, Petocz P, Allman-Farinelli M, Samman S.** 2011. B vitamin status, dietary intake and length of stay in a sample of elderly rehabilitation patients. J. Nutr. Health Aging **15:**485-489.
- 179. **Martens JH, Barg H, Warren MJ, Jahn D.** 2002. Microbial production of vitamin B₁₂. Appl. Microbiol. Biotechnol. **58:**275-285.
- 180. **Roth JR, Lawrence JG, Rubenfield M, Kieffer-Higgins S, Church GM.** 1993. Characterization of the cobalamin (vitamin B₁₂) biosynthetic genes of *Salmonella typhimurium*. J. Bacteriol. **175:**3303-3316.
- 181. **Perlman D.** 1959. Microbial synthesis of cobamides. Adv. Appl. Microbiol. 1:87-122.

- 182. **Debussche L, Thibaut D, Cameron B, Crouzet J, Blanche F.** 1993. Biosynthesis of the corrin macrocycle of coenzyme B₁₂ in *Pseudomonas denitrificans*. J. Bacteriol. **175:**7430-7440.
- 183. Blanche F, Cameron B, Crouzet J, Debussche L, Thibaut D, Vuilhorgne M, Leeper FJ, Battersby AR. 1995. Vitamin B₁₂: how the problem of its biosynthesis was solved. Angew. Chem. Int. Ed. Engl. **34:**383-411.
- 184. **Battersby AR.** 1994. How nature builds the pigments of life: the conquest of vitamin B₁₂. Science **264**:1551-1557.
- 185. **Scott AI.** 1996. Travels of an organic chemist along nature's pathways. Bioorg. Med. Chem. **4:**965-985.
- 186. **Cameron B, Briggs K, Pridmore S, Brefort G, Crouzet J.** 1989. Cloning and analysis of genes involved in coenzyme B₁₂ biosynthesis in *Pseudomonas denitrificans*. J. Bacteriol. **171:**547-557.
- 187. Crouzet J, Cameron B, Cauchois L, Rigault S, Rouyez MC, Blanche F, Thibaut D, Debussche L. 1990. Genetic and sequence analysis of an 8.7-kilobase *Pseudomonas denitrificans* fragment carrying eight genes involved in transformation of precorrin-2 to cobyrinic acid. J. Bacteriol. 172:5980-5990.
- 188. Crouzet J, Cauchois L, Blanche F, Debussche L, Thibaut D, Rouyez MC, Rigault S, Mayaux JF, Cameron B. 1990. Nucleotide sequence of a *Pseudomonas denitrificans* 5.4-kilobase DNA fragment containing five *cob* genes and identification of structural genes encoding S-adenosyl-L-methionine: uroporphyrinogen III methyltransferase and cobyrinic acid a,c-diamide synthase. J. Bacteriol. 172:5968-5979.
- 189. **Moore SJ, Warren MJ.** 2012. The anaerobic biosynthesis of vitamin B₁₂. Biochem. Soc. Trans. **40:**581-586.
- 190. **Kang Z, Wang Y, Gu P, Wang Q, Qi Q.** 2011. Engineering *Escherichia coli* for efficient production of 5-aminolevulinic acid from glucose. Metab. Eng. **13:**492-498.
- 191. **Sasaki K, Watanabe M, Tanaka T, Tanaka T.** 2002. Biosynthesis, biotechnological production and applications of 5-aminolevulinic acid. Appl. Microbiol. Biotechnol. **58:**23-29.
- 192. **Moser J, Lorenz S, Hubschwerlen C, Rompf A, Jahn D.** 1999. *Methanopyrus kandleri* glutamyl-tRNA reductase. J. Biol. Chem. **274:**30679-30685.
- 193. **Frankenberg N, Heinz DW, Jahn D.** 1999. Production, purification, and characterization of a Mg²⁺-responsive porphobilinogen synthase from *Pseudomonas aeruginosa*. Biochemistry **38:**13968-13975.
- 194. **Petrovich RM, Litwin S, Jaffe EK.** 1996. *Bradyrhizobium japonicum* porphobilinogen synthase uses two Mg(II) and monovalent cations. J. Biol. Chem. **271:**8692-8699.

- 195. **Jaffe EK.** 2000. The porphobilinogen synthase family of metalloenzymes. Acta Crystallogr. D Biol. Crystallogr. **56:**115-128.
- 196. **Raux E, Schubert HL, Warren MJ.** 2000. Biosynthesis of cobalamin (vitamin B₁₂): a bacterial conundrum. Cell. Mol. Life Sci. **57:**1880-1893.
- 197. **Jordan PM, Warren MJ.** 1987. Evidence for a dipyrromethane cofactor at the catalytic site of *E. coli* porphobilinogen deaminase. FEBS Lett. **225:**87-92.
- 198. **Blanche F, Debussche L, Thibaut D, Crouzet J, Cameron B.** 1989. Purification and characterization of S-adenosyl-L-methionine: uroporphyrinogen III methyltransferase from *Pseudomonas denitrificans*. J. Bacteriol. **171:**4222-4231.
- 199. **Warren MJ, Roessner CA, Santander PJ, Scott AI.** 1990. The *Escherichia coli cysG* gene encodes S-adenosylmethionine-dependent uroporphyrinogen III methylase. Biochem. J. **265:**725-729.
- 200. **Thibaut D, Couder M, Crouzet J, Debussche L, Cameron B, Blanche F.** 1990. Assay and purification of S-adenosyl-L-methionine:precorrin-2 methyltransferase from *Pseudomonas denitrificans*. J. Bacteriol. **172:**6245-6251.
- 201. Warren MJ, Roessner CA, Ozaki S, Stolowich NJ, Santander PJ, Scott AI. 1992. Enzymatic synthesis and structure of precorrin-3, a trimethyldipyrrocorphin intermediate in vitamin B₁₂ biosynthesis. Biochemistry **31:**603-609.
- 202. **Spencer P, Stolowich NJ, Sumner LW, Scott AI.** 1998. Definition of the redox states of cobalt-precorrinoids: investigation of the substrate and redox specificity of CbiL from *Salmonella typhimurium*. Biochemistry **37:**14917-14927.
- 203. Scott AI, Roessner CA, Stolowich NJ, Spencer JB, Min C, Ozaki SI. 1993. Biosynthesis of vitamin B₁₂. Discovery of the enzymes for oxidative ring contraction and insertion of the fourth methyl group. FEBS Lett. **331:**105-108.
- 204. Schroeder S, Lawrence AD, Biedendieck R, Rose RS, Deery E, Graham RM, McLean KJ, Munro AW, Rigby SE, Warren MJ. 2009. Demonstration that CobG, the monooxygenase associated with the ring contraction process of the aerobic cobalamin (vitamin B₁₂) biosynthetic pathway, contains an Fe-S center and a mononuclear nonheme iron center. J. Biol. Chem. **284**:4796-4805.
- 205. **Min C, Atshaves BP, Roessner CA, Stolowich NJ, Spencer JB, Scott AI.** 1993. Isolation, structure, and genetically engineered synthesis of precorrin-5, the pentamethylated intermediate of vitamin B₁₂ biosynthesis. J. Am. Chem. Soc. **115:**10380-10381.
- 206. **Blanche F, Thibaut D, Famechon A, Debussche L, Cameron B, Crouzet J.** 1992. Precorrin-6x reductase from *Pseudomonas denitrificans*: purification and characterization of the enzyme and identification of the structural gene. J. Bacteriol. **174:**1036-1042.

- 207. **Thibaut D, Blanche F, Debussche L, Leeper FJ, Battersby AR.** 1990. Biosynthesis of vitamin B₁₂: structure of precorrin-6x octamethyl ester. Proc. Natl. Acad. Sci. U. S. A. **87:**8800-8804.
- 208. **Blanche F, Famechon A, Thibaut D, Debussche L, Cameron B, Crouzet J.** 1992. Biosynthesis of vitamin B₁₂ in *Pseudomonas denitrificans*: the biosynthetic sequence from precorrin-6y to precorrin-8x is catalyzed by the *cobL* gene product. J. Bacteriol. **174:**1050-1052.
- 209. **Thibaut D, Couder M, Famechon A, Debussche L, Cameron B, Crouzet J, Blanche F.** 1992. The final step in the biosynthesis of hydrogenobyrinic acid is catalyzed by the *cobH* gene product with precorrin-8x as the substrate. J. Bacteriol. **174:**1043-1049.
- 210. **Debussche L, Thibaut D, Cameron B, Crouzet J, Blanche F.** 1990. Purification and characterization of cobyrinic acid a,c-diamide synthase from *Pseudomonas denitrificans*. J. Bacteriol. **172:**6239-6244.
- 211. **Debussche L, Couder M, Thibaut D, Cameron B, Crouzet J, Blanche F.** 1992. Assay, purification, and characterization of cobaltochelatase, a unique complex enzyme catalyzing cobalt insertion in hydrogenobyrinic acid a,c-diamide during coenzyme B₁₂ biosynthesis in *Pseudomonas denitrificans*. J. Bacteriol. **174:**7445-7451.
- 212. Lundqvist J, Elmlund D, Heldt D, Deery E, Soderberg CA, Hansson M, Warren M, Al-Karadaghi S. 2009. The AAA(+) motor complex of subunits CobS and CobT of cobaltochelatase visualized by single particle electron microscopy. J. Struct. Biol. 167:227-234.
- 213. **Reid JD, Hunter CN.** 2004. Magnesium-dependent ATPase activity and cooperativity of magnesium chelatase from *Synechocystis* sp. PCC6803. J. Biol. Chem. **279:**26893-26899.
- 214. **Heldt D, Lawrence AD, Lindenmeyer M, Deery E, Heathcote P, Rigby SE, Warren MJ.** 2005. Aerobic synthesis of vitamin B₁₂: ring contraction and cobalt chelation. Biochem. Soc. Trans. **33:**815-819.
- 215. **Debussche L, Couder M, Thibaut D, Cameron B, Crouzet J, Blanche F.** 1991. Purification and partial characterization of Cob(I)alamin adenosyltransferase from *Pseudomonas denitrificans*. J. Bacteriol. **173:**6300-6302.
- 216. **Blanche F, Couder M, Debussche L, Thibaut D, Cameron B, Crouzet J.** 1991. Biosynthesis of vitamin B₁₂: stepwise amidation of carboxyl groups b, d, e, and g of cobyrinic acid a,c-diamide is catalyzed by one enzyme in *Pseudomonas denitrificans*. J. Bacteriol. **173:**6046-6051.
- 217. Romao CV, Ladakis D, Lobo SA, Carrondo MA, Brindley AA, Deery E, Matias PM, Pickersgill RW, Saraiva LM, Warren MJ. 2011. Evolution in a family of chelatases facilitated by the introduction of active site asymmetry and protein oligomerization. Proc. Natl. Acad. Sci. U. S. A. 108:97-102.

- 218. **Scott AI, Stolowich NJ, Wang J, Gawatz O, Fridrich E, Muller G.** 1996. Biosynthesis of vitamin B₁₂: factor IV, a new intermediate in the anaerobic pathway. Proc. Natl. Acad. Sci. U. S. A. **93:**14316-14319.
- 219. **Kajiwara Y, Santander PJ, Roessner CA, Perez LM, Scott AI.** 2006. Genetically engineered synthesis and structural characterization of cobalt-precorrin 5A and -5B, two new intermediates on the anaerobic pathway to vitamin B₁₂: definition of the roles of the CbiF and CbiG enzymes. J. Am. Chem. Soc. **128**:9971-9978.
- 220. Wang J, Stolowich NJ, Santander PJ, Park JH, Scott AI. 1996. Biosynthesis of vitamin B₁₂: concerning the identity of the two-carbon fragment eliminated during anaerobic formation of cobyrinic acid. Proc. Natl. Acad. Sci. U. S. A. 93:14320-14322.
- 221. Moore SJ, Lawrence AD, Biedendieck R, Deery E, Frank S, Howard MJ, Rigby SE, Warren MJ. 2013. Elucidation of the anaerobic pathway for the corrin component of cobalamin (vitamin B₁₂). Proc. Natl. Acad. Sci. U. S. A. 110:14906-14911.
- 222. **Roessner CA, Williams HJ, Scott AI.** 2005. Genetically engineered production of 1-desmethylcobyrinic acid, 1-desmethylcobyrinic acid a,c-diamide, and cobyrinic acid a,c-diamide in *Escherichia coli* implies a role for CbiD in C-1 methylation in the anaerobic pathway to cobalamin. J. Biol. Chem. **280**:16748-16753.
- 223. **Vevodova J, Graham RM, Raux E, Warren MJ, Wilson KS.** 2005. Crystallization and preliminary structure analysis of CobE, an essential protein of cobalamin (vitamin B₁₂) biosynthesis. Acta Crystallogr. Sect. F Struct. Biol. Cryst. Commun. **61:**442-444.
- **Fonseca MV, Escalante-Semerena JC.** 2001. An *in vitro* reducing system for the enzymic conversion of cobalamin to adenosylcobalamin. J. Biol. Chem. **276**:32101-32108.
- 225. **Thompson TB, Thomas MG, Escalante-Semerena JC, Rayment I.** 1999. Three-dimensional structure of adenosylcobinamide kinase/adenosylcobinamide phosphate guanylyltransferase (CobU) complexed with GMP: evidence for a substrate-induced transferase active site. Biochemistry **38:**12995-13005.
- 226. **Thomas MG, Thompson TB, Rayment I, Escalante-Semerena JC.** 2000. Analysis of the adenosylcobinamide kinase/adenosylcobinamide-phosphate guanylyltransferase (CobU) enzyme of *Salmonella typhimurium* LT2. Identification of residue His-46 as the site of guanylylation. J. Biol. Chem. **275**:27576-27586.
- 227. **Maggio-Hall LA, Escalante-Semerena JC.** 1999. *In vitro* synthesis of the nucleotide loop of cobalamin by *Salmonella typhimurium* enzymes. Proc. Natl. Acad. Sci. U. S. A. **96:**11798-11803.
- 228. **Keck B, Munder M, Renz P.** 1998. Biosynthesis of cobalamin in *Salmonella typhimurium*: transformation of riboflavin into the 5,6-dimethylbenzimidazole moiety. Arch. Microbiol. **171:**66-68.

- 229. **Horig JA, Renz P.** 1980. Biosynthesis of vitamin B₁₂. Some properties of the 5,6-dimethylbenzimidazole-forming system of *Propionibacterium freudenreichii* and *Propionibacterium shermanii*. Eur. J. Biochem. **105**:587-592.
- 230. **Zayas CL, Escalante-Semerena JC.** 2007. Reassessment of the late steps of coenzyme B₁₂ synthesis in *Salmonella enterica*: evidence that dephosphorylation of adenosylcobalamin-5'-phosphate by the CobC phosphatase is the last step of the pathway. J. Bacteriol. **189:**2210-2218.
- 231. Holliday GL, Thornton JM, Marquet A, Smith AG, Rebeille F, Mendel R, Schubert HL, Lawrence AD, Warren MJ. 2007. Evolution of enzymes and pathways for the biosynthesis of cofactors. Nat. Prod. Rep. 24:972-987.
- 232. **Mandal M, Breaker RR.** 2004. Gene regulation by riboswitches. Nat. Rev. Mol. Cell Biol. **5:**451-463.
- 233. Nahvi A, Sudarsan N, Ebert MS, Zou X, Brown KL, Breaker RR. 2002. Genetic control by a metabolite binding mRNA. Chem. Biol. 9:1043.
- 234. **Kadner RJ.** 1978. Repression of synthesis of the vitamin B₁₂ receptor in *Escherichia coli*. J. Bacteriol. **136:**1050-1057.
- 235. **Lundrigan MD, Kadner RJ.** 1989. Altered cobalamin metabolism in *Escherichia coli btuR* mutants affects *btuB* gene regulation. J. Bacteriol. **171:**154-161.
- 236. **Lundrigan MD, Koster W, Kadner RJ.** 1991. Transcribed sequences of the *Escherichia coli btuB* gene control its expression and regulation by vitamin B₁₂. Proc. Natl. Acad. Sci. U. S. A. **88:**1479-1483.
- 237. **Gallo S, Oberhuber M, Sigel RK, Krautler B.** 2008. The corrin moiety of coenzyme B₁₂ is the determinant for switching the *btuB* riboswitch of *E. coli*. Chembiochem **9:**1408-1414.
- 238. **Gallo S, Mundwiler S, Alberto R, Sigel RK.** 2011. The change of corrin-amides to carboxylates leads to altered structures of the B₁₂-responding btuB riboswitch. Chem. Commun. (Camb.) **47:**403-405.
- 239. **Johnson JE, Jr., Reyes FE, Polaski JT, Batey RT.** 2012. B₁₂ cofactors directly stabilize an mRNA regulatory switch. Nature **492:**133-137.
- 240. **Peselis A, Serganov A.** 2012. Structural insights into ligand binding and gene expression control by an adenosylcobalamin riboswitch. Nat. Struct. Mol. Biol. **19:**1182-1184.
- 241. **Roth JR, Lawrence JG, Bobik TA.** 1996. Cobalamin (coenzyme B₁₂): synthesis and biological significance. Annu. Rev. Microbiol. **50:**137-181.
- 242. **Schauer K, Rodionov DA, de Reuse H.** 2008. New substrates for TonB-dependent transport: do we only see the 'tip of the iceberg'? Trends Biochem. Sci. **33:**330-338.

- 243. **Gruber K, Puffer B, Krautler B.** 2011. Vitamin B₁₂-derivatives-enzyme cofactors and ligands of proteins and nucleic acids. Chem. Soc. Rev. **40**:4346-4363.
- 244. **Bradbeer C, Reynolds PR, Bauler GM, Fernandez MT.** 1986. A requirement for calcium in the transport of cobalamin across the outer membrane of *Escherichia coli*. J. Biol. Chem. **261:**2520-2523.
- 245. Cadieux N, Bradbeer C, Kadner RJ. 2000. Sequence changes in the Ton box region of BtuB affect its transport activities and interaction with TonB protein. J. Bacteriol. 182:5954-5961.
- 246. Chimento DP, Mohanty AK, Kadner RJ, Wiener MC. 2003. Substrate-induced transmembrane signaling in the cobalamin transporter BtuB. Nat. Struct. Biol. 10:394-401.
- 247. **Shultis DD, Purdy MD, Banchs CN, Wiener MC.** 2006. Outer membrane active transport: structure of the BtuB:TonB complex. Science **312:**1396-1399.
- 248. **Gumbart J, Wiener MC, Tajkhorshid E.** 2007. Mechanics of force propagation in TonB-dependent outer membrane transport. Biophys. J. **93:**496-504.
- 249. **Borths EL, Locher KP, Lee AT, Rees DC.** 2002. The structure of *Escherichia coli* BtuF and binding to its cognate ATP binding cassette transporter. Proc. Natl. Acad. Sci. U. S. A. **99:**16642-16647.
- 250. Cadieux N, Bradbeer C, Reeger-Schneider E, Koster W, Mohanty AK, Wiener MC, Kadner RJ. 2002. Identification of the periplasmic cobalamin-binding protein BtuF of *Escherichia coli*. J. Bacteriol. **184:**706-717.
- 251. **James KJ, Hancock MA, Gagnon JN, Coulton JW.** 2009. TonB interacts with BtuF, the *Escherichia coli* periplasmic binding protein for cyanocobalamin. Biochemistry **48:**9212-9220.
- 252. Carter DM, Miousse IR, Gagnon JN, Martinez E, Clements A, Lee J, Hancock MA, Gagnon H, Pawelek PD, Coulton JW. 2006. Interactions between TonB from *Escherichia coli* and the periplasmic protein FhuD. J. Biol. Chem. **281**:35413-35424.
- 253. **Locher KP, Lee AT, Rees DC.** 2002. The *E. coli* BtuCD structure: a framework for ABC transporter architecture and mechanism. Science **296:**1091-1098.
- 254. **Krewulak KD, Vogel HJ.** 2008. Structural biology of bacterial iron uptake. Biochim. Biophys. Acta **1778:**1781-1804.
- 255. **Hvorup RN, Goetz BA, Niederer M, Hollenstein K, Perozo E, Locher KP.** 2007. Asymmetry in the structure of the ABC transporter-binding protein complex BtuCD-BtuF. Science **317:**1387-1390.

- 256. **Korkhov VM, Mireku SA, Locher KP.** 2012. Structure of AMP-PNP-bound vitamin B₁₂ transporter BtuCD-F. Nature **490**:367-372.
- 257. **Banerjee R, Ragsdale SW.** 2003. The many faces of vitamin B₁₂: catalysis by cobalamin-dependent enzymes. Annu. Rev. Biochem. **72:**209-247.
- 258. **Janssen DB, Oppentocht JE, Poelarends GJ.** 2001. Microbial dehalogenation. Curr. Opin. Biotechnol. **12:**254-258.
- 259. **Linkfield TG, Tiedje JM.** 1990. Characterization of the requirements and substrates for reductive dehalogenation by strain DCB-1. J. Ind. Microbiol. **5:**9-15.
- 260. **Neumann A, Siebert A, Trescher T, Reinhardt S, Wohlfarth G, Diekert G.** 2002. Tetrachloroethene reductive dehalogenase of *Dehalospirillum multivorans*: substrate specificity of the native enzyme and its corrinoid cofactor. Arch. Microbiol. **177:**420-426.
- 261. Holscher T, Krajmalnik-Brown R, Ritalahti KM, Von Wintzingerode F, Gorisch H, Loffler FE, Adrian L. 2004. Multiple nonidentical reductive-dehalogenase-homologous genes are common in *Dehalococcoides*. Appl. Environ. Microbiol. **70:**5290-5297.
- 262. **Brown KL.** 2005. Chemistry and enzymology of vitamin B₁₂. Chem. Rev. **105**:2075-2149.
- 263. **Matthews RG.** 2001. Cobalamin-dependent methyltransferases. Acc. Chem. Res. **34:**681-689.
- 264. **Thauer RK.** 1998. Biochemistry of methanogenesis: a tribute to Marjory Stephenson. 1998 Marjory Stephenson Prize Lecture. Microbiology **144:**2377-2406.
- 265. **Ragsdale SW.** 2006. Metals and their scaffolds to promote difficult enzymatic reactions. Chem. Rev. **106:**3317-3337.
- 266. **Goulding CW, Postigo D, Matthews RG.** 1997. Cobalamin-dependent methionine synthase is a modular protein with distinct regions for binding homocysteine, methyltetrahydrofolate, cobalamin, and adenosylmethionine. Biochemistry **36:**8082-8091.
- 267. **Dixon MM, Huang S, Matthews RG, Ludwig M.** 1996. The structure of the C-terminal domain of methionine synthase: presenting S-adenosylmethionine for reductive methylation of B₁₂. Structure **4:**1263-1275.
- 268. **Bandarian V, Pattridge KA, Lennon BW, Huddler DP, Matthews RG, Ludwig ML.** 2002. Domain alternation switches B₁₂-dependent methionine synthase to the activation conformation. Nat. Struct. Biol. **9:**53-56.

- 269. Koutmos M, Datta S, Pattridge KA, Smith JL, Matthews RG. 2009. Insights into the reactivation of cobalamin-dependent methionine synthase. Proc. Natl. Acad. Sci. U. S. A. 106:18527-18532.
- 270. Kung Y, Ando N, Doukov TI, Blasiak LC, Bender G, Seravalli J, Ragsdale SW, Drennan CL. 2012. Visualizing molecular juggling within a B₁₂-dependent methyltransferase complex. Nature **484**:265-269.
- 271. **Reitzer R, Gruber K, Jogl G, Wagner UG, Bothe H, Buckel W, Kratky C.** 1999. Glutamate mutase from *Clostridium cochlearium*: the structure of a coenzyme B₁₂-dependent enzyme provides new mechanistic insights. Structure **7:**891-902.
- 272. **Gruber K, Reitzer R, Kratky C.** 2001. Radical shuttling in a protein:ribose pseudorotation controls alkyl-radical transfer in the coenzyme B₁₂ dependent enzyme glutamate mutase. Angew. Chem. Int. Ed. Engl. **40:**3377-3380.
- 273. **Masuda J, Shibata N, Morimoto Y, Toraya T, Yasuoka N.** 2000. How a protein generates a catalytic radical from coenzyme B₁₂: X-ray structure of a diol-dehydratase-adeninylpentylcobalamin complex. Structure **8:**775-788.
- 274. Shibata N, Tamagaki H, Hieda N, Akita K, Komori H, Shomura Y, Terawaki S, Mori K, Yasuoka N, Higuchi Y, Toraya T. 2010. Crystal structures of ethanolamine ammonia-lyase complexed with coenzyme B₁₂ analogs and substrates. J. Biol. Chem. **285**:26484-26493.
- 275. **Berkovitch F, Behshad E, Tang KH, Enns EA, Frey PA, Drennan CL.** 2004. A locking mechanism preventing radical damage in the absence of substrate, as revealed by the x-ray structure of lysine 5,6-aminomutase. Proc. Natl. Acad. Sci. U. S. A. **101:**15870-15875.
- 276. **Wolthers KR, Levy C, Scrutton NS, Leys D.** 2010. Large-scale domain dynamics and adenosylcobalamin reorientation orchestrate radical catalysis in ornithine 4,5-aminomutase. J. Biol. Chem. **285**:13942-13950.
- 277. **Sintchak MD, Arjara G, Kellogg BA, Stubbe J, Drennan CL.** 2002. The crystal structure of class II ribonucleotide reductase reveals how an allosterically regulated monomer mimics a dimer. Nat. Struct. Biol. **9:**293-300.
- 278. Larsson KM, Logan DT, Nordlund P. 2010. Structural basis for adenosylcobalamin activation in AdoCbl-dependent ribonucleotide reductases. ACS Chem. Biol. 5:933-942.
- 279. **Hoffman RM, Erbe RW.** 1976. High *in vivo* rates of methionine biosynthesis in transformed human and malignant rat cells auxotrophic for methionine. Proc. Natl. Acad. Sci. U. S. A. **73:**1523-1527.
- 280. **Fowler B, Whitehouse C, Wenzel F, Wraith JE.** 1997. Methionine and serine formation in control and mutant human cultured fibroblasts: evidence for methyl trapping and characterization of remethylation defects. Pediatr. Res. **41:**145-151.

- 281. Willard HF, Ambani LM, Hart AC, Mahoney MJ, Rosenberg LE. 1976. Rapid prenatal and postnatal detection of inborn errors of propionate, methylmalonate, and cobalamin metabolism: a sensitive assay using cultured cells. Hum. Genet. 34:277-283.
- 282. **Silagi S, Darlington G, Bruce SA.** 1969. Hybridization of two biochemically marked human cell lines. Proc. Natl. Acad. Sci. U. S. A. **62:**1085-1092.
- 283. Siniscalco M, Klinger HP, Eagle H, Koprowski H, Fujimoto WY, Seegmiller JE. 1969. Evidence for intergenic complementation in hybrid cells derived from two human diploid strains each carrying an X-linked mutation. Proc. Natl. Acad. Sci. U. S. A. 62:793-799.
- Watkins D, Rosenblatt DS. 1988. Genetic heterogeneity among patients with methylcobalamin deficiency. Definition of two complementation groups, *cblE* and *cblG*. J. Clin. Invest. 81:1690-1694.
- 285. **Watkins D, Rosenblatt DS.** 2011. Inherited disorders of folate and cobalamin transport and metabolism. *In* Valle D, Beaudet AL, Vogelstein B, Kinzler KW, Antonarakis SE, Ballabio A (ed.), The online metabolic & molecular bases of inherited disease. McGraw-Hill, New York.
- 286. **Froese DS, Gravel RA.** 2010. Genetic disorders of vitamin B₁₂ metabolism: eight complementation groups--eight genes. Expert Rev. Mol. Med. **12:**e37.
- 287. Watkins D, Ru M, Hwang HY, Kim CD, Murray A, Philip NS, Kim W, Legakis H, Wai T, Hilton JF, Ge B, Dore C, Hosack A, Wilson A, Gravel RA, Shane B, Hudson TJ, Rosenblatt DS. 2002. Hyperhomocysteinemia due to methionine synthase deficiency, *cblG*: structure of the *MTR* gene, genotype diversity, and recognition of a common mutation, P1173L. Am. J. Hum. Genet. 71:143-153.
- 288. **Gherasim C, Lofgren M, Banerjee R.** 2013. Navigating the B₁₂ road: assimilation, delivery, and disorders of cobalamin. J. Biol. Chem. **288:**13186-13193.
- 289. Chen LH, Liu ML, Hwang HY, Chen LS, Korenberg J, Shane B. 1997. Human methionine synthase. cDNA cloning, gene localization, and expression. J. Biol. Chem. 272:3628-3634.
- 290. Leclerc D, Wilson A, Dumas R, Gafuik C, Song D, Watkins D, Heng HH, Rommens JM, Scherer SW, Rosenblatt DS, Gravel RA. 1998. Cloning and mapping of a cDNA for methionine synthase reductase, a flavoprotein defective in patients with homocystinuria. Proc. Natl. Acad. Sci. U. S. A. 95:3059-3064.
- 291. **Olteanu H, Banerjee R.** 2001. Human methionine synthase reductase, a soluble P-450 reductase-like dual flavoprotein, is sufficient for NADPH-dependent methionine synthase activation. J. Biol. Chem. **276**:35558-35563.

- 292. **Wolthers KR, Basran J, Munro AW, Scrutton NS.** 2003. Molecular dissection of human methionine synthase reductase: determination of the flavin redox potentials in full-length enzyme and isolated flavin-binding domains. Biochemistry **42:**3911-3920.
- 293. **Wolthers KR, Scrutton NS.** 2007. Protein interactions in the human methionine synthase-methionine synthase reductase complex and implications for the mechanism of enzyme reactivation. Biochemistry **46**:6696-6709.
- 294. **Yamada K, Gravel RA, Toraya T, Matthews RG.** 2006. Human methionine synthase reductase is a molecular chaperone for human methionine synthase. Proc. Natl. Acad. Sci. U. S. A. **103:**9476-9481.
- 295. **Rosenberg LE, Lilljeqvist AC, Hsia YE, Rosenbloom FM.** 1969. Vitamin B₁₂ dependent methylmalonicaciduria: defective B₁₂ metabolism in cultured fibroblasts. Biochem. Biophys. Res. Commun. **37:**607-614.
- 296. **Mahoney MJ, Rosenberg LE, Mudd SH, Uhlendorf BW.** 1971. Defective metabolism of vitamin B₁₂ in fibroblasts from children with methylmalonicaciduria. Biochem. Biophys. Res. Commun. **44:**375-381.
- 297. **Mahoney MJ, Hart AC, Steen VD, Rosenberg LE.** 1975. Methylmalonicacidemia: biochemical heterogeneity in defects of 5'-deoxyadenosylcobalamin synthesis. Proc. Natl. Acad. Sci. U. S. A. **72:**2799-2803.
- 298. **Dobson CM, Wai T, Leclerc D, Wilson A, Wu X, Dore C, Hudson T, Rosenblatt DS, Gravel RA.** 2002. Identification of the gene responsible for the *cblA* complementation group of vitamin B₁₂-responsive methylmalonic acidemia based on analysis of prokaryotic gene arrangements. Proc. Natl. Acad. Sci. U. S. A. **99:**15554-15559.
- 299. Horster F, Baumgartner MR, Viardot C, Suormala T, Burgard P, Fowler B, Hoffmann GF, Garbade SF, Kolker S, Baumgartner ER. 2007. Long-term outcome in methylmalonic acidurias is influenced by the underlying defect (mut⁰, mut̄, cblA, cblB). Pediatr. Res. 62:225-230.
- 300. **Padovani D, Labunska T, Banerjee R.** 2006. Energetics of interaction between the G-protein chaperone, MeaB, and B₁₂-dependent methylmalonyl-CoA mutase. J. Biol. Chem. **281:**17838-17844.
- 301. **Korotkova N, Lidstrom ME.** 2004. MeaB is a component of the methylmalonyl-CoA mutase complex required for protection of the enzyme from inactivation. J. Biol. Chem. **279:**13652-13658.
- 302. **Padovani D, Banerjee R.** 2006. Assembly and protection of the radical enzyme, methylmalonyl-CoA mutase, by its chaperone. Biochemistry **45:**9300-9306.
- 303. **Padovani D, Banerjee R.** 2009. A G-protein editor gates coenzyme B₁₂ loading and is corrupted in methylmalonic aciduria. Proc. Natl. Acad. Sci. U. S. A. **106:**21567-21572.

- 304. Froese DS, Kochan G, Muniz JR, Wu X, Gileadi C, Ugochukwu E, Krysztofinska E, Gravel RA, Oppermann U, Yue WW. 2010. Structures of the human GTPase MMAA and vitamin B₁₂-dependent methylmalonyl-CoA mutase and insight into their complex formation. J. Biol. Chem. **285**:38204-38213.
- 305. **Takahashi-Iniguez T, Garcia-Arellano H, Trujillo-Roldan MA, Flores ME.** 2011. Protection and reactivation of human methylmalonyl-CoA mutase by MMAA protein. Biochem. Biophys. Res. Commun. **404:**443-447.
- 306. **Dobson CM, Wai T, Leclerc D, Kadir H, Narang M, Lerner-Ellis JP, Hudson TJ, Rosenblatt DS, Gravel RA.** 2002. Identification of the gene responsible for the *cblB* complementation group of vitamin B₁₂-dependent methylmalonic aciduria. Hum. Mol. Genet. **11:**3361-3369.
- 307. Lerner-Ellis JP, Gradinger AB, Watkins D, Tirone JC, Villeneuve A, Dobson CM, Montpetit A, Lepage P, Gravel RA, Rosenblatt DS. 2006. Mutation and biochemical analysis of patients belonging to the *cblB* complementation class of vitamin B₁₂-dependent methylmalonic aciduria. Mol. Genet. Metab. 87:219-225.
- 308. **Leal NA, Park SD, Kima PE, Bobik TA.** 2003. Identification of the human and bovine ATP:Cob(I)alamin adenosyltransferase cDNAs based on complementation of a bacterial mutant. J. Biol. Chem. **278:**9227-9234.
- 309. **Padovani D, Labunska T, Palfey BA, Ballou DP, Banerjee R.** 2008. Adenosyltransferase tailors and delivers coenzyme B₁₂. Nat Chem Biol **4:**194-196.
- 310. **Stich TA, Yamanishi M, Banerjee R, Brunold TC.** 2005. Spectroscopic evidence for the formation of a four-coordinate Co²⁺ cobalamin species upon binding to the human ATP:cobalamin adenosyltransferase. J. Am. Chem. Soc. **127:**7660-7661.
- 311. **Yamanishi M, Labunska T, Banerjee R.** 2005. Mirror "base-off" conformation of coenzyme B₁₂ in human adenosyltransferase and its downstream target, methylmalonyl-CoA mutase. J. Am. Chem. Soc. **127:**526-527.
- 312. **Leal NA, Olteanu H, Banerjee R, Bobik TA.** 2004. Human ATP:Cob(I)alamin adenosyltransferase and its interaction with methionine synthase reductase. J. Biol. Chem. **279**:47536-47542.
- 313. **Mera PE, Escalante-Semerena JC.** 2010. Dihydroflavin-driven adenosylation of 4-coordinate Co(II) corrinoids: are cobalamin reductases enzymes or electron transfer proteins? J. Biol. Chem. **285**:2911-2917.
- 314. **Schubert HL, Hill CP.** 2006. Structure of ATP-bound human ATP:cobalamin adenosyltransferase. Biochemistry **45:**15188-15196.
- 315. **Padovani D, Banerjee R.** 2009. A rotary mechanism for coenzyme B₁₂ synthesis by adenosyltransferase. Biochemistry **48:**5350-5357.

- 316. **Lofgren M, Banerjee R.** 2011. Loss of allostery and coenzyme B₁₂ delivery by a pathogenic mutation in adenosyltransferase. Biochemistry **50**:5790-5798.
- 317. **Zhang J, Wu X, Padovani D, Schubert HL, Gravel RA.** 2009. Ligand-binding by catalytically inactive mutants of the *cblB* complementation group defective in human ATP:cob(I)alamin adenosyltransferase. Mol. Genet. Metab. **98:**278-284.
- 318. **Fan C, Bobik TA.** 2008. Functional characterization and mutation analysis of human ATP:Cob(I)alamin adenosyltransferase. Biochemistry **47:**2806-2813.
- 319. Saridakis V, Yakunin A, Xu X, Anandakumar P, Pennycooke M, Gu J, Cheung F, Lew JM, Sanishvili R, Joachimiak A, Arrowsmith CH, Christendat D, Edwards AM. 2004. The structural basis for methylmalonic aciduria. The crystal structure of archaeal ATP:cobalamin adenosyltransferase. J. Biol. Chem. 279:23646-23653.
- 320. **St Maurice M, Mera PE, Taranto MP, Sesma F, Escalante-Semerena JC, Rayment I.** 2007. Structural characterization of the active site of the PduO-type ATP:Co(I)rrinoid adenosyltransferase from *Lactobacillus reuteri*. J. Biol. Chem. **282:**2596-2605.
- 321. **Zhang J, Dobson CM, Wu X, Lerner-Ellis J, Rosenblatt DS, Gravel RA.** 2006. Impact of *cblB* mutations on the function of ATP:cob(I)alamin adenosyltransferase in disorders of vitamin B₁₂ metabolism. Mol. Genet. Metab. **87:**315-322.
- 322. Lempp TJ, Suormala T, Siegenthaler R, Baumgartner ER, Fowler B, Steinmann B, Baumgartner MR. 2007. Mutation and biochemical analysis of 19 probands with *mut*⁰ and 13 with *mut*⁻ methylmalonic aciduria: identification of seven novel mutations. Mol. Genet. Metab. **90:**284-290.
- 323. Mancia F, Keep NH, Nakagawa A, Leadlay PF, McSweeney S, Rasmussen B, Bosecke P, Diat O, Evans PR. 1996. How coenzyme B₁₂ radicals are generated: the crystal structure of methylmalonyl-coenzyme A mutase at 2 Å resolution. Structure 4:339-350.
- 324. **Mancia F, Evans PR.** 1998. Conformational changes on substrate binding to methylmalonyl-CoA mutase and new insights into the free radical mechanism. Structure **6:**711-720.
- 325. **Mancia F, Smith GA, Evans PR.** 1999. Crystal structure of substrate complexes of methylmalonyl-CoA mutase. Biochemistry **38:**7999-8005.
- 326. **Marsh EN, Harding SE, Leadlay PF.** 1989. Subunit interactions in *Propionibacterium shermanii* methylmalonyl-CoA mutase studied by analytical ultracentrifugation. Biochem. J. **260:**353-358.
- 327. **Jansen R, Kalousek F, Fenton WA, Rosenberg LE, Ledley FD.** 1989. Cloning of full-length methylmalonyl-CoA mutase from a cDNA library using the polymerase chain reaction. Genomics **4:**198-205.

- 328. **Brass EP, Ruff LJ.** 1989. Effect of carnitine on propionate metabolism in the vitamin B₁₂-deficient rat. J. Nutr. **119:**1196-1202.
- 329. **Rosenblatt DS, Hosack A, Matiaszuk NV, Cooper BA, Laframboise R.** 1985. Defect in vitamin B₁₂ release from lysosomes: newly described inborn error of vitamin B₁₂ metabolism. Science **228:**1319-1321.
- 330. **Vassiliadis A, Rosenblatt DS, Cooper BA, Bergeron JJ.** 1991. Lysosomal cobalamin accumulation in fibroblasts from a patient with an inborn error of cobalamin metabolism (*cblF* complementation group): visualization by electron microscope radioautography. Exp. Cell Res. **195:**295-302.
- 331. **Watkins D, Rosenblatt DS.** 1986. Failure of lysosomal release of vitamin B₁₂: a new complementation group causing methylmalonic aciduria (*cblF*). Am. J. Hum. Genet. **39:**404-408.
- 332. Rutsch F, Gailus S, Miousse IR, Suormala T, Sagne C, Toliat MR, Nurnberg G, Wittkampf T, Buers I, Sharifi A, Stucki M, Becker C, Baumgartner M, Robenek H, Marquardt T, Hohne W, Gasnier B, Rosenblatt DS, Fowler B, Nurnberg P. 2009. Identification of a putative lysosomal cobalamin exporter altered in the *cblF* defect of vitamin B₁₂ metabolism. Nat. Genet. 41:234-239.
- 333. Gailus S, Suormala T, Malerczyk-Aktas AG, Toliat MR, Wittkampf T, Stucki M, Nurnberg P, Fowler B, Hennermann JB, Rutsch F. 2010. A novel mutation in *LMBRD1* causes the *cblF* defect of vitamin B₁₂ metabolism in a Turkish patient. J. Inherit. Metab. Dis. 33:17-24.
- 334. **Miousse IR, Watkins D, Rosenblatt DS.** 2011. Novel splice site mutations and a large deletion in three patients with the *cblF* inborn error of vitamin B₁₂ metabolism. Mol. Genet. Metab. **102:**505-507.
- 335. **Armour CM, Brebner A, Watkins D, Geraghty MT, Chan A, Rosenblatt DS.** 2013. A patient with an inborn error of vitamin B₁₂ metabolism (*cblF*) detected by newborn screening. Pediatrics **132:**e257-261.
- 336. Oladipo O, Rosenblatt DS, Watkins D, Miousse IR, Sprietsma L, Dietzen DJ, Shinawi M. 2011. Cobalamin F disease detected by newborn screening and follow-up on a 14-year-old patient. Pediatrics 128:e1636-1640.
- 337. **Alfadhel M, Lillquist YP, Davis C, Junker AK, Stockler-Ipsiroglu S.** 2011. Eighteen-year follow-up of a patient with cobalamin F disease (*cblF*): report and review. Am. J. Med. Genet. A **155a**:2571-2577.
- 338. Chapel A, Kieffer-Jaquinod S, Sagne C, Verdon Q, Ivaldi C, Mellal M, Thirion J, Jadot M, Bruley C, Garin J, Gasnier B, Journet A. 2013. An extended proteome map of the lysosomal membrane reveals novel potential transporters. Mol. Cell. Proteomics 12:1572-1588.

- 339. **Tseng LT, Lin CL, Tzen KY, Chang SC, Chang MF.** 2013. LMBD1 serves as a specific adaptor for insulin receptor internalization. J. Biol. Chem. **288**:32424-32432.
- 340. Wang YH, Chang SC, Huang C, Li YP, Lee CH, Chang MF. 2005. Novel nuclear export signal-interacting protein, NESI, critical for the assembly of hepatitis delta virus. J. Virol. 79:8113-8120.
- 341. **Huang C, Jiang JY, Chang SC, Tsay YG, Chen MR, Chang MF.** 2013. Nuclear export signal-interacting protein forms complexes with lamin A/C-Nups to mediate the CRM1-independent nuclear export of large hepatitis delta antigen. J. Virol. **87:**1596-1604.
- 342. Coelho D, Kim JC, Miousse IR, Fung S, du Moulin M, Buers I, Suormala T, Burda P, Frapolli M, Stucki M, Nurnberg P, Thiele H, Robenek H, Hohne W, Longo N, Pasquali M, Mengel E, Watkins D, Shoubridge EA, Majewski J, Rosenblatt DS, Fowler B, Rutsch F, Baumgartner MR. 2012. Mutations in *ABCD4* cause a new inborn error of vitamin B₁₂ metabolism. Nat. Genet. 44:1152-1155.
- 343. **Kim JC, Lee NC, Hwu PW, Chien YH, Fahiminiya S, Majewski J, Watkins D, Rosenblatt DS.** 2012. Late onset of symptoms in an atypical patient with the *cblJ* inborn error of vitamin B₁₂ metabolism: diagnosis and novel mutation revealed by exome sequencing. Mol. Genet. Metab. **107:**664-668.
- 344. **Holzinger A, Kammerer S, Roscher AA.** 1997. Primary structure of human PMP69, a putative peroxisomal ABC-transporter. Biochem. Biophys. Res. Commun. **237:**152-157.
- 345. **Kashiwayama Y, Seki M, Yasui A, Murasaki Y, Morita M, Yamashita Y, Sakaguchi M, Tanaka Y, Imanaka T.** 2009. 70-kDa peroxisomal membrane protein related protein (P70R/ABCD4) localizes to endoplasmic reticulum not peroxisomes, and NH2-terminal hydrophobic property determines the subcellular localization of ABC subfamily D proteins. Exp. Cell. Res. **315**:190-205.
- 346. **Shani N, Jimenez-Sanchez G, Steel G, Dean M, Valle D.** 1997. Identification of a fourth half ABC transporter in the human peroxisomal membrane. Hum. Mol. Genet. **6:**1925-1931.
- 347. Liu LX, Janvier K, Berteaux-Lecellier V, Cartier N, Benarous R, Aubourg P. 1999. Homo- and heterodimerization of peroxisomal ATP-binding cassette half-transporters. J. Biol. Chem. 274:32738-32743.
- 348. **Hillebrand M, Verrier SE, Ohlenbusch A, Schafer A, Soling HD, Wouters FS, Gartner J.** 2007. Live cell FRET microscopy: homo- and heterodimerization of two human peroxisomal ABC transporters, the adrenoleukodystrophy protein (ALDP, ABCD1) and PMP70 (ABCD3). J. Biol. Chem. **282**:26997-27005.
- 349. Wanders RJ, Visser WF, van Roermund CW, Kemp S, Waterham HR. 2007. The peroxisomal ABC transporter family. Pflugers Arch. 453:719-734.

- 350. **Kikuchi M, Hatano N, Yokota S, Shimozawa N, Imanaka T, Taniguchi H.** 2004. Proteomic analysis of rat liver peroxisome: presence of peroxisome-specific isozyme of Lon protease. J. Biol. Chem. **279:**421-428.
- 351. **Islinger M, Luers GH, Li KW, Loos M, Volkl A.** 2007. Rat liver peroxisomes after fibrate treatment. A survey using quantitative mass spectrometry. J. Biol. Chem. **282:**23055-23069.
- Wiese S, Gronemeyer T, Ofman R, Kunze M, Grou CP, Almeida JA, Eisenacher M, Stephan C, Hayen H, Schollenberger L, Korosec T, Waterham HR, Schliebs W, Erdmann R, Berger J, Meyer HE, Just W, Azevedo JE, Wanders RJ, Warscheid B. 2007. Proteomics characterization of mouse kidney peroxisomes by tandem mass spectrometry and protein correlation profiling. Mol. Cell. Proteomics 6:2045-2057.
- 353. Gopinath K, Venclovas C, Ioerger TR, Sacchettini JC, McKinney JD, Mizrahi V, Warner DF. 2013. A vitamin B₁₂ transporter in *Mycobacterium tuberculosis*. Open Biol. 3:120175.
- 354. Lerner-Ellis JP, Tirone JC, Pawelek PD, Dore C, Atkinson JL, Watkins D, Morel CF, Fujiwara TM, Moras E, Hosack AR, Dunbar GV, Antonicka H, Forgetta V, Dobson CM, Leclerc D, Gravel RA, Shoubridge EA, Coulton JW, Lepage P, Rommens JM, Morgan K, Rosenblatt DS. 2006. Identification of the gene responsible for methylmalonic aciduria and homocystinuria, *cblC* type. Nat. Genet. 38:93-100.
- 355. Nogueira C, Aiello C, Cerone R, Martins E, Caruso U, Moroni I, Rizzo C, Diogo L, Leao E, Kok F, Deodato F, Schiaffino MC, Boenzi S, Danhaive O, Barbot C, Sequeira S, Locatelli M, Santorelli FM, Uziel G, Vilarinho L, Dionisi-Vici C. 2008. Spectrum of *MMACHC* mutations in Italian and Portuguese patients with combined methylmalonic aciduria and homocystinuria, *cblC* type. Mol. Genet. Metab. 93:475-480.
- 356. Lerner-Ellis JP, Anastasio N, Liu J, Coelho D, Suormala T, Stucki M, Loewy AD, Gurd S, Grundberg E, Morel CF, Watkins D, Baumgartner MR, Pastinen T, Rosenblatt DS, Fowler B. 2009. Spectrum of mutations in *MMACHC*, allelic expression, and evidence for genotype-phenotype correlations. Hum. Mutat. 30:1072-1081.
- 357. **Kraus JP.** 2009. *cblC*: advances in defining the *MMACHC* mutation spectrum. Hum. Mutat. **30:**v.
- 358. Liu MY, Yang YL, Chang YC, Chiang SH, Lin SP, Han LS, Qi Y, Hsiao KJ, Liu TT. 2010. Mutation spectrum of *MMACHC* in Chinese patients with combined methylmalonic aciduria and homocystinuria. J. Hum. Genet. **55**:621-626.
- 359. **Backe PH, Ytre-Arne M, Rohr AK, Brodtkorb E, Fowler B, Rootwelt H, Bjoras M, Morkrid L.** 2013. Novel deletion mutation identified in a patient with late-onset combined methylmalonic acidemia and homocystinuria, *cblC* Type. JIMD Rep. **11:**79-85.

- 360. **Profitlich LE, Kirmse B, Wasserstein MP, Diaz GA, Srivastava S.** 2009. High prevalence of structural heart disease in children with *cblC*-type methylmalonic aciduria and homocystinuria. Mol. Genet. Metab. **98:**344-348.
- 361. **Rosenblatt DS, Aspler AL, Shevell MI, Pletcher BA, Fenton WA, Seashore MR.** 1997. Clinical heterogeneity and prognosis in combined methylmalonic aciduria and homocystinuria (*cblC*). J. Inherit. Metab. Dis. **20:**528-538.
- 362. **Mellman I, Willard HF, Youngdahl-Turner P, Rosenberg LE.** 1979. Cobalamin coenzyme synthesis in normal and mutant human fibroblasts. Evidence for a processing enzyme activity deficient in *cblC* cells. J. Biol. Chem. **254:**11847-11853.
- 363. **Andersson HC, Shapira E.** 1998. Biochemical and clinical response to hydroxocobalamin versus cyanocobalamin treatment in patients with methylmalonic acidemia and homocystinuria (*cblC*). J. Pediatr. **132:**121-124.
- 364. **Morel CF, Lerner-Ellis JP, Rosenblatt DS.** 2006. Combined methylmalonic aciduria and homocystinuria (*cblC*): phenotype-genotype correlations and ethnic-specific observations. Mol. Genet. Metab. **88:**315-321.
- 365. Yu HC, Sloan JL, Scharer G, Brebner A, Quintana AM, Achilly NP, Manoli I, Coughlin CR, 2nd, Geiger EA, Schneck U, Watkins D, Suormala T, Van Hove JL, Fowler B, Baumgartner MR, Rosenblatt DS, Venditti CP, Shaikh TH. 2013. An X-linked cobalamin disorder caused by mutations in transcriptional coregulator *HCFC1*. Am. J. Hum. Genet. 93:506-514.
- 366. **Koutmos M, Gherasim C, Smith JL, Banerjee R.** 2011. Structural basis of multifunctionality in a vitamin B₁₂-processing enzyme. J. Biol. Chem. **286:**29780-29787.
- 367. **Plesa M, Kim J, Paquette SG, Gagnon H, Ng-Thow-Hing C, Gibbs BF, Hancock MA, Rosenblatt DS, Coulton JW.** 2011. Interaction between MMACHC and MMADHC, two human proteins participating in intracellular vitamin B₁₂ metabolism. Mol. Genet. Metab. **102:**139-148.
- 368. **Froese DS, Zhang J, Healy S, Gravel RA.** 2009. Mechanism of vitamin B₁₂-responsiveness in *cblC* methylmalonic aciduria with homocystinuria. Mol. Genet. Metab. **98:**338-343.
- 369. Froese DS, Healy S, McDonald M, Kochan G, Oppermann U, Niesen FH, Gravel RA. 2010. Thermolability of mutant MMACHC protein in the vitamin B₁₂-responsive *cblC* disorder. Mol. Genet. Metab. **100**:29-36.
- 370. **Kim J, Gherasim C, Banerjee R.** 2008. Decyanation of vitamin B₁₂ by a trafficking chaperone. Proc. Natl. Acad. Sci. U. S. A. **105**:14551-14554.
- 371. **Kim J, Hannibal L, Gherasim C, Jacobsen DW, Banerjee R.** 2009. A human vitamin B₁₂ trafficking protein uses glutathione transferase activity for processing alkylcobalamins. J. Biol. Chem. **284:**33418-33424.

- 372. Froese DS, Krojer T, Wu X, Shrestha R, Kiyani W, von Delft F, Gravel RA, Oppermann U, Yue WW. 2012. Structure of MMACHC reveals an arginine-rich pocket and a domain-swapped dimer for its B₁₂ processing function. Biochemistry **51**:5083-5090.
- 373. Hannibal L, Kim J, Brasch NE, Wang S, Rosenblatt DS, Banerjee R, Jacobsen DW. 2009. Processing of alkylcobalamins in mammalian cells: A role for the MMACHC (*cblC*) gene product. Mol. Genet. Metab. 97:260-266.
- 374. **Sillaots SL, Hall CA, Hurteloup V, Rosenblatt DS.** 1992. Heterogeneity in *cblG*: differential retention of cobalamin on methionine synthase. Biochem. Med. Metab. Biol. **47:**242-249.
- 375. Fofou-Caillierez MB, Mrabet NT, Chery C, Dreumont N, Flayac J, Pupavac M, Paoli J, Alberto JM, Coelho D, Camadro JM, Feillet F, Watkins D, Fowler B, Rosenblatt DS, Gueant JL. 2013. Interaction between methionine synthase isoforms and MMACHC: characterization in *cblG*-variant, *cblG* and *cblC* inherited causes of megaloblastic anemia. Hum. Mol. Genet. 22:4591-4601.
- 376. Goodman SI, Moe PG, Hammond KB, Mudd SH, Uhlendorf BW. 1970. Homocystinuria with methylmalonic aciduria: two cases in a sibship. Biochem. Med. 4:500-515.
- 377. **Willard HF, Mellman IS, Rosenberg LE.** 1978. Genetic complementation among inherited deficiencies of methylmalonyl-CoA mutase activity: evidence for a new class of human cobalamin mutant. Am. J. Hum. Genet. **30:**1-13.
- 378. Suormala T, Baumgartner MR, Coelho D, Zavadakova P, Kozich V, Koch HG, Berghauser M, Wraith JE, Burlina A, Sewell A, Herwig J, Fowler B. 2004. The *cblD* defect causes either isolated or combined deficiency of methylcobalamin and adenosylcobalamin synthesis. J. Biol. Chem. **279**:42742-42749.
- 379. Coelho D, Suormala T, Stucki M, Lerner-Ellis JP, Rosenblatt DS, Newbold RF, Baumgartner MR, Fowler B. 2008. Gene identification for the *cblD* defect of vitamin B₁₂ metabolism. N. Engl. J. Med. **358:**1454-1464.
- 380. **Stucki M, Coelho D, Suormala T, Burda P, Fowler B, Baumgartner MR.** 2012. Molecular mechanisms leading to three different phenotypes in the *cblD* defect of intracellular cobalamin metabolism. Hum. Mol. Genet. **21:**1410-1418.
- 381. Miousse IR, Watkins D, Coelho D, Rupar T, Crombez EA, Vilain E, Bernstein JA, Cowan T, Lee-Messer C, Enns GM, Fowler B, Rosenblatt DS. 2009. Clinical and molecular heterogeneity in patients with the *cblD* inborn error of cobalamin metabolism. J. Pediatr. 154:551-556.
- **Yogev O, Pines O.** 2011. Dual targeting of mitochondrial proteins: mechanism, regulation and function. Biochim. Biophys. Acta **1808**:1012-1020.

- 383. **Mellman IS, Youngdahl-Turner P, Willard HF, Rosenberg LE.** 1977. Intracellular binding of radioactive hydroxocobalamin to cobalamin-dependent apoenzymes in rat liver. Proc. Natl. Acad. Sci. U. S. A. **74:**916-920.
- 384. **Kolhouse JF, Allen RH.** 1977. Recognition of two intracellular cobalamin binding proteins and their identification as methylmalonyl-CoA mutase and methionine synthetase. Proc. Natl. Acad. Sci. U. S. A. **74:**921-925.
- 385. **Bottger V, Bottger A.** 2009. Epitope mapping using phage display peptide libraries. Methods Mol. Biol. **524:**181-201.
- 386. **James KJ, Hancock MA, Moreau V, Molina F, Coulton JW.** 2008. TonB induces conformational changes in surface-exposed loops of FhuA, outer membrane receptor of *Escherichia coli*. Protein Sci. **17:**1679-1688.
- 387. **Rodi DJ, Janes RW, Sanganee HJ, Holton RA, Wallace BA, Makowski L.** 1999. Screening of a library of phage-displayed peptides identifies human bcl-2 as a taxolbinding protein. J. Mol. Biol. **285:**197-203.
- 388. Rodi DJ, Agoston GE, Manon R, Lapcevich R, Green SJ, Makowski L. 2001. Identification of small molecule binding sites within proteins using phage display technology. Comb. Chem. High Throughput Screen. 4:553-572.
- 389. **Sidhu SS, Fairbrother WJ, Deshayes K.** 2003. Exploring protein-protein interactions with phage display. Chembiochem **4:**14-25.
- 390. **Goodyear CS, Silverman GJ.** 2008. Phage-display methodology for the study of protein-protein interactions: overview. CSH Protoc. **2008**:pdb top48.
- 391. **Nobbmann U, Connah M, Fish B, Varley P, Gee C, Mulot S, Chen J, Zhou L, Lu Y, Shen F, Yi J, Harding SE.** 2007. Dynamic light scattering as a relative tool for assessing the molecular integrity and stability of monoclonal antibodies. Biotechnol. Genet. Eng. Rev. **24:**117-128.
- 392. **Santiago PS, Moura F, Moreira LM, Domingues MM, Santos NC, Tabak M.** 2008. Dynamic light scattering and optical absorption spectroscopy study of pH and temperature stabilities of the extracellular hemoglobin of *Glossoscolex paulistus*. Biophys. J. **94:**2228-2240.
- 393. **Slotboom DJ, Duurkens RH, Olieman K, Erkens GB.** 2008. Static light scattering to characterize membrane proteins in detergent solution. Methods **46:**73-82.
- 394. **Schuck P.** 2000. Size-distribution analysis of macromolecules by sedimentation velocity ultracentrifugation and lamm equation modeling. Biophys. J. **78:**1606-1619.
- 395. **Schuck P.** 1998. Sedimentation analysis of noninteracting and self-associating solutes using numerical solutions to the Lamm equation. Biophys. J. **75:**1503-1512.

- 396. **Erickson HP.** 2009. Size and shape of protein molecules at the nanometer level determined by sedimentation, gel filtration, and electron microscopy. Biol. Proced. Online **11:**32-51.
- 397. **Schuh S, Rosenblatt DS, Cooper BA, Schroeder ML, Bishop AJ, Seargeant LE, Haworth JC.** 1984. Homocystinuria and megaloblastic anemia responsive to vitamin B₁₂ therapy. An inborn error of metabolism due to a defect in cobalamin metabolism. N. Engl. J. Med. **310**:686-690.
- 398. **Shevell MI, Rosenblatt DS.** 1992. The neurology of cobalamin. Can. J. Neurol. Sci. **19:**472-486.
- 399. **Gravel RA, Mahoney MJ, Ruddle FH, Rosenberg LE.** 1975. Genetic complementation in heterokaryons of human fibroblasts defective in cobalamin metabolism. Proc. Natl. Acad. Sci. U. S. A. **72:**3181-3185.
- 400. **Carrillo-Carrasco N, Chandler RJ, Venditti CP.** 2012. Combined methylmalonic acidemia and homocystinuria, *cblC* type. I. Clinical presentations, diagnosis and management. J. Inherit. Metab. Dis. **35**:91-102.
- 401. Pagliarini DJ, Calvo SE, Chang B, Sheth SA, Vafai SB, Ong SE, Walford GA, Sugiana C, Boneh A, Chen WK, Hill DE, Vidal M, Evans JG, Thorburn DR, Carr SA, Mootha VK. 2008. A mitochondrial protein compendium elucidates complex I disease biology. Cell 134:112-123.
- 402. **Laue TM, Shah BD, Ridgeway TM, Pelletier SL.** 1992. Computer-aided interpretation of analytical sedimentation data for proteins, p. 90-125. *In* Harding SE, Rowe AJ, Horton JC (ed.), Analytical ultracentrifugation in biochemistry and polymer Science. The Royal Society of Chemistry, Cambridge.
- 403. **Whitmore L, Wallace BA.** 2004. DICHROWEB, an online server for protein secondary structure analyses from circular dichroism spectroscopic data. Nucleic Acids Res. **32:**W668-673.
- 404. **Sreerama N, Woody RW.** 2000. Estimation of protein secondary structure from circular dichroism spectra: comparison of CONTIN, SELCON, and CDSSTR methods with an expanded reference set. Anal. Biochem. **287:**252-260.
- 405. **McGuffin LJ, Bryson K, Jones DT.** 2000. The PSIPRED protein structure prediction server. Bioinformatics **16:**404-405.
- 406. **Ward JJ, Sodhi JS, McGuffin LJ, Buxton BF, Jones DT.** 2004. Prediction and functional analysis of native disorder in proteins from the three kingdoms of life. J. Mol. Biol. **337:**635-645.
- 407. **Bond CS, Schuttelkopf AW.** 2009. ALINE: a WYSIWYG protein-sequence alignment editor for publication-quality alignments. Acta Crystallogr. D Biol. Crystallogr. **65:**510-512.

- 408. **Mandava S, Makowski L, Devarapalli S, Uzubell J, Rodi DJ.** 2004. RELIC--a bioinformatics server for combinatorial peptide analysis and identification of protein-ligand interaction sites. Proteomics **4:**1439-1460.
- 409. Pettersen EF, Goddard TD, Huang CC, Couch GS, Greenblatt DM, Meng EC, Ferrin TE. 2004. UCSF Chimera--a visualization system for exploratory research and analysis. J. Comput. Chem. 25:1605-1612.
- 410. Myszka DG. 1999. Improving biosensor analysis. J. Mol. Recognit. 12:279-284.
- 411. **Borgstahl GE.** 2007. How to use dynamic light scattering to improve the likelihood of growing macromolecular crystals. Methods Mol. Biol. **363:**109-129.
- 412. **Kelly SM, Jess TJ, Price NC.** 2005. How to study proteins by circular dichroism. Biochim. Biophys. Acta **1751:**119-139.
- 413. **Sreerama N, Woody RW.** 2004. Computation and analysis of protein circular dichroism spectra. Methods Enzymol. **383:**318-351.
- 414. **Jeong J, Kim J.** 2011. Glutathione increases the binding affinity of a bovine B₁₂ trafficking chaperone bCblC for vitamin B₁₂. Biochem. Biophys. Res. Commun. **412:**360-365.
- 415. **Sugase K, Dyson HJ, Wright PE.** 2007. Mechanism of coupled folding and binding of an intrinsically disordered protein. Nature **447:**1021-1025.
- 416. **Gunasekaran K, Tsai CJ, Kumar S, Zanuy D, Nussinov R.** 2003. Extended disordered proteins: targeting function with less scaffold. Trends Biochem. Sci. **28:**81-85.
- 417. Fong JH, Shoemaker BA, Garbuzynskiy SO, Lobanov MY, Galzitskaya OV, Panchenko AR. 2009. Intrinsic disorder in protein interactions: insights from a comprehensive structural analysis. PLoS Comput. Biol. 5:e1000316.
- 418. **Claros MG, Vincens P.** 1996. Computational method to predict mitochondrially imported proteins and their targeting sequences. Eur. J. Biochem. **241:**779-786.
- 419. **Sharma VS, Pilz RB, Boss GR, Magde D.** 2003. Reactions of nitric oxide with vitamin B₁₂ and its precursor, cobinamide. Biochemistry **42:**8900-8908.
- 420. **Cracan V, Padovani D, Banerjee R.** 2010. IcmF is a fusion between the radical B₁₂ enzyme isobutyryl-CoA mutase and its G-protein chaperone. J. Biol. Chem. **285:**655-666.
- 421. **Banerjee R, Gherasim C, Padovani D.** 2009. The tinker, tailor, soldier in intracellular B₁₂ trafficking. Curr. Opin. Chem. Biol. **13:**484-491.
- 422. **Stover PJ, Field MS.** 2011. Trafficking of intracellular folates. Adv. Nutr. 2:325-331.

- 423. **Frenkel EP, Kitchens RL.** 1975. Intracellular localization of hepatic propionyl-CoA carboxylase and methylmalonyl-CoA mutase in humans and normal and vitamin B₁₂ deficient rats. Br. J. Haematol. **31:**501-513.
- 424. **Deme JC, Miousse IR, Plesa M, Kim JC, Hancock MA, Mah W, Rosenblatt DS, Coulton JW.** 2012. Structural features of recombinant MMADHC isoforms and their interactions with MMACHC, proteins of mammalian vitamin B₁₂ metabolism. Mol. Genet. Metab. **107:**352-362.
- 425. **Pear WS, Nolan GP, Scott ML, Baltimore D.** 1993. Production of high-titer helper-free retroviruses by transient transfection. Proc. Natl. Acad. Sci. U. S. A. **90:**8392-8396.
- 426. **Watkins D.** 1998. Cobalamin metabolism in methionine-dependent human tumour and leukemia cell lines. Clin. Invest. Med. **21:**151-158.
- 427. Hatchell EC, Colley SM, Beveridge DJ, Epis MR, Stuart LM, Giles KM, Redfern AD, Miles LE, Barker A, MacDonald LM, Arthur PG, Lui JC, Golding JL, McCulloch RK, Metcalf CB, Wilce JA, Wilce MC, Lanz RB, O'Malley BW, Leedman PJ. 2006. SLIRP, a small SRA binding protein, is a nuclear receptor corepressor. Mol. Cell 22:657-668.
- 428. **Bourgeron T, Rustin P, Chretien D, Birch-Machin M, Bourgeois M, Viegas-Pequignot E, Munnich A, Rotig A.** 1995. Mutation of a nuclear succinate dehydrogenase gene results in mitochondrial respiratory chain deficiency. Nat. Genet. **11:**144-149.
- 429. **Okado-Matsumoto A, Fridovich I.** 2001. Subcellular distribution of superoxide dismutases (SOD) in rat liver: Cu,Zn-SOD in mitochondria. J. Biol. Chem. **276**:38388-38393.
- 430. **Petrova VY, Drescher D, Kujumdzieva AV, Schmitt MJ.** 2004. Dual targeting of yeast catalase A to peroxisomes and mitochondria. Biochem. J. **380**:393-400.
- 431. **Dinur-Mills M, Tal M, Pines O.** 2008. Dual targeted mitochondrial proteins are characterized by lower MTS parameters and total net charge. PLoS One **3:**e2161.
- 432. **Knox C, Sass E, Neupert W, Pines O.** 1998. Import into mitochondria, folding and retrograde movement of fumarase in yeast. J. Biol. Chem. **273**:25587-25593.
- 433. **Strobel G, Zollner A, Angermayr M, Bandlow W.** 2002. Competition of spontaneous protein folding and mitochondrial import causes dual subcellular location of major adenylate kinase. Mol. Biol. Cell **13:**1439-1448.
- 434. **Rossmanith W.** 2011. Localization of human RNase Z isoforms: dual nuclear/mitochondrial targeting of the *ELAC2* gene product by alternative translation initiation. PLoS One **6:**e19152.

- 435. **Rutsch F, Gailus S, Suormala T, Fowler B.** 2011. *LMBRD1*: the gene for the *cblF* defect of vitamin B_{12} metabolism. J. Inherit. Metab. Dis. **34:**121-126.
- 436. **Boulter JM, Wang DN.** 2001. Purification and characterization of human erythrocyte glucose transporter in decylmaltoside detergent solution. Protein Expr. Purif. **22:**337-348.
- 437. **Rath A, Glibowicka M, Nadeau VG, Chen G, Deber CM.** 2009. Detergent binding explains anomalous SDS-PAGE migration of membrane proteins. Proc. Natl. Acad. Sci. U. S. A. **106:**1760-1765.
- 438. **Duong F.** 2003. Binding, activation and dissociation of the dimeric SecA ATPase at the dimeric SecYEG translocase. EMBO J. **22:**4375-4384.
- 439. **Maillard AP, Lalani S, Silva F, Belin D, Duong F.** 2007. Deregulation of the SecYEG translocation channel upon removal of the plug domain. J. Biol. Chem. **282:**1281-1287.
- 440. **van der Does C, de Keyzer J, van der Laan M, Driessen AJ.** 2003. Reconstitution of purified bacterial preprotein translocase in liposomes. Methods Enzymol. **372:**86-98.
- 441. **Xu J, Liu Y, Yang Y, Bates S, Zhang JT.** 2004. Characterization of oligomeric human half-ABC transporter ATP-binding cassette G2. J. Biol. Chem. **279:**19781-19789.
- 442. **Wojnar P, Lechner M, Merschak P, Redl B.** 2001. Molecular cloning of a novel lipocalin-1 interacting human cell membrane receptor using phage display. J. Biol. Chem. **276:**20206-20212.
- 443. **Hesselink RW, Findlay JB.** 2013. Expression, characterization and ligand specificity of lipocalin-1 interacting membrane receptor (LIMR). Mol. Membr. Biol. **30:**327-337.
- 444. Guimaraes CP, Domingues P, Aubourg P, Fouquet F, Pujol A, Jimenez-Sanchez G, Sa-Miranda C, Azevedo JE. 2004. Mouse liver PMP70 and ALDP: homomeric interactions prevail *in vivo*. Biochim. Biophys. Acta **1689**:235-243.
- 445. **Vigonsky E, Ovcharenko E, Lewinson O.** 2013. Two molybdate/tungstate ABC transporters that interact very differently with their substrate binding proteins. Proc. Natl. Acad. Sci. U. S. A. **110:**5440-5445.
- 446. **Lewinson O, Lee AT, Locher KP, Rees DC.** 2010. A distinct mechanism for the ABC transporter BtuCD-BtuF revealed by the dynamics of complex formation. Nat. Struct. Mol. Biol. **17:**332-338.
- 447. **Gherasim C, Hannibal L, Rajagopalan D, Jacobsen DW, Banerjee R.** 2013. The Cterminal domain of CblD interacts with CblC and influences intracellular cobalamin partitioning. Biochimie **95:**1023-1032.
- 448. Carter DM, Gagnon JN, Damlaj M, Mandava S, Makowski L, Rodi DJ, Pawelek PD, Coulton JW. 2006. Phage display reveals multiple contact sites between FhuA, an outer membrane receptor of *Escherichia coli*, and TonB. J. Mol. Biol. **357**:236-251.

- 449. Pawelek PD, Croteau N, Ng-Thow-Hing C, Khursigara CM, Moiseeva N, Allaire M, Coulton JW. 2006. Structure of TonB in complex with FhuA, *E. coli* outer membrane receptor. Science **312**:1399-1402.
- 450. **Pavlidou M, Hanel K, Mockel L, Willbold D.** 2013. Nanodiscs allow phage display selection for ligands to non-linear epitopes on membrane proteins. PLoS One **8:**e72272.
- 451. **Mah W, Deme JC, Watkins D, Fung S, Janer A, Shoubridge EA, Rosenblatt DS, Coulton JW.** 2013. Subcellular location of MMACHC and MMADHC, two human proteins central to intracellular vitamin B₁₂ metabolism. Mol. Genet. Metab. **108:**112-118.
- 452. **Gailus S, Hohne W, Gasnier B, Nurnberg P, Fowler B, Rutsch F.** 2010. Insights into lysosomal cobalamin trafficking: lessons learned from *cblF* disease. J. Mol. Med. (Berl.) **88:**459-466.
- 453. **Takahashi K, Kimura Y, Kioka N, Matsuo M, Ueda K.** 2006. Purification and ATPase activity of human ABCA1. J. Biol. Chem. **281:**10760-10768.
- 454. Shintre CA, Pike AC, Li Q, Kim JI, Barr AJ, Goubin S, Shrestha L, Yang J, Berridge G, Ross J, Stansfeld PJ, Sansom MS, Edwards AM, Bountra C, Marsden BD, von Delft F, Bullock AN, Gileadi O, Burgess-Brown NA, Carpenter EP. 2013. Structures of ABCB10, a human ATP-binding cassette transporter in apo- and nucleotide-bound states. Proc. Natl. Acad. Sci. U. S. A. 110:9710-9715.
- 455. **Borths EL, Poolman B, Hvorup RN, Locher KP, Rees DC.** 2005. *In vitro* functional characterization of BtuCD-F, the *Escherichia coli* ABC transporter for vitamin B₁₂ uptake. Biochemistry **44:**16301-16309.